Estrogen receptor alpha and p90 ribosomal S6 kinase in homeostasis and disease.

By

Zachary M. Sandusky

Dissertation

Submitted to the Faculty of the

Graduate School of Vanderbilt University

in partial fulfillment of the requirements

for the degree of

DOCTOR OF PHILOSOPHY

In

Cancer Biology

December 12, 2020

Nashville, Tennessee

Approved:

Deborah A. Lannigan, Ph.D.

Barbara M. Fingleton, Ph.D.

Ann Richnmond, Ph.D.

Kevin G. Osteen, Ph.D.

Charles C. Hong, M.D. Ph.D.

Table of Contents

List of Figures

List of Tables

List of Publications

1. Ludwik, K.A.*, **Sandusky, Z.M.***, Wright, E.B., Lannigan, D.A. FACS protocol for direct comparison of isolated in vivo cell populations. Accepted with revisions; Star Protocols, 2020

2. **Sandusky, Z.M.,** Cadar, A.G., Wright, E.B., Li, Y., Li., M., Hong, C., O'Doherty, G., Lannigan, D. RSK1/2 inhibition enhances doxorubicin-induced ERK1/2 activation to provide cardioprotection. Submitted; Journal of Molecular and Cellular Cardiology, 2020

3. Li Y*., **Sandusky Z.M.***, Vemula R., Wu B., Zhang Q., Fukuda S., Li M., Lannigan D.A., O'Doherty G.A. Regioselective Synthesis of a C-4" Carbamate, C-6" n-Pr Substituted Cyclitol Analogue of SL0101. *Org Lett* **22**, 1448-1452 (2020)

4. Ludwik K.A.*, **Sandusky Z.M.***, Stauffer K.M., Boyd K.L., Stricker T.P., and Lannigan D.A. RSK2 controls adult estrogen homeostasis by inhibiting ERK1/2 mediated degradation of estrogen receptor alpha. Cell Rep. 32(3) 2020

5. Li M., Li Y., Ludwik K.A., **Sandusky Z.M.**, Lannigan D.A., and O'Doherty G.A. Stereoselective Synthesis and Evaluation of C6″-Substituted 5a-Carbasugar Analogues of SL0101 as Inhibitors of RSK1/2. Org Lett. 19(9) 2017

6. Ludwik K.A., Campbell J.P., Li M., Li Y., **Sandusky Z.M.**, Pasic L., Sowder M.E., Brenin D.R., Pietenpol J.A., O'Doherty G.A., and Lannigan D.A. Development of a RSK Inhibitor as a Novel Therapy for Triple-Negative Breast Cancer. Mol Cancer Ther. 15(11) 2016

7. Li M.*, Mrozowski R.M.*, **Sandusky Z.M.***, Shan M., Song, X., Wu B., Zhang Q., Lannigan D.A., and O'Doherty G.A. Synthesis and Structure-Activity Relationship Study of 5a-Carbasugar Analogues of SL0101. ACS Med Chem Lett. 6(1) 2014

8. Mrozowski R.M.*, **Sandusky Z.M.*,** Vemula R.*, Wu B., Zhang Q., Lannigan D.A., and O'Doherty G.A. De novo synthesis and biological evaluation of C6"-substituted C4"-amide analogues of SL0101. Org Lett. 16(22) 2014

*denotes co-first author

Chapter 1

1. Introduction

The American Cancer Society estimates that over 250,000 new cases of invasive breast cancer are diagnosed annually in the United States. Subtyping breast cancer and the identification of targeted therapies have greatly improved our ability to manage the disease. However, major clinical challenges still exist including resistance to therapy and metastasis.

The majority of breast cancers are estrogen receptor alpha positive (ER+), indicating their hormone-responsive nature. These patients are treated with targeted therapies against estrogen signaling. Estrogen receptor alpha (ERalpha) is a ligand activated transcription factor that promotes cell proliferation in both the normal breast and ER+ breast cancer. Thus, understanding the processes underlying estrogen signaling homeostasis can improve the identification of novel therapies for ER+ breast cancer.

The Ser/Thr kinase family, ribosomal S6 kinases (RSK1 - 4), has been implicated in the etiology of various human diseases, including breast cancer, cardiovascular disease, fibrosis, and others, yet there are no clinical RSK inhibitors. RSKs are downstream effectors of the mitogen-activated kinase kinase (MEK 1/2) – extracellular regulated kinase (ERK1/2) pathway. RSK is capable of phosphorylating both cytoplasmic and nuclear substrates involved in cell proliferation, survival, and motility. Despite the disrupted RSK activity in a variety of human diseases, the underlying mechanisms are poorly understood.

While studying RSK2-knockout mice (RSK2-KO), we discovered a role for RSK2 in homeostasis of estrogen signaling (Figure 1.1). RSK2 has been implicated in ER+ breast cancer, however the role in normal mammary physiology was unknown. In chapter 2, we describe the identification of ERalpha regulation by ERK1/2 – RSK2 in normal mammary epithelial cells. We discovered that RSK2 is a negative regulator of normal ERalpha signaling,

and RSK2-KO mammary ER+ cells have increased oxidative stress and DNA-damage. These findings have important implications for ER+ breast cancer and women taking exogenous estrogen therapies.

In the second part of this thesis, we investigate targeting RSK2 signaling in cardiac pathophysiology and breast cancer. Based on reports that increased RSK activity is associated with human cardiovascular damage, we hypothesized that activation of RSK is also involved in adverse cardiovascular events of cancer chemotherapy. In chapter 3, we demonstrate the potential of a RSK inhibitor to prevent anthracycline chemotherapy-induced cardiac toxicity in vivo. This study confirms clinical reports of a pathological role for increased cardiac RSK activity.

In chapter 4, we demonstrate that targeting RSK 1/2 in the aggressive, ER-negative, triple-negative breast cancer (TNBC) subtype can prevent the establishment and proliferation of metastasis. These preclinical proof of concept studies in chapters 3 and 4 suggest that targeting RSK is dual strategy in cancer, both reducing the side effects of chemotherapy and preventing cancer progression. To accompany these studies, we developed a novel RSK inhibitor, C5-n-propyl-cyclitol SL0101 (C5"), with increased drug like properties. The synthesis and evaluation of C5" is described in chapters 5 – 8. Overall, these studies increase our understanding of RSK in homeostasis and pathophysiology.

Figure 1.1 ERK1/2 – RSK2 signaling maintains estrogen homeostasis in adult mice. In wild-type mouse mammary glands, ERK1/2 activity is restricted by RSK2. In RSK2-knockout mice, ERK1/2 drives increased ERalpha transcription and degradation. The increased estrogen signaling participates in a feed forward loop with ERK1/2 activity. Loss of RSK2 is associated with oxidative stress and DNA damage. This ultimately results in loss of ER+ cells and insufficient hormone dependent mammary alveolar expansion during pregnancy.

Figure 1. 1 ERK1/2 – RSK2 signaling maintains estrogen homeostasis in adult mice.
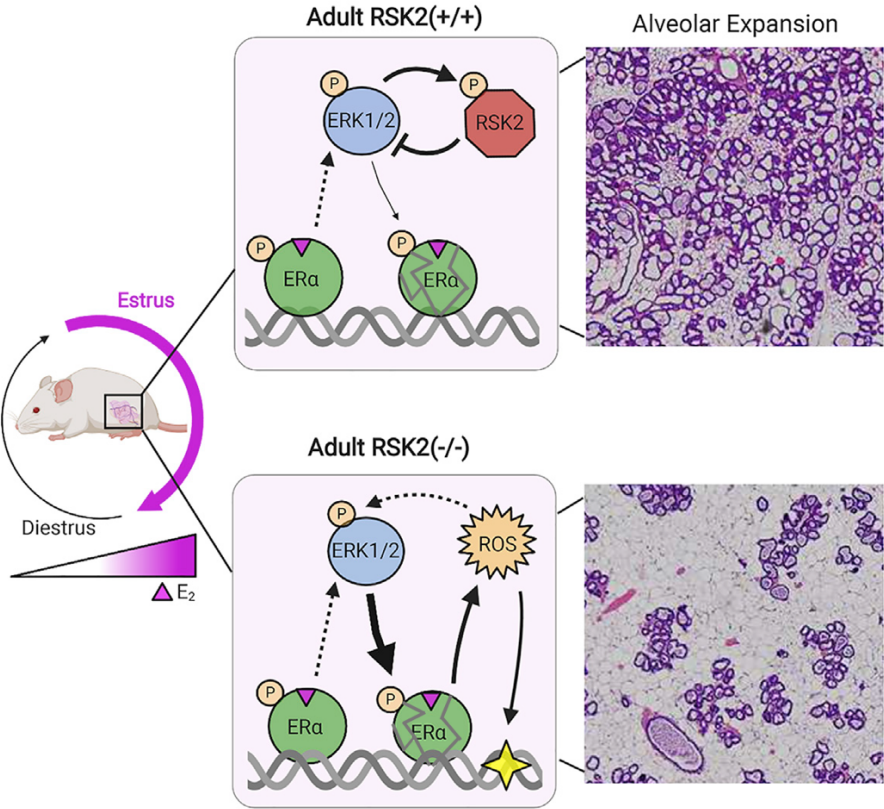
Estrogen physiology and exogenous estrogen containing therapies

Estrogens are a family of steroid hormones which are also widely used pharmaceuticals. Estrogens bind and activate the transcription factor, estrogen receptor alpha (ERalpha; gene name ESR1). In addition to their role in hormone signaling, estrogens have been proposed as carcinogens due to ERalpha induced mitogenic gene expression and due to the chemical ability of estrogen to intercalate with DNA (*1, 2*). This is further evidenced by association between exogenous exposure and increased breast cancer risk (*3, 4*). Estrogens are commonly recognized as the major female reproductive hormone, but estrogen signaling is also required for male fertility and the development and homeostasis of non-reproductive tissues including the bone, brain, and cardiovascular system (*5-7*). Estrogen signaling is now recognized to have a broad role in human homeostasis and pathophysiology.

The three major endogenous estrogens are estrone, estradiol, and estriol (Figure 1.2 A). Estradiol (E2) is produced by the ovaries and is the most potent and abundant estrogen in premenopausal women (*8, 9*). Estrone is the predominant estrogen in postmenopausal women and is produced by aromatase enzymes in peripheral tissues (*10*). Estriol is the least potent of these endogenous estrogens and is predominantly generated by the placenta during pregnancy. E2 can be produced from testosterone by aromatase enzymes (gene name CYP19A1), as well as from estrone by hydroxysteroid dehydrogenase enzymes. The production of estrogens by aromatase enzymes occurs in peripheral tissues other than the ovaries, including adrenals, adipose, brain, breast, and testes (*11*). Due to tissue specific expression of factors involved in estrogen producers and estrogen receptors, it is difficult to estimate estrogen exposures.

E2 has a high affinity for ERalpha ($Kd \sim 0.1 - 1$ nM) (*8, 9*). Estrogens are cholesterol derived and lipophilic, therefore they readily cross cell membranes and accumulate in adipose tissue. In premenopausal women, the concentration of E2 in circulation is approximately $0.2 - 3$ nM and estrogens are carried by serum albumins and sex hormone globulins (*12-14*). The concentration of estrogen in breast tissue is estimated to be ten-fold higher than the levels in

circulation (*15, 16*). Accumulation in the breast is likely due to the adipose tissue and expression of aromatase enzymes.

Estrogen exposure is linked to increased breast cancer risk in large epidemiology studies (*6*) . Reproductive factors such as early menarche, late menopause, and nulliparity increase relative reproductive cycles, therefore estrogen exposure and breast cancer risk. Endogenous estrogen levels are regulated in cyclic pattern by the female reproductive cycle. Endocrine signaling through the hypothalamic-pituitary-gonad axis stimulates the production of female sex hormones, including estrogens by the ovaries (*17*). Estrogen levels are highest in circulation during the follicular phase of the reproductive cycle, with the peak in estrogen driving ovulation. The follicular phase is controlled by release of follicle stimulating hormone (FSH) from the pituitary. After ovulation, during the luteal phase of the cycle, progesterone is the predominant hormone produced by the ovary and prepares the uterus and breast for pregnancy (*18, 19*). Monitoring the reproductive cycle is a useful tool to study the effects of hormone signaling in the physiological setting (*20*). This ensures studying hormone signaling in true complexity, as cross-talk exists in the form of feedback loops for hormone levels and activation of their receptors (*21*).

Targeting estrogen signaling is a major pharmaceutical strategy. Exogenous estrogens are used in oral contraceptives and hormone replacement therapy (*22*). These therapies are used by over 140 million women annually worldwide (*23*). Most current contraceptives contain the exogenous estrogen 17alpha-estradiol. This synthetic estrogen is orally available and shows similar affinity for ERalpha as E2 (*8*). To address the breast cancer risk associated with contraceptive use, current formulations contain lower estrogen concentrations although the risk has not been completely resolved (*23-25*). Relatively more safe alternative pharmaceutical contraceptives include inserts, which have decreased systemic hormone exposure. The majority of non-hormonal contraceptives are at the preclinical stage (*26*).

For postmenopausal hormone replacement therapy, the predominant exogenous estrogen is equine-derived conjugated estrogens, primarily estrone and equillin. Hormone replacement therapy is associated with increased breast cancer risk in a randomized, multicenter, placebo-controlled study (*6*). Hormone replacement therapy was significantly associated with other events, including increased risk of cardiovascular events and decreased bone fractures, supporting the role for estrogen signaling in non-reproductive tissues (*27*). Risk could be reduced by restricting therapy use to the perimenopausal period. However, identifying non-hormonal therapies for postmenopausal symptoms such as hot flashes and bone fractures will require better understanding of estrogen signaling in tissues of the nervous and skeletal system.

The most common breast cancer subtype is hormone responsive, ERalpha-positive (ER+) breast cancer, which is treated with ERalpha-targeted therapy. Premenopausal ER+ patients are treated with tamoxifen, which is an ERalpha antagonist in the breast. Postmenopausal women are treated with more efficacious inhibitors of estrogen signaling, such as ERalpha degraders (fulvestrant) and aromatase inhibitors (letrozole). In a clinical study of the prophylactic use of tamoxifen, which is orally available and well tolerated, treatment decreased the incidence of breast cancer (*28*). This study supports previous preclinical research that estrogen signaling is a major target in breast cancer.

Figure 1.2 Introduction to ERalpha and RSK biology. A) The structure of the major

endogenous human estrogens, estrone, estradiol, and estriol (upper panel) and the exogenous

estrogens 17alpha-ethinyl estradiol and equilin (lower panel). B) Estrogen receptor alpha post

translational modifications. ERalpha domain structure is shown with the location of post

translational modifications (solid circles) or hotspot mutations (open circles). The color of the

circle represents the original modified residue. Amino acid labeling is relative to human

ERalpha. The y-axis represents the number of published reports demonstrating the presence of

the modification in human ER+ breast cancer tissue. C) The structure of the most common

RSK-specific inhibitors. The NTKD inhibitors SL0101, BI-D1870, and BIX 02565 (upper panel)

and the CTKD inhibitor FMK (lower panel).

Figure 1. 2 Introduction to ERalpha and RSK biology

A

Estrone

Estradiol (E2)

Estriol

17alpha-Ethinylestradiol

Equilin

B

Clinical reports

ERalpha

AF-1   DBD   Hinge   AF-2

1   184   264   302   595

Modification type: ● Post translational modification   ○ Hot spot missense mutation

Modified residue: ● Serine (S)   ● Threonine (T)   ● Lysine (K)   ○ Glutamate (E)
● Tyrosine (Y)   ● Cysteine (C)   ● Arginine (R)   ○ Aspartate (D)

C

SL0101   BI-D1870   BIX 02565

FMK

9
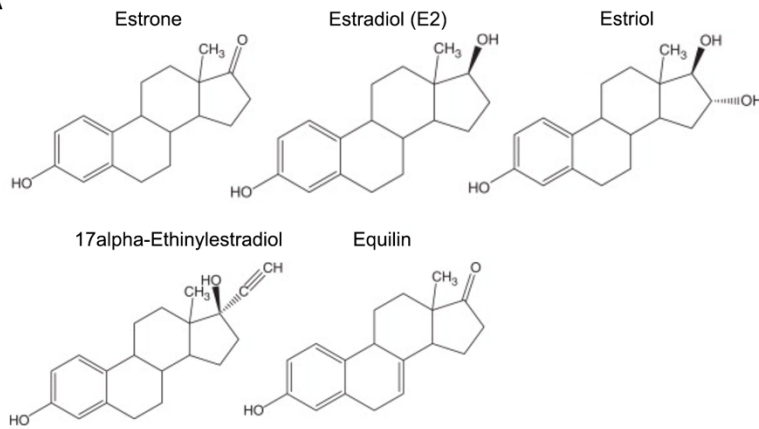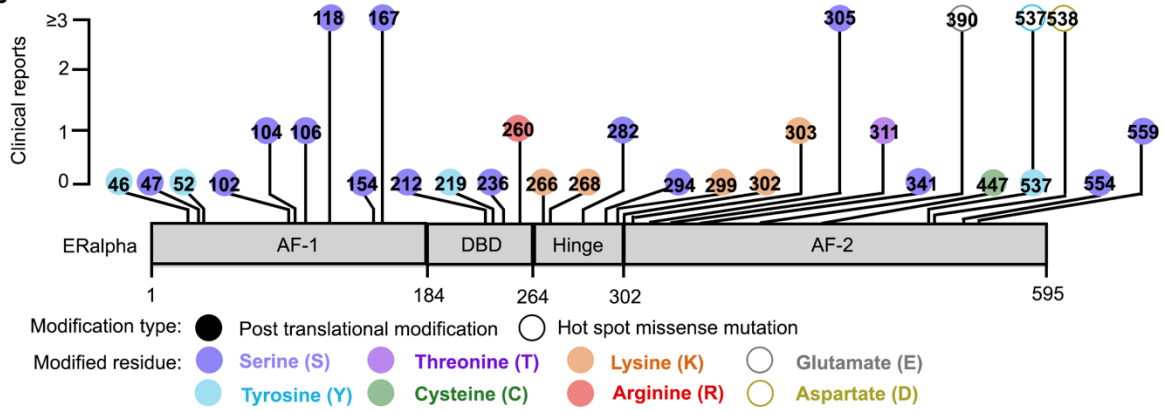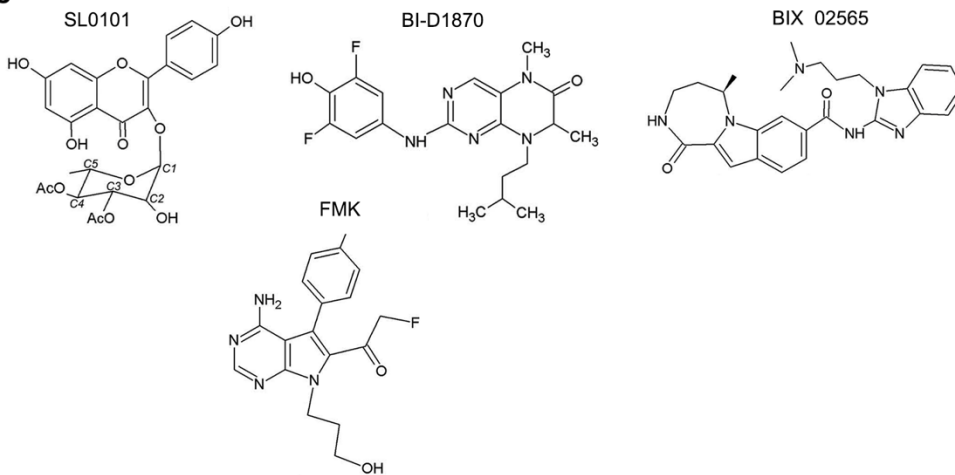
Estrogen receptor alpha signaling and post translational modifications

Estrogen signaling is central to development and homeostasis of the breast epithelium (*29*). Estrogens primarily exert their biological activity in the breast through the ligand-activated transcription factor, estrogen receptor alpha (ERalpha). Full transcriptional activation of ERalpha requires ligand binding and post-translational modification (PTMs), primarily through kinase mediated phosphorylation. Following the discovery of ERalpha, it was soon recognized that ERalpha undergoes rapid proteasomal degradation in response to ligand and this is required for transcriptional activity (*30*). ERalpha PTMs can mediate receptor stability, co-activator assembly, and transcriptional activity of ERalpha (*31*). Many of these studies are performed using transformed breast cancer cell lines and the key regulatory mechanisms under normal physiology are poorly understood. More recently, studies performed using human samples or transgenic mice are increasingly necessary for identifying and validating mechanisms of ERalpha transcription.

Transgenic mouse models and tissue recombination studies demonstrate that ERalpha is the major estrogen receptor for mammary gland development and breast cancer (*29, 32, 33*). Since the discovery of ERalpha, other estrogen receptors have been identified based on sequence homology. Estrogen receptor beta, the most closely related to ERalpha, is also required for reproductive fertility, however, only ERalpha is required for mammary development (*34*). Transgenic knockout mice for other receptors have been developed but a mammary gland phenotype has not been reported. These include knockout mouse models for the membrane bound G-protein coupled estrogen receptor (GPR30) (*35*), and estrogen related receptors (ERRa, ERRb, ERRg), which are nuclear orphan receptors (*36*). Together, current knowledge suggests that ERalpha is the major estrogen receptor for proliferation of the mammary epithelium.

The domain structure of ERalpha is well conserved with other nuclear hormone receptors. ERalpha is composed of two activator function domains and both are required for full

transcriptional activation. The N-terminal activator function-1 (AF-1) domain is ligand independent and contains the majority of identified ERalpha PTM sites (Figure 1.2 B). The C-terminal activator function-2 (AF-2) domain contains the ligand binding pocket and mediates interaction of ERalpha with co-activators. Between the AF-1 and AF-2 domain is the DNA-binding domain, composed of two zinc fingers, and the hinge domain, containing the nuclear localization sequence. Activation of ERalpha results in dimerization and binding to estrogen response elements, which are predominantly found at distal enhancers. However, ERalpha can also activate transcription through other DNA-bound factors such as AP-1 and RUNX transcription factors. To accomplish gene expression ERalpha recruits co-activators such as chromatin- and histone-modifying enzymes (*37*). The set of genes regulated by ERalpha has been predominantly studied in breast cancer cell lines and includes growth factors, cytokines, and cell cycle genes.

Approximately twenty seven ERalpha PTMs have been identified, the majority of which are phosphorylations to the AF-1 domain (Figure 1.2 B) (*31*). These PTMs have been primarily studied in breast cancer cell lines and have been shown to promote ligand-independent ERalpha activation and resistance to ERalpha targeted therapy. Of all the ERalpha PTMs, only three have been reported in more than one report using clinical samples. The extracellular regulated kinase (ERK1/2) phosphorylates ERalpha Ser-118 (*38*) and increased phosphor-Ser-118 correlates with increased phospho-ERK1/2 in ER+ breast cancer patients (*39*). Similarly, ERalpha Ser-167 is phosphorylated by AKT and RSK, and increased activation of these pathways is correlated with increased phospho-Ser167 (*40*). The phospho-Ser-118 and phospho-Ser-167 ERalpha have increased DNA binding and transcription activity in vitro and phospho-Ser-118 ERalpha recruits distinct transcription factors (*41*). Surprisingly, phosphorylation at these sites in clinical samples is associated with favorable response to tamoxifen (*31, 39, 40, 42-46*). This suggests that these sites are biomarkers for intact estrogen signaling that is tamoxifen sensitive in ER+ breast cancers. This was surprising because in vitro,

11

these phosphorylations were believed to promote tamoxifen resistance, supporting the need for more physiological models of ER+ breast cancer. ERalpha Ser-305 is located in the AF-2 domain of ERalpha and phospho-Ser-305 is associated with a worse prognosis with tamoxifen in ER+ breast cancer patients (*47-49*). This suggests that phospho-Ser-305 can mediate ligand-independent ERalpha activation and tamoxifen resistance (*50*). Ser305 is phosphorylated by PKA, however, it is unknown if activation of these pathways correlates with increased phospho-Ser305 in clinical samples (*51*). A myriad of pathways regulate ERalpha in transformed breast cancer cell lines. However, very few ERalpha PTMs have been validated in clinical samples. This suggest that the other ERalpha PTMs are less physiologically important in ER+ breast cancer or that the suitable tools, such as antibodies, to detect changes in these PTMs are not available.

Recurrent mutations in the ligand binding domain of ERalpha have been identified. These mutations were not discovered until recently and are detected exclusively in the metastasis of ER+ breast cancer patients who progressed on ERalpha targeted therapy (*52*). These mutations include E380Q, Y537S, and D538G. These mutations result in ligand-independent activation of ERalpha and a prometastatic gene expression program.

The ubiquitin-proteasome system, commonly recognized for a role in cellular proteostasis, is also required for cell signaling pathways, transcription activity, and the cell cycle (*53, 54*). Ligand binding to ERalpha, and other nuclear hormone receptors, induces proteolysis through the 26S proteasome (*55-57*). The observation of ligand induced ERalpha degradation in vivo was reported over fifty years ago. Furthermore, inhibition of the 26S proteasome blocks ERalpha transcription, demonstrating the important link between ERalpha degradation and transcription activity (*30*). The phosphorylation of ERalpha Ser-118 (*58*), Ser-294 (*59*), Ser-341 (*60*), and Tyr-537 (*61*) which are associated with ERalpha transcriptional activation and co-activator recruitment, are also known to mediate ERalpha protein stability in transformed breast cancer cell lines. Proteins are targeted for degradation through the 26S proteasome by E3-

ligase mediated lysine poly-ubiquitination. Notably, in vitro studies have identified many E3 ligases that regulate ERalpha protein stability and serve as transcription co-activators. However, the specific E3 ligase for ERalpha under normal physiological conditions is unknown (*62*). Furthermore, the mechanisms of proteasome mediated control of ERalpha transcription is poorly understood. It is possible that the proteasome is responsible for recycling ERalpha off the DNA for multiple rounds of transcription (*63-65*). This is supported by studies demonstrating pulses of ERalpha recruitment to the chromatin under saturating estradiol levels, although this model has been contrasted. ERalpha Lys-302 and Lys-303 ubiquitination have been identified using in vitro studies, and mediate ERalpha transcription activity and protein stability (*66-68*). It is also possible that other lysines residues on ERalpha are ubiquitinated. The only E3 ligase that has been associated with ERalpha protein levels in vivo is E6AP (*69*). However, this study was largely observational and the ability of E6AP to directly ubiquitinate ERalpha is unknown.

Taken together, it is clear that complex mechanisms control ERalpha transcription and ERalpha appears to be hijacked in ER+ breast cancer. Diverse ERalpha PTMs exist that mediate ERalpha transcriptional activity and have prognostic importance in ER+ breast cancer. It is not fully understood how the PTM code of ERalpha can mediate transcriptional activation and co-activator recruitment. Understanding the role of ERalpha phosphorylation in vivo and the role of specific ERalpha coactivors from the ubqiutin-proteasome system will aid identification of novel treatment strategies for ER+ breast cancer. Furthermore, these novel treatments may benefit other disease associated with disrupted estrogen signaling.

Estrogen receptor alpha is a driver of normal mammary development and breast cancer

The mammary gland is an arborized network of ducts embedded in an adipose-rich stroma. The mammary ducts are composed of an epithelial bilayer, with an inner layer of luminal cells and a basal layer of myoepithelial cells. The majority of breast cancers arise from the epithelium (*70*). In the normal mammary gland, the myoepithelial cells contract to release milk that is produced in ER-negative luminal cells during lactation. ER-positive (ER+) luminal cells are termed sensor cells, as they detect estrogen and relay the signal in a paracrine manner through expression of growth factors (*37, 71*). This process is required for coordinated development of the mammary epithelium during puberty, as well as pregnancy and lactation (*32, 33*).

The combination of transgenic mouse models, tissue transplantation studies, and lineage tracing have allowed a deep mechanistic understanding of normal mammary gland development. Interestingly, FOXA1, GATA3, and RUNX1 are commonly mutated in ER+ breast cancer at rates of 4%, 29%, and 7% (*72*) and these transcription factors are also critical for normal development of mammary ER+ cells (Table 1.1) (*73-75*) (*75*) (*76*). The MAPK pathway components, MAP3K1 and MAP2K4, are mutated in approximately 18% and 9% of ER+ breast cancers (*72*). A role for these genes in control of ERalpha levels in the normal developing mammary gland is unknown, but other MAPK component such as the p38MAPK-MSK1 pathway and ERK1/2-p90RSK pathway have been shown to control ERalpha levels in the normal mammary gland (*77, 78*). Together, these studies support the hypothesis that breast cancer hijacks normal developmental programs.

A summary of transgenic mouse models used to study ER+ mammary epithelial cells is provided in Table 1.1. These models have greatly improved our understanding of normal ER+ luminal cell homeostasis and future research will use these tools to increase our understanding of ER+ breast cancer. In brief there are several key takeaways from these studies. First, ERalpha is required for normal pubertal mammary gland development and lactation, whereas

14

ERbeta is dispensable (*29, 32-34*). Mammary specific expression of ERalpha truncation mutants revealed that both the AF-1 and AF-2 domains are required for ERalpha-dependent mammary development (*79*). Future studies investigating the role of individual residues, such as Ser118, will provide important insight into the physiological relevance of p-Ser118 in the normal mammary gland. Second, tissue recombination studies and transgenic mouse models support the conclusion that ERalpha in the mammary epithelium, not the stroma, regulates mammary gland development (*32, 33*). Control of development requires ERalpha-induced expression of the EGF family ligand, amphiregulin (*71*). Finally, lineage tracing experiments support the conclusion that ER+ luminal cells, ER-negative luminal cells, and myoepithelial cells are three distinct lineages in the postnatal mammary gland (*80-82*). Two recent lineage tracing studies used independent transgenic models to label ER+ luminal cells and discovered that the ER+ luminal subpopulation is maintained by long-lived lineage-restricted progenitor cells (*80, 81*). The conclusion that the ER+ luminal lineage is heterogenous and contains progenitor cells could explain the heterogeneity observed in ER+ breast cancers (*83*). The existence of a luminal progenitor population was surprising, as ER+ luminal cells were traditionally imagined as terminally differentiated and post-mitotic cells. The possibility of an ER+ luminal cell progenitor has important implications for ER+ breast cancer cell of origin research, and the identification of these cells will be aided by advanced transgenic mouse models (*84*).

Table 1. 1 Analysis of normal mammary ER+ cells in transgenic mice.

Transgenic model	Mammary gland phenotype	Reference
Esr1[tm1Ksk] (ERalpa-KO)	The first germline Esr1 knockout. Generated by targeting the start codon. Mammary phenotype includes absence of epithelial duct outgrowth during puberty. Also defects in uterus, ovary, and bone.	(*85*)
MMTV-Cre/Esr1^{fl/fl}	Germline targeting of Esr1 specifically in mammary epithelial cells using the MMTV promoter. Mammary glands have an absence of pubertal duct growth, branching, and terminal end development. This supports an epithelial intrinsic role for ERalpha in the mammary gland.	(*32*)
WAP-Cre/Esr1^{fl/fl}	The WAP (whey acidic protein) promoter is used to target the lactation stage in mammary epithelial cells during adult development. Targeting Esr1 in this stage allowed normal pubertal development and resulted in defective alveologenesis and lactation. A loss of progesterone receptor positive cells was also observed. This phenotype is more severe after multiple pregnancies.	(*32*)
Esr1 C451A	This transgenic mouse models germline expression of an ERalpha palmitoylation deficient mutant. Delayed pubertal mammary development and loss of progesterone receptor positive cells was observed. However, systemic effects such as disrupted E2 levels are reported.	(*86*)
Esr1 AF1[0]	Germline expression of an ESR1 truncated mutant with deletion of the AF-1 domain. The model has systemic effects including increased E2 levels. Mammary epithelial transplants from mutant mice into wild-type hosts revealed an absence of epithelial duct development during puberty.	(*79*)
Esr1 AF2[0]	Germline expression of an ESR1 truncation mutant with deletion of the ligand binding domain. This mouse displays similar phenotypes to the AF-1 domain mutant, including absence of epithelial duct development during puberty.	(*79*)
Esr1-rtTA/TetO-Cre/Rosa-YFP	This transgenic knock-in mouse expresses the tetracycline transactivator (rtTA) downstream of a copy of the ESR1 promoter. The rtTA drives conditional expression of YFP for lineage tracing ER+ cells in the mammary gland. This strategy revealed that a restricted subset of adult mammary stem/progenitor cells sustain ER+ cell development, homeostasis, and regeneration.	(81)
Esr1-Cre/Ai9-RFP (Esr1-RFP)	This knock-in mouse models expresses Cre recombinase under control of a copy of the natural Esr1 promoter crossed with an RFP reporter strain induced by Cre. This mouse will enable future studies to label ER+ cells for identification, isolation, and tracing.	(*84*)
Prominin1-CreER[T2]/R26R-tdTomato	This transgenic knock in mouse expresses an inducible Cre under control of the endogenous Prom1 (CD133) locus. Prominin1 is a marker of a subset of ER+ mammary luminal cells. This strategy revealed that Prom1 expressing cells	(*80*)

	give rise to exclusively ER+ cells even after serial transplantation.	
Rps6ka3-KO (RSK2-KO)	Germline knockout of RSK2 results in decreased ERa protein levels in the mammary gland and loss of ER+ cells. This is also observed after transplantation of RSK2-KO mammary epithelial cells into wild-type hosts. The disrupted estrogen signaling in the adult mammary gland results in inefficient alveolar expansion and lactation.	(*78*)
MMTV-Cre/p38a^{fl/fl}	Germline deletion of p38alpha in mammary epithelial cells using the MMTV promoter. Results in decreased ER+ cells and ESR1 mRNA expression possibly due to a defect in luminal progenitor cells.	(*77*)
Foxa1-KO	Germline Foxa1 knockout is perinatal lethal therefore the authors employed mammary transplants into wild-type hosts to demonstrate FOXA1 is required for epithelial duct development during puberty and required for ESR1 expression.	(*74*)
MMTV-Cre/Runx1^{fl/fl}	Germline deletion of Runx1 specifically in mammary epithelial cells using the MMTV promoter. This model revealed a role for RUNX1 is homeostasis of general luminal cells and ER+ cells. The loss of ER+ cells could be rescued by deletion of P53, suggesting activation of a cell cycle checkpoint.	(*73*)
MMTV-Cre/Gata3^{fl/fl}	Germline deletion of Gata3 specifically in mammary epithelial cells using the MMTV promoter. These studies revealed a role for GATA3 as a major regulator of the mammary luminal lineage. Loss of GATA3 results in loss of luminal cells including decreased ER+ cells and lactation insufficiency.	(*76*)
MMTV-Cre/Id4^{fl/fl}	Germline deletion of Id4 in the mammary gland using the MMTV promoter using this mouse model revealed delayed development of mammary ducts and increased expression of ER in luminal and basal cells. However, upon further analysis these mice also display significant ovarian defects which confound the mammary results.	(*87*)
WAP-Cre/Foxm1^{fl/fl}	Deletion of Foxm1 in the adult mammary gland using the WAP promoter. Loss of Foxm1 increased mammary expression of GATA3 and ERalpha, suggesting that Foxm1 suppresses this pathway Additionally, the authors demonstrate that Foxm1 overexpression results in expansion luminal progenitor cells.	(*88*)
MMTV-Ube3a (E6AP[WT])	Transgenic knock in mouse with overexpression of full length E6AP in mammary epithelial cells using the MMTV promoter. E6AP overexpression is associated with a minor duct development defect and decreased ERalpha protein levels, although the effects are primarily studied on progesterone receptor.	(*69*)
Esr2-KO (ERbeta-KO)	Germline knockout of Esr2. The mice were initially reported to display normal mammary gland development and	(*34, 89*)

	lactation followed by reports of minor defects in these processes.	
Gpr30-KO (GPER-KO)	Germline knockout of the membrane bound g protein-coupled estrogen receptor GPER. The role in normal development of the mammary gland was not reported. However, GPER-KO were crossed with the mouse model of luminal breast cancer PyMT, which revealed that GPER supports breast cancer progression but does not impair ER+ cell numbers.	(*35*)
Esrra-KO (ERRa-KO)	Germline knockout of estrogen related receptor alpha in mice is reported, however, the mammary gland phenotype is unknown.	(*36*)

Ribosomal S6 kinase (RSK) biology and inhibitors

The ribosomal S6 kinase (RSK) family of Ser/Thr protein kinases (RSK 1 – 4) were discovered based on their role in phosphorylation of S6 and regulation of cap-dependent protein translation (*90-92*). RSKs are downstream effectors of the mitogen activated protein kinase kinase (MEK 1/2) – extracellular regulated kinase (ERK 1/2) signaling pathway (*93*). RSKs are expressed in independent and overlapping tissues (*94*), and isoform specific activities have been reported. RSKs are activated by various stimuli, including growth factors, cytokines, and oxidative stress. In cell based experiments RSK signaling promotes cell survival (*95*), cell cycle (*96, 97*), and cell motility (*98, 99*), therefore RSK has been implicated in human diseases including breast cancer.

RSKs are composed of two distinct kinase domains (*100*). The N-terminal kinase domain (NTKD) belongs to the AGC protein kinase family. The C-terminal kinase domain (CTKD) belongs to the calcium/calmodulin-dependent protein kinase family. RSK is activated by a serious of phosphorylation events that begins with ERK 1/2 dependent phosphorylation and activation of the CTKD. The only known role for the CTKD is autophosphorylation of the RSK hinge region to create a PDK1 binding site. PDK1 phosphorylates RSK Ser-221 for activation of the NTKD (*101, 102*). The NTKD then phosphorylates substrates with the AGC kinase substrate motif, RxRxxS/T.

RSK signaling is involved in the etiology of diverse human diseases. Inactivating mutations in RSK2 (gene name RPS6KA3) result in the developmental disorder Coffin Lowry syndrome (*103-106*). This syndrome is associated with diseases such as mental retardation, skeletal and cardiac defects (*107*). The genes encoding RSK1, RSK3, and RSK4 are not associated with genetic diseases. Triple knockout mice for RSK1, RSK2, and RSK3 have been reported and are viable (*108*). The role of RSK in cancer is interesting as RSK 1/2 appear to

promote cancer whereas RSK 3/4 may be tumor suppressors (*109-111*). This suggests

preferentially targeting RSK 1/2 in cancer. The role of RSK in other human diseases such as

cardiovascular disease, fibrosis, and infectious disease, has been previously reviewed by our

laboratory (*112*).

Despite evidence that RSK is an important drug target, there are no RSK-specific

inhibitors with sufficient pharmacokinetics for clinical use. To address this need many RSK

specific inhibitors are undergoing preclinical development. BI-D1870, BIX 02565, and SL0101

are small molecule RSK inhibitors with similar potency (IC50 0.1 – 1 microM) (Figure 1.2 C)

(*112*). FMK is a unique RSK inhibitor in that it covalently binds a gatekeeper residue specifically

conserved in the CTKD of RSK1, 2, and 4. Our laboratory discovered the small molecule NTKD

inhibitor, SL0101 (*113*), which is RSK specific but demonstrate poor stability in vivo. Therefore,

recent efforts have identified an improved SL0101 analogue , C5"-n-propyl-cyclitol-SL0101 (C5")

with increased potency and stability in vivo (*78, 114, 115*).

Chapter 2

RSK2 maintains adult estrogen homeostasis by inhibiting ERK1/2-mediated degradation of estrogen receptor alpha

Adapted from: (*78*)

Summary

In response to estrogens, estrogen receptor alpha (ERalpha), a critical regulator of homeostasis, is degraded through the 26S proteasome. However, despite the continued presence of estrogen prior to menopause, ERalpha protein levels are maintained. We discovered that ERK1/2-RSK2 activity oscillates during the estrous cycle. In response to high estrogen levels ERK1/2 is activated and phosphorylates ERalpha to drive ERalpha degradation and estrogen-responsive gene expression. Reduction of estrogen levels result in ERK1/2 deactivation. RSK2 maintains redox homeostasis, which prevents sustained ERK1/2 activation. In juveniles ERK1/2-RSK2 activity is not required. Mammary gland regeneration demonstrated that ERK1/2-RSK2 regulation of ERalpha is intrinsic to the epithelium. Reduced RSK2 and enrichment in an estrogen-regulated gene signature occurs in individuals taking oral contraceptives. RSK2 loss enhances DNA damage, which may account for the elevated breast cancer risk with the use of exogenous estrogens. These findings implicate RSK2 as a critical component for the preservation of estrogen homeostasis.

Introduction

The importance of estrogen signaling is highlighted by the numerous physiological alterations, which occur during menopause, oophorectomy or anti-estrogen therapy (*116*). In the adult human estrogen levels are highest in the follicular phase reaching a level of ~ 1 nM and decrease approximately five-fold in the luteal phase of the menstrual cycle (*117*). In the mouse the estrous cycle is divided into four stages, which is based on vaginal cytology, and is comprised of proestrus, estrus, metestrus and diestrus. The highest level of estrogen ~ 0.2 nM occurs during proestrus and then decreases by approximately three-fold in diestrus (*118*). All estrogen receptor (ER) positive tissues respond to fluctuations in estrogen levels. The mammary gland undergoes extensive morphological changes as estrogen levels change (*119*) and therefore, it is an ideal organ in which to investigate the mechanisms that regulate estrogen homeostasis. Estrogen acts primarily through the steroid hormone receptors, estrogen receptor alpha (ERalpha) and ERbeta. In the mammary gland ERalpha is of particular importance for its contributions to gland development (*32*). Whereas, mammary gland development is normal in the absence of ERbeta (*89*). Therefore, to examine estrogen homeostasis in the mammary gland we focused our studies on ERalpha.

Estrogen binding to the receptor results in ERalpha degradation through the 26S proteasome pathway, and both are required for activation of estrogen-responsive gene expression (*61, 62, 64, 120, 121*). However, it is puzzling how this degradation-coupled transcription is regulated to maintain ERalpha protein levels, as theoretically estrogen levels are sufficient throughout the menstrual cycle to continuously drive degradation (*9*). Therefore, it might be expected that ERalpha levels would eventually drop below that required to generate a physiological response. Yet, both ERalpha levels and estrogen responsiveness are maintained to allow progression into the next menstrual cycle but the mechanisms regulating ERalpha degradation are unknown (*30, 122*). Maintenance of responsiveness is of particular relevance to individuals taking estrogen containing oral contraceptives in which estrogen levels do not

fluctuate compared to the normal menstrual cycle (*117*) and in transgendered individuals where estrogen levels can reach supra-physiological levels (*123*).

We hypothesized that a negative regulatory mechanism must exist to limit ERalpha degradation to preserve ERalpha levels and, as a result, maintain estrogen responsiveness. To identify this mechanism, we focused on estrogen and its control of the EGFR signaling pathway because of the importance of EGFR in mammary gland development (*124*), cell fate specification (*125*) and breast cancer (*126*). Stimulation of EGFR activates the MEK-ERK1/2 signaling cascade. Activated ERK1/2 and its downstream effector, RSK, directly phosphorylate ERalpha at Ser-118 and Ser-167, respectively (*38, 127*). These sites increase ERalpha transcriptional activity in cell-based systems. In a transgenic mouse model RSK2 nuclear accumulation in the mammary gland drives high grade ER+ ductal carcinoma in situ (*128*). As cancer often exploits mechanisms important in development and homeostasis, we investigated the contributions of ERK1/2-RSK2 signaling to normal ERalpha biology.

Unexpectedly, we discovered a novel regulatory mechanism in which the ERK1/2-RSK2 pathway acts as a developmentally regulated switch that is required for maintaining ERalpha protein levels in the mammary gland and uterus in the adult but not in the juvenile. ERK1/2 is activated during the estrus phase of the cycle as a consequence of an estrogen pulse that occurs in proestrus. Activated ERK1/2 phosphorylates ERalpha, driving the degradation of ERalpha and estrogen-responsive gene expression. To enable estrogen responsiveness for the subsequent cycle ERK1/2 is inactivated when estrogen levels are low. Active RSK2 limits the response to estrogen by maintaining redox homeostasis, which prevents ERK1/2 activation in response to reactive oxygen species (ROS). In the RSK2 knockout (RSK2-KO) and in individuals taking oral contraceptives, decreased RSK2 levels are correlated with an enriched signature for estrogen-responsive gene expression. These observations may explain the mechanism underlying the increase in breast cancer risk that is observed for individuals taking exogenous estrogens as reduced RSK2 is correlated with increased DNA damage.

Materials and Methods

Mice

All procedures involving animals were done in accordance with current federal (NIH Guide for Care and Use of Laboratory Animals) and university guidelines and were approved by the University of Virginia and Vanderbilt University Institutional Animal Care and Use Committee. Female WT or RSK2-KO mice (105) between six and fourteen weeks old were studied. The age of animals in specific experiments are indicated in the figures with adult animals ranging from twelve to fourteen weeks. For whole mount analysis the 4th mammary gland was fixed and stained in Carmine Alum. Ductal distance was measured from the nipple to the tip of the longest duct. The number of secondary branches along the longest primary branch were counted.

The stages of the estrous cycle were determined by cytological analysis of vaginal swabs (129) (20). For all experiments requiring matched estrous stages, the cycles were monitored for 2 weeks prior to end point to ensure continuous cycling.

Mammary epithelial cells were isolated with modifications (125). Briefly, mammary glands were isolated from donor mice, minced, and digested in DMEM/F12 supplemented with 2mg/ml Collagenase A and 100U/ml Pen/Strep for 2.5h in 37 o C 5% CO_2 incubator. Digested material was pelleted at 180xG for 5 min and the pellet was suspended in DNAse I (1000U/ml) for 3-5 min in 37 o C in 5% CO_2. Fetal bovine serum (FBS) was added and the digested tissue was pelleted at 180xG for 10 min. The pellet was washed with phosphate-buffer saline, pelleted, suspended in Accumax (StemCell Technologies Inc.) and placed in Thermomixer at 37 o C for 10 min. Digested material was pelleted at 180xG for 3 min, suspended in 5x trypsin for 5 min at 37 o C. Trypsin was quenched with FBS and cells were pelleted and suspended in phosphate buffered saline (PBS) or DMEM/F12. The cell preparation was filtered through 70-micrometer mesh to obtain single cell suspensions. For mammary gland regenerations, 4x107 cells/ml of

single cells in DMEM/F12 were mixed 1:1 with matrigel. 10 microL of cell suspension in matrigel was injected into the cleared 4th mammary fat pad of a recipient 3wk old mouse (130). To inhibit the 26S proteasome pathway or RSK1/2 in vivo female mice in estrus (12 wk) were injected intraperitoneally (IP) with vehicle or PS-341 at 5 mg/kg in 2% DMSO, 30% PEG, and 68% saline or C5″-n-propyl cyclitol SL0101 at 40mg/kg in one part DMSO and nine parts 25% hydroxypropyl-beta-cyclodextrin. Animals in the PS-341 study were euthanized 4h after injection and animals in the RSK1/2 study were injected twice at 7 h interval before euthanasia.

Cell line studies

TM3 cells were purchased and cultured according to ATCC. Cells were maintained in log-phase and screened for Mycoplasma by PCR. Prior to experiments, cells were serum-starved in phenol red-free media for 48 h followed by addition of vehicle, C5"-n-propyl-cyclitol SL0101 (20 microM, 6h), BI-D1870 (10 microM, 6h), trametinib (1 microM, 6h), or U0126 (10 microM, 6h). In experiments with MG-132, cells were pretreated (10 microM, 1h). For analysis of Ser-118 upshift, cells were serum-starved as above and treated with phorbol 12-myristate 13-acetate (10) (0.5 microM, 20 min), EGF and FGF7 cocktail (12.5 nM each, 5 min), C5" (20 microM for 2 h). In experiments with trametinib, cells were pretreated (1 microM, 2h). Cells were lysed and analyzed (127).

Transduction

Constructs to generate lentivirus including psPAX2, pMD2.G, and pLVTHM were provided by D. Trono, Ph.D. (Swiss Institute of Technology, Lausanne, Switzerland). The pLV-Venus lentivirus construct was provided by Ian Macara, Ph.D. (Vanderbilt University, Nashville, TN). Lentiviral production was performed using Lipofectamine 3000 (Invitrogen) according to the manufacturer's instructions. S118A-ERalpha and S167A-ERalpha were generated using Q5 site-directed mutagenesis.

Fluorescence Activated Cell Sorting (FACS)

For FACS, single epithelial cells (106 cells/ml) obtained from mammary glands in PBS were incubated with Cell Trace Violet (1microM) and Zombie Yellow (1:250) for 20 min at room temperature. Cells were washed and suspended in 5% FBS in PBS. Cells were blocked with 10% normal rat serum in 5% FBS for 10 min at 4 o C, followed by incubation with biotin-conjugated primary antibodies against lineage markers for 10 min at 4o C. The cells were incubated with primary antibodies for 20 min at 4 o C, washed and suspended in 5% FBS. Cells were analyzed using FACSCantoII or sorted using FACSAriaII. Flow cytometry data were analyzed using Cytobank version 6.2. Further reagents details are provided in the Key Resource Table.

EdU labeling was performed (82) in mice staged in proestrus were injected intraperitoneally with 10 mg/ml EdU in PBS (100 mg/kg) and then administered EdU in the drinking water (1 mg/ml). The estrus stage was monitored, and mammary glands were isolated in metestrus (2 days after EdU injection). Mammary cells were isolated and analyzed for EdU incorporation using the Click-iT Edu Flow Cytometry Assay Kit, followed by the antibody staining as described above carried out in 1xClick-iT saponin based permeabilization buffer. Further reagents details are provided in the Key Resource Table (Table 2.1).

Immunostaining

Mouse organs were fixed in buffered 10% formalin for 2 d and then placed in 70% ethanol. The fixed samples were paraffin-embedded, and sectioned. Sections were deparaffinized and antigen retrieval performed in tris-EDTA buffer pH 8.0 or citrate buffer pH 6.0 or pH 7.0 (Table 2.1). The sections were blocked in 10% bovine serum albumin (BSA) in PBS and incubated with primary antibody in 3% BSA in PBS o/n at 4 oC. The sections were washed and incubated with secondary antibody for 1 h in room temperature. For detection of Venus-tagged ERalpha in TM3 cells, 1x104 cells were seeded on laminin-coated glass coverslips. After treatment, cells were fixed in 4% PFA in PBS (pH 7.4, 15 min). Antibodies are listed in the Key Resource Table. For immunofluorescence staining, cells were fixed in 4% PFA in PBS (pH 7.4, 15 min) and

permeabilized with 0.1% Triton X-100 in PBS (15 min), DNA was stained with Hoechst in PBS (10 min) and coverslips mounted using Fluoro-Gel (Electron Microscopy Sciences). Images were collected with a laser-scanning microscope (LSM 510/Meta/FCS, Carl Zeiss Inc.).

RNA analysis

For RNA isolation, 5x104 EpCAMhiCD49f+Sca1+Cd49b- cells were FACS sorted and total RNA extraction (RNeasy Micro Kit) was performed. The RNA quality was tested using Agilent 100 Bioanalyzer (RIN 8). Libraries were constructed and sequenced by Genewiz LLC. Reads were aligned to the mm10 mouse genome with STAR, the transcripts were assembled using Gencode version 15 as gene models. Genes and transcripts were quantified with HTSeq. Two samples were clear outliers and were discarded. Batch correction was done with SVA, and differential gene expression analysis was performed with DESeq2. Gene set enrichment was done with GSEA using MSigDB and GSVA using GSKB mouse gene sets. RNASeq data is available at Gene Expression Omnibus under accession GSE113323.

For qRT-PCR RNA (1microg) was reverse transcribed using High Capacity cDNA Reverse Transcription Kit. Analysis was performed using IQ RealTime SyberGreen PCR Supermix (BioRad Laboratories) on the C1000Thermal Cycler CFX96 Real-Time System (128). The deltaCt was calculated using GAPDH as a control. Primers are listed in the Key Resource Table.

Raw reads from the sequencing of normal breast tissue at different stages of menstrual cycle (131) were normalized using DESeq2 according to the estimated size of the libraries. Based on unsupervised hierarchical clustering, 5 samples were rejected as outliers and Z-scores were calculated correcting for sequencing batch.

Quantification and statistical analysis

Statistical analyses were performed using GraphPad Prism 6. The statistical test used is reported in the figure legends. Additional ANOVA values for complex comparisons are provided (Table 2.2).

Table 2. 1: Key Resource Table.

REAGENT or RESOURCE	SOURCE	IDENTIFIER
Antibodies		
Rat anti-keratin 8	University of Iowa	TROMA-I
Chicken anti-keratin14	BioLegend	SIG-3476
Rabbit anti-pRSK (Thr359/Ser363) (Tris)	Santa Cruz Biotechnology, Inc.	sc-12898-R
Mouse anti-ERα 6F11 (Citrate)	Thermo Fisher Scientific Inc.	MA5-13304
Mouse anti-γH2A.X (Ser139) (Tris)	EMD Millipore	JBW301
Rabbit anit-pERK1/2 (pTEpY) (Tris)	Promega	V803A
Rabbit anti-peEF2 (Thr56) (Tris)	Cell Signal Technology	2331
Mouse anti-GATA3 (Tris)	Thermo Fisher Scientific Inc.	1A12-1D9
Rabbit anti-AR	Thermo Fisher Scientific Inc.	MA5-13426
Rabbit anti-E cadherin	Cell Signal Technology	3195
Mouse anti-ERK	BD Biosciences	610124

Donkey anti-rabbit 647	Invitrogen	A31573
Donkey anti-mouse 647	Invitrogen	A31571
Goat anti-rat 546	Invitrogen	A11081
Goat anti-chicken 488	Invitrogen	A11039
Biotin anti-CD140	Biolegend	APA5
Biotin anti-CD31	Biolegend	MEC13.3
Biotin anti-Ter-119	Biolegend	TER-119
Biotin anti-CD45	Biolegend	30-F11
Brilliant Violet 510 Streptavidin	Biolegend	405233
Anti-Sca1-PerCP	Biolegend	405233
Anti-Sca1-FITC	Biolegend	D7
Anti-CD49b-APC/Cy7	Biolegend	DX5
Anti-EpCAM-APC	Biolegend	G8.8
Anti-CD49f-PE/Cy7	Biolegend	GoH3
Chemicals, Peptides, and Recombinant Proteins		
Cell Trace Violet	Life Technologies Corp.	C34557
Zombie Yellow	Biolegend	423104
EdU (5-Ethynyl-2'-deoxyuridine)	Life Technologies Corp.	NEO87011604
Bortezomib (PS-341)	Calbiochem	50-431-40001
BI-D1870	Enzo Life Sciences	BML-EI407
Trametinib	Selleck Chem	S2673
U0126	Sigma	U120
MG-132	Calbiochem	474790
17-β estradiol (E_2)	Sigma	E2758

Phorbol 12-myristate 13-acetate (*10*)	Sigma	P1585
EGF	Calbiochem	324831
FGF7	R&D Systems	251KG010CF
Experimental Models: Organisms/Strains		
Mouse: C57BL/6J[RSK2-/-](RSK2-KO)	Institut de Genetique et Biologie Moleculaire et Cellulaire, C.U. de Strasbourg, France	Andre Hanauer, PhD.
Cell line: TM3	ATCC	CRL-1714
Commercial Assays		
Click-iT™ Plus EdU Alexa Fluor™ 488 Flow Cytometry Assay Kit	Thermo Fisher Scientific Inc.	C10632
Click-iT™ Plus OPP Alexa Fluor™ 647 Protein Synthesis Assay Kit	Thermo Fisher Scientific Inc.	C10458
CellROX™ Green Reagent	Thermo Fisher Scientific Inc.	C10444
RNeasy Micro Kit	Qiagen	74004
qRT-PCR primers		
f-GAPDHm	AGAACATCATCCCTGCATCCA	
r-GAPDHm	CAGATCCACGACGGACACATT	
f-GATA3m	GATGTAAGTCGAGGCCCAAG	
r-GATA3m	GCAGGCATTGCAAAGGTAGT	
f-ESR1m	TTACGAAGTGGGCATGATGA	

r-ESR1m	CCTGAAGCACCCATTTCATT	
Plasmids		
pLVTHM	D. Trono, Ph.D.	Addgene; 12260
pSPAX2	D. Trono, Ph.D.	Addgene; 12247
pMD2.G	D. Trono, Ph.D.	Addgene; 12259
Software and Algorithms		
LSM-FCS/ ZEN	Carl Zeiss, Inc.	N/A
Openlab 5.5.0 / Volocity 6.2.1	PerkinElmer Inc.	N/A
GraphPad Prism 6.0a	GraphPad Spftware Inc.	N/A
Morpheus	Broad Institute	https://software.broadinstitute.org/morpheus/
BioRender	BioRender	https://biorender.com/

Table 2. 2: ANOVA summary.

Supplemental Table 1: ANOVA TABLE				
Figure 1B (WT vs. RSK2-KO)				
ANOVA summary				
F	18.62			
P value	< 0.0001			
P value summary	****			
Are differences among means statistically significant? (P < 0.05)	Yes			
R square	0.867			
Number of families	1			
Number of comparisons per family	4			
Alpha	0.05			
Holm-Sidak's multiple comparisons test	Mean Diff.	Significant?	Summary	Adjusted P Value
WT PE vs. KO PE	0.5386	Yes	*	0.0265
WT E vs. KO E	0.3825	Yes	*	0.0376
WT ME vs. KO ME	1.081	Yes	****	< 0.0001
WT DE vs. KO DE	0.6243	Yes	**	0.0065
Figure 1B (Estrous stages)				
ANOVA summary				
F	215.3			

P value	< 0.0001			
P value summary	****			
Are differences among means statistically significant? (P < 0.05)	Yes			
R square	0.5039			
Number of families	1			
Number of comparisons per family	3			
Alpha	0.05			
Dunnett's multiple comparisons test	Mean Diff.	Significant?	Summary	Adjusted P Value
WT E vs. WT PE	-0.1718	Yes	**	0.0042
WT E vs. WT ME	-0.8292	Yes	****	< 0.0001
WT E vs. WT DE	-1.132	Yes	****	< 0.0001
Figure 1C				
ANOVA summary				
F	11.09			
P value	< 0.0001			
P value summary	****			
Are differences among means statistically significant? (P < 0.05)	Yes			
R square	0.7281			
Number of families	1			

Number of comparisons per family	4			
Alpha	0.05			
Holm-Sidak's multiple comparisons test	Mean Diff.	Significant?	Summary	Adjusted P Value
WT 12 PE vs. KO 12 PE	22.28	Yes	**	0.0023
WT 12 E vs. KO 12 E	20.57	Yes	**	0.0023
WT 12 ME vs. KO 12 ME	22.14	Yes	***	0.0002
WT 12 DE vs. KO 12 DE	15.79	Yes	**	0.0023
Figure 2B				
ANOVA summary				
F	106.4			
P value	< 0.0001			
P value summary	****			
Are differences among means statistically significant? (P < 0.05)	Yes			
R square	0.8944			
Number of families	1			
Number of comparisons per family	4			
Alpha	0.05			
Holm-Sidak's multiple comparisons test	Mean Diff.	Significant?	Summary	Adjusted P Value

ML WT (E) vs. ML KO (E)	19.18	Yes	****	< 0.0001
LP WT vs. LP KO	0.9114	No	ns	0.9613
AP WT vs. AP KO	-0.7909	No	ns	0.9613
U WT vs. U KO	-19.2	Yes	****	< 0.0001
Figure 2C				
ANOVA summary				
F	13.56			
P value	< 0.0001			
P value summary	****			
Are differences among means statistically significant? (P < 0.05)	Yes			
R square	0.655			
Number of families	1			
Number of comparisons per family	4			
Alpha	0.05			
Holm-Sidak's multiple comparisons test	Mean Diff.	Significant?	Summary	Adjusted P Value
ML WT (PE) vs. ML KO (PE)	24.18	Yes	**	0.0031
ML WT (E) vs. ML KO (E)	19.1	Yes	****	< 0.0001
ML WT (ME) vs. ML KO (ME)	18.64	Yes	*	0.0197

ML WT (DE) vs. ML KO (DE)	11.79	Yes	*	0.0461
Figure 2F				
ANOVA summary				
F	1.881			
P value	0.1471			
P value summary	ns			
Are differences among means statistically significant? (P < 0.05)	No			
R square	0.116			
Number of families	1			
Number of comparisons per family	2			
Alpha	0.05			
Holm-Sidak's multiple comparisons test	Mean Diff.	Significant?	Summary	Adjusted P Value
6wk WT vs. 6 KO	0.2369	No	ns	0.8948
WT 8wk vs. KO 8wk	4	No	ns	0.3524
Figure 2H				
ANOVA summary				
F	8.896			
P value	< 0.0001			
P value summary	****			

Are differences among means statistically significant? (P < 0.05)	Yes			
R square	0.6402			
Number of families	1			
Number of comparisons per family	3			
Alpha	0.05			
Holm-Sidak's multiple comparisons test	Mean Diff.	Significant?	Summary	Adjusted P Value
WT6 vs. KO6	0.9722	No	ns	0.6945
WT8 vs. KO8	4	No	ns	0.583
WT10 vs. KO10	23.32	Yes	****	< 0.0001
Figure 3A				
ANOVA summary				
F	6.893			
P value	0.0012			
P value summary	**			
Are differences among means statistically significant? (P < 0.05)	Yes			
R square	0.7338			
Number of families	1			
Number of comparisons per family	4			

Alpha	0.05			
Holm-Sidak's multiple comparisons test	Mean Diff.	Significant?	Summary	Adjusted P Value
8wkWT vs. 6wkWT	0.2	No	ns	0.4754
10wkWTE vs. 6wkWT	0.4374	No	ns	0.2435
12wk WTE vs. 6wkWT	1.196	Yes	***	0.0003
12wkKOE vs. 6wkKO	0.7278	Yes	*	0.0379
Figure 3C				
ANOVA summary				
F	10.98			
P value	0.0016			
P value summary	**			
Significant diff. among means (P < 0.05)?	Yes			
R squared	0.6281			
Number of families	1			
Number of comparisons per family	3			
Alpha	0.05			
Tukey's multiple comparisons test	Mean Diff.	Significant?	Summary	Adjusted P Value
WTE vs. WTDE	0.7499	Yes	**	0.0042
WTE vs. WTPE	0.9749	Yes	**	0.0096
WTDE vs. WTPE	0.2251	No	ns	0.7157
Figure 4C				

ANOVA summary				
F	6.587			
P value	0.0251			
P value summary	*			
Are differences among means statistically significant? (P < 0.05)	Yes			
R square	0.7671			
Number of families	1			
Number of comparisons per family	3			
Alpha	0.05			
Holm-Sidak's multiple comparisons test	Mean Diff.	Significant?	Summary	Adjusted P Value
KO_E vs. WT_E	181.5	Yes	*	0.0329
KO_E vs. KO_DE	239.8	Yes	*	0.024
KO_E vs. WT_DE	196	Yes	*	0.0329
Figure 4D				
ANOVA summary				
F	11.53			
P value	0.0028			
P value summary	**			
Are differences among means statistically significant? (P < 0.05)	Yes			

39

R square	0.8122			
Number of families	1			
Number of comparisons per family	3			
Alpha	0.05			
Holm-Sidak's multiple comparisons test	Mean Diff.	Significant?	Summary	Adjusted P Value
WTV vs. WTPS	-0.05347	No	ns	0.6881
KOV vs. KOPS	-0.7145	Yes	**	0.0016
WTV vs. KOV	0.4995	Yes	**	0.0092
Figure 6A				
ANOVA summary				
F	7.01			
P value	0.0021			
P value summary	**			
Significant diff. among means (P < 0.05)?	Yes			
R squared	0.5126			
Number of families	1			
Number of comparisons per family	3			
Alpha	0.05			
Sidak's multiple comparisons test	Mean Diff.	Significant?	Summary	Adjusted P Value
WT E vs. WT DE	0.7597	Yes	**	0.002

KO E vs. KO DE	0.2441	No	ns	0.6895
WT DE vs. KO DE	-0.6181	Yes	*	0.0437
Figure 6B				
ANOVA summary				
F	574.1			
P value	< 0.0001			
P value summary	****			
Are differences among means statistically significant? (P < 0.05)	Yes			
R square	0.9957			
Number of families	1			
Number of comparisons per family	4			
Alpha	0.05			
Dunnett's multiple comparisons test	Mean Diff.	Significant?	Summary	Adjusted P Value
V vs. 216	0.6396	Yes	****	< 0.0001
V vs. BID	0.4211	Yes	****	< 0.0001
V vs. Tram	0.1658	Yes	****	< 0.0001
V vs. U0126	0.2126	Yes	****	< 0.0001
Figure 6E				
ANOVA summary				
F	25.58			
P value	< 0.0001			

P value summary	****			
Are differences among means statistically significant? (P < 0.05)	Yes			
R square	0.895			
Number of families	1			
Number of comparisons per family	3			
Alpha	0.05			
Sidak's multiple comparisons test	Mean Diff.	Significant?	Summary	Adjusted P Value
WT-V vs. WT-216	100	Yes	****	< 0.0001
167-V vs. 167-216	53.26	Yes	**	0.0013
118-V vs. 118-216	-22.7	No	ns	0.2554
Figure 6I				
ANOVA summary				
F	42.55			
P value	< 0.0001			
P value summary	****			
Are differences among means statistically significant? (P < 0.05)	Yes			
R square	0.9466			
Number of families	1			

Number of comparisons per family	5			
Alpha	0.05			
Dunnett's multiple comparisons test	Mean Diff.	Significant?	Summary	Adjusted P Value
V vs. 216	100	Yes	****	< 0.0001
V vs. Ebs	-56.73	Yes	**	0.0011
V vs. NAC	-1.255	No	ns	0.9999
V vs. 216+Ebs	0.1907	No	ns	> 0.9999
V vs. 216+NAC	-2.203	No	ns	0.9997
Figure 6J				
ANOVA summary				
F	11.29			
P value	0.0052			
P value summary	**			
Are differences among means statistically significant? (P < 0.05)	Yes			
R square	0.9039			
Number of families	1			
Number of comparisons per family	5			
Alpha	0.05			
Dunnett's multiple comparisons test	Mean Diff.	Significant?	Summary	Adjusted P Value

veh vs. 216	-100	Yes	**	0.0046
veh vs. NAC	4.143	No	ns	0.9988
veh vs. Ebs	7.899	No	ns	0.9856
veh vs. NAC+216	2.002	No	ns	0.9999
veh vs. Ebs+216	-4.961	No	ns	0.9981
Figure 7C				
ANOVA summary				
F	4483			
P value	< 0.0001			
P value summary	****			
Are differences among means statistically significant? (P < 0.05)	Yes			
R square	0.9989			
Number of families	1			
Number of comparisons per family	2			
Alpha	0.05			
Dunnett's multiple comparisons test	Mean Diff.	Significant?	Summary	Adjusted P Value
v vs. 216	100	Yes	****	< 0.0001
v vs. no OPP	110.7	Yes	****	< 0.0001
Figure 7E				
ANOVA summary				
F	53.24			

P value	< 0.0001			
P value summary	****			
Are differences among means statistically significant? (P < 0.05)	Yes			
R square	0.8331			
Number of families	1			
Number of comparisons per family	3			
Alpha	0.05			
Holm-Sidak's multiple comparisons test	Mean Diff.	Significant?	Summary	Adjusted P Value
WT WT vs. KO WT	2.2	Yes	****	< 0.0001
WT KO vs. KO KO	2.495	Yes	****	< 0.0001
WT WT vs. KO KO	3.167	Yes	****	< 0.0001
Figure 7F				
ANOVA summary				
F	8.231			
P value	0.0056			
P value summary	**			
Are differences among means statistically significant? (P < 0.05)	Yes			
R square	0.5784			
Number of families	1			

Number of comparisons per family	3			
Alpha	0.05			
Tukey's multiple comparisons test	Mean Diff.	Significant?	Summary	Adjusted P Value
F vs. L	1.323	Yes	*	0.0023
F vs. OC	1.565	Yes	**	0.0007
L vs. OC	0.2425	No	ns	0.8481
Figure 7G				
ANOVA summary				
F	16.2			
P value	0.0003			
P value summary	***			
Are differences among means statistically significant? (P < 0.05)	Yes			
R square	0.7137			
Number of families	1			
Number of comparisons per family	3			
Alpha	0.05			
Tukey's multiple comparisons test	Mean Diff.	Significant?	Summary	Adjusted P Value
F vs. L	-370.8	Yes	**	0.0403
F vs. OC	-425.5	Yes	***	0.0086

L vs. OC	-54.69	No	ns	0.8938

Supplemental Figure 2B				
ANOVA summary				
F	15.15			
P value	< 0.0001			
P value summary	****			
Are differences among means statistically significant? (P < 0.05)	Yes			
R square	0.6152			
Number of families	1			
Number of comparisons per family	10			
Alpha	0.05			
Holm-Sidak's multiple comparisons test	Mean Diff.	Significant?	Summary	Adjusted P Value
Lum WT (PE) vs. Lum KO (PE)	2.92	No	ns	0.9759
Lum WT (E) vs. Lum KO (E)	-3.972	No	ns	0.9001
Lum WT (ME) vs. Lum KO (ME)	11.03	No	ns	0.3438
Lum WT (DE) vs. Lum KO (DE)	-0.8083	No	ns	0.9883

6wk WT Lum vs. 6wk KO Lum	-0.7805	No	ns	0.9883
6wk WT Basal vs. 6wk KO Basal	2.215	No	ns	0.9759
Basal WT (PE) vs. Basal KO (PE)	-3.224	No	ns	0.9759
Basal WT (E) vs. Basal KO (E)	5.276	No	ns	0.7059
Basal WT (ME) vs. Basal KO (ME)	-4.4	No	ns	0.9759
Basal WT (DE) vs. Basal KO (DE)	0.8421	No	ns	0.9883
Supplemental Figure 2D (upper panel)				
ANOVA summary				
F	14.08			
P value	< 0.0001			
P value summary	****			
Are differences among means statistically significant? (P < 0.05)	Yes			
R square	0.6827			
Number of families	1			
Number of comparisons per family	6			
Alpha	0.05			

Holm-Sidak's multiple comparisons test	Mean Diff.	Significant?	Summary	Adjusted P Value
LP WT (PE) vs. LP KO (PE)	0.6	No	ns	0.6675
LP WT (E) vs. LP KO (E)	0.7409	No	ns	0.4535
LP WT (ME) vs. LP KO (ME)	0.685	No	ns	0.6675
LP WT (DE) vs. LP KO (DE)	1.354	No	ns	0.2605
LP WT 6 wk vs. LP KO 6 wk	1.357	No	ns	0.2605
LP WT 8wk vs. LP KO 8wk	0.8333	No	ns	0.5929
Supplemental Figure 2D (middle panel)				
ANOVA summary				
F	25.68			
P value	< 0.0001			
P value summary	****			
Are differences among means statistically significant? (P < 0.05)	Yes			
R square	0.788			
Number of families	1			
Number of comparisons per family	6			

Alpha	0.05			
Holm-Sidak's multiple comparisons test	Mean Diff.	Significant?	Summary	Adjusted P Value
AP WT (PE) vs. AP KO (PE)	-1	No	ns	0.9127
AP WT (E) vs. AP KO (E)	-0.8557	No	ns	0.8246
AP WT (ME) vs. AP KO (ME)	-0.95	No	ns	0.9127
AP WT (DE) vs. AP KO (DE)	-0.2083	No	ns	0.9127
AP WT 6 wk vs. AP KO 6 wk	-0.9667	No	ns	0.8246
AP WT 8wk vs. AP KO 8 wk	0.4833	No	ns	0.9127
Supplemental Figure 2D (lower panel)				
ANOVA summary				
F	10.23			
P value	< 0.0001			
P value summary	****			
Are differences among means statistically significant? (P < 0.05)	Yes			
R square	0.597			
Number of families	1			

Number of comparisons per family	6			
Alpha	0.05			
Holm-Sidak's multiple comparisons test	Mean Diff.	Significant?	Summary	Adjusted P Value
U WT 6 wk vs. U KO 6 wk	-4.556	No	ns	0.4122
U WT 8wk vs. U KO 8wk	-4.417	No	ns	0.4122
U WT (PE) vs. U KO (PE)	-22.25	Yes	***	0.001
U WT (E) vs. U KO (E)	-18.63	Yes	****	< 0.0001
U WT (ME) vs. U KO (ME)	-18.46	Yes	**	0.004
U WT (DE) vs. U KO (DE)	-10.75	Yes	*	0.046
Supplemental Figure 2F (upper panel)				
ANOVA summary				
F	48.26			
P value	< 0.0001			
P value summary	****			
Are differences among means statistically significant? (P < 0.05)	Yes			
R square	0.9013			
Number of families	1			

Number of comparisons per family	4			
Alpha	0.05			
Holm-Sidak's multiple comparisons test	Mean Diff.	Significant?	Summary	Adjusted P Value
4wt vs. 4ko	-0.01537	No	ns	0.9784
6wt vs. 6ko	-0.1672	No	ns	0.9784
8wt vs. 8ko	-0.2023	No	ns	0.9784
10wt vs. 10ko	0.32	No	ns	0.9784
Supplemental Figure 2F (lower panel)				
ANOVA summary				
F	10.14			
P value	< 0.0001			
P value summary	****			
Are differences among means statistically significant? (P < 0.05)	Yes			
R square	0.6827			
Number of families	1			
Number of comparisons per family	4			
Alpha	0.05			
Holm-Sidak's multiple comparisons test	Mean Diff.	Significant?	Summary	Adjusted P Value
4wt vs. 4ko	2	No	ns	0.8956

6wt vs. 6ko	-3.8	No	ns	0.8956
8wt vs. 8ko	-2.214	No	ns	0.8956
10wt vs. 10ko	-1.5	No	ns	0.8956
Supplemental Figure 4B				
ANOVA summary				
F	6.587			
P value	0.0251			
P value summary	*			
Are differences among means statistically significant? (P < 0.05)	Yes			
R square	0.7671			
Number of families	1			
Number of comparisons per family	3			
Alpha	0.05			
Holm-Sidak's multiple comparisons test	Mean Diff.	Significant?	Summary	Adjusted P Value
KO_E vs. WT_E	181.5	Yes	*	0.0329
KO_E vs. KO_DE	239.8	Yes	*	0.024
KO_E vs. WT_DE	196	Yes	*	0.0329
Supplemental Figure 4D				
ANOVA summary				
F	32.99			
P value	0.0004			

P value summary	***			
Are differences among means statistically significant? (P < 0.05)	Yes			
R square	0.9428			
Number of families	1			
Number of comparisons per family	3			
Alpha	0.05			
Holm-Sidak's multiple comparisons test	Mean Diff.	Significant?	Summary	Adjusted P Value
WT-sham vs. WT-OVX	-0.3735	No	ns	0.0523
KO-sham vs. KO-OVX	-1.381	Yes	***	0.0003
WT-sham vs. KO-sham	0.9988	Yes	**	0.0021
Supplemental Figure 7F				
ANOVA summary				
F	16.37			
P value	0.0004			
P value summary	***			
Are differences among means statistically significant? (P < 0.05)	Yes			
R square	0.7318			
Number of families	1			

| Number of comparisons per family	3			
Alpha	0.05			
Holm-Sidak's multiple comparisons test	Mean Diff.	Significant?	Summary	Adjusted P Value
F vs. L	-307.9	Yes	**	0.0032
F vs. HC	-349.3	Yes	***	0.0008
L vs. HC	-41.37	No	ns	0.6384

Results

RSK2 is required to maintain ERalpha homeostasis in the adult mammary gland

In the mouse estrogen levels are highest during proestrus, akin to the follicular stage in humans (*132*). Analysis of ERalpha in the mammary gland of wild type (WT) mice in situ using quantitative immunofluorescence (IF) revealed that ERalpha protein levels varied during the estrous cycle (Figs. 2.1 A, B). In the WT, the lowest ERalpha protein levels occurred during estrus, which is consistent with observations that ERalpha protein degradation increases in response to the estrogen pulse in proestrus (Table 2.2) (*55*). Staging of the estrous cycle was determined by analysis of vaginal cytology and uterine wet weight (*129*) (Fig. 2.2 A). WT and RSK2-KO mice moved through the estrous cycle in a similar manner (Fig. 2.2 B). In the RSK2-KO glands ERalpha levels were consistently lower than the WT across all estrous stages (Figs. 2.1 A, B, 2.2 C). These results were unexpected as RSK2 phosphorylation of ERalpha stimulates transcription (*127*) and would, presumably, increase ERalpha degradation. Therefore, based on these observations we would expect that loss of RSK2 would increase ERalpha protein levels.

**Figure 2.1 RSK2 regulates ERalpha protein levels in the adult mammary gland throughout the estrous cycle.** (A) ERalpha protein expression in the adult mammary gland of WT and RSK2-KO mice during the estrous cycle. Scale bar = 20 micrometers. (B) ERalpha protein levels are lower in the RSK2-KO at all stages of the estrous cycle in adult mammary glands as determined by IF. ERalpha protein levels normalized to the average level observed in the WT mice at proestrus (median ± quartile, n ≥ 3 mice/genotype and stage, one-way ANOVA with Holm-Sidak's correction for multiple comparisons). (C) Loss of RSK2 results in a decrease in the number of ERalpha cells relative to K8+ cells at all stages of the estrous cycle in adult mammary glands (median ± quartile, n ≥ 4 mice/genotype, ≥ 150 cells/mouse, one-way ANOVA with Holm-Sidak's correction for multiple comparisons). See Figure 2.2 and Table 2.1.

Figure 2. 1 RSK2 regulates ERalpha protein levels in the adult mammary gland throughout the estrous cycle.
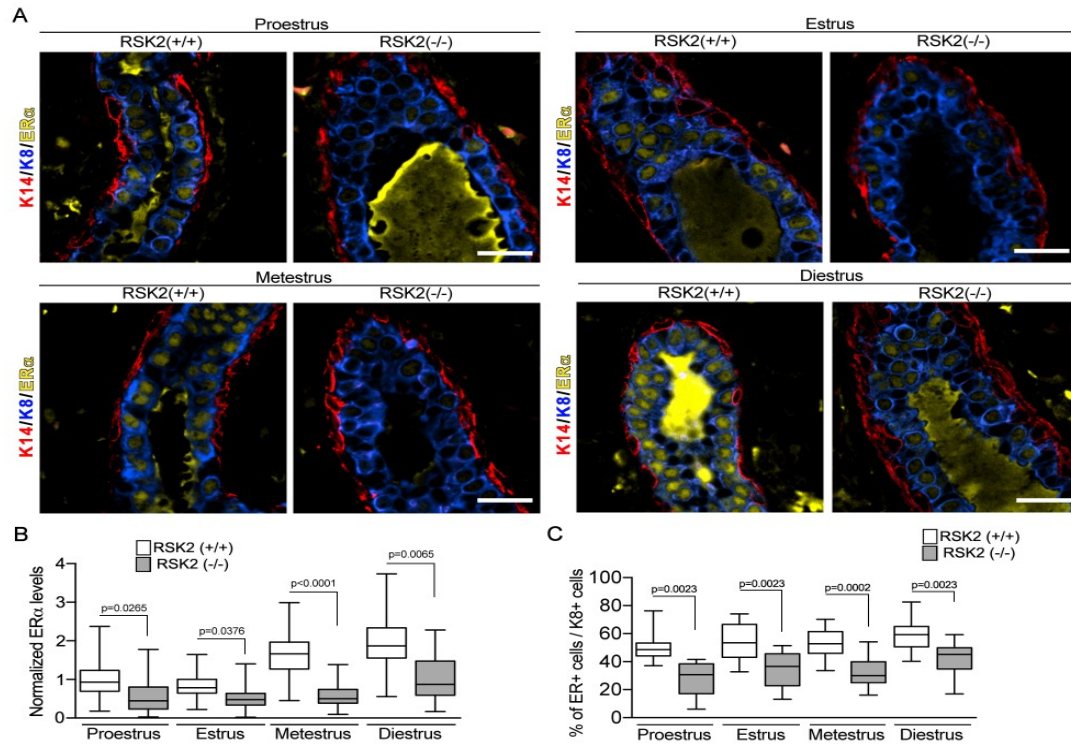
Figure 2.2 Estrogen responsiveness in WT and RSK2-KO mice. (A) Uterine wet weight is

similar in WT and RSK2-KO. (median ± quartile, n≥8 mice/genotype, Student's t-test). (B)

Cycling through the estrous cycle is similar in WT and RSK2-KO mice. Left graph: (mean ±

S.D., n≥10 mice/genotype); Right graph: Representative cycle. (C) ERalpha protein expression

levels are reduced in RSK2-KO at all stages of the estrous cycle in adult mammary glands. The

graphs were generated from data shown in Figs. 2.1 B and C.

Figure 2. 2 Estrogen responsiveness in WT and RSK2-KO mice.
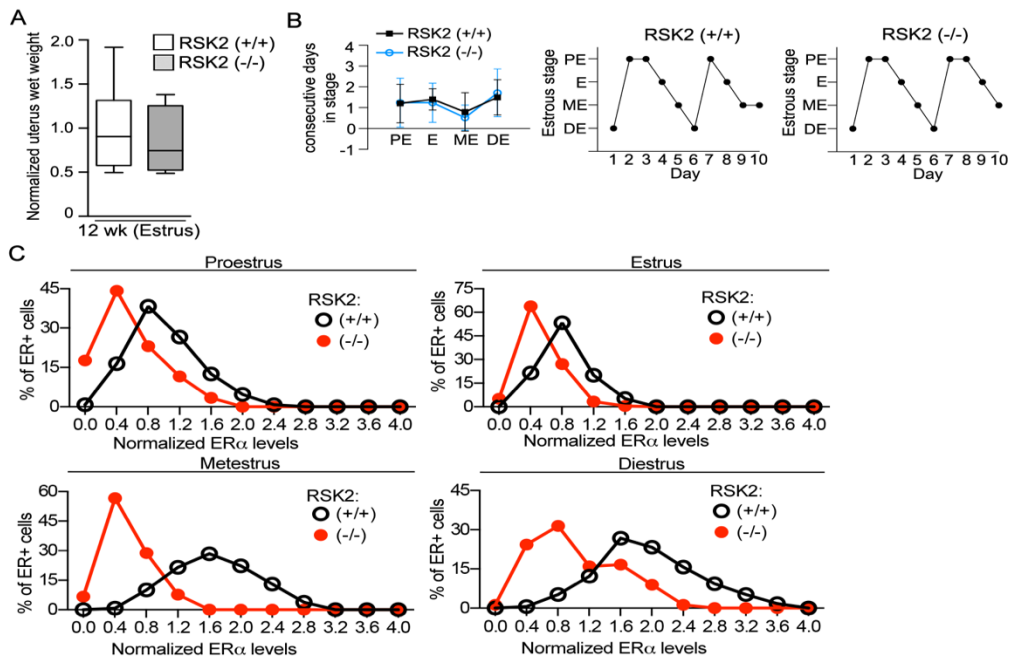
To further investigate the decrease in ERalpha levels that occur in the RSK2-KO glands we analyzed cell populations within the adult mammary glands by fluorescence-activated cell sorting (FACS). A novel FACS protocol that allowed the simultaneous analysis of WT and RSK2-KO mammary epithelial cells (MECs) was developed in which one of the genotypes was permanently marked and equal numbers of cells from the marked and unmarked genotypes were mixed (Fig. 2.3 A). The marked genotype was varied, and live cells and lineage-negative MECs determined (Fig. 2.4 A). The luminal and basal populations were clearly separated using epithelial cell adhesion molecule (EpCAM) and integrin alpha 6 (CD49f) (Fig. 2.3 B). The distributions were fairly similar in adult WT and RSK2-KO mice at each stage of the estrous cycle (Fig. 2.4 B). Further fractionation of the luminal cells by stem cells antigen-1 (Sca1) and integrin alpha 2 (CD49b) resulted in four populations with the gates for each experiment established using a fluorescence minus one strategy (Fig. 2.4 C) (*133*). The EpCAM^{hi}CD49f$^+$Sca1$^+$CD49b$^-$ population, which consists primarily of ERalpha cells (*82*), is referred to as non-clonogenic luminal (NCL) due to its lack of colony-forming potential in vitro and engrafting ability in vivo. The EpCAM^{hi}CD49f$^+$Sca$^-$CD49b$^+$ and EpCAM^{hi}CD49f$^+$Sca$^+$CD49b$^+$ are luminal progenitors, which express low or high levels of luminal differentiation markers, respectively (*82*). The EpCAM^{hi}CD49f$^+$Sca$^-$Cd49b$^-$ population is currently undefined. In comparison to the WT at estrus the NCL population was decreased in the RSK2-KO with a concomitant increase in the undefined population but no change in the luminal progenitor populations (Figs. 2.3 B, 2.4 D). These observations are consistent with those observed in situ in which fewer ERalpha cells were observed in the RSK2-KO (Figs. 2.1 C, 2.2C). A decrease in ERalpha protein levels was also observed in NCL cells isolated during FACS, consistent with our *in situ* analysis (Figs. 2.1 A, B, 2.3 D). At each stage of the estrous cycle a reduction in the NCL population was observed (Figs. 2.3 C, 2.4 D).

RSK2-KO is a constitutive knockout and therefore, we evaluated the contributions of systemic and intrinsic mechanisms that facilitate RSK2 regulation of the ERalpha population.

61

To perform these analyses mammary epithelial cells from WT and RSK2-KO mice were separately introduced into the cleared 4th mammary fat pads of a WT recipient. The glands from the transplanted cells regenerated to similar extents (Fig. 2.4 E). In regenerated glands loss of RSK2 also resulted in a decrease in the NCL population (Fig. 2.3 E), indicating that the effects on the ERalpha population caused by the loss of RSK2 are intrinsic to the mammary epithelial cells.

As ERalpha is absolutely required for mammary gland development (*134*) we analyzed the mammary gland at different ages starting at puberty. No detectable difference in the expansion of the mammary gland into the fat pad or branching during development was observed (Fig. 2.4 F). Analysis by FACS showed that all cell populations were similar between RSK2-KO and WT in juveniles (Figs. 2.3 F, 2.4 B, D). Consistent with these data in situ analysis of the juvenile mammary glands showed similar ERalpha protein levels (Fig. 2.3 G) and number of ERalpha cells (Fig. 2.3 H). We conclude that RSK2 regulates the ERalpha population only in the adult, which explains the absence of a developmental defect.

Figure 2.3 RSK2 maintains the EpCAM^{hi}CD49f$^+$Sca1$^+$CD49b$^-$ (NCL) population within the adult mammary gland throughout the estrous cycle. (A) Schematic of FACS protocol. (B) FACS analysis of adult mammary glands isolated from females during estrus. Gating strategy of luminal cells by further subdivision using Sca-1 and CD49b. The percentage of NCL cells within the luminal population at estrus decreases in adult RSK2-KO mice (median ± quartile, n ≥ 6 mice/genotype, one-way ANOVA with Holm-Sidak's correction for multiple comparisons). (C) Loss of RSK2 results in a reduction in the percentage of NCL cells at all stages of the estrous cycle in adult mammary glands (median ± quartile, n≥3 mice/genotype and stage, one-way ANOVA with Holm-Sidak's correction for multiple comparisons). proestrus =PE; estrus =E; metestrus = ME; diestrus =DE (D) ERalpha protein levels are decreased in cells isolated from the NCL population of RSK2-KO mice (median ± quartile, n=3 mice/genotype, > 20 cells/mouse, Student's t-test). Scale bar = 10 micrometers. Fn =fluorescence (E) RSK2 regulation of the NCL population is intrinsic to the epithelium (median ± quartile, n=3 mice/genotype, Student's t-test). (F) The percentage of NCL cells within the luminal population is similar between WT and RSK2-KO juvenile females (median ± quartile, n ≥ 3 mice/genotype and age group, one-way ANOVA with Holm-Sidak's correction for multiple comparisons). (G) The levels of ERalpha protein expression and the (H) number of ERalpha cells relative to K8+ cells are similar in WT and RSK2-KO juvenile females (median ± quartile, n=3 mice/genotype, ≥ 5 fields/mouse, one-way ANOVA with Holm-Sidak's correction for multiple comparisons). Scale bar = 20 miicrometers.

Figure 2. 3 RSK2 maintains the EpCAM^{hi}CD49f$^+$Sca1$^+$CD49b$^-$ (NCL) population within the adult mammary gland throughout the estrous cycle.
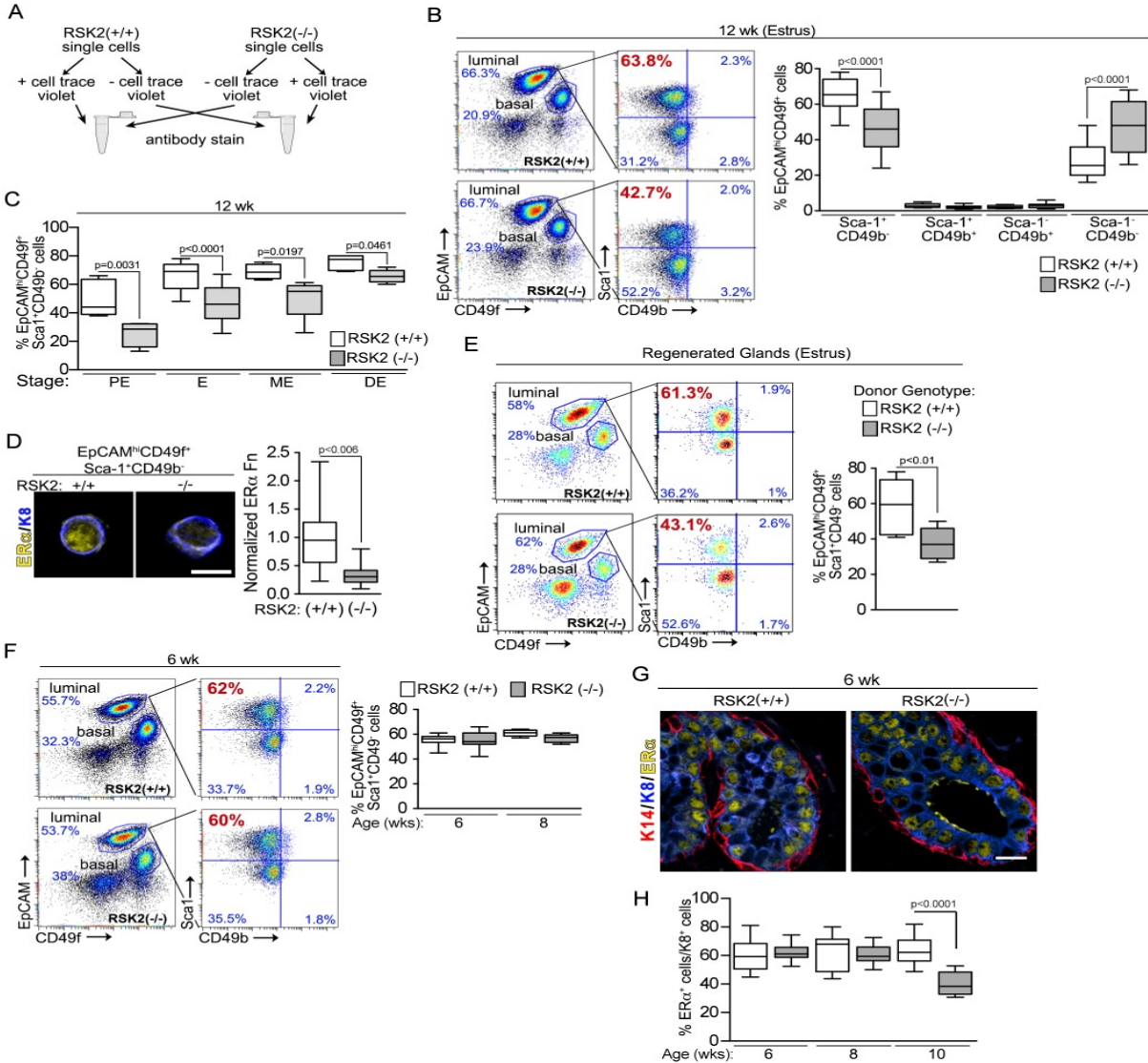
Figure 2.4 Analysis of WT and RSK2-KO mammary glands. (A) Gating strategy for flow

cytometry analysis and sorting of mouse mammary epithelium. Cells were gated for forward

(FCS-A) and side (SSC-A) scatter to remove debris. Single cells (p2) gated by FSC-H/A were

then gated for live cells (ZombieYellow negative). Lineage$^+$ (Cd140a$^+$; CD31$^+$; Ter-119$^+$; and

CD45$^+$) cells were gated out. CellTraceViolet (CTV) positive and negative populations were

separated. (B) FACS analysis of luminal and basal epithelial populations in the mammary gland

(median ± quartile, n≥4 mice/genotype and stage, one-way ANOVA with Holm-Sidak's

correction for multiple comparisons) (Table S1). solid=luminal, hatched = basal (C)

Fluorescence minus one strategy for determining the gates for Sca1 and CD49b. (D) FACS

analysis of luminal progenitor and undefined epithelial populations (median ± quartile, n ≥ 3

mice/genotype and stage, one-way ANOVA with Holm-Sidak's correction for multiple

comparisons) (Table S1). (E) Representative whole mount image of the regenerated 4th

mammary gland from WT or RSK2-KO ~ 20 wk after transplantation at 3 wk. Scale bar = 1 mm.

(F) Mammary gland development is similar in WT and RSK2-KO. (median ± quartile, n≥2

mice/genotype, one-way ANOVA with Holm-Sidak's correction for multiple comparisons) (Table

S1). Scale bar = 2 mm.

Figure 2. 4 Analysis of WT and RSK2-KO mammary glands.
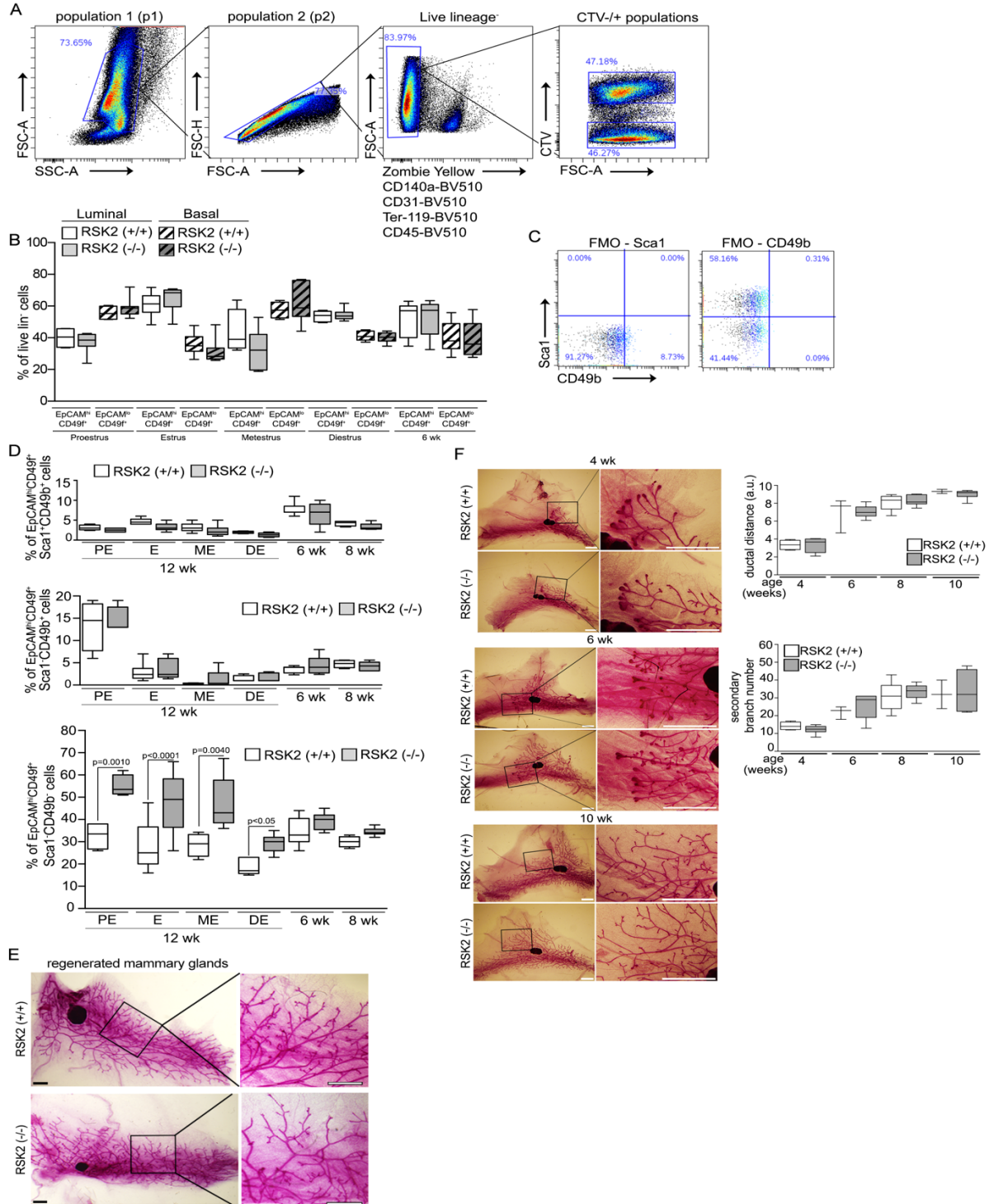
*ERK1/2-RSK2 signaling is dependent on estrogens*

At the onset of puberty estrogen increases the levels of growth factors (*135, 136*), which, theoretically, would result in RSK activation through its upstream activator, ERK1/2 (*137*). C57BL/6J mice initiate cycling by ~ six weeks (*138*), although we observed that cycling was irregular until ~ ten to twelve weeks of age. Interestingly, ERK1/2, as shown by Thr202/Tyr204 phosphorylation (pERK1/2), was not active until the animals were ≥ ten weeks old and the levels of active ERK1/2 were similar at estrus between the WT and RSK2-KO at the same age (Fig. 2.5 A). A causal relationship between estrogen and ERK1/2 activity was demonstrated by the observations that ERK1/2 activation was prevented by oophorectomy at six weeks (Fig. 2.5 B). ERK1/2 activation in the WT occurs in estrus after the estrogen burst in proestrus and then decreases during diestrus when estrogen levels are lowest (Fig. 2.5 C). The inactivation of ERK1/2 appears to be consistent with increased phosphatase activity as the protein levels of ERK1/2 do not change between estrus and diestrus (Fig. 2.6 B). We conclude that the ability of estrogen to activate ERK1/2 and regulate its cyclic activation appears as the mice sexually mature.

Active ERK1/2 was primarily confined to the luminal compartment and was present in ER+ cells (Fig. 2.6 C). To confirm that RSK was activated in the WT mammary gland an anti-active RSK antibody (pRSK) was used. RSK is activated in response to coordinated inter- and intra- molecular phosphorylation events (*139*), which is identical within the RSK family and therefore, identification of the active state of a particular RSK is not possible. However, active RSK was not detectable in the adult RSK2-KO mammary glands indicating that RSK2 is the predominant active RSK isoform (Fig. 2.6 D). These results demonstrate that in the WT estrogen activates ERK1/2-RSK2 signaling and that this activation corresponds with the ability of RSK2 to regulate ERalpha protein levels (Figs. 2.1 B, 2.5 C).

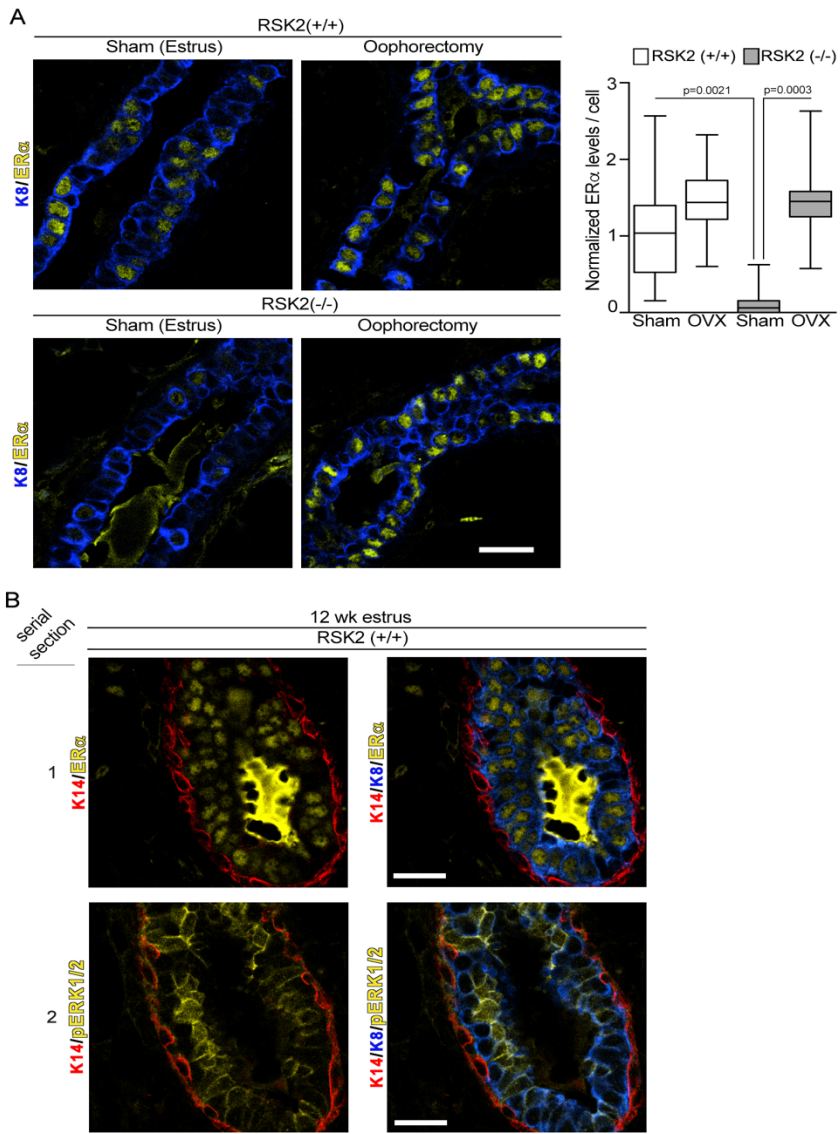**Figure 2.5 ERK1/2-RSK2 signaling is activated only in the adult mammary gland.** (A)

ERK1/2 activity is increased in the adult compared to juvenile animals (median ± quartile, n ≥ 2

mice/genotype and age, ≥ 3 fields/mouse, one-way ANOVA with Holm-Sidak's correction for

multiple comparisons). Scale bar = 20 micrometers. (B) ERK1/2 activity in the mammary gland

depends on estrogen (median ± quartile, n ≥2 mice/genotype and procedure, ≥ 3 fields/mouse,

Student's t-test). Scale bar = 20 micrometers. (C) ERK1/2 activity varies during the estrous

cycle in the WT in the adult mammary gland (median ± quartile, n≥ 2mice/genotype, ≥ 3

fields/mouse, one-way ANOVA with Tukey's correction for multiple comparisons). Scale bar =

20 micrometers. (D) Active nuclear RSK2 is the predominant RSK in adult mammary glands.

Scale bar = 20 micrometers.

Figure 2. 5 ERK1/2-RSK2 signaling is activated only in the adult mammary gland.
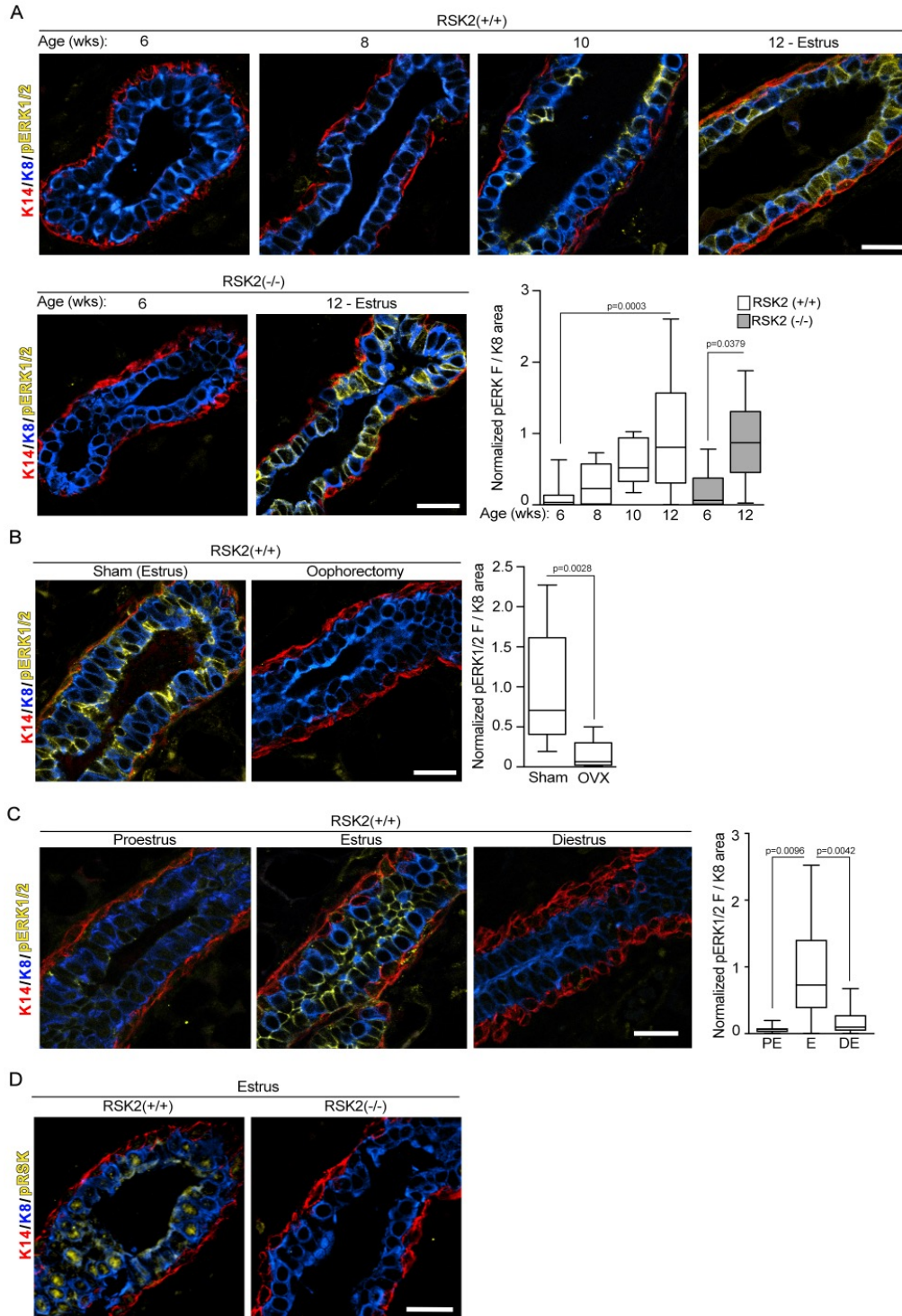
Figure 2.6 ERK1/2 is active in ER+ cells. (A) ERalpha protein levels increase in response to oophorectomy (median ± quartile, n ≥2 mice/genotype and procedure, ≥ 3 fields/mouse, one-way ANOVA with Holm-Sidak's correction for multiple comparisons) (Table S1). Scale bar= 20 micrometers. (B) The image on the left is shown without K8 to facilitate the visualization of ERalpha and pERK1/2. Serial sections were necessary to avoid antibody interference. Scale bar = 20 micrometers.

Figure 2. 6 ERK1/2 is active in ER+ cells.

A

RSK2(+/+)

Sham (Estrus)   Oophorectomy

K8/ERα

RSK2(-/-)

Sham (Estrus)   Oophorectomy

K8/ERα

□ RSK2 (+/+) ■ RSK2 (-/-)

p=0.0021   p=0.0003

Normalized ERα levels / cell

Sham OVX Sham OVX

B

serial section

12 wk estrus
RSK2 (+/+)

1   K14/ERα   K14/K8/ERα

2   K14/pERK1/2   K14/K8/pERK1/2

RSK2 negatively regulates proteasome-coupled transcription in the adult mammary gland

To identify a mechanism that would explain the reduced ERalpha protein levels with the loss of RSK2 we performed transcriptomic analyses on the NCL population (Supplemental information table 2, available online). Estrus was chosen as changes in gene expression would be occurring in response to the estrogen pulse that happened in proestrus. We contrasted these data with that obtained in diestrus, which has the lowest estrogen levels. The transcriptomic analysis of the RSK2-KO showed 2747 differentially expressed genes (DEG) between estrus and diestrus as compared to 39 in the WT between estrus and diestrus (Figs. 2.7 A, 2.8 A). The transcriptomic data of RSK2-KO at estrus showed a significant correlation with a signature obtained from the ERalpha breast cancer cell line, MCF-7, 24h after estrogen treatment (Figs. 2.7 B, C) (Table S3) (*140*).   This correlation was not driven by cell cycle genes (Fig. 2.8 B) (Table 2.3). No significant correlation with the estrogen-responsive gene signature was obtained for the WT at estrus (Figs. 2.7 B, C). ESR1 (gene encoding ERalpha) mRNA levels were similar between WT and RSK2-KO (Fig. 2.8 C), eliminating the possibility that ERalpha mRNA expression levels accounted for the transcriptomic differences. Taken together, these data demonstrate that estrogen signaling is higher in the RSK2-KO than the WT and therefore, we conclude that RSK2 acts to inhibit estrogen-responsive gene expression.

Estrogen-responsive gene expression is interconnected with ERalpha destruction through the 26S proteasome pathway (*55, 62, 120, 121, 141*). Therefore, it would be expected that ERalpha degradation would be greater in the RSK2-KO than the WT. To investigate this possibility the rate of in vivo ERalpha degradation was determined using the 26S proteasome inhibitor, PS-341(*62*). In the WT gland ERalpha levels did not substantially change in response to proteasome inhibition. However, in the RSK2-KO gland ERalpha protein levels increased by ~ five-fold in response to PS-341 and therefore, ERalpha degradation is much higher in the absence of RSK2 (Fig. 2.7 D). This increased degradation explains our in situ observations that ERalpha levels are lower in the RSK2-KO compared to the WT (Figs. 2.1 A, B, 2.2 C).

Reduced ERalpha protein levels in the RSK2-KO could be the result of decreased RSK2 kinase activity or loss of the RSK2 protein. To distinguish between these mechanisms RSK2 activity was inhibited i*n vivo* by the specific RSK1/2 inhibitor, *C5″-n*-propyl cyclitol SL0101 (C5") (*115*) (*142*). ERalpha protein levels were reduced by the RSK1/2 inhibitor (Fig. 2.7 E). To demonstrate that the inhibitor was on target we used phosphorylation of the elongation translation factor 2 (peEF2) as a biomarker (*143*) (Fig. 2.8 D). We conclude that RSK2 kinase activity is important in ERalpha degradation.

Table 2. 3 Statistical analysis of gene set overlaps from the NCL populations.

| Gene sets in overlap		Fisher's exact test for overlap
Genes UP in R2KO-E vs R2KO-DE	E2_24h_UP	0.00001
Genes DOWN in R2KO-E vs R2KO-DE	E2_24h_DOWN	0.00001
Genes UP in R2KO-E vs R2KO-DE	Cell cycle genes	0.0007
Genes UP in WT-E vs WT-DE	E2_24h_UP	no overlap
Genes DOWN in WT-E vs WT-DE	E2_24h_DOWN	no overlap
Genes UP in WT-E vs WT-DE	Cell cycle genes	0.5785

Figure 2.7 RSK2 is a negative regulator of ERalpha-mediated signaling. (A) RSK2-KO

mice show higher number of DEGs between estrus and diestrus (right panel) than WT (left

panel). Genes with a fold-change ≥ |1.5| (log2(fold-change) ≥ |0.5|) and an FDR adjusted p <

0.05 are shown as black dots and genes with a fold-change < |1.5| (log2(fold-change) < |0.5|)

and an FDR adjusted p-value > 0.05 are shown as grey dots. The dashed line indicates the cut

off values. (B) Heat map illustrating that the gene expression of NCL cells isolated from RSK2-

KO mice in estrus correlates with a 24 h estrogen-regulated gene signature identified from

MCF-7 cells (*140*). (C) Quantitative assessment of enrichment for estrogen-regulated genes.

Cumulative Z-scores were generated for each mouse by summing individual Z-scores of genes

up regulated in estrogen-regulated signature and subtracting individual Z-scores of genes down

regulated (mean ± S.D., each point represents a mouse, one-way ANOVA with Holm-Sidak's

correction for multiple comparisons). (D) Loss of RSK2 increases ERalpha turnover. Adult

mice staged at estrus were treated with vehicle or PS-341 (5 mg/kg) IP for 4 h before

euthanasia and isolation of the mammary gland. ERalpha protein levels were normalized to

those observed in the WT mice at estrus (median ± quartile, n=3 mice/genotype and condition, ≥

200 cells/mouse, one-way ANOVA with Holm-Sidak's correction for multiple comparisons).

Scale bar = 20 micrometers. (E) RSK2 kinase activity is necessary to maintain ERalpha protein

levels. Adult mice staged at estrus were treated with vehicle or *C5″-n*-propyl cyclitol SL0101

(C5") (40mg/kg) IP twice every 7 h before euthanasia and isolation of the mammary gland

(median ± quartile, n≥3 mice/genotype, ≥3 fields/mouse, Student's t-test).

Figure 2. 7 RSK2 is a negative regulator of ERalpha-mediated signaling.

76
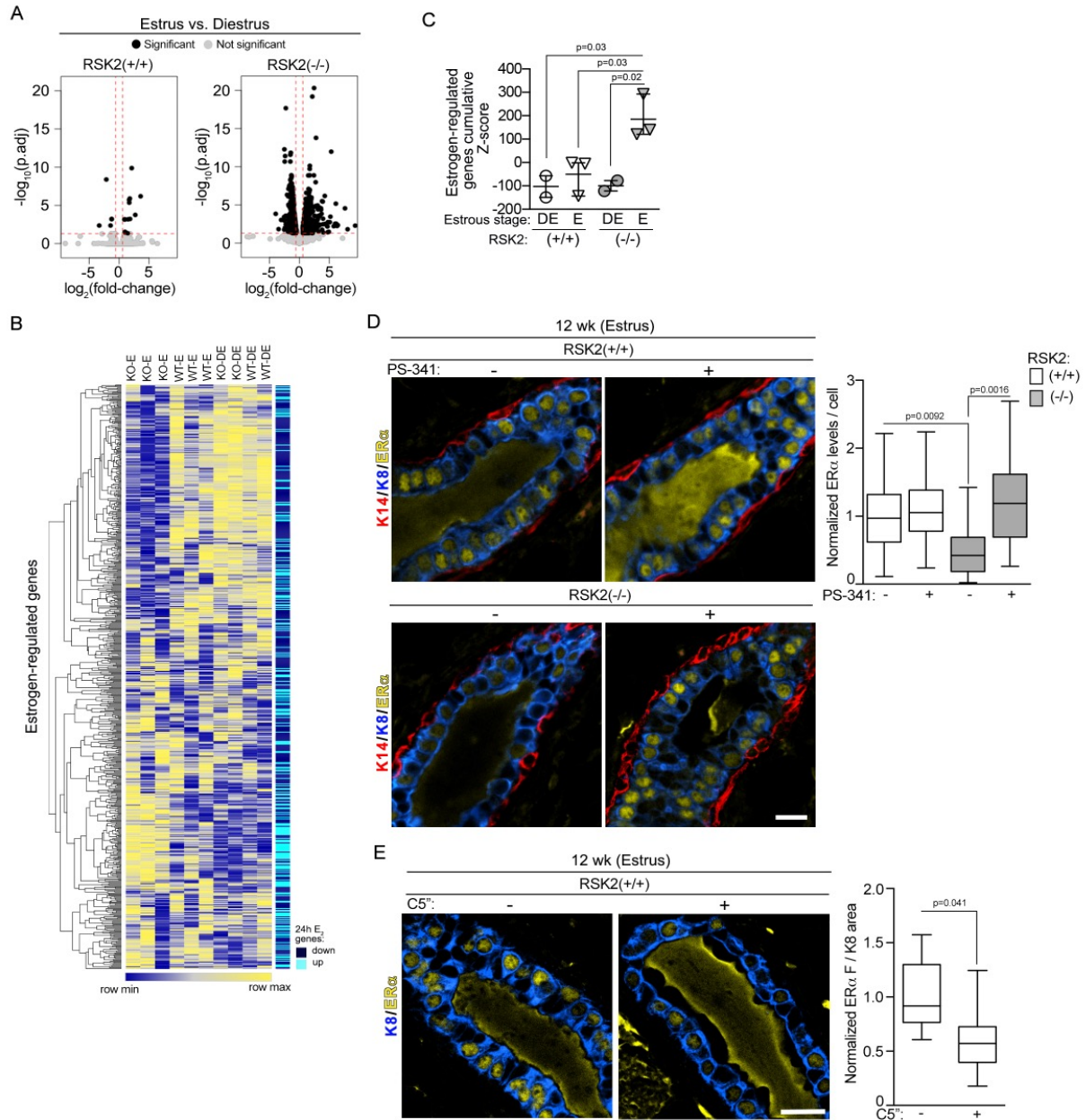
Figure 2.8 Transcriptomic analysis of the NCL population. (A) Principal component (*144*)

analysis of the transcriptomic data. (B) Proliferation genes do not drive the enrichment for

estrogen -regulated signature in RSK2 KO estrus mice. Cumulative Z-scores were generated

for each mouse by summing individual Z-scores of genes up regulated in estrogen-regulated

signature in which the cell cycle genes were removed and subtracting individual Z-scores of

genes down regulated. (median ± quartile, one-way ANOVA with Holm-Sidak's correction for

multiple comparisons) (Table S1). (C) ESR1 and GATA3 mRNA levels are similar in NCL cells

isolated from RSK2-KO and WT mice during the estrus stage (mean ± S.D., n=3 mice/genotype

in triplicate, Student's t-test). (D) On target increase in peEF2 *in vivo* by *C5″-n*-propyl cyclitol

SL0101 (C5"). Adult mice staged at estrus were treated with vehicle or *C5″* (40 mg/kg) IP twice

every 7 h before euthanasia and isolation of the mammary gland (median ± quartile, n ≥ 2

mice/genotype in triplicate, Student's t-test).

**Figure 2. 8 Transcriptomic analysis of the NCL population.**
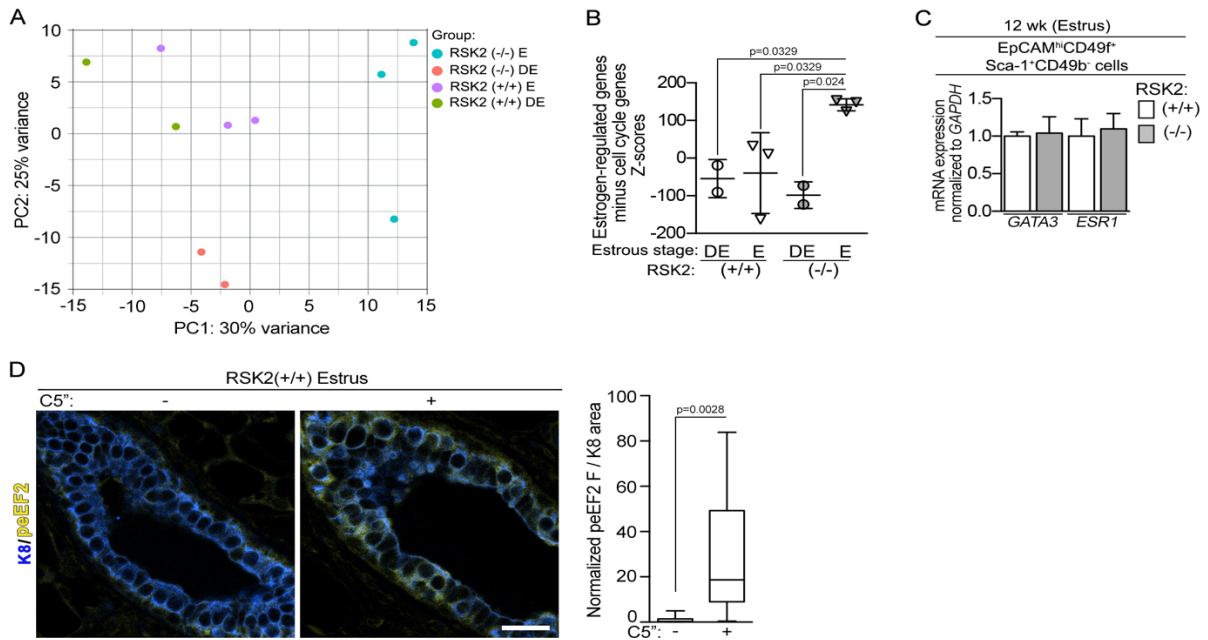
RSK2 maintains ERalpha protein levels in adult reproductive tissue

We next investigated whether RSK2 preserved ERakpha protein levels in other

estrogen-responsive tissues. We focused on the female reproductive tract, as we observed a

40% reduction in the fertility rate in crosses between RSK2-KO females and males (Fig. 2.9 A).

RSK2-KO males crossed with heterozygote females had similar fertility rates to that of the WT

crosses, indicating that the reduced fertility is associated with the RSK2-KO females. Ovaries in

the RSK2-KO and WT mice showed all stages of follicular development and the presence of the

corpora luteum (Fig. 2.9 B, 2.11 A), demonstrating that hormonal signaling (*145*) through the

hypothalamic-pituitary-ovarian axis is not impaired in RSK2-KO mice. The uterus expresses

high levels of ERalpha which is present in stromal cells as well as glandular and luminal

epithelium. In comparison to the WT, the ERalpha protein levels were substantially decreased

in the epithelial but not in the stromal cells in RSK2-KO mice (Fig. 2.9 C). Interestingly, ERK1/2

activity was detected in the uterine epithelium but not in the stroma cells, providing further

evidence of the connection between ERK1/2-RSK2 signaling and the regulation of ERalpha

protein levels (Fig. 2.9 D). Uterine wet weight and total uterine width was similar in the WT and

RSK2-KO, which is consistent with the literature as stromal cells are thought to mediate uterine

expansion (Figs. 2.10A, B) (*129, 146*). These data indicate that RSK2 regulates ERalpha

protein levels in multiple tissues.

Figure 2.9 RSK2 maintains ERalpha protein levels in the uterine epithelium. (A) RSK2-KO

mice show a fertility defect (n ≥ 15 dams/genotype, Chi-squared test p=0.0299). (B) The

hypothalamic-pituitary-ovarian axis is not disrupted in RSK2-KO females. H&E sections of

ovaries isolated from adult mice in estrus. Scale bar = 1 mm PF=primary follicle; SF=secondary

follicle; TF=tertiary follicle; CL=corpus luteum. (C) RSK2-KO have reduced ERalpha protein

levels in the glandular and luminal epithelium of the uterus (median ± quartile, n=3

mice/genotype, > 120 cells/mouse, Student's t-test). Scale bar = 40 micrometers. GE =

glandular epithelium; S = stroma; LE = luminal epithelium (D) Active ERK1/2 is confined to the

epithelium of the uterus. Scale bar = 40 micrometers.

Figure 2. 9 RSK2 maintains ERalpha protein levels in the uterine epithelium.

81
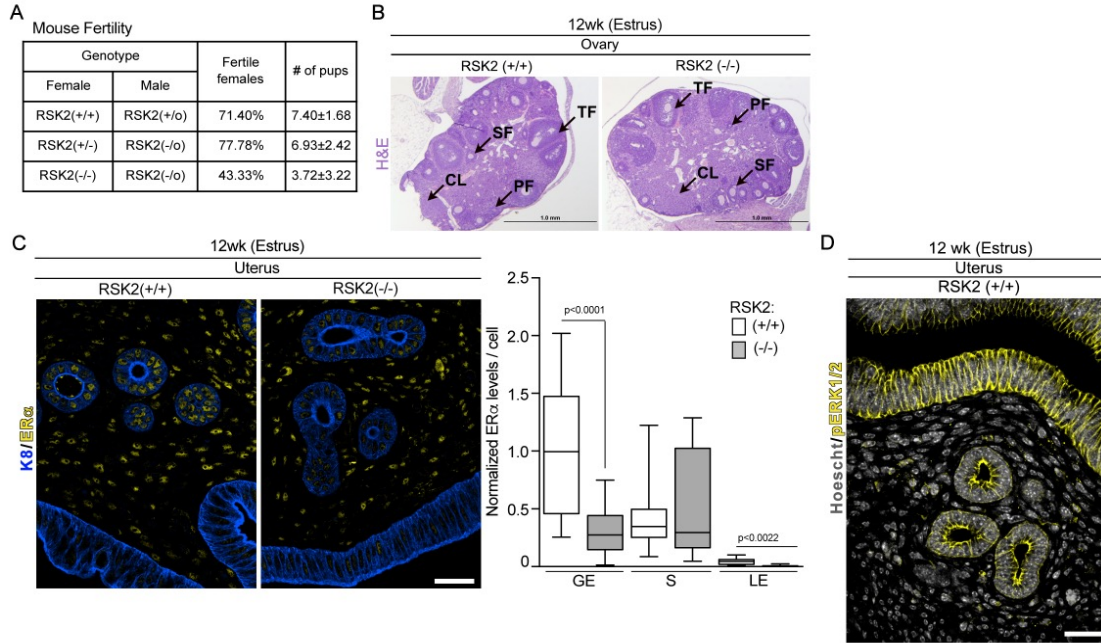
Figure 2.10 The hypothalamic-pituitary-ovarian axis is not impaired in RSK2-KO mice. (A)

Representative H&E images of ovaries. Scale bar = 1 mm. (B) Luminal height in the uterus in

the WT and RSK2-KO are similar. Measurements from ≥30 randomly selected regions from

each animal (median ± quartile, n≥3 mice/genotype, ≥ 3 fields/mouse, Student's t-test).

Figure 2. 10 The hypothalamic-pituitary-ovarian axis is not impaired in RSK2-KO mice.
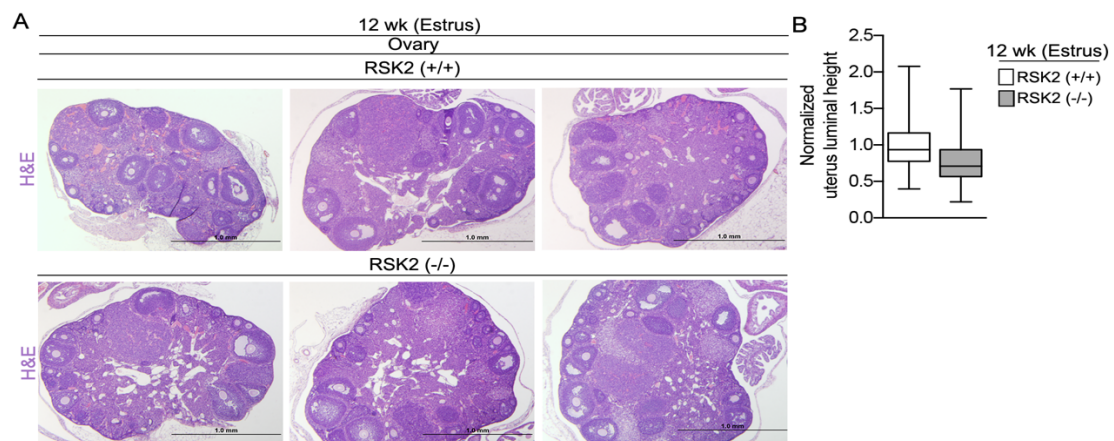
ERK1/2 drives ERalpha degradation through phosphorylation of Ser-118 on ERalpha

To address the mechanism by which RSK2 regulates ERalpha protein levels we initially focused on GATA3, as GATA3 and ERalpha regulate each other's expression via a positive feedback mechanism in breast cancer (*147*). Therefore, it is conceivable that RSK2 indirectly regulates ERalpha protein levels through GATA3. However, no difference in GATA3 mRNA levels was observed between WT and RSK2-KO mice (Fig. 2.8 C). Furthermore, GATA3 protein levels in the uterine glandular epithelium (*148*) are extremely low whereas ERalpha protein levels are very high (Figs. 2.11 A). We conclude that RSK2 regulation of ERalpha through GATA3 is unlikely.

Interestingly, in contrast to the WT mice ERK1/2 activity remains elevated in the RSK2-KO mice during diestrus (Fig. 2.12 A) and coincident with these observations ERalpha protein levels remain lower in the RSK2-KO (Figs. 2.1 A, B, 2.2 C). Therefore, we investigated whether ERK1/2 activity was a driver of ERalpha degradation. In support of this hypothesis when we prevented ERK1/2 activation by oophorectomizing RSK2-KO mice we observed that the levels of ERalpha were rescued to WT levels (Fig. 2.5 A). To perform further mechanistic studies we used the normal mouse Leydig cell line, TM3, which expresses ERalpha but does not form tumors in vivo. Survival of the TM3 line was dependent on RSK2, which prevented knockout out approaches. However, short term treatment with two structurally distinct RSK inhibitors decreased ERalpha protein levels, which was prevented by inhibition of the 26S proteasome (Figs. 2.11 B, C). This effect is specific as androgen receptor protein levels do not change in response to RSK1/2 inhibition (Fig. 2.11 D). ERK1/2 activity increased in response to the RSK inhibitors (Fig. 2.11 B), which is consistent with our observations at diestrus in the RSK2-KO mice. MEK inhibition by trametinib or U0126, did not decrease ERalpha levels. Taken together, these results indicate that ERK1/2 activity increases ERalpha degradation through the 26S proteasome.

It is hypothesized that degradation of phosphorylated ERalpha occurs at a faster rate than the unphosphorylated (*149*). Therefore, we investigated whether the ERK1/2 and RSK2 phosphorylation of ERalpha (*38, 127*) regulated ERalpha turnover. GFP-tagged ERalpha mutants were generated in which the ERK1/2 phosphorylation site, Ser-118 (S118A- ERalpha), or the RSK2 site, Ser-167 (S167A- ERalpha was mutated to Ala. In response to ERK1/2 activation mutation of Ser-167 did not alter ERalpha turnover; however, mutation of Ser-118 prevented ERalpha destruction (Fig. 2.11 E). An electrophoretic mobility shift assay was used to confirm phosphorylation of Ser-118 in response to RSK1/2 inhibition because phospho-specific antibodies to human ERalpha do not recognize the mouse protein (*150*) (Fig. 2.12 B). We conclude that ERK1/2 phosphorylation of Ser-118 targets ERalpha for destruction and that RSK2 negatively regulates ERK1/2 activity to protect ER alpha from degradation.

RSK2 negatively regulates ERK1/2 activity by controlling oxidative stress levels

To investigate the mechanism by which RSK2 negatively regulates ERK1/2 we determined whether a loss of RSK2 resulted in increased oxidative stress. In support of this hypothesis an increase in ROS is associated with estrogen-regulated transcription (*151*) and ROS activates ERK1/2 (*152*). Therefore, in the RSK2-KO the increased estrogen-regulated transcription could result in elevated ROS levels compared to WT, resulting in ERK1/2 activation. The presence of gamma-H2AX provides a readout for the formation of DNA double stranded breaks, which occur in response to oxidative stress (*153*). Consistent with our hypothesis gamma-H2AX was elevated in the RSK2-KO (Fig. 2.11 F). Analysis of the genes up regulated in the RSK2-KO at estrus compared to diestrus revealed enrichment for genes associated with oxidative stress (Fig. 2.12 C). Additionally, an over-representation of genes associated with the glutathione metabolic process, suggesting that the cells were experiencing oxidative stress and attempting to compensate by increasing glutathione production. Consistent with the in vivo data RSK2 inhibition in the TM3 line exhibited elevated ROS (Fig. 2.11 G) and

DNA damage (Fig. 2.11 H). Importantly, reduction of ROS by two structurally distinct anti-oxidants rescued ERalpha levels in the presence of RSK2 inhibition (Fig. 2.11 I) and prevented ERK1/2 activation (Fig. 2.11 J). Taken together, these data demonstrate that RSK2 maintains estrogen homeostasis by preventing the activation of ERK1/2 by ROS.

Figure 2.11 ERK1/2 drives ERalpha degradation through phosphorylation of Ser-118. (A)

ERK1/2 activity remains elevated during diestrus in the adult mammary gland (median ±

quartile, n= 3 mice, ≥ 3 fields/mice, Student's t-test). (B) RSK2 is a negative regulator of

ERK1/2 activity. Serum starved TM3 were treated for 6 h with vehicle, *C5″-n*-propyl cyclitol

SL0101 (C5") (20 microM), BI-D1870 (10 microM), trametinib (1 microM) or U0126 (10 microM).

The white vertical line indicates that conditions not relevant to the manuscript were removed.

ERalpha levels were normalized to Ran and then to the vehicle (mean, n=3, one-way ANOVA

with Dunnett's correction for multiple comparisons). (C) RSK1/2 inhibition stimulates ERα

degradation through the 26S proteasome pathway. Serum starved TM3 were treated for 6 h

with vehicle, C5″ (20 microM) with or without a 1 h pre-treatment with MG132 (10 µM). (D)

RSK2 does not regulate androgen receptor (AR) degradation. Serum starved TM3 were treated

for 6 h with vehicle or *C5″* (20 microM). AR levels were normalized to Ran and then to the

vehicle (mean, n=3 in duplicate, Student's t-test). (E) Phosphorylation of Ser-118A is required

for ERalpha degradation. Cells transduced with WT or mutant ERalpha-VENUS were treated

with vehicle or C5" (20 microM) as in (B). The range was normalized to WT ERalpha(mean,

n=3, >150 cells/condition/experiment, one-way ANOVA with Holm-Sidak's correction for multiple

comparisons). Scale bar = 10 micrometers. (F) Loss of RSK2 increases double stranded DNA

breaks (gamma-H2AX foci) in the mammary gland (median ± quartile, n≥4 mice/genotype, ≥3

fields/mouse, Student's t-test). (G) RSK1/2 inhibition increases ROS. Serum starved TM3 were

treated as in (B). The data were normalized to the range with and without C5" (20 microM)

(mean, n=3, >100 cells/condition/experiment, Student's t-test). (H) RSK1/2 inhibition increases

DNA damage in vitro. Cells treated for 72 h with vehicle or C5" (20 microM). The data were

normalized to the range with and without C5" (mean, n=3, >80 cells/condition/experiment,

Student's t-test). (I) Inhibition of ROS rescues ERalpha levels. Serum starved TM3 were

treated for 6 h with vehicle or C5" (20 microM) with or without ebselen (Ebs) (50 microM) or N-

acetyl cysteine (NAC) (15 mM) for the final 2 h. The range was normalized to ERalpha levels in

the absence of anti-oxidants (mean, n=3, >50 cells/condition/experiment, one-way ANOVA with Dunnett's correction for multiple comparisons). (J) Inhibition of ROS inhibits ERK1/2 activation. Cells treated and analyzed as in (I).

Figure 2. 11 ERK1/2 drives ERalpha degradation through phosphorylation of Ser-118.
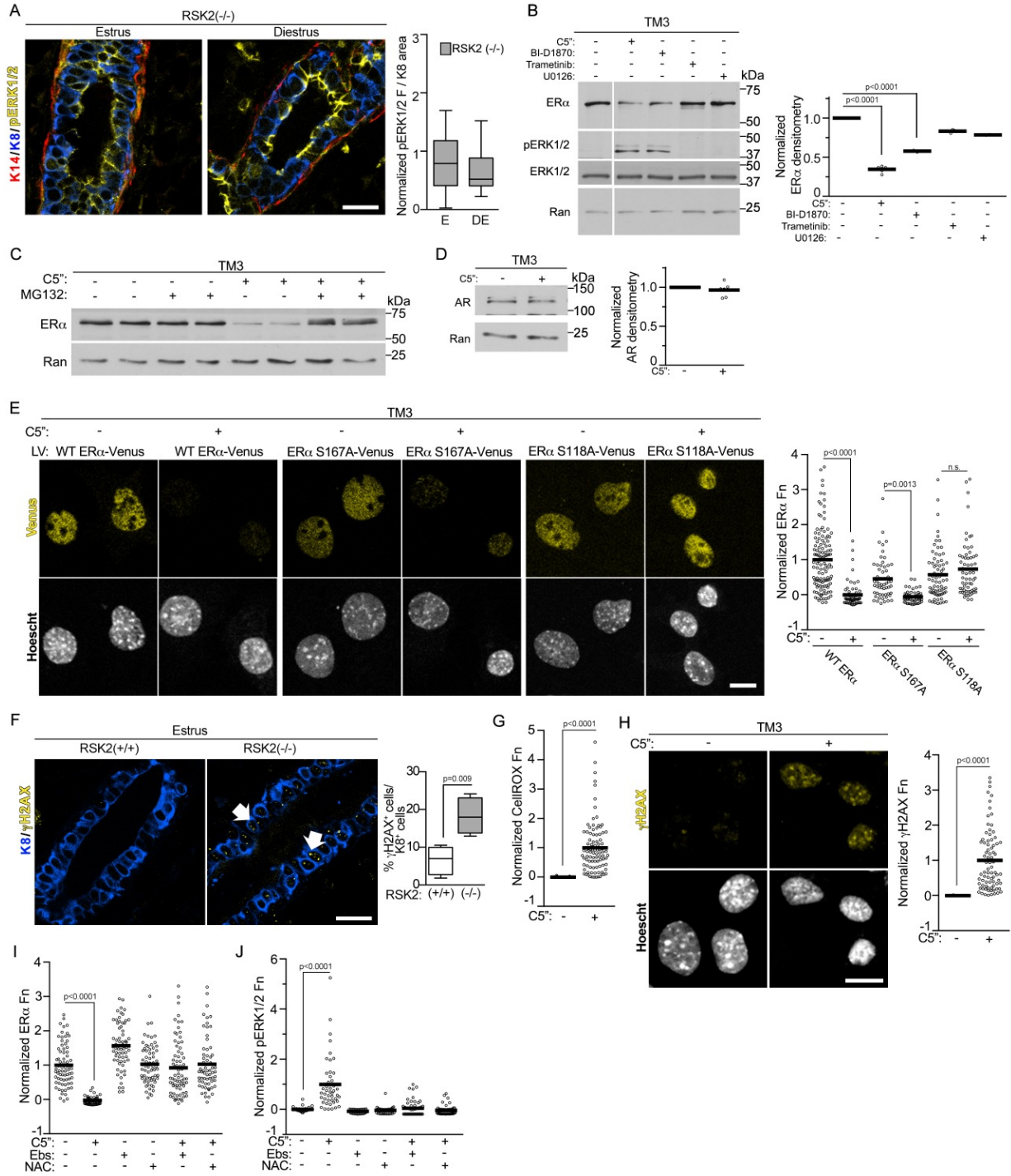
Figure 2.12 Phosphorylation of Ser-118 ERalpha correlates with degradation of ERalpha.

(A) GATA3 is expressed at very low levels in the uterus compared to the mammary gland.

Scale bar = 20 micrometers. (B) Ser118- ERalpha phosphorylation occurs in response to agents

that stimulate ERalpha degradation. Serum starved TM3 were treated with PMA (0.5 microM,

20 min) or an EGF/FGF7 cocktail (12.5 nM each, 5 min) with or without *C5″* (20 microM, 2h) or

trametinib (1 microM, 1 h as a pretreatment). The white vertical line indicates that conditions

not relevant to the manuscript were removed.

Figure 2. 12 Phosphorylation of Ser-118 ERalpha correlates with degradation of ERalpha.
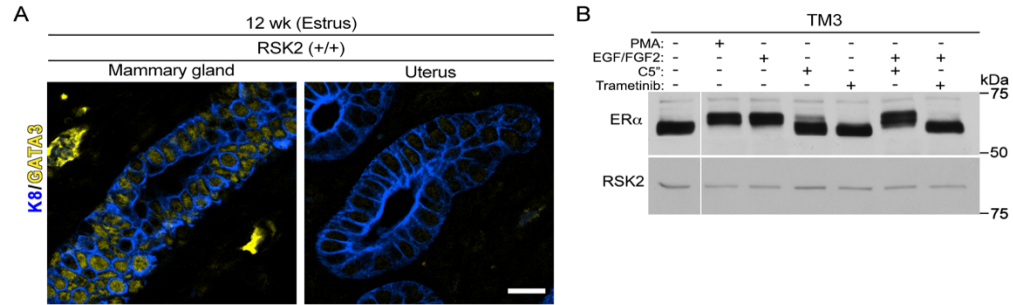
RSK2 integrates estrogen-mediated transcription and translational responses to maintain

homeostasis

There was no evidence of hyperplasia in the RSK2-KO glands, which was surprising because of their increased expression of cell cycle genes. In fact, the rate of proliferation was decreased in the NCL population of RSK2-KO (Figs. 2.13 A, 2.14 A, B), which is consistent with the reduced number of ERalpha cells observed in these mice (Figs. 2.1 C, 2.3 B, C). Because of this disconnect between the gene expression and proliferation data we investigated whether RSK2 was important in translational regulation in the ERalpha population (*154*). As a readout for translational activity in vivo we measured eEF2 phosphorylation (peEF2). The levels of peEF2 were higher at diestrus in the RSK2-KO (Fig. 2.13 B), which is consistent with inhibition of protein synthesis (*143*). We also observed that RSK1/2 inhibition decreased protein synthesis in the TM3 line (Fig. 2.13 C). Taken together, these data support a model in which RSK2 regulation of translation contributes to the physiological responses induced by estrogen.

To further evaluate the physiological importance of RSK2 in estrogen responsiveness we investigated the remodeling of the mammary gland that occurs during pregnancy. This remodeling is dependent on the ERalpha cells within the mammary gland, which act as sensors to facilitate alveolar expansion and lactation (*32, 135*). Alveolar expansion in the whole animal knockout (Fig. 2.13 D) and in glands regenerated from RSK2-KO (Fig. 2.14 C) were reduced, consistent with the decrease in the ERalpha population observed in the RSK2-KO glands. Pup weight was reduced in litters arising from RSK2-KO crosses, which could be rescued by fostering RSK2-KO pups to WT dams (Fig. 2.13 E, 2.15D). These results argue that the reduced alveolar expansion in the RSK2-KO dams does not provide sufficient nutrition for the pups rather than a developmental defect in the offspring. These results support our hypothesis that RSK2 is a critical regulator of estrogen responsiveness in vivo.

Estrogen homeostasis in the human breast

To evaluate whether RSK2 also functions in regulating estrogen responsiveness in humans we examined transcriptomic data obtained from normal breast tissue at different stages of the menstrual cycle or from women who were taking oral contraceptives (*131*). In women taking oral contraceptives the levels of synthetic estrogen remain elevated over the time the drugs are administered. In individuals in the luteal phase and in those taking oral contraceptives (Fig. 2.13 F) a significant correlation was observed with the estrogen-responsive gene signature obtained from the ERalpha breast cancer cell line, MCF-7 (*140*). Interestingly, RSK2 mRNA levels were inversely correlated with the estrogen-responsive gene signature (Figs. 2.13 G, 2.14 E), which is consistent with the RSK2-KO data. This correlation was not driven by cell cycle genes (Fig. 2.14 F). We propose that individuals who take oral contraceptives are subject to prolonged estrogen-responsive gene expression in comparison to individuals who are normally cycling.

Figure 2.13 RSK2 is necessary for alveolar expansion. (A) RSK2-KO NCL cells show a decrease in proliferation as compared to the WT. RSK2-KO or WT MECs were used to regenerate the mammary gland in a WT mouse. These mice were staged in proestrus and administered 5-ethynyl-2'-deoxyuridine (EdU) throughout one estrus cycle. The mammary glands were isolated and analyzed by FACS (n=3 glands/genotype; paired Student's t-test). (B) RSK2 regulates eEF2K activity in vivo (median ± quartile, n ≥ 3 mice/genotype, ≥ 5 fields/mouse, Student's t-test). (C) Inhibition of RSK1/2 decreases translation in vitro. Serum starved TM3 were treated for 6 h with vehicle or C5" (20 microM). The range was normalized to the o-propargyl-puromycin (*84*) in the absence and presence of C5" (mean, n ≥ 3, >150 cells/condition/experiment, one-way ANOVA with Holm-Sidak's correction for multiple comparisons). (D) Alveolar expansion is reduced in RSK2-KO dams as shown by H&E stains of mammary glands isolated from dams 1 d after birth (median ± quartile, n ≥ 3 mice/genotype, ≥ 3 fields/mouse, Student's t-test). Scale bar = 1 mm. (E) Pups nursed by RSK2-KO dams are smaller than those nursed by WT dams. Weanling weight at 21 d nursed by a dam with the indicated genotype (median ± quartile, n=3 litters matched for size/dam genotype, one-way ANOVA with Holm-Sidak's correction for multiple comparisons). (F) The estrogen-regulated signature is enriched in the luteal phase or with oral contraceptive use. Cumulative patient Z-scores were generated for each individual by summing individual Z-scores of genes up regulated in estrogen-regulated signature and subtracting individual Z-scores of genes down regulated (mean ± S.D., n=8, F=follicular, 3 L=luteal, 4=OC oral contraceptive, one-way ANOVA with Tukey's correction for multiple comparisons). (G) RSK2 mRNA levels are decreased in response to the luteal phase or oral contraceptives based on Z-score analysis as in (F). (H) Schematic illustrating maintenance of estrogen homeostasis by RSK2. See discussion for further explanation.

Figure 2. 13 RSK2 is necessary for alveolar expansion.
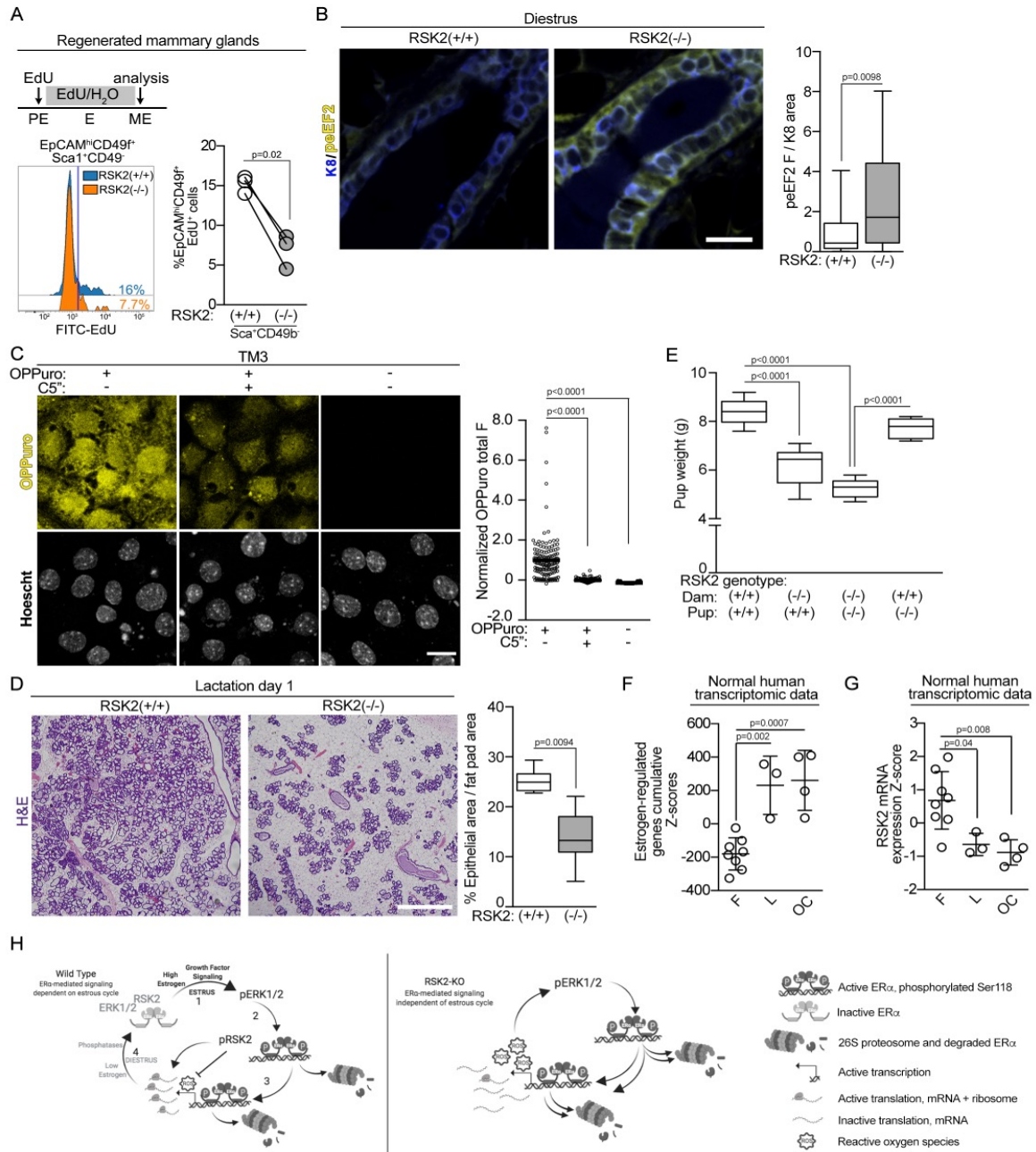
Figure 2.14 RSK2-KO dams fail to provide adequate nutrition for their pups. (A)

Fluorescence minus one strategy for determining the gate for FITC-EdU. (B) FACS analysis of

proliferation of mammary glands using RSK2-KO or WT MECs regenerated in a WT mouse.

(n=3 glands/genotype; paired Student's t-test). (C) Alveolar expansion is reduced in mammary

glands regenerated from RSK2-KO mammary epithelial cells as shown by the H&E stains of

mammary glands isolated from the same WT dam 1 d after birth. Scale bar = 1 mm. (D)

Representative images of WT and RSK2-KO pups at 21 d nursed by either WT or RSK2-KO

dams. (E) Heat map illustrating that estrogen-regulated signature is enriched in the luteal phase

and by oral contraceptive use. (F) Proliferation genes do not drive the enrichment for the

estrogen-regulated signature in individuals in the luteal phase or those taking oral

contraceptives. Cumulative Z-scores were generated for each individual by summing individual

Z-scores of genes up regulated in estrogen-regulated signature and subtracting individual Z-

scores of genes down regulated. (mean ± S.D., one-way ANOVA with Holm-Sidak's correction

for multiple comparisons) (Table 2.2).

Figure 2. 14 RSK2-KO dams fail to provide adequate nutrition for their pups.
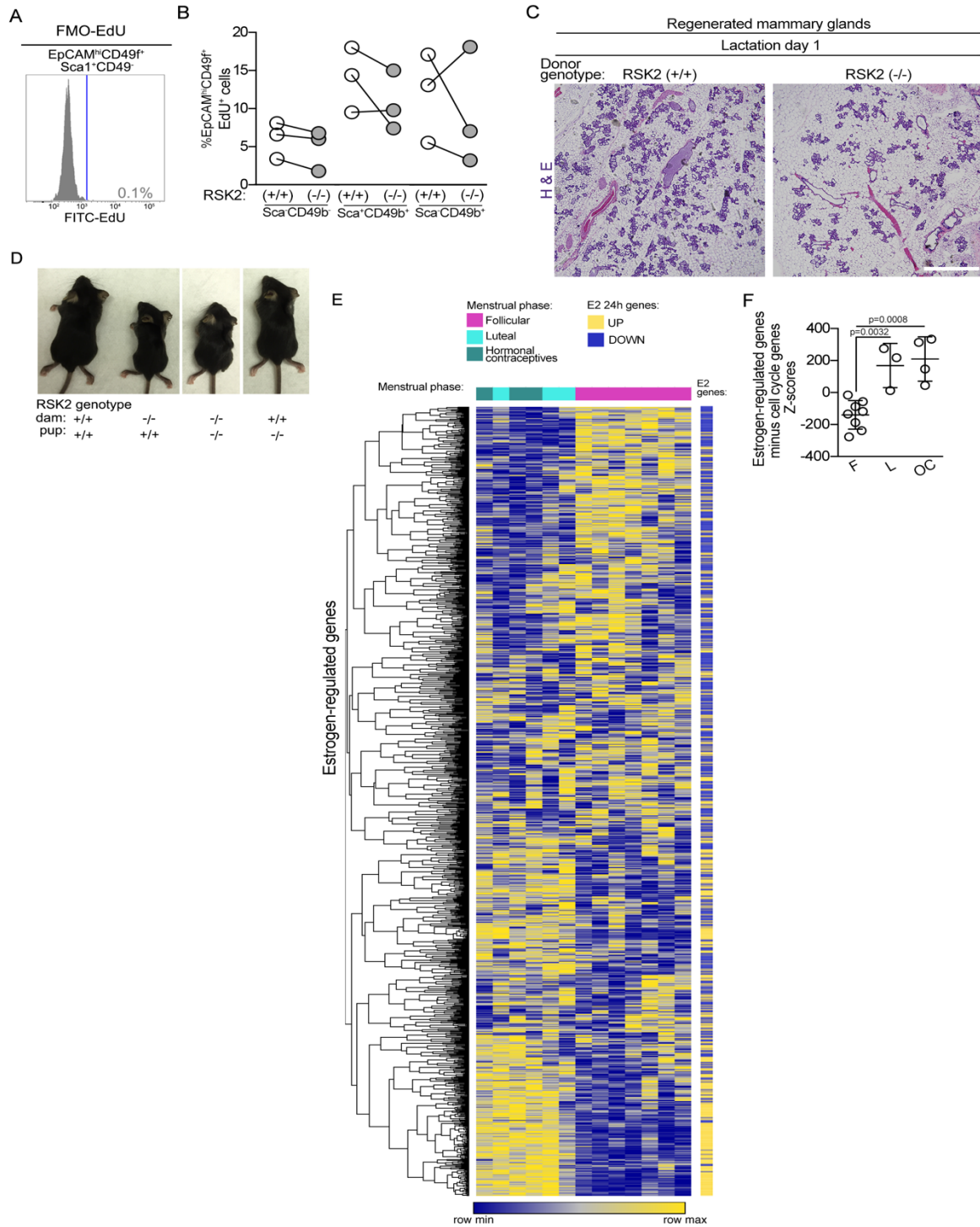
Discussion

All ER+ tissues respond to estrogen signaling and therefore, are subject to the normal fluctuations in the levels of estrogen that occur throughout the estrous cycle. The importance of estrogen signaling is highlighted by the numerous physiological alterations, which occur during menopause, oophorectomy or anti-estrogen therapy (*116*). Here, we provide the first evidence that growth factor signaling through the ERK1/2-RSK2 pathway is required to maintain cyclic estrogen responsiveness *in vivo*. In the schematic for the WT (Fig. 2.13 H, left) in step one, we propose that the estrogen pulse in proestrus activates growth factor pathway signaling. This hypothesis is based on observations in neuroendocrine tissues that ERK1/2 is activated after the estrogen surge (*155*). Consistent with these data we found in the mammary gland that ERK1/2 was activated in estrus and this activation was dependent on estrogen. The second step of the schematic shows we identified that ERK1/2 phosphorylates ERalpha to enhance degradation through the 26S proteasome pathway, as mutation of the ERK1/2 phosphorylation site, Ser-118, prevents ERalpha degradation. The most likely mechanism for the increased ERalpha turnover is through creation of a phosphodegron at Ser-118, which results in E3 ligase recruitment (*144*). In step three we determined that activated ERK1/2 drives ERalpha degradation to enhance estrogen-responsive gene expression. Additionally, activated RSK2, which regulates protein synthesis (*154*), was identified to be important in translation of the estrogen-mediated gene program. The physiological importance of RSK2 translational regulation is demonstrated by the reduced pup size and decreased fertility in the RSK2-KO females. We propose that the fertility defect is most likely explained by decreased translation in the glandular epithelium due to loss of RSK2, as estrogen-induced glandular secretions are known to be important for implantation (*156*). To reset the cycle we propose in step four that ERK1/2 is dephosphorylated and inactivated by phosphatases. This hypothesis is based on observations in neutrophils that estrogen upregulates expression of ERK1/2 phosphatases

(*157*) and our data demonstrating that total ERK1/2 protein levels do not vary with estrogen levels. The cycle is then reinitiated at the next proestrus.

In contrast to temporal activation of ERK1/2 during the estrus cycle we show in the schematic for the RSK2-KO (Fig. 2.13 H, right) the disruption of this homeostatic mechanism due to loss of RSK2. We determined that loss of RSK2 maintains activation of ERK1/2 in diestrus, which results in increased estrogen-responsive gene expression. We identified that loss of RSK2 resulted in elevated ROS levels and we hypothesize that this increased ROS inhibits phosphatase activity. This hypothesis is supported by studies showing that oxidation of the reactive site cysteine in ERK1/2 phosphatases results in their inactivation (*158, 159*). We speculate that the increased ROS is a result of elevated estrogen-responsive gene expression, which is known to occur (*151*), and to increased energy requirements. This later hypothesis is supported by gene ontology analysis of the NCL population at estrus which showed an over-representation of genes associated with the mitochondria. We conclude that RSK2 regulates estrogen-responsive gene expression by controlling redox homeostasis. These findings represent a previously unidentified function for RSK2. Negative regulation of estrogen-responsive gene expression by RSK2 was unexpected, as its contributions to ERalpha breast cancer are well established (*43, 128, 160*).

We show the importance of ERK1/2 in regulating ERalpha degradation in vivo. Phosphorylation of ERalpha at Ser-118 has been reported to occur by a number of different kinases and has been associated with increased ERalpha-mediated transcription in breast cancer cells (*38, 150, 161-165*). Furthermore, mutation of Ser-118 to Ala in an ectopic expression system prevented degradation (*166*). Numerous ubiquitin ligases have been reported to regulate ERalpha stability and components of the 26S proteasome are found in association with ERalpha on the chromatin in studies using breast cancer cells (*30*). It is unclear whether the degradation mechanism differs between breast cancer and normal

physiology as ERalpha protein levels are higher in breast cancer (*167*), which does suggest that the homeostatic mechanisms have been disrupted.

We also report the analysis of gene expression in the purified NCL population. Relatively few differences in DEG were detected in the WT between estrus and diestrus as compared to the RSK2-KO. We propose that the increased gene expression is driven by the continuous ERalpha transcriptional activation in response to activated ERK1/2 in the RSK2-KO. To accurately compare gene expression in the WT and RSK2-KO we developed a FACS protocol that permitted mixing the genotypes and sorting simultaneously. This approach eliminated artifacts due to differences in staining between preparations.

RSK2 regulation of estrogen responsiveness occurs in the mature gland but not during puberty. It is possible that unopposed estrogen action is required to facilitate the extensive remodeling of the gland that begins at puberty. However, in the adult this extensive proliferative response could lead to dysfunction and hyperproliferation within the gland. In human females we observed an inverse relationship between RSK2 mRNA levels, and an estrogen-responsive gene signature in the breast tissue of women in the luteal phase or on oral contraceptives. Consistent with these observations RSK2 mRNA levels also decreased in endometrial tissue of women in the luteal compared to the follicular phase (*168*). ERalpha protein levels are known to decrease in women taking hormone replacement therapy, suggesting increased ERalpha-mediated transcription-coupled degradation occurs in these individuals (*167*). We speculate that RSK2 levels are decreased in individuals in which normal estrogen levels are disrupted resulting in chronic activation of ERK1/2 and dysregulated estrogen-mediated transcription. This increase in estrogen-mediated signaling could lead to an increase in DNA damage as we observed in the RSK2-KO mice, and may account for the higher risk of breast cancer associated with the use of hormonal contraceptives and hormone replacement therapy (*23, 169-172*).

Chapter 3

RSK1/2 inhibition enhances doxorubicin-induced ERK1/2 activation to provide cardioprotection

Adapted from: (Sandusky et al., 2020, submitted: Journal of Molecular and Cellular Cardiology).

Abstract

The chemotherapeutic agent, doxorubicin, is a widely used and efficacious treatment for some types of breast cancers and leukemias. However, its usefulness is limited by cardiotoxicity. Doxorubicin activates ERK1/2 but the importance of this activation to the cardiotoxic effects observed with doxorubicin are not clear. The Ser/Thr protein kinases, RSK, are downstream effectors of ERK1/2, and are implicated in diminished cardiac function. We found that RSK1/2 inhibition and doxorubicin, together, potentiated ERK1/2 activity and prevented doxorubicin cardiotoxicity both in vitro and in vivo. Inhibition of ERK1/2 was unable to rescue doxorubicin-induced cardiotoxicity. The efficacy of doxorubicin to reduce the viability of breast cancer cells was not diminished by RSK1/2 inhibition. These results demonstrate that in cardiomyocytes RSK over rides the anti-apoptotic activity of ERK1/2 in the presence of doxorubicin. This mechanism is not present in breast cancer cells. Thus agents that inhibit RSK have the potential to reduce doxorubicin-induced cardiotoxicity while maintaining the potency of doxorubicin as a chemotherapeutic.

Introduction

Doxorubicin (*131*), an anthracycline antibiotic, is used to treat approximately one million

cancer patients per year, primarily with breast cancer and leukemia (*173*). DOX is correlated

with cardiotoxicity in 3-26% of treated patients. Dexrazoxane (DXZ) is the only FDA-approved

agent for prevention of DOX-induced cardiotoxicity. DXZ, an EDTA-derivative, is thought to act

by chelating iron to prevent the futile cycle between iron and DOX that results in toxic

superoxide radicals. The clinical use of DXZ has been limited based on side effects and reports

that it reduces DOX efficacy (*174*). Beta-blockers, ACE inhibitors and angiotensin receptor

blockers have also been used prophylactically to prevent DOX cardiotoxicity but their efficacy in

ameliorating cardiac dysfunction remains controversial (*173*). DOX is an extremely effective

chemotherapeutic agent and identifying whether a targetable pathway exists to ameliorate DOX-

induced cardiotoxicity is a major goal for improvement of cancer patient outcomes.

ERK1/2 activity is crucial for cardiac homeostasis as demonstrated by the observations

that an increase in cardiovascular adverse events (CVAEs) is associated with melanoma

patients treated with BRAF and MEK1/2 inhibitors. However, these results seem at odds with

the observations that DOX treatment activates ERK1/2 and has been implicated as a possible

mechanism for DOX-induced cardiotoxicity (*175*). To better understand these conflicting

observations, we focused on RSK, a family of Ser/Thr kinases, which are downstream effectors

of ERK1/2. RSK has not been associated with chemotherapeutic-induced CVAEs but is

activated in failing hearts (*176*). Additionally, over expression of RSK in the hearts of transgenic

mice increases their susceptibility to cardiac damage (*177*). Based on these studies we

hypothesized that active RSK contributes to DOX-induced cardiotoxicity. Consistent with this

hypothesis we demonstrated that RSK1/2 inhibition decreased DOX-induced cardiotoxicity in

vitro and in vivo. RSK1/2 inhibition enhanced DOX-induced activation of ERK1/2 in neonatal rat

ventricular cardiomyocytes (NRVMs) but not in breast cancer cell lines. These observations are

consistent with the importance of ERK1/2 in maintaining cardiac function. Reduced RSK1/2

102

activity further decreased breast cancer cell line viability in the presence of DOX. We propose

that RSK1/2 inhibition can be used to protect the heart from DOX-induced cardiotoxicity by

enhancing ERK1/2 activity in cardiomyocytes, while preserving the efficacy of DOX as a

chemotherapeutic agent.

Materials and methods

Mice

All procedures involving mice were performed in accordance with current federal (NIH Guide for

Care and Use of Laboratory Animals) and university guidelines as approved by the Vanderbilt

University Institutional Animal Care and Use Committee. Female, adult (12 week), wild-type

C57BL/6J mice (Jackson Laboratory, stock #000664) were randomized by initial body weight

and monitored for changes in weight weekly during treatment.

DOX-induced cardiotoxicity

Mice were treated with IP injection of 5 mg/kg DOX (Sigma, #D1515) or vehicle (saline) and 40

mg/kg C-5"-n-propyl cyclitol SL0101 (C5") (114) or vehicle (1 part DMSO and 9 parts 25%

hydroxypropyl-beta-cyclodextrin in H2O). Mice were treated with C5" or vehicle 2 h before DOX

and 24 and 48 h after DOX. This treatment schedule was performed each week for five weeks.

Left ventricle M-mode echocardiography measurements were acquired with a Vevo 2100

Imaging System. Echocardiograms (178) were performed on non-anesthetized mice by the

Vanderbilt Cardiac Pathophysiology Core.

For tissue analysis, animals were euthanized, and organs were fixed in 10% neutral buffered

formalin for 2 d and stored in 70% ethanol. The fixed tissues were paraffin embedded and

sectioned. Sections were deparaffinized, stained with Masson's trichrome (Vanderbilt

Translational Pathology Shared Resource), and imaged on a light microscope (OMAX,

#M83EZ-C03S), digital camera (OMAX, # A35140U), and ToupeLite software (ToupTek).

Cardiomyocyte isolation and cell culture

NRVMs were isolated (179) and cultured in DMEM (Gibco, # 11885) supplemented with 7% heat-inactivated fetal bovine serum and 1% penicillin/streptomycin. The cells were plated on 10 mg/ml mouse tail laminin (Invitrogen, # 23017) coated dishes and cultured at 37oC and 5% CO2. Media changes occurred every 24 h and experiments performed on culture day three.

Cell viability assay

MDA-MB-231 and HDQ-P1 cell lines were obtained, cultured, and authenticated as directed by the American Type Culture Collection (ATCC) or by the German Collection of Microorganisms and Cell Culture, respectively.

For viability assays, $7x10^4$ NRVMs or $4x10^3$ HDQ-P1s or $4x10^3$ MDA-MB-231s were seeded per well of a 96 well plate. Cells were treated with the indicated concentration of each agent or vehicle (DMSO). NRVM viability was measured at 30 h and cancer cell proliferation was measured at 48 h using CellTiter-Glo Luminescent Viability Assay Kit (Promega, # PRG7572) and a GloMax Discover reader with Glomax Discover v3.0 software (Promega).

ATP assay

For cellular ATP measurements, $7x10^4$ NRVMs were seeded per well of a 96 well plate. Cells were treated with the indicated drug concentration or vehicle (DMSO) for 16 h and ATP measured using CellTiter-Glo Luminescent Viability Assay Kit. Proliferation in the controls cells was not observed over this time frame. Trametinib (Selleck Chem, # S2673) and BI-D1870 (Enzo Life, # BML-EI407) were dissolved in DMSO and used at the indicated concentrations.

ROS assay

$1.5x10^5$ NRVMs were seeded per well of an 8 well LabTek (Thermo Fisher # 155409). Cells were treated with the indicated concentration of each drug for 16 h, washed, and incubated for 30 min in the dark at 37oC with 10 mM H2DCFDA (Invitrogen cat# D399). After staining, cells were washed and returned to the incubator for 5 min before live cell imaging on a Nikon Eclipse Ti widefield microscope using Volocity software v6.2.1 (Quorum Technologies).

Western blot

For western blot analysis, 2x106 NRMVs, 3.5x105 HDQ-P1s or 3.5x103 MDA-MB-231s were seeded per 6 cm dish. Pretreatment with C5" at the indicated concentration for 2 h was followed by treatment with the indicated concentration of DOX or epirubicin (EPI) for 14 h. Cell lysates were collected, normalized for total protein, electrophoresed by SDS-PAGE and immunoblotted. Primary antibodies; anti-phospho RSK (T359/S363) (Santa Cruz Biotechnology, # SC12898), anti-phospho (pTEpY) ERK1/2 (Promega, # V803A), anti-RSK1 (Santa Cruz Biotechnology, # SC231), anti-ERK1/2 (BD Biosciences, # 610123), anti-cleaved PARP (Cell Signal Technology, # 9542), and anti-Ran (BD Biosciences, #610341).

Immunofluorescence

1x106 NRVMs were seeded per well of a 12 well plate on sterile coverslips coated with mouse 10 mg/ml laminin (Invitrogen, # 2301715). Cells were treated with the indicated concentrations of each agent or vehicle (DMSO). Cells were fixed in 4% paraformaldehyde (pH 7.4) in phosphate buffered saline (PBS) for 15 min, permeabilized in 0.05% Triton X-100 in PBS for 15 min and blocked ON at 4oC in 10% bovine serum albumin (BSA) in PBS. Cells were incubated with gH2AX (Ser139) antibody (Millipore, # 05-636) ON in the dark at 4oC followed by a rabbit anti-mouse Alexa Fluor 488 (Thermo Fisher, #A-11059). DNA was stained with 2 mg/ml Hoescht 33342 (Thermo fisher, #H1399) Images were collected with a laser-scanning microscope (LSM 510/META/FCA, ZEISS) and ZEN software (ZEISS).

Quantification and statistical analysis

Image analysis was performed using Openlab 5.5.0 (Agilent) or ImageJ64 (National Institute of Health) software. Statistical analysis was performed using Prism 6 (GraphPad) software. The statistical test used is reported in the figure legends. Only significant p-values are shown.

Results

Inhibition of RSK1/2 activates ERK1/2 to protect rat neonatal cardiomyocytes from doxorubicin toxicity

In agreement with the literature DOX activated ERK1/2 as determined by an antibody that detects the MEK1/2-catalyzed phosphorylation within the ERK1/2 activation motif (pERK1/2) in isolated NRVMs (Fig. 3.1 A) (*180*). Epirubicin (EPI), a doxorubicin derivative that reportedly has fewer cardiotoxicity side effects, also activated ERK1/2 (Fig. 3.1 A). As expected, DOX decreased the viability of NRVMs (Fig. 3.1 B). RSK was also activated in response to DOX and EPI as determined by an antibody that detects RSK autophosphorylation, which is necessary for its catalytic activity (pRSK). Activation of RSK occurred in response to ERK1/2 activity as shown by the MEK1/2 inhibitor, trametinib (Tram). We recently developed a specific inhibitor of RSK1/2, *C*-5"-*n*-propyl cyclitol SL0101 (C5"), which demonstrates *in vivo* efficacy against breast cancer metastasis (*115*). *C*5" decreased basal RSK activation and prevented the DOX-induced increase in RSK activation (Fig. 3.1 A). RSK1/2 inhibition in combination with DOX or EPI further increased ERK1/2 activity above that observed with DOX. *C*5" rescued viability in the presence of DOX in a dose dependent manner (Fig. 3.1 B). DOX decreased viability by induction of apoptosis, as shown by cleaved PARP (Fig. 3.1 C). C5"in the presence of DOX prevented PARP cleavage (Fig. 3.1 C), indicating that RSK1/2 inhibition acts to protect cardiac cells from DOX-induced apoptosis. Taken together, these data suggest that it is RSK1/2 activity and not ERK1/2 activity that mediates DOX-induced cardiotoxicity. These data may reconcile the disparate observations on ERK1/2 involvement in DOX-induced apoptosis in cardiomyocytes, as the extent of RSK activation in these various studies was not determined (*175*).

Increased reactive oxygen species (ROS) levels are thought to be an important mechanism of DOX-induced cardiotoxicity (*180*). The elevation in ROS results from redox

cycling of DOX with intracellular iron, which disrupts mitochondrial oxidative respiration. To determine whether RSK1/2 facilitates this mitochondrial toxicity live cell imaging with the indicator dye, H2DCFDA was used to measure ROS levels. DOX increased ROS levels nearly eight-fold but RSK1/2 inhibition in combination with DOX restored ROS levels to basal levels (Fig. 3.1 D). DOX decreases mitochondrial respiration (*181*) and consistent with those data ATP levels were reduced by DOX treatment but rescued by *C5"* (Fig. 3.1 E). A structurally distinct RSK inhibitor, BI-D1870 (*148*), also rescued ATP levels in the presence of DOX. MEK1/2 inhibition was unable to restore ATP levels, which is consistent with the observations that ERK1/2 activity is important for cardiac homeostasis.

The pleiotropic mechanisms of DOX-associated cardiotoxicity include the intercalation of DOX with DNA and stabilization of a ternary complex consisting of topoisomerase 2b, which results in DNA damage (*182*). DOX increased the number of cells staining for gH2AX, a marker of DNA double stranded breaks, and *C5"* was able to reduce this damage (Fig. 3.1 F). Importantly, as observed by the nuclear staining, DOX levels were not decreased in response to RSK1/2, which eliminates the possibility that RSK1/2 protects cardiomyocytes by limiting their exposure to DOX. We propose that the increase in ERK1/2 activity that occurs in the presence of DOX and RSK1/2 inhibition aids in protecting cardiomyocytes.

Targeted therapies are currently not available for triple negative breast cancer (TNBC) and DOX is currently part of a first line treatment regimen (*183*)). Therefore, we evaluated the efficacy of *C5"* in combination with DOX in the TNBC cell lines, HDQP-1 and MDA-MB-231. HDQP-1 cells are ~ five-fold more sensitive to inhibition of proliferation by *C5"* than MDA-MB-231 cells (*115*). Importantly, the combination of *C5"* and DOX resulted in loss of viability in both lines (Fig. 3.1 G). DOX activated ERK1/2 in both TNBC lines but in contrast to the cardiomyocytes the combination of *C5"* and DOX did not further increase ERK1/2 activation (Fig. 3.1 H). Overall, these pre-clinical observations show that *C5"* will not limit DOX anti-tumor efficacy, an important concern for DXZ.

Figure 3.1 RSK1/2 inhibition, but not MEK inhibition, protects neonatal rat ventricular cardiomyocytes (NRVMs) from DOX toxicity. A, RSK1/2 inhibition increases ERK1/2 activity in the presence of DOX or EPI. NVRMs were pre-treated with vehicle, C5" or Tram 2 h before DOX or EPI. The samples were normalized to the housekeeping protein, Ran or total ERK1/2 (n=2). B, RSK activity is required for DOX cardiotoxicity. The samples were treated as in A and normalized to the vehicle control (mean ± S.D., n=2 in quadruplicate, ANOVA with Tukey's correction for multiple comparisons). C, Inhibition of RSK1/2 prevents DOX-induced cleaved-PARP. Cells were treated and normalized as in A (n=2). D, RSK1/2 inhibition prevents DOX-induced ROS. Cells were treated as in A and the fluorescence intensity was normalized to the vehicle (n=1 in sextuplet, 6 fields/condition, ANOVA with Tukey's correction for multiple comparisons). Scale bar = 50 mm. E, DOX-induced decreased ATP levels are rescued by inhibition of RSK1/2. The samples were treated as in A and normalized to the vehicle control (n≥ 2 in triplicate except for BI-D1870, ANOVA with Sidak's correction for multiple comparisons). F, DOX-induced DNA damage is prevented by RSK1/2 inhibition. The samples were treated as in A (n=2 in duplicate, six images/ condition, > 44 cells/image, ANOVA with Tukey's correction for multiple comparisons). Scale bar = 50 mm. G, Inhibition of RSK1/2 does not protect TNBC lines from DOX toxicity. TNBC lines were pre-treated with vehicle or C5" before DOX and the data normalized to the vehicle control. (n=2 in triplicate, ANOVA with Dunnett's correction for multiple comparisons). H, RSK1/2 inhibition in combination with DOX does not potentiate ERK1/2 activity in TNBC lines. The samples were treated as in H and normalized to Ran (n=2, in duplicate).

Figure 3. 1 RSK1/2 inhibition, but not MEK inhibition, protects neonatal rat ventricular cardiomyocytes (NRVMs) from DOX toxicity.

109
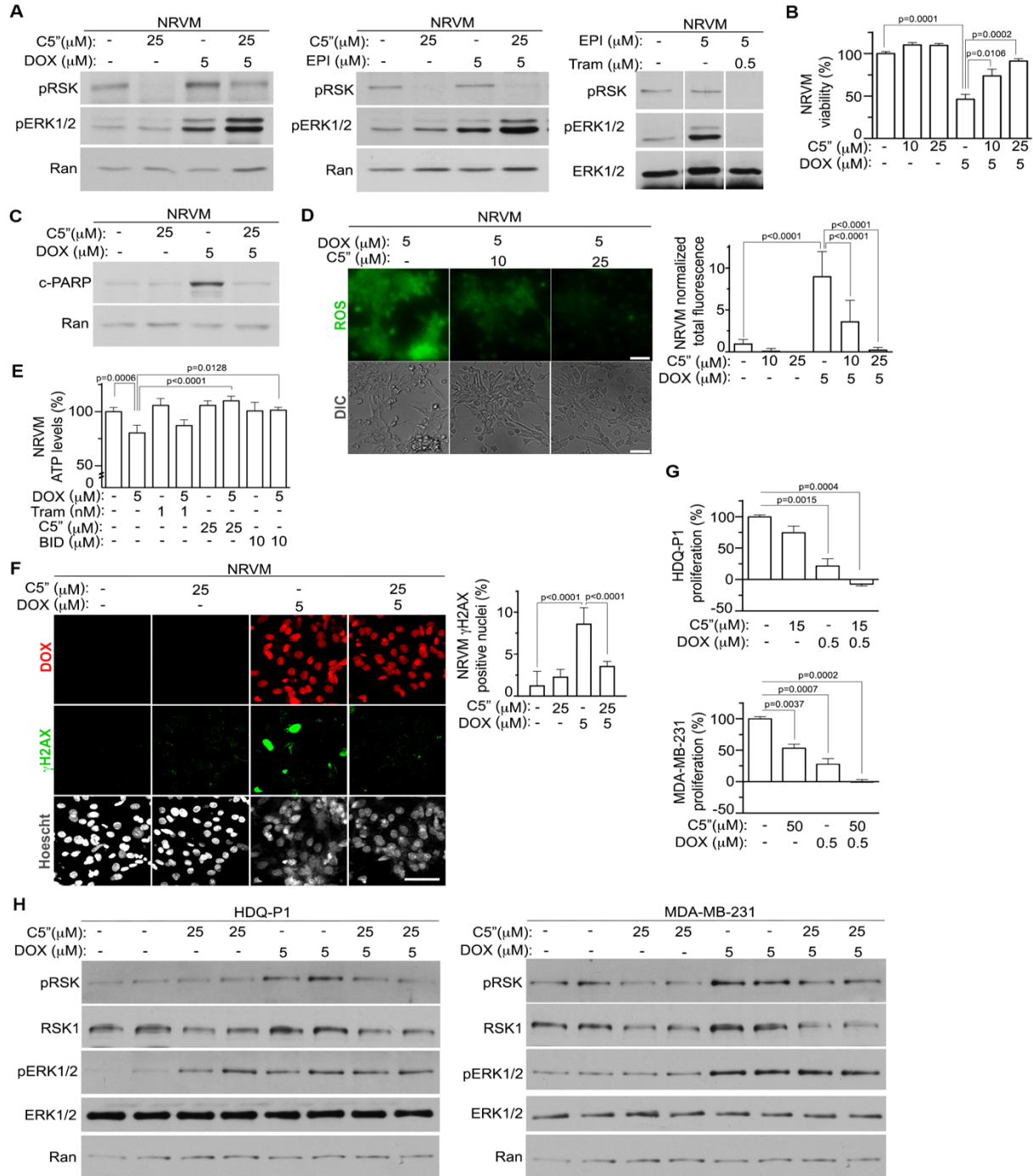
RSK1/2 inhibition prevents the doxorubicin-induced decrease in cardiac function in vivo

Based on the *in vitro* observations, the ability of RSK1/2 to limit DOX-induced CVAEs was investigated *in vivo*. *C*5" was administered 3 h before DOX treatment, which was followed by a second administration of *C*5" 24 and 48 h after DOX. This treatment regimen was repeated weekly for five weeks (Fig. 3.2 A). This dosing and scheduling regimen for DOX is known to reduce cardiac function (*182*). Two weeks after the final treatment, high-resolution echocardiography was performed on conscious mice (Fig. 3.2 B). In the control animals the values for the various measurements were similar to those reported on conscious animals (*184*) (Table 3.1). In the hearts of DOX-treated mice the left ventricle end-systolic volume (LVESV) was increased and the LV ejection fraction (LVEF) was decreased indicating that DOX impaired LV contractility function (Figs. 3.2C, D, Table 3.1). Consistent with these observations the LV anterior wall at systole was reduced (Fig. 3.2 E, Table 3.1). Importantly, mice treated with *C*5" prevented the DOX-induced impairment of LV cardiac function (Figs. 3.2 C, D, E, Table 3.1). DOX prevented the weight gain that occurred in the control animals and *C*5" was unable to restore the weight gain (Fig. 3.2 F). DOX is known to target the cells lining the intestine due to their rapid proliferation, and RSK1/2 inhibition does not prevent this damage but importantly does not exacerbate the effect. Treatment with *C*5" by itself resulted in an increased heart rate but had no effect on any of the other measured parameters (Figs. 3.2C, D, E, Table 3.1). At the end of the experiment hearts were collected and analyzed for evidence of histological damage. To assess damage we stained cardiac sections with Masson's Trichrome which stains fibrotic collagen fibers blue. Histological assessment showed no overt damage between any of the groups (Fig. 3.2 G).

Figure 3.2 Targeting RSK1/2 activity prevents DOX-induced disruption of cardiac function in vivo. A, Schematic representation of treatment schedule. B, Representative echo M-mode images from conscious mice after indicated treatments (n ≥ 3 mice/group). C, Inhibiting RSK1/2 prevents DOX-induced increase in left ventricle end systolic (LVES) volume but does not affect left ventricle end diastolic (LVED) volume. Each point represents a mouse. D, The DOX-induced decrease in cardiac ejection fraction is prevented by RSK1/2 inhibition. Each point represents a mouse. E, Inhibiting RSK1/2 prevents Dox-induced disruption of LV anterior wall (LVAW) systolic volume but does not affect LVAW diastolic volume. Each point represents a mouse. F, DOX prevents weight gain, which is not prevented by RSK1/2 inhibition. Weight change refers to the weight after the treatments versus to the start of the treatments. Each point represents a mouse. G, Masson's trichrome stain of representative cardiac sections from the different treatment groups. Cardiac cells (pink) and fibrous collagen fibers (blue) (n ≥3 mice/group). (PM = papillary muscle, LV Wall = left ventricle wall). Scale bar = 0.5 mm.

Figure 3. 2 Targeting RSK1/2 activity prevents DOX-induced disruption of cardiac function in vivo.

112
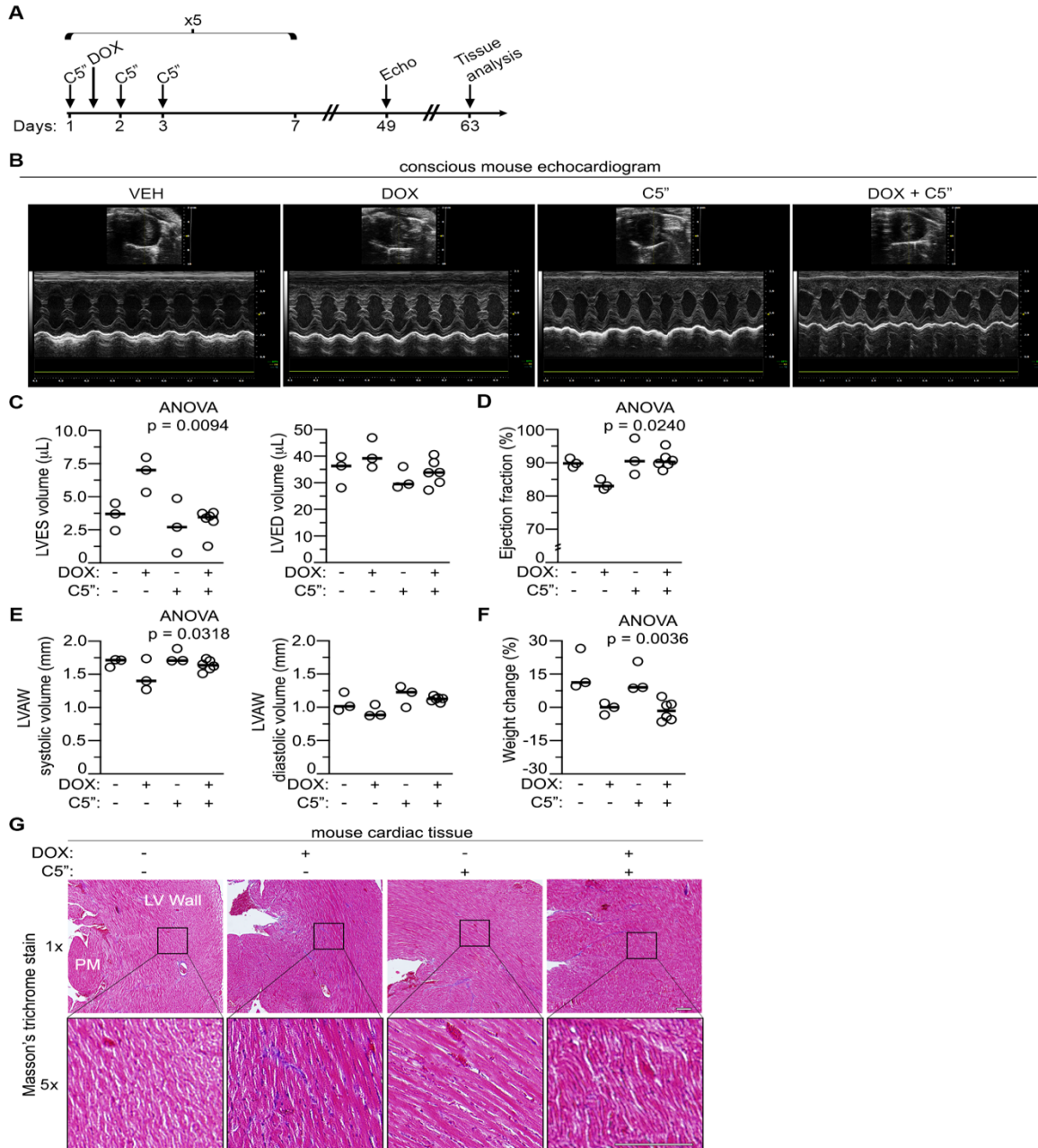
Table 3. 1: Echo summary table.

Treatment	Veh			DOX			C5"			DOX + C5"			
	AVG	SD	N	AVG	SD	N	AVG	SD	N	AVG	SD	N	ANOVA (p)
Heart Rate (BPM)	670.04	8.47	3	638.34	40.57	3	712.48	13.25	3	678.52	13.73	6	0.0086
Diameter; s (mm)	1.21	0.14	3	1.56	0.12	3	1.05	0.34	3	1.15	0.16	6	0.0380
Diameter; d (mm)	2.98	0.22	3	3.18	0.18	3	2.86	0.15	3	2.95	0.17	6	NS
Volume;s (*185*)	3.55	1.04	3	6.77	1.33	3	2.78	2.06	3	3.15	0.95	6	0.0094
Volume;d (*185*)	34.78	6.02	3	40.69	5.68	3	31.40	4.13	3	33.89	4.83	6	NS
Stroke Volume (*185*)	31.23	4.99	3	33.92	4.48	3	28.62	2.74	3	30.74	4.30	6	NS

Ejection Fraction (%)	89.95	1.33	3	83.43	1.54	3	91.49	5.54	3	90.79	2.60	6	0.0240
Fractional Shortening (%)	59.55	1.83	3	51.10	1.65	3	63.48	10.58	3	61.24	4.48	6	NS
Cardiac Output (mL/min)	20.92	3.29	3	21.53	1.40	3	20.37	1.58	3	20.88	3.18	6	NS
LV Mass (mg)	104.12	15.25	3	88.30	24.93	3	98.74	5.42	3	94.38	10.46	6	NS
LV Mass Cor (mg)	83.30	12.20	3	70.64	19.95	3	78.99	4.34	3	75.50	8.37	6	NS
LVAW;d (mm)	1.07	0.14	3	0.93	0.09	3	1.18	0.16	3	1.12	0.04	6	NS
LVAW;s (mm)	1.68	0.06	3	1.47	0.24	3	1.77	0.11	3	1.64	0.08	6	0.0318

LVID;d (mm)	2.96	0.20	3	3.09	0.24	3	2.75	0.23	3	2.85	0.19	6	NS
LVID;s (mm)	1.57	0.29	3	1.63	0.12	3	1.29	0.25	3	1.35	0.18	6	NS
LVPW;d (mm)	0.97	0.08	3	0.83	0.07	3	0.97	0.07	3	0.83	0.08	6	NS
LVPW;s (mm)	1.45	0.10	3	1.40	0.03	3	1.59	0.16	3	1.50	0.14	6	NS

Discussion

Taken together, our data supports a model in which active ERK1/2 is necessary for maintaining cardiac function whereas the ERK1/2 downstream effector, RSK, is responsible for chemotherapy-induced CVAEs. This hypothesis is based on the observations that RSK1/2 inhibition prevented DOX-induced cardiotoxicity *in vitro* and *in vivo* despite increasing ERK1/2 activity in cardiomyocytes. Furthermore, inhibition of ERK1/2 activity was unable to reduce DOX-induced cardiotoxicity. Reducing RSK1/2 activity inhibits proliferation of numerous breast cancer lines in vitro and in vivo (*115*) whereas no effect was observed with cardiomyocytes using similar doses of *C5*". Our data supports the continued development of RSK inhibitors for clinical use as RSK1/2 inhibition in combination with DOX will potentially reduce cardiotoxicity and improve patient outcome.

Chapter 4

Development of a RSK inhibitor as a novel therapy for triple-negative breast cancer

Adapted from: (115)

Summary

Metastatic breast cancer is an incurable disease and identification of novel therapeutic opportunities is vital. Triple-negative breast cancer (TNBC) frequently metastasizes and high levels of activated p90RSK (RSK), a downstream MEK-ERK1/2 effector, are found in TNBC. We demonstrate, using direct pharmacologic and genetic inhibition of RSK1/2, that these kinases contribute to the TNBC metastatic process in vivo. Kinase profiling showed that RSK1 and RSK2 are the predominant kinases targeted by the new inhibitor, which is based on the natural product SL0101. Further evidence for selectivity was provided by the observations that silencing RSK1 and RSK2 eliminated the ability of the analogue to further inhibit survival or proliferation of a TNBC cell line. In vivo, the new derivative was as effective as the FDA-approved MEK inhibitor trametinib in reducing the establishment of metastatic foci. Importantly, inhibition of RSK1/2 did not result in activation of AKT, which is known to limit the efficacy of MEK inhibitors in the clinic. Our results demonstrate that RSK is a major contributor to the TNBC metastatic program and provide preclinical proof of-concept for the efficacy of the novel SL0101 analogue in vivo.

Introduction

Metastatic breast cancer remains incurable, with therapy limited to slowing disease progression (*186*). In particular, triple- negative breast cancer (TNBC) patients have increased probability of death due to metastasis compared with other breast cancer subtypes (*187*). TNBC is characterized by its lack of currently available targeted markers. However, the MEK-ERK1/2 cascade is now considered as a viable drug target for TNBC (*188-191*). In genetic analysis of basal-like breast cancers, which includes ~70% of TNBCs, activated MEK-ERK1/2 signaling is thought to occur in ~80% of the tumors (*72, 188, 192*). In addition, numerous TNBC cell lines possess an activated RAS-transcriptional program and enhanced sensitivity to MEK inhibition (*185, 193*). In support of these preclinical observations, a complete response was observed in a phase Ib trial using a combination of trametinib, a MEK inhibitor, and gemcitabine, a nucleotide analogue, in a TNBC patient who had failed multiple therapies (*189*). Based on these data various MEK inhibitors are being tested in clinical trials, which include TNBC patients (*194*).

However, treating patients with drugs that inhibit "global regulators" such as MEK causes a number of side effects that result in limited efficacy (*194*). We postulate that inhibiting downstream effectors of MEK like the Ser/Thr protein kinase, p90RSK (RSK), will have fewer side effects because it controls a more limited set of targets. RSK phosphorylates various substrates that control diverse cellular processes, including metastasis (*98, 99, 195-197*). Approximately, 85% of TNBC patient samples have activated RSK, which is identified by the presence of phosphorylated residues critical for its activity (*198*). Taken together, these observations suggest that RSK is a viable target for TNBC.

RSK contains two nonidentical functional kinase domains referred to as the N-terminal (NTKD) and C-terminal (CTKD) (*137*). The CTKD functions to regulate RSK activation, whereas the NTKD, which belongs to the AGC kinase family, is responsible for substrate phosphorylation (*137*). In a screen of botanical extracts we identified the first RSK inhibitor, SL0101 (**1a**), which

118

was isolated from *Forsteronia refracta* (*99*). SL0101 is an extremely specific allosteric inhibitor for the NTKD (*99, 113, 199, 200*).

In addition to SL0101, other RSK inhibitors have been described. However, the currently available NTKD inhibitors are not RSK specific (*199*) (*201, 202*) (*203, 204*) or demonstrate poor pharmacokinetics (*205, 206*). Covalent inhibitors of the RSK CTKD (*207-209*), targeting autoactivation, are also available and have limited off-target effects. However, CTKD inhibitors do not inhibit an activated kinase and the autoactivation mechanism can be bypassed (*207*), suggesting that the clinical utility of CTKD inhibitors is limited.

Because of the selectivity of SL0101 for RSK we continue to improve its drug-like properties through extensive structure–activity–relationship (SAR) analysis. We have now identified a SL0101 analogue, *C5″-n*-propyl cyclitol SL0101 (**1b**), which retains specificity for RSK1/2 and is more potent in *in vitro* and cell-based assays than the parent compound. This improved analogue inhibits proliferation, survival in a nonadherent environment, and migration of TNBC lines but, unlike MEK inhibitors, does not activate the AKT pathway. Inhibition of RSK1/2 using (**1b**) or silencing RSK1 or RSK2 inhibited TNBC metastatic colonization *in vivo*. Moreover, (**1b**) was as effective as the FDA-approved MEK inhibitor, trametinib. Taken together, these results indicate that RSK1/2 are viable drug targets for TNBC metastasis.

Materials and Methods

Animals

Animal procedures had approval of the Vanderbilt University Institutional Animal Care and Use Committee. For in vivo metastatic models, NOD-SCID-IL2Rgamma (NSG) mice (6–8 weeks; Jackson Laboratory) were injected in the left cardiac ventricle with 1×10^5 cells/100 microL PBS. Mice injected with MCF-7 cells received a 17beta-estradiol pellet (0.36-mg 60-day release; Innovative Research of America). Mice bearing MCF-7 metastasis were injected

intraperitoneally with vehicle [10% (2-hydroxypropyl)-beta-cyclodextrin (HPBCD) in 10% DMSO] or (1b) (40 mg/kg) 2 hours prior to euthanasia (day 50). Mice injected with HDQ-P1-Luc were randomized and at 2 hours after injection were treated for 5 days with HPBCD, (1b) (40 mg/kg) intraperitoneally Q12 hours or trametinib (2 mg/kg; Santa Cruz Biotechnology, Inc.) intraperitoneally Q24 hours. For bioluminescence imaging, mice were injected intraperitoneally with RediJect d-Luciferin (1.5 mg; PerkinElmer, Inc.) and imaged with a Xenogen IVIS using Living Image acquisition software (Xenogen Corp.). For ex vivo imaging, organs were placed in d-Luciferin (150 microg/mL PBS). After imaging, tissue was fixed in 4% buffered formalin and paraffin-embedded.

In vitro cell assays

Cell lines were obtained and cultured as directed by ATCC or by German Collection of Microorganisms and Cell Culture. Stocks were prepared within one to two passages after receipt and new stocks thawed frequently and passaged <6 months. Authentication was based on growth rate, morphology, and absence of mycoplasma. Serum-starved cells were pretreated for 2 hours with vehicle or inhibitor. MCF-7 cells were treated with phorbol 12-myristate 13-acetate (PMA; Sigma) for 20 minutes. Cells were lysed as described previously (210).

For motility assays 2.5×105 cells were plated on fibronectin-coated (5 microg/mL; Corning) 2-chamber Lab Teks (Thermo Fisher Scientific). After 48 hours, cells were pretreated with vehicle or inhibitors for 2 h and scratched with a P200 pipette tip. After washing, HEPES (50 millimol/L; Thermo Fisher Scientific)-buffered media with vehicle or inhibitor was added and images taken every 20 minutes using Nikon Eclipse Ti microscope and an Orca R2 digital CCD camera (Hamamatsu). Migration velocity was quantified using Volocity software (PerkinElmer, Inc.). Additional details are in Supplementary Data.

For two-dimensional (2D) proliferation assays, 2×105 cells/well in 24-well or 103 cells/well in 96-well were seeded. For 3D proliferation, 1.5×103 cells/well in 96-well were plated in 2% matrigel (MG; Corning, Inc.) onto 100% MG. Inhibitor or vehicle was added and proliferation

was measured at 48 to 72 hours using CellTiterGlo reagent (Promega Corp.) with a GloMax Discover luminometer (Promega Corp.).

For survival assays, cells were seeded at 1.5×10^3 cells/well in 96-well poly-HEMA–coated plates (Corning, Inc.) and vehicle or inhibitors added and bioluminescence measured at 48 to 72 hours.

The IC50 values for proliferation and survival were determined using nonlinear regression analysis (GraphPad Prism version 6.0a).

Immunostaining

Section preparation and antibodies are listed in Supplementary Data. Fluorescent images were obtained with a laser-scanning microscope (510/Meta/FCS Carl Zeiss, Inc.). Objectives were: mouse tissue 40× Plan-Neofluar oil NA 1.3 (zoom 0.7×); human tissue 20× NA 0.8. Images were acquired using LSM-FCS software (Carl Zeiss, Inc.), quantitated using Openlab 5.5.0 (PerkinElmer, Inc.), and processed in Photoshop version CS6 version 13.0 (Adobe).

In vitro kinase assays

RSK2 kinase assays performed as described previously (210). The kinase screen was performed using the ZLYTE screen (Thermo Fisher Scientific, Inc.).

Statistical analysis

Statistical analyses (GraphPad Prism 6.0a) using the Mann–Whitney test (two-sided) unless indicated. *P < 0.05 was statistically significant.

Results

SL0101 analogue with improved in vitro *and cell-based efficacy*

In prior SAR studies of the flavonoid glycoside, SL0101 (**1a**), we determined that replacement of the C5-methyl group on the pyranose with an *n*-propyl moiety (**1c**), improved the IC_{50} by >25-fold but that the compound had limited aqueous solubility (*210*). In addition, we

121

determined that exchanging the rhamnose with a cyclitol (**1d**), improved the cell-based efficacy for inhibition of proliferation but this compound was not RSK specific (*211*). We hypothesized that combining the modifications would improve the potency for RSK inhibition while maintaining specificity for RSK. Consistent with our hypothesis *C5″-n*-propyl cyclitol SL0101 (**1b**) has a six-fold improved IC_{50} in an *in vitro* kinase assay for RSK inhibition compared to SL0101 (**1a**; Fig. 4.1 A). Furthermore, (**1b**) inhibited the proliferation in 2D culture of the estrogen receptor α–positive (ER^+) breast cancer line, MCF-7, with an IC_{50} of approximately 8 micromol/L versus approximately 50 micromol/L for SL0101 (Fig 4.1 B). Previously, we found that the proliferation of the immortalized but untransformed breast line, MCF-10A, is less dependent on RSK for proliferation than the MCF-7 line (*211*). Consistent with these observations, only a slight decrease in MCF-10A proliferation occurred at the highest concentrations of (**1b**) (Fig. 4.1 B). The efficacy of SL0101 diminishes after >48 hours in *in vitro* culture (*113*). One advantage in replacing the rhamnose with a cyclitol moiety is that the cyclitol should be resistant to acid catalyzed anomeric bond hydrolysis, which should increase stability. To test this possibility we incubated MCF-7 cells with (**1b**) (25 micromol/L) for varying lengths of time. In agreement with our rationale, only a minor increase in proliferation over a 96-hour time course was observed when MCF-7 cells were incubated with (**1b**) (Fig. 4.1C). In contrast, there was a 100% increase in proliferation from 48 to 96 hours in the presence of SL0101 (100 micromol/L). These data indicate that the modifications to generate the SL0101 analogue (**1b**) resulted in a more potent RSK inhibitor than the parent compound.

*Specificity of C5″-*n*-propyl cyclitol SL0101 (1b) for RSK1/2*

SL0101 (**1a**) is highly selective for RSK (*99, 199*) which is most likely due to the fact that SL0101 inhibits RSK by an allosteric mechanism (*200*). Therefore, to evaluate the specificity of (**1b**), we compared its ability to inhibit RSK substrates in comparison to SL0101 (**1a**). In agreement with previous results, SL0101 induces an increase in the phosphorylation of eukaryotic elongation factor 2 (p-eEF2) in MCF-7 cells, which also occurred with (**1b**) (Fig. 4.1

D). This increase is due to the activation of eEF2 kinase, which is inhibited by RSK (*143*).

Furthermore, both RSK inhibitors decreased the phosphorylation of Ser167-ERα, an important

marker for anti-estrogen responsiveness (*212*). SL0101 and (**1b**) also decreased the

phosphorylation of the ribosomal protein, S6 (pS6), a known RSK downstream effector (Fig. 4.1

E) (*91*). Previously, we identified that silencing RSK2 reduced cyclin D1 levels (*213*), and

consistent with these results RSK inhibition decreased cyclin D1 levels. In a more global

analysis, *in vitro* kinase assays were performed against a panel of 247 purified kinases, which

contained representatives from all kinase families (Fig. 4.2). At 10 micromol/L of (**1b**), RSK1 and

RSK2 were the top hits, with colony stimulating factor 1 receptor (CSF1R) and mitogen-

activated protein kinase kinase kinase kinase (MAP4K4) being inhibited by approximately 37%

compared with RSK2 (Fig. 4.1F). CSF1R regulates macrophage function, and inhibitors are

currently in development as cancer therapies. MAP4K4 is an endothelial protein kinase, and

inhibitors are being developed as antidiabetic drugs (*214*). Thus, the off-target effects of (**1b**)

are very limited. Neither of these off-target effects is viewed as problematic for further drug

development. Taken together, these data demonstrate that (**1b**) is very specific for RSK1/2.

RSK inhibition in vivo

The overall goal of our studies is to develop a RSK inhibitor for *in vivo* use. To evaluate

the ability of (**1b**) to inhibit RSK1/2 *in vivo*, we used an MCF-7 metastatic model because most

of our prior characterization of SL0101 was performed using this line. MCF-7 cells that stably

express luciferase (MCF-7-Luc) were introduced by intracardiac (IC) injection into NSG mice,

and metastasis were established for ~50 days. Before treatment we determined that the tumor

burden between animals was equivalent (Fig. 4.1 G). Two hours after treatment with (**1b**) or

vehicle, the animals were euthanized and the tibia isolated, as ER$^+$ tumors frequently

metastasize to the bone. Moreover, MCF-7 cells within the tibia were easily identified by their

positive staining with cytokeratin 8 (K8) (Fig. 4.1 H). The levels of the RSK target, pS6, were

123

decreased by >2.5-fold with (**1b**). These results demonstrate that (**1b**) is able to attain a

sufficient concentration to induce pharmacodynamic changes *in vivo*.

Figure 4.1 C5"-n-propyl cyclitol SL0101. (1b) shows improved potency compared to the parent compound. A, structure and IC50 for selected SL0101 analogues. B, efficacy of (1a) and (1b) in inhibiting proliferation of MCF-7 and MCF-10A cells. Symbol, mean ± SD (n ≥ 2, triplicate; *, P < 0.01 compared to vehicle). C, the in vitro stability of (1b) (25 millimol/L) is increased in comparison to (1a) (100 millimol/L). Bar, mean (n = 2, quadruplicate; *, P < 0.0001). D, analysis of lysates from MCF-7 cells pretreated with (1a), (1b), or DMSO for 2 hours and treated with or without 500 nmol/L PMA (20 minutes). E, representative images of MCF-7 cells treated as in D. Scale bar, 10 mm. Bar graph showing the decrease in pS6 (n ≥ 30 cells). F, representation of (1b) specificity in a kinase screen indicating percentage of inhibition at 10 mmol/L compared to RSK2. G, bioluminescence images of NSG mice at day 50 after IC injection with MCF-7-Luc cells. H, representative paraffin embedded tibia sections from mice in G treated with (40 mg/kg) or vehicle 2 hours prior to euthanasia. Scale bar, 40 mm. Bar graph showing the decrease in pS6 (n = 6 sections/mouse).

Figure 4. 1 C5"-n-propyl cyclitol SL0101 (1b) shows improved potency compared to the parent compound.
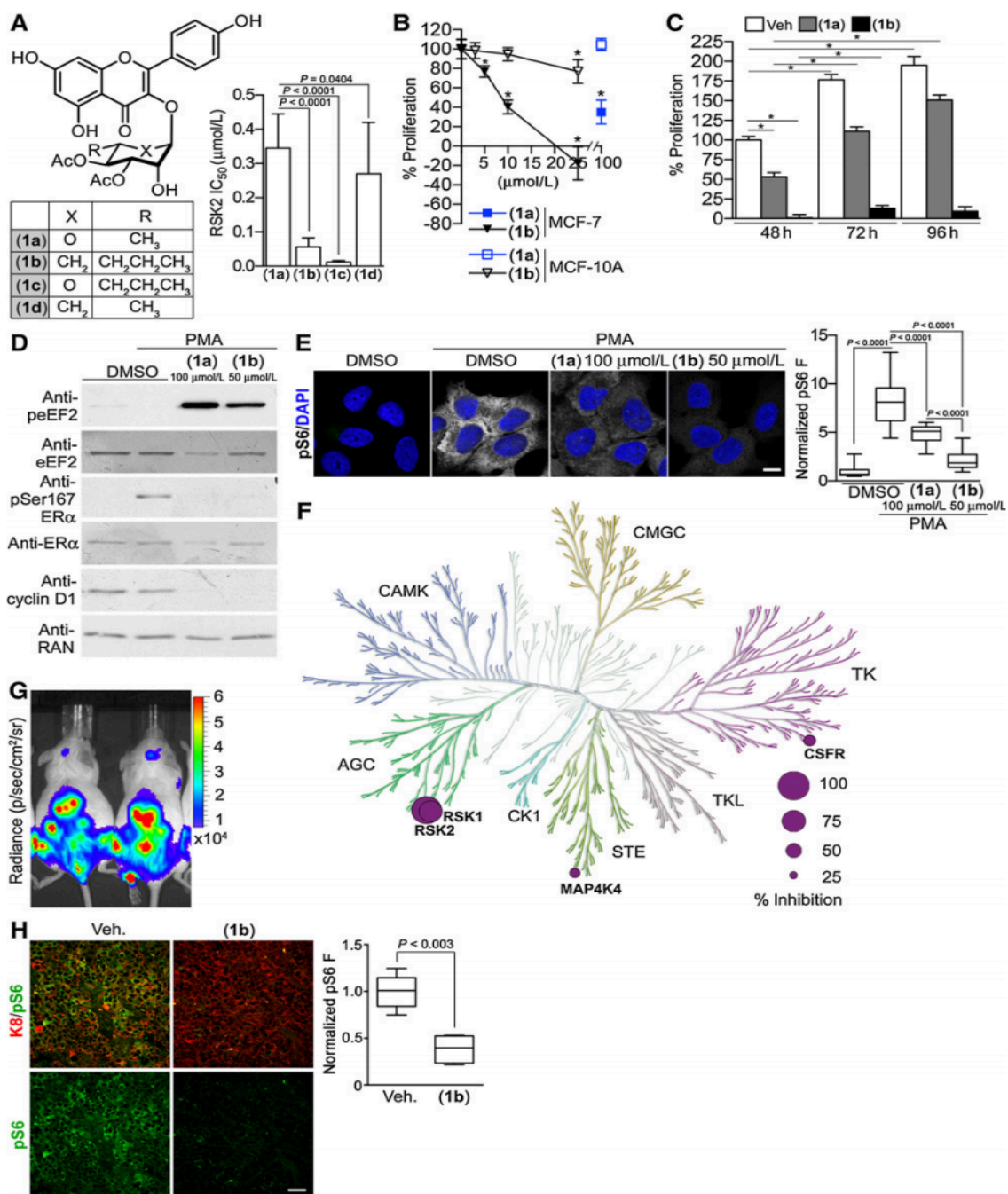
Figure 4.2 Schematic of the human kinome was reproduced courtesy of Cell Signaling Technology, Inc. (www.cellsignal.com). Kinases screened with (1b) are listed.

Figure 4. 2: Kinome screen with (1b) Chapter 4: Supp Fig 1

Figure S1
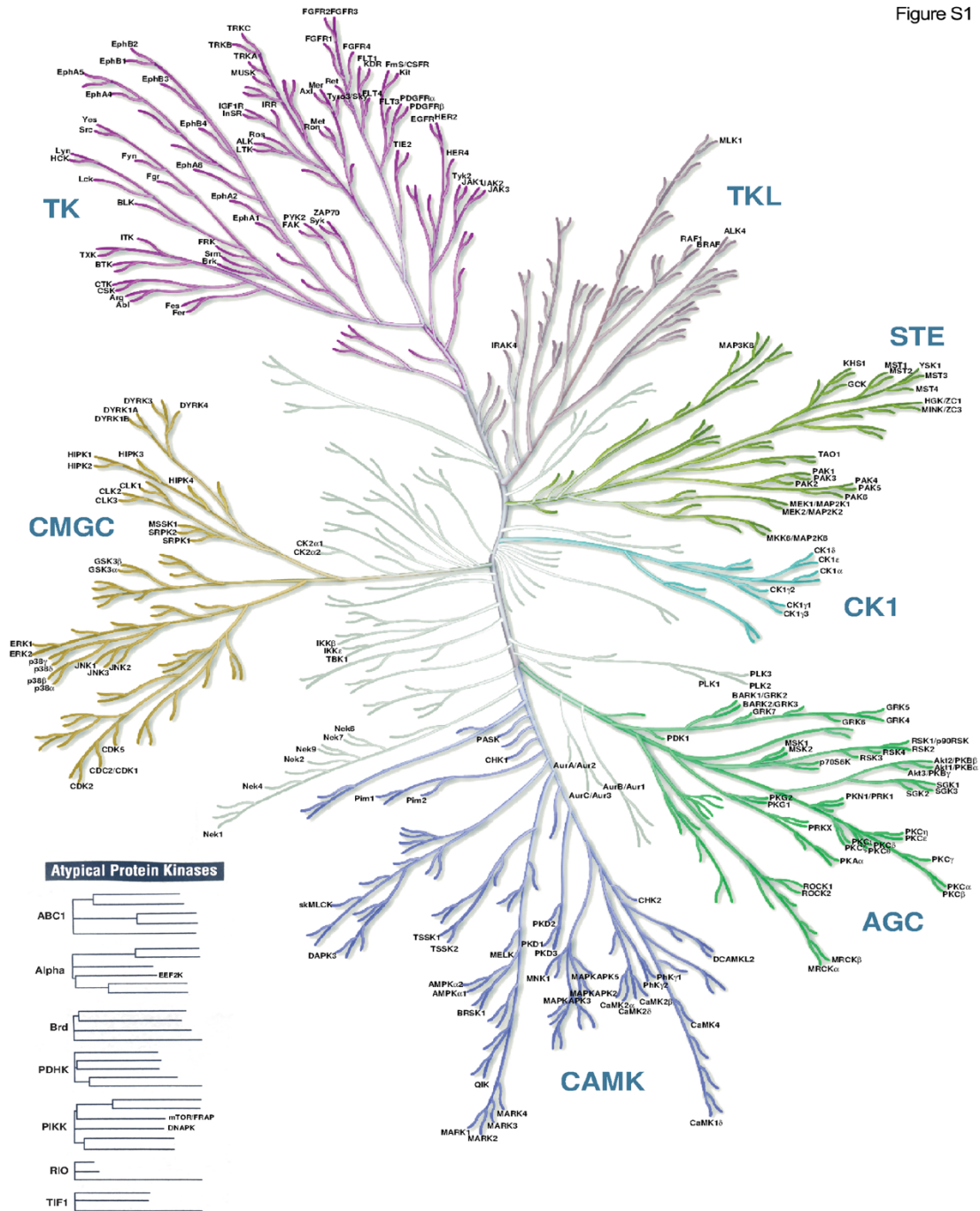
RSK as a drug target for TNBC

RSK has been proposed as a drug target for TNBC based on observations that ~85% of TNBC tumors have activated RSK. In agreement with these observations we found that the levels of activated RSK (pRSK) were higher in TNBC tumors than normal tissue (Fig. 4.3 A, B and Table 4.1). The levels of activated RSK varied considerably within and between tumors. Moreover, in TNBC tumor tissue-activated RSK could be present in the nucleus, cytoplasm, or both whereas it was mainly cytoplasmic in normal breast cells. The differences in subcellular localization suggest that the substrates regulated by RSK differ between normal and TNBC tissue. Taken together, these results are consistent with RSK as a viable drug target for TNBC.

To investigate whether activated RSK was functionally important in TNBC, we chose a panel of eight cell lines representing five different TNBC subtypes (*215*). We observed that activated RSK was present at different levels in these lines (Fig. 4.3 C, D). In 2D culture, the proliferation of all the TNBC lines was inhibited at a lower concentration of (**1b**) than SL0101 (**1a**) (Fig. 4.4 A). The lines from the mesenchymal subtype, CAL-120 and MDA-MB-231, were relatively resistant whereas the basal-like 2 (BL2), HDQ-P1, and HCC70 were among the most sensitive (Fig. 4.5 A). The BL2 lines are of interest clinically because this subtype is correlated with the poorest response to neoadjuvant chemotherapy (*216*). To better understand these observations, we compared the levels of activated RSK normalized to total RSK1 and RSK2, which should reflect RSK1/2 specific activity (Fig. 4.3 E). The anti-RSK2 antibody is less sensitive than the anti-RSK1 antibody and this difference was accounted for by normalizing to recombinant proteins. We observed an inverse relationship between the IC_{50} for (**1b**) and the specific activity of the combined isoforms (Supplementary Fig. S2B), consistent with the hypothesis that higher RSK specific activity increases sensitivity to the inhibitor. In a separate analysis, active RSK was normalized to RSK2 or RSK1 separately and a statistically significant inverse correlation was observed for RSK2 (Fig. 4.5 B).

Table 4.1 Patient statistics. Median age 53.

Table 4. 1 Patient statistics.

Patient ID	Race	Age
T1	Caucasian	64
T2	African-American	52
T3	Caucasian	28
T4	African-American	60
T5	Other	43
T6	African-American	56
T7	African-American	53
T8	Caucasian	55
N1	Caucasian	62
N2	Caucasian	39
N3	Caucasian	35

Figure 4.3 Active RSK in TNBC. A, activated RSK levels are increased in TNBC. Bar, median

± quartile (n ≥ 5 field/tissue sample). B, representative paraffin-embedded sections of normal

breast and TNBC tissue stained for the cytokeratins 8 (K8), 14 (K14), and phospho-

Thr359/phospho-Ser363 RSK (pRSK). Scale bar, 20 mm. C, analysis of TNBC cell lysates

normalized using the housekeeping protein RAN. D, quantitation of the levels of pRSK

normalized to RAN (n = 3). E, comparison of pRSK relative to total RSK1 and RSK2 for various

TNBC lines. To control for antibody sensitivity, the levels of RSK1 and RSK2 were determined

using purified, recombinant protein.

Figure 4. 3 Active RSK in TNBC.
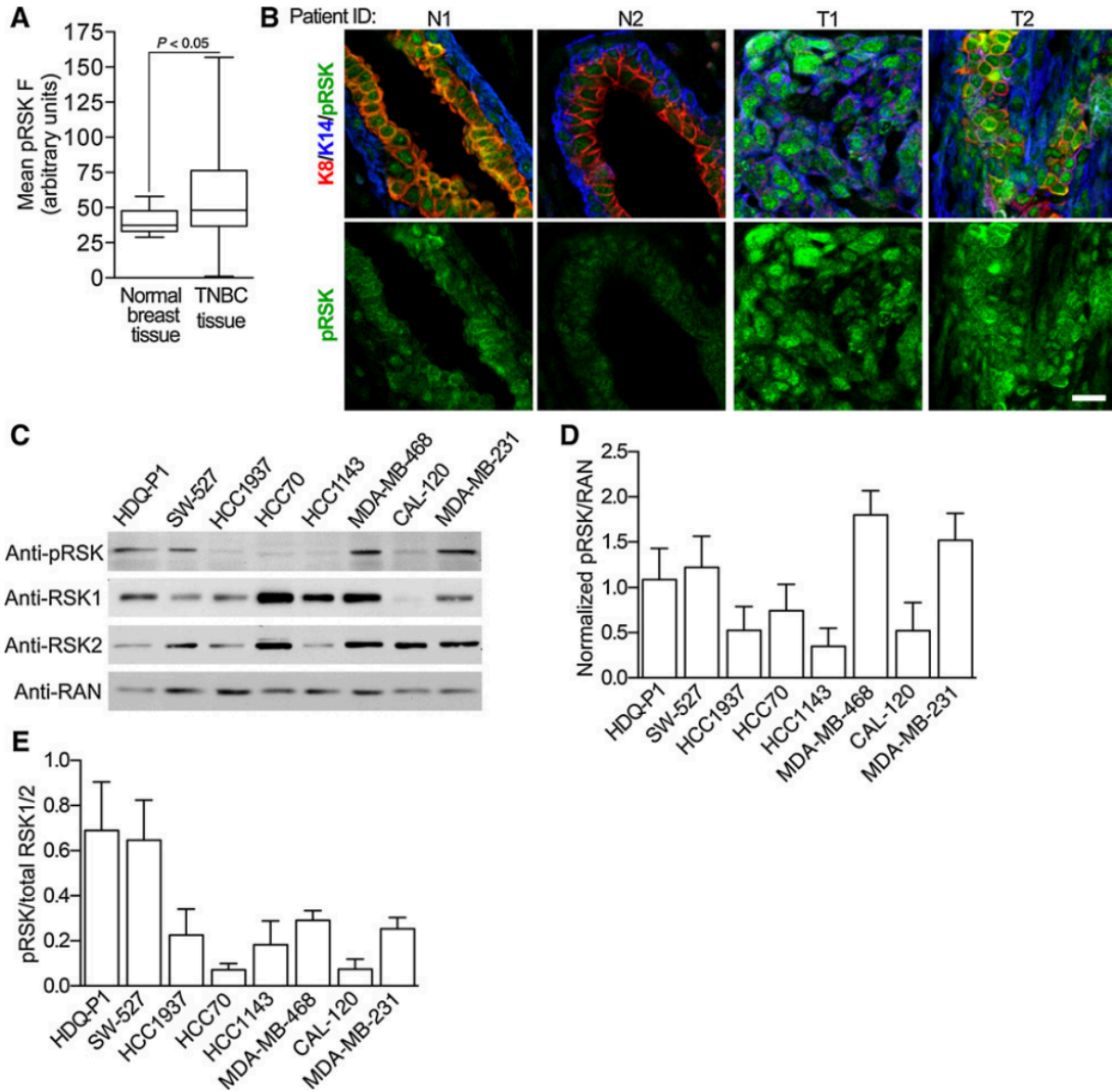
Figure 4.4 RSK is required for TNBC proliferation. (A) Efficacy of (1a) and (1b) in inhibiting proliferation of various TNBC lines. Symbol, mean ± S.D. (n ≥ 2, triplicate). (B) Correlation of IC50 for inhibition of proliferation by (1b) versus activated RSK normalized to total RSK1 and RSK2 levels.

Figure 4. 4 RSK is required for TNBC proliferation.

135
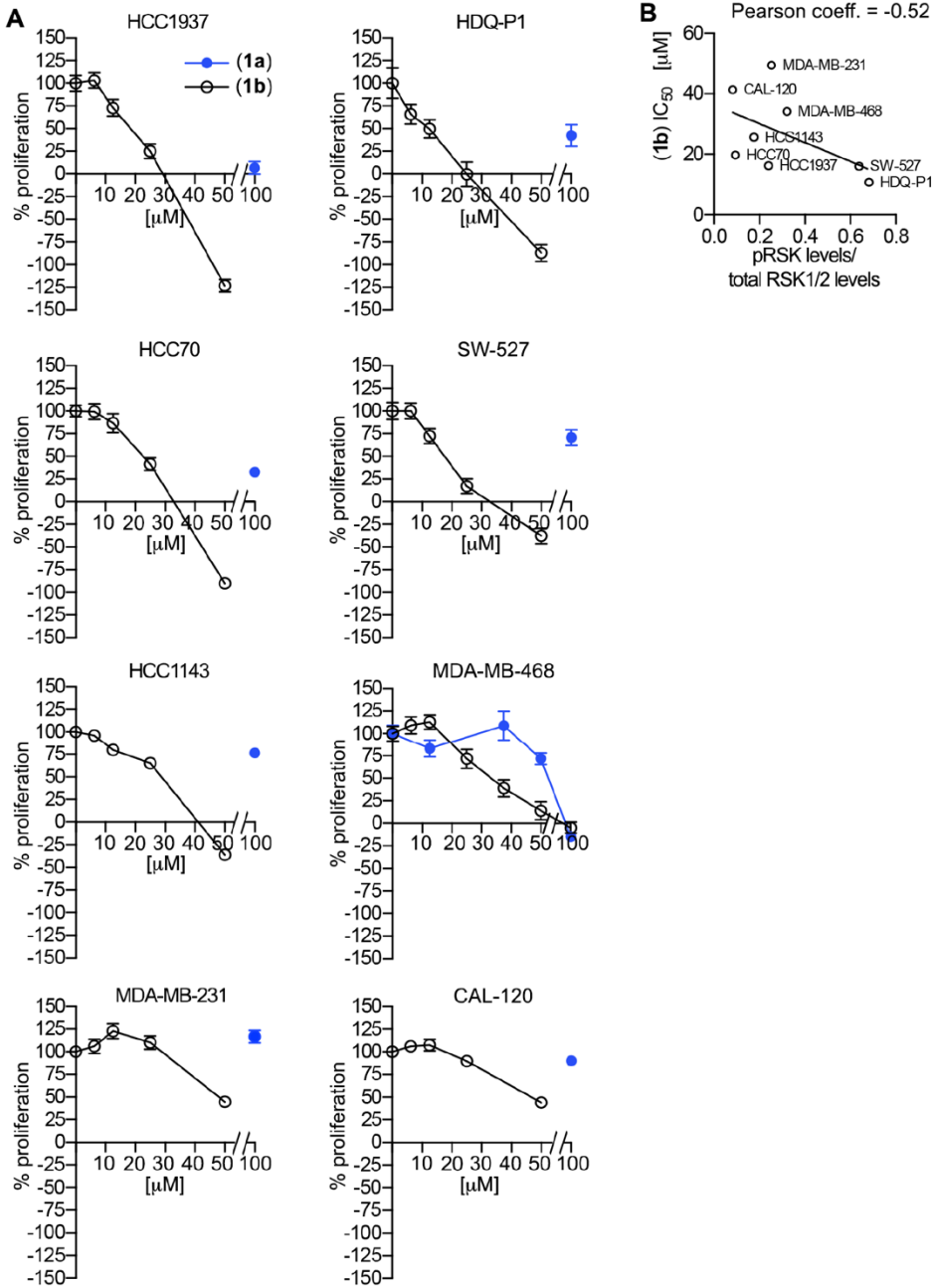
To evaluate specificity we investigated the efficacy of (**1b**) in the context of RSK1/2 silencing. As expected, loss of RSK1/2 decreased 2D proliferation by approximately 60% in MDA-MB-231 cells (Fig. 4.5 C, D). Importantly, silencing RSK1/2 resulted in loss of sensitivity to (**1b**) (Fig. 4.5 D). These results support the conclusion that (**1b**) is specific for RSK1/2 and also demonstrate that RSK1/2 are primarily responsible for regulating the proliferation of MDA-MB-231 cells.

Proliferation of the MDA-MB-231 line is reported to be more sensitive to RSK inhibition in 3D versus 2D (*205*). In agreement, we observed that the IC$_{50}$ for (**1b**) is approximately 8 micromol/L in 3D and approximately 50 micromol/L in 2D (Fig. 4.5 E). Surprisingly, HDQ-P1 and HCC70 were unable to proliferate in 3D, suggesting that these lines have more stringent requirements for proliferation than MDA-MB-231.

The ability of cancer cells to survive in circulation is an important step in metastasis and therefore, we analyzed survival in ultra-low adhesion plates. Survival of HDQ-P1, HCC70, and MDA-MB-231 was dependent on RSK and the IC$_{50}$ for inhibition of survival by (**1b**) was approximately 30, 15, and 3 micromol/L, respectively (Fig. 4.5 F). Silencing RSK1/2 in MDA-MB-231 cells decreased survival by approximately 75% and was not further inhibited by (**1b**) (Fig. 4.5 G). These results demonstrate that the survival of some TNBC lines depends on RSK and confirm that (**1b**) is a very specific RSK inhibitor.

RSK has been implicated in regulating motility (*99*) and we investigated this possibility using the scratch assay. In all lines tested, (**1b**) reduced cell velocity to the same extent as SL0101 but at lower concentrations (Fig. 4.5 H, I, J and Fig. 4.6 A, B, C and Supplementary Movies S1–S3 (available in online version)). The motility of HCC70 was reduced by approximately 50%, and in MDA-MB-231 and HDQ-P1 cells motility was decreased by at least 75%. Apoptosis was not detected with the doses and time course used in the scratch assay (Fig. 4.6 D). Taken together, our results demonstrate that inhibition of RSK by (**1b**) reduces

proliferation, survival in a nonadherent environment and motility, which are essential

components of the metastatic process.

Figure 4.5 RSK is required for TNBC proliferation, survival, and motility. A, IC50s for (1b) in MCF-7 and TNBC lines. Bar, median ± range (n ≥ 2, ≥ quadruplicate). B, correlation of IC50 for inhibition of proliferation by (1b) of TNBC lines versus activated RSK normalized to total RSK2 levels. C, analysis of lysates from MDA-MB-231 cells transduced with scramble (scrbl) or double transduced with RSK1/2 targeting shRNAs. Bar, nonrelevant lanes removed. ns, nonspecific. D, efficacy of (1b) in inhibiting proliferation of MDA-MB-231 cells transduced as in C. Symbol, mean ± SD (n ≥ 2, triplicate; *, P < 0.03 compared to vehicle). E, bar graph showing (1b) IC50 for MDA-MB-231 proliferation in 2D and 3D. Bar, median ± range (n ≥ 2, ≥ quadruplicate). F, IC50s for (1b) for survival of TNBC lines. Bar, median range (n 2, triplicate). G, efficacy of (1b) in inhibiting survival of MDA-MB-231 cells transduced as in B. Symbol, mean ± SD (n ≥ 2, triplicate; *, P < 0.01 compared to vehicle). Scatter plots showing efficacy of (1a) and (1b) in inhibiting motility of (H) MDA-MB-231, (I) HCC70, and (J) HDQ-P1. Each circle represents a cell trace. Bar, median (n ± 2, 30 cells/treatment).

Figure 4. 5 RSK is required for TNBC proliferation, survival, and motility.
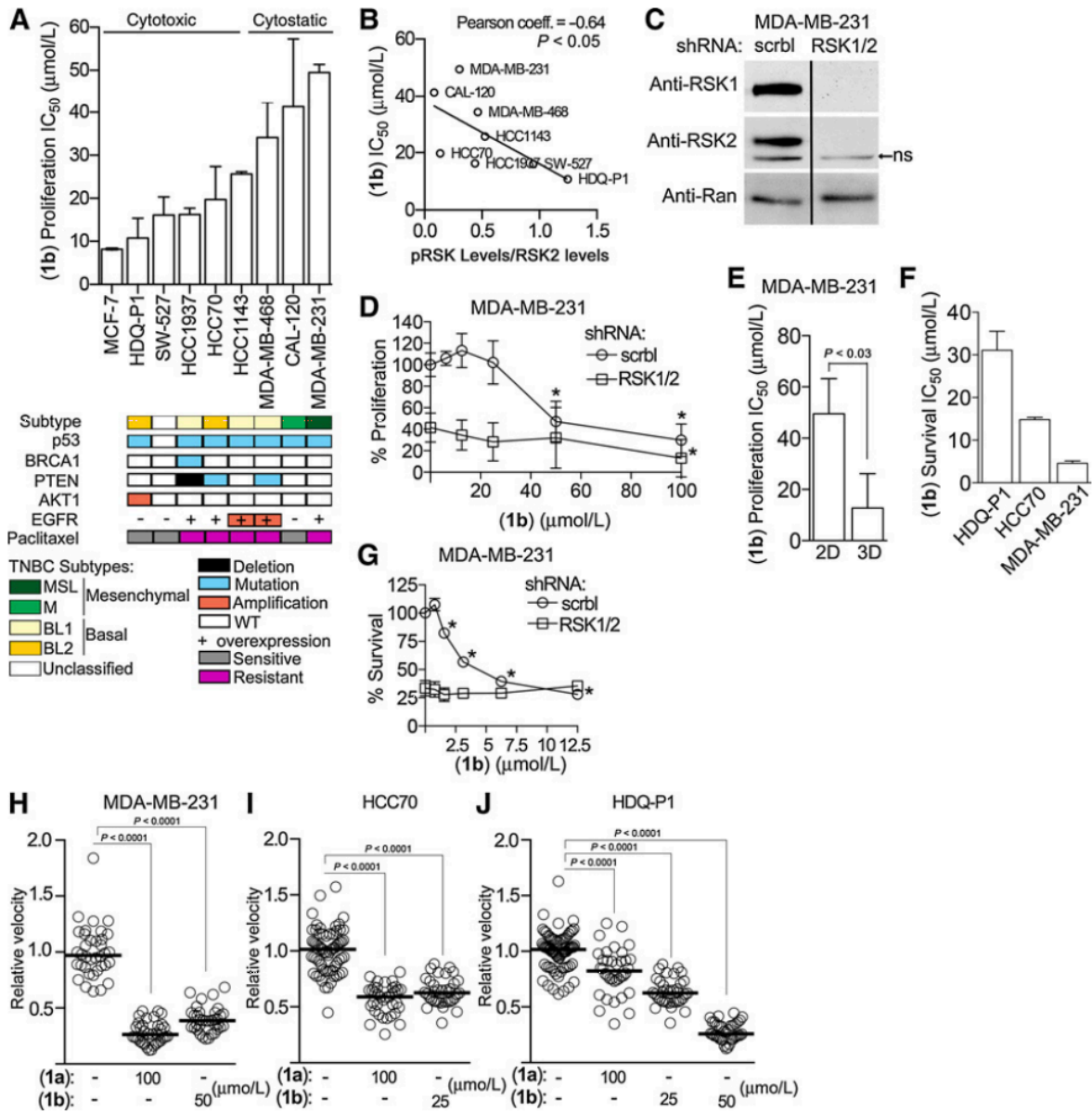
Figure 4.6 RSK regulates TNBC cell motility. (A) (1b) and (1a) inhibit proliferation of the indicated cell lines as measured by the scratch assay. The cells were plated as a confluent monolayer on fibronectin, pre-treated with vehicle or inhibitors for 2 h and a wound introduced into the monolayer. The movement of the cells was monitored over time. The velocity of individual cells was calculated from their distance traveled over the time and normalized to the vehicle control. Representative DIC images and cell traces (as shown by the colored lines) of (A) MDA-MB-231, (B) HCC70 and (C) HDQ-P1 cells. (D) Lysates were obtained from cells treated with vehicle or (1b) for a 10 h time period, which was the maximum length that the scratch assay was performed. Arrows indicate location of full length and cleaved products. The absence of cleaved products indicates that apoptosis was not occurring. MW markers are shown on the right. ns=nonspecific.

Figure 4. 6 RSK regulates TNBC cell motility.

141
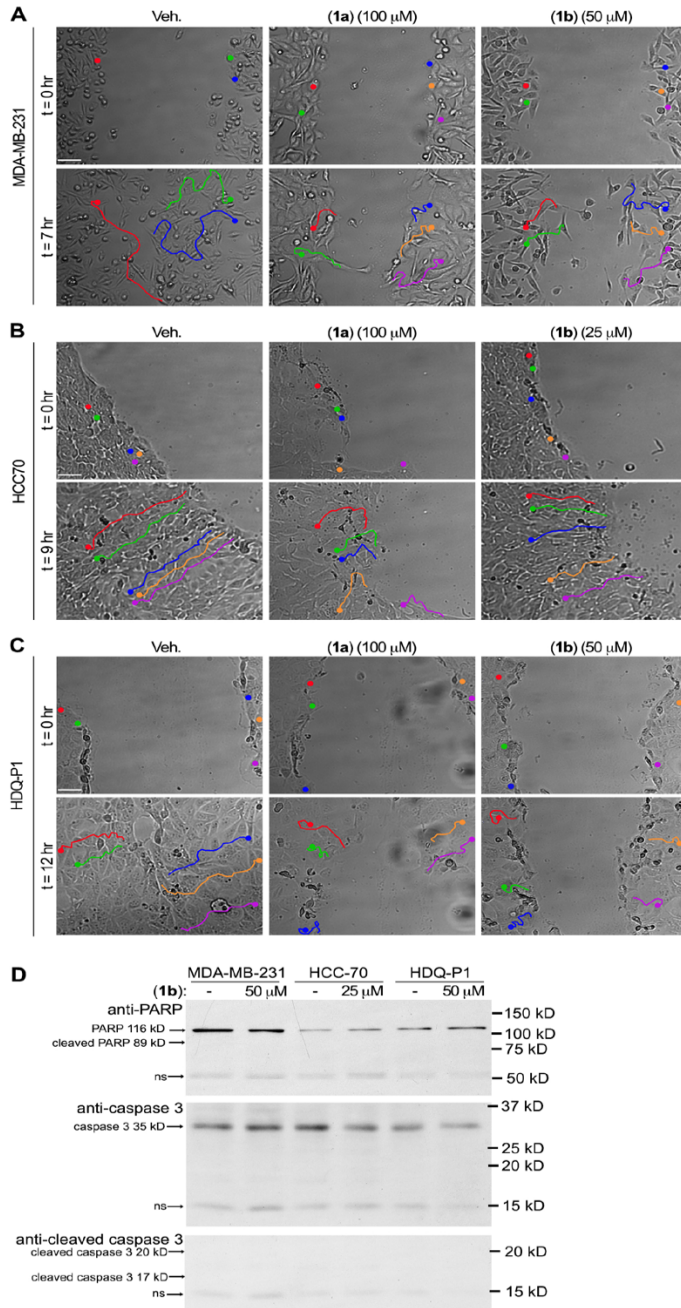
Silencing RSK decreases TNBC metastasis in vivo

To identify the contributions of RSK1 and RSK2 to metastasis, we used an *in vivo* metastatic MDA-MB-231 model in which luciferase was stably expressed (MDA-MB-231-Luc). MDA-MB-231-Luc cells were transduced with control, RSK1- or RSK2-specific shRNAs (Fig. 4.8 A). The cells were quality controlled for their luciferase signal, and equal numbers of cells were introduced by IC injection into female NSG mice (Fig. 4.8 B). This model will identify whether RSK1 or RSK2 contribute to the metastatic processes that includes metastatic colonization and proliferation at the metastatic site. At day 19 silencing RSK1 or RSK2 decreased the total metastatic burden, as determined by bioluminescence, by more than three-fold (Fig. 4.7 A, B and Fig. 4.8 C). This decrease in metastatic burden is further supported by the observations that silencing RSK1 or RSK2 increased survival by approximately 40% to 60% (Fig. 4.7 C). Silencing RSK1 or RSK2 reduced the number of metastatic foci by nearly half (Fig. 4.7 D), and remained constant over the duration of the experiment. The number of bioluminescent foci was linearly correlated with the number of metastatic foci as determined by histology (Fig. 4.8 D). Therefore, we conclude that the increased whole animal bioluminescence from day 5 onwards reflects proliferation at the metastatic sites (Fig. 4.7 E). Thus, silencing RSK1 or RSK2 decreased proliferation from day 12 to day 19 more than three-fold compared to the control. We also conclude that the decrease in metastatic foci reflects that RSK1 or RSK2 is necessary for metastatic colonization. This decrease in metastatic foci was not organ dependent (Fig. 4.7 F). *Ex vivo* analysis of bioluminescence was also performed as it improved the resolution for determining individual metastatic foci. These results of the *ex vivo* bioluminescence (Fig. 4.7 G, H) and the histologic analysis (Fig. 4.8 E, F) were consistent. We conclude that RSK1/2 regulate numerous steps that comprise the metastatic process, which results in improved survival.

Figure 4.7 RSK1 and RSK2 contribute to the metastatic phenotype. A, representative bioluminescence images of NSG mice injected IC with MDA-MB-231-Luc cells transduced with scramble (scrbl), RSK1-, or RSK2-targeting shRNAs (t = 19 days). B, RSK1 and RSK2 decreased the metastatic burden in mice from A (t = 19 days; n = 8 mice/group). C, Kaplan–Meier curves from A (n = 8 mice/group; test = log-rank). D, the number of metastatic foci is constant in mice from A. Symbol, mean. E, total bioluminescence in mice from A is decreased with RSK1 or RSK2 silencing. Each line represents a mouse; the data are fold change over day 6. F, loss of RSK1 or RSK2 decreased the number of metastatic foci in numerous organs in mice from A (t = 19 days). Bar, mean ± SD (n = 8 mice/group). *, P < 0.05. G, representative ex vivo bioluminescence images of livers of mice from A. H, ex vivo analysis confirms that silencing RSK1 or RSK2 decreased the number of metastatic foci in the livers from A. Bar, median quartile (n = 4 mice/group).

Figure 4. 7 RSK1 and RSK2 contribute to the metastatic phenotype.
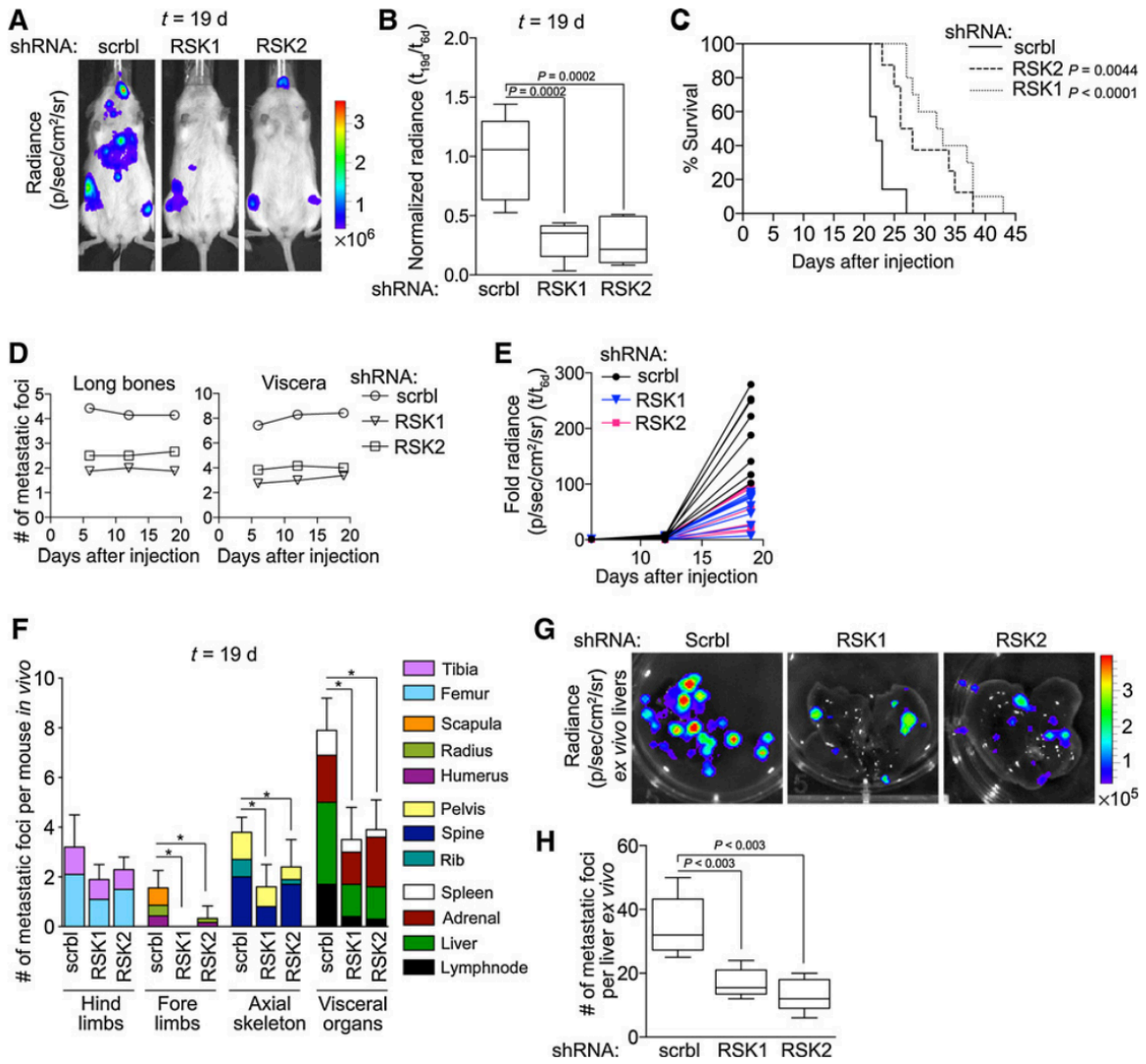
Figure 4.8 RSK1 and RSK2 contribute to TNBC metastasis. (A) Analysis of lysates

generated from MDAMB-231 transduced with scramble (scrbl), RSK1 or RSK2-targeting

shRNAs. (B) The luminescence signal correlates with the cell number of MDA-MB-231-Luc cells

transduced with scramble (scrbl), RSK1- or RSK2- targeting shRNAs. (C) Bioluminescence

images of NSG mice injected IC with MDA-MB-231-Luc cells transduced with scramble (scrbl),

RSK1- or RSK2- targeting shRNAs. (D) The number of metastatic foci in livers in mice from (C)

detected by histology correlates with the number of metastatic foci in livers detected by ex vivo

bioluminescence imaging. (n= 8 mice/group, 4 sections/mouse) (E) Representative

paraffinembedded H&E sections of mouse livers from (C). Arrowheads indicate tumor foci. (F)

Silencing RSK1 or RSK2 reduces the number of liver metastatic foci as detected by H&E. Bar,

median + quartile (n = 8 mice/group, ≥4 sections/mouse).

Figure 4. 8 RSK1 and RSK2 contribute to TNBC metastasis.
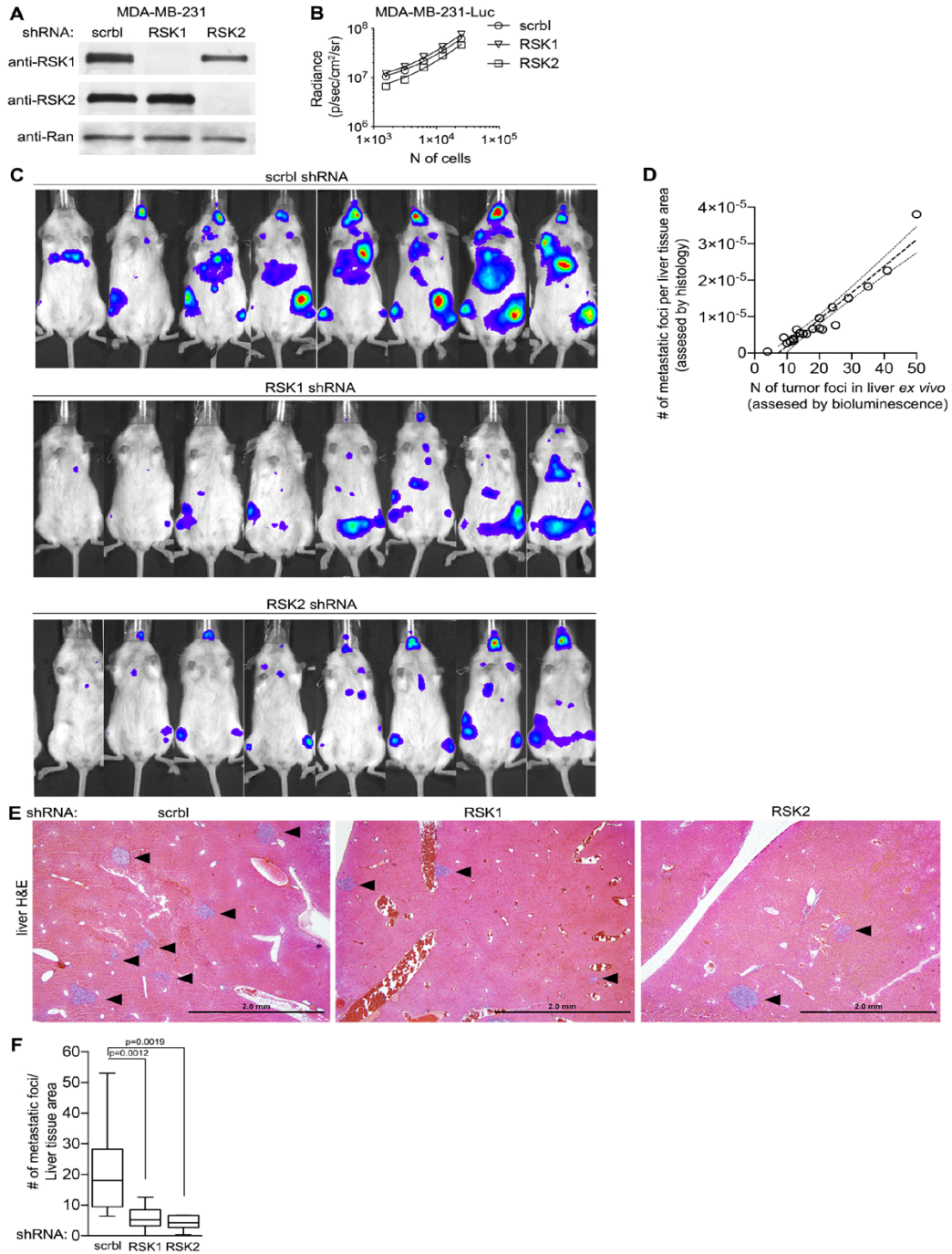
*Inhibition of RSK decreases metastatic colonization*

We investigated whether (**1b**) would be sufficiently efficacious to decrease metastatic colonization *in vivo*. For these experiments we used the HDQ-P1 model because of the clinical importance of the BL2 subtype. This model has not previously been used as an *in vivo* metastatic model. To validate the model, HDQ-P1 cells were transduced with luciferase (HDQ-P1-Luc) and introduced by IC injection into male NSG mice. At 24 hours after injection, the cells were widespread through the animal, but by day 5 the cells were primarily localized to the liver, adrenal glands, and testes (Fig. 4.10). This model is in contrast to the widely used MDA-MB-231 IC metastatic model, in which the cells primarily metastasize to the bone. TNBC primarily metastasizes to lymph nodes and viscera more often than to the bone, and the HDQ-P1 model better recapitulates these clinical observations.

To evaluate the efficacy of (**1b**), we compared it to a drug that is in the same class as (**1b**) and therefore, would be expected to generate a similar phenotype. The MEK inhibitor, trametinib, is approved for melanoma and is currently in multiple clinical trials including those for breast cancer (*217*). MEK inhibition will decrease ERK1/2 activity and reduce RSK activation (*137*). HDQ-P1-Luc cells were introduced by IC injection into female NSG mice and treatment began 2 hours after injection. The animals were imaged just before treatment to ensure viability and distribution of the cells *in vivo*. This approach recapitulates the clinical scenario of tumor cells within the circulation, which have been proposed to act as a negative prognostic marker and demonstrate similar therapeutic responsiveness as the metastatic tumor (*186*). By 24 hours both (**1b**) and trametinib decreased the total *in vivo* bioluminescence by three-fold (Fig. 4.9 A, B). Moreover, the number of metastatic foci in both the skeleton and the viscera was reduced by drug treatment (Fig. 4.9 C). Treatments were stopped on day 5 and on day 6 the total *in vivo* bioluminescence was reduced three-fold by drug treatment in comparison to the control (Fig. 4.9 D). To confirm these findings, we measured the bioluminescence of the liver and adrenal glands *ex vivo* and observed a five-fold reduction in metastatic burden in mice treated

147

with either drug (Fig. 4.9 E, F, G, H). We conclude that inhibition of RSK or its upstream

activator, MEK, decreases metastatic colonization. Moreover, these observations with HDQ-P1

confirm those obtained with MDA-MB-231.

Figure 4.9 Pharmacological inhibition of metastatic colonization by (1b). A, bioluminescence images of NSG mice injected IC with HDQ-P1-Luc cells at t=1 and 24 hours after injection. At 2 hours after injection, mice were treated with vehicle, (1b) (40 mg/kg) i.p. Q12h or trametinib (tram) (2 mg/kg) i.p. Q24h. Inhibition of RSK or MEK decreases total metastatic burden (B) and the number of metastatic foci in individual organs (t= 24 hours; C). Bar,mean ± SD (n = 4 mice/group; *, P < 0.05). D, inhibition of RSK or MEK decrease total metastatic burden (t = 6 days; n = 4 mice/group). Representative ex vivo bioluminescence images of livers (E) and adrenal glands (G; t = 6 days). Ex vivo analysis confirms that inhibiting RSK or MEK activity decreased the metastatic burden in livers (F) and adrenals (H; n = 4 mice/group).

Figure 4. 9 Pharmacological inhibition of metastatic colonization by (1b).
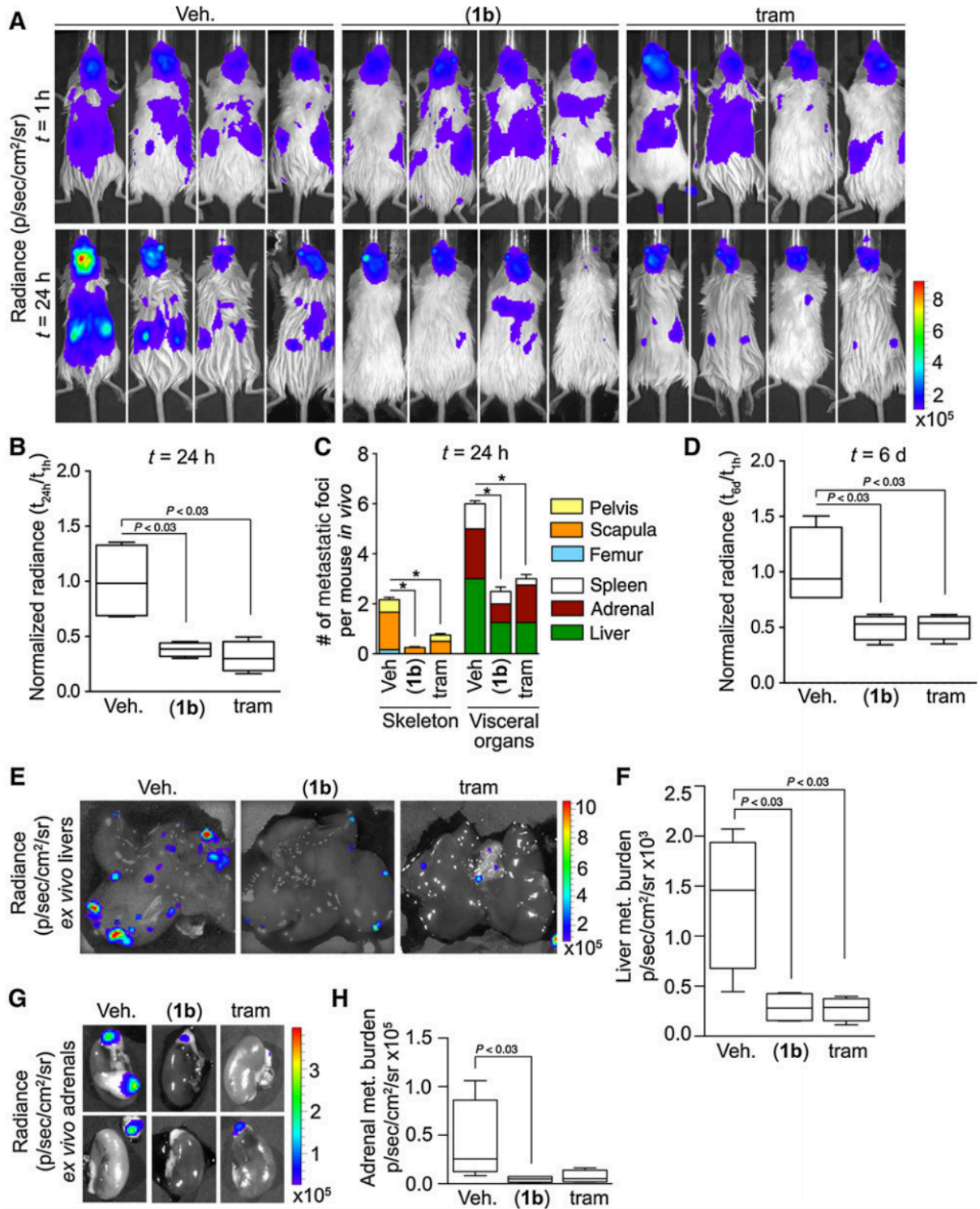
Figure 4.10 The HDQ-P1 line preferentially targets to the viscera. (A) Representative bioluminescence images at the indicated times of male NSG mice injected IC with HDQ-P1-Luc cells. (B) Total bioluminescence signal from HDQ-P1-Luc metastases stabilizes within the viscera in mice from (A). Symbol, mean ± S.D. (n= 4 mice).

**Figure 4. 10 The HDQ-P1 line preferentially targets to the viscera.**
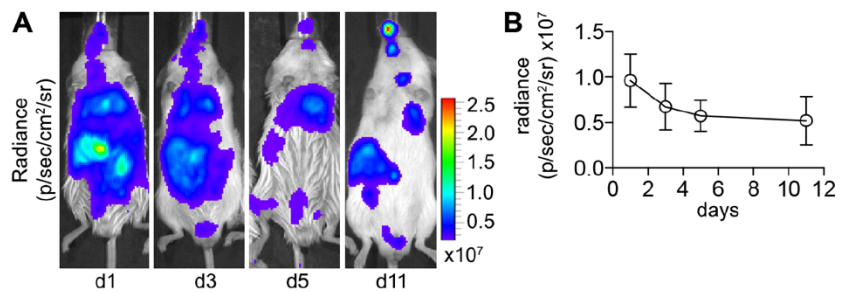
Inhibition of RSK does not activate AKT

Inhibiting "global regulators" such as MEK results in a number of side effects and their ability to induce an effective clinical response appears limited (*194*). MEK inhibition can result in activation of AKT (*218*) (*219*) and based on these results there are clinical trials underway combining MEK inhibitors with an AKT or PI3K inhibitor. Consistent with the literature, we observed that treatment of MDA-MB-231 cells with trametinib enhanced the levels of phosphoSer 473 AKT (pAKT), which is necessary for AKT activity (Fig. 4.11 A). In contrast, activation of AKT was not observed in response to (**1b**). In comparison to MDA-MB-231, HDQ-P1 have high basal levels of active AKT but consistent with the results observed in MDA-MB-231, (**1b**) did not increase AKT activity in contrast to trametinib (Fig. 4.11 B). Taken together, these results indicate that RSK inhibition by itself will effectively target the TNBC metastatic process but not have the undesirable side effect of activating AKT.

Figure 4.11 (1b) does not activate AKT. Analysis of lysates from MDA-MB-231 (A) and HDQ-P1 cells (B) treated with vehicle, trametinib (1 mmol/L), or (1b) (25 mmol/L) for 2 hours. Bar, separate gels.

Figure 4. 11 (1b) does not activate AKT.
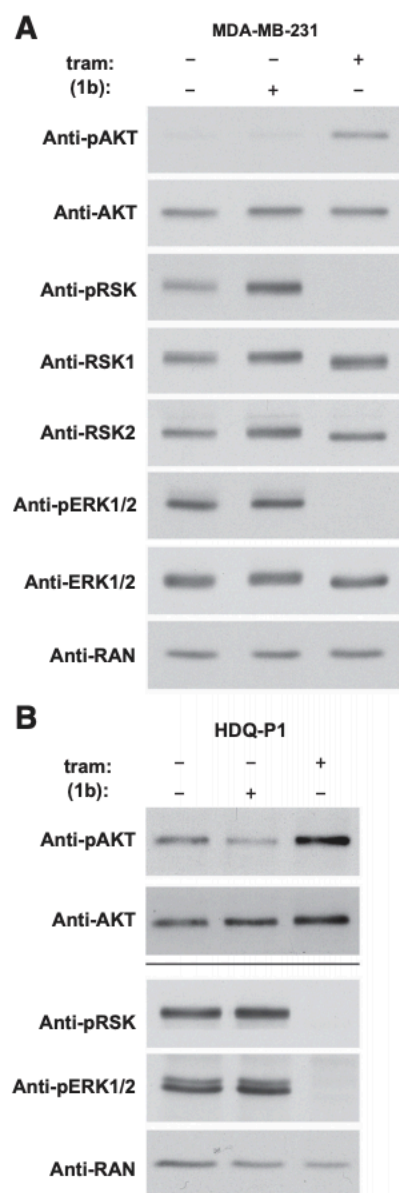
Discussion

The importance of RSK in regulating metastasis *in vivo* has not been thoroughly investigated. Kang and colleagues (*96*) reported that silencing RSK2 decreased metastatic colonization to the lymph nodes using a human head and neck squamous cell carcinoma line. They further followed up on these observations using the RSK CTKD inhibitor, FMK-MEA, which resulted in a modest decrease in metastatic tumor burden from 97% to 79% (*220*). In a screen Lara and colleagues (*221*) identified that loss of RSK1 increased motility in lung cancer lines but in contrast Zhou and colleagues (*222*) found that inhibition of RSK activity was associated with decreased motility in lung cancer lines. It is possible that the discrepancy between these studies results from the ability of RSK1 to act as a scaffold and regulate other signaling pathways. RSK has also been proposed as a drug target for TNBC based on observations that it decreased the levels of the surface marker CD44, which is reported to be associated with cancer stem cells (*198*). We demonstrated using genetic and pharmacologic approaches *in vitro* and *in vivo* that reducing RSK1/2 activity or RSK1 or RSK2 levels inhibits multiple steps within the metastatic program. Furthermore, we confirmed that activated RSK is present in the majority of TNBCs. Our results strongly suggest that RSK is a viable drug target for TNBC metastasis.

We also report the generation and validation of a novel SL0101 analogue, *C5″-n*-propyl cyclitol SL0101 (**1b**) that is specific for RSK1/2. The specificity of the inhibitor for RSK1/2 is demonstrated by our observations that silencing RSK1/2 eliminates responsiveness to (**1b**) in MDA-MB-231 proliferation and survival assays. In *in vitro* assays using multiple TNBC cell lines the new analogue inhibits the major steps involved in the metastatic process, which include motility, proliferation and survival in a nonadherent environment. In addition, (**1b**) was as effective at inhibiting metastatic colonization *in vivo* as the FDA-approved MEK inhibitor, trametinib. Activation of the AKT pathway is proposed as a mechanism to account for the lack of efficacy of selumetinib, a MEK inhibitor, in combination with the anti-estrogen, fulvestrant, in a phase II clinical trial (*223*). We propose that inhibitors of RSK will offer greater flexibility in

designing combination cancer therapies than MEK inhibitors, as there will be no positive

feedback loop that results in activation of AKT.

Chapter 5

De novo synthesis and biological evaluation of C6″-substituted C4″-amide analogues of SL0101

Adapted from: (232)

Summary

In an effort to improve upon the in vivo half-life of the known ribosomal S6 kinase (RSK) inhibitor SL0101, C4″-amide/C6″-alkyl substituted analogues of SL0101 were synthesized and evaluated in cell-based assays. The analogues were prepared using a de novo asymmetric synthetic approach, which featured Pd-π-allylic catalyzed glycosylation for the introduction of a C4″-azido group. Surprisingly replacement of the C4″-acetate with a C4″-amide resulted in analogues that were no longer specific for RSK in cell-based assays.

Figure 5. 1 Graphical abstract.
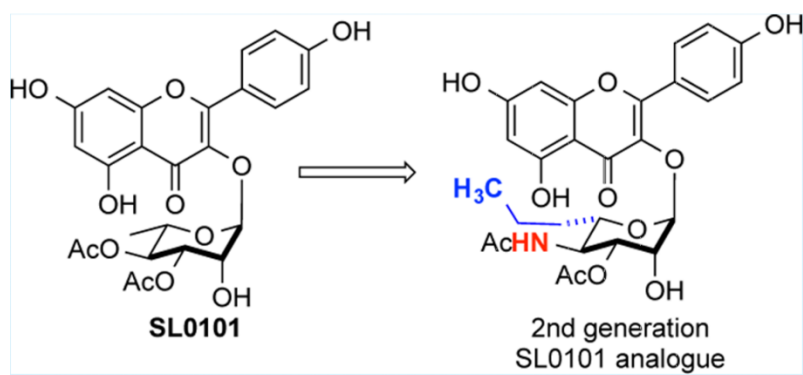
Introduction

The ribosomal S6 kinases (RSKs) are a family of Ser/Thr kinases, which are downstream effectors of the extracellular signal-regulated kinase 1/2 pathways. RSK appears to be involved in the etiology of a number of different cancers and, importantly, regulates a motility/invasive gene program. RSK is a dual kinase domain protein with the N-terminal kinase domain (NTKD) responsible for phosphorylation of target substrates (*224*). In a screen of botanical extracts SL0101 (1), a flavonoid glycoside, was identified as an inhibitor of the NTKD of RSK (*114*). SL0101 (1) is a relatively selective inhibitor for RSK with a Ki of ~1 microM. From the crystal structure of SL0101 (1) complexed with the NTKD isoform of RSK25 and de novo synthetic studies, we identified analogues (2 and 3) with C6″-substitutions of the rhamnose that showed improved efficacy in the in vitro kinase assays (*224*).
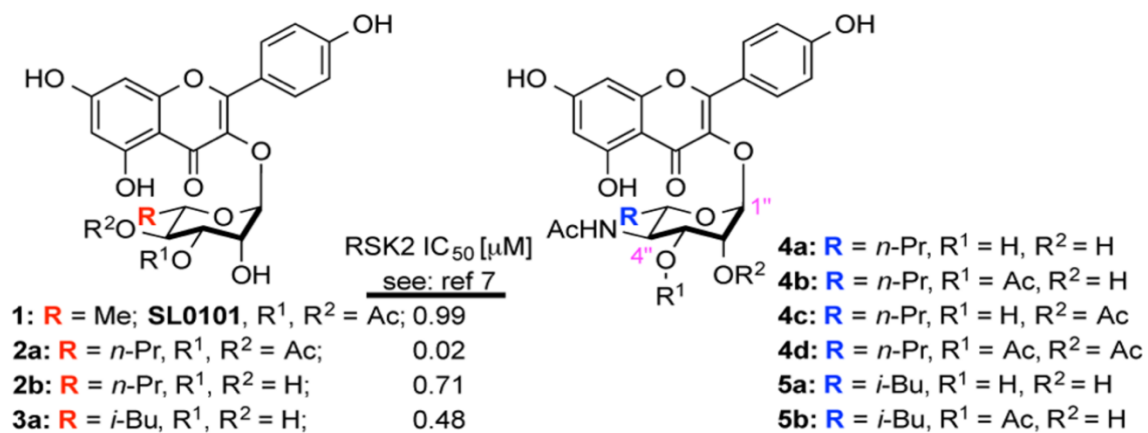
Materials and methods

H and 13C spectra were recorded on 270 MHz, 400 MHz and 600 MHz spectrometers. Chemical shifts were reported relative to benzene-d6 (δ 7.16 ppm), CDCl3 (δ 7.26 ppm), CD3OD (δ 3.31 ppm), acetone-d6 (δ 2.05 ppm) for 1 H, and benzene-d6 (δ 127.68 ppm), CDCl3 (δ 77.0 ppm), CD3OD (δ 49.15 ppm), acetone-d6 (δ 29.92 ppm) for 13C. Optical rotations were measured with a digital polarimeter at sodium D line (589 nm) and were reported in concentration of g/100 mL at 25 ºC in the solvent specified. Infrared (IR) spectra were obtained on a FT-IR spectrometer. Flash chromatography was performed using the indicated solvent system on silica gel standard grade 60 (230-400 mesh). Rf values are reported for analytical TLC using the specified solvents and 0.25 mm silica gel 60 F254 plates that were visualized by UV irradiation (254 nm) or by staining with KMnO4 stain or p-anisaldehyde stain. Ethyl ether, tetrahydrofuran, methylene chloride, toluene, and triethylamine were dried by passing through activated alumina (8 x 14 mesh) column with argon gas pressure. Commercial

reagents were used without purification unless otherwise noted. Air and/or moisture-sensitive reactions were carried out under an atmosphere of argon/nitrogen using oven/flamed-dried glassware and standard syringe/septum techniques. Melting points are uncorrected.

Results

SL0101 (1) has a short biological half-life in vivo (*224*), which is presumably due to hydrolysis of the C3″/C4″-acetates which are necessary for high affinity. To identify less labile groups that could replace the ester without loss of affinity, we investigated replacing the C4″-acetate with a C4″-acetamide in combination with the C6″-alkyl substitution that we previously identified (*224*). Specifically, we targeted six C4″-acetamide analogues 4a–d and 5a–b (Figure 5.2).

Figure 5. 2 C4''-amide analogues of SL0101.

RSK2 IC$_{50}$ [µM]
see: ref 7

1: R = Me; **SL0101**, R^1, R^2 = Ac; 0.99
2a: R = n-Pr, R^1, R^2 = Ac; 0.02
2b: R = n-Pr, R^1, R^2 = H; 0.71
3a: R = i-Bu, R^1, R^2 = H; 0.48

4a: R = n-Pr, R^1 = H, R^2 = H
4b: R = n-Pr, R^1 = Ac, R^2 = H
4c: R = n-Pr, R^1 = H, R^2 = Ac
4d: R = n-Pr, R^1 = Ac, R^2 = Ac
5a: R = i-Bu, R^1 = H, R^2 = H
5b: R = i-Bu, R^1 = Ac, R^2 = H

Retrosynthetically, we envisioned that C4″-acetamide substituted analogues 6 could arise from C4″-azido sugar 7a, which could be prepared from enone sugar 7c via allylic carbonate 7b (Fig. 5.3). Previously we have shown that C4 allylic azides such as 7a could be prepared from C4 allylic carbonates like 7b via Pd-catalyzed allylic alkylation. However, this approach was not compatible for pyran rings with a C1 kaempferol group. To address this issue, a Pd-glycosylation method was developed for the direct incorporation of a C4 azido sugar.

Our synthesis started with exposure of flavonol 9 and Boc-pyranone 13 to our typical glycosylation conditions (2.5 mol % Pd2(DBA)3·CHCl3 and 10 mol % of PPh3 in CH2Cl2 at 0 °C; 95%), which produced glycosylated pyranone 14 with complete α-selectivity (Fig. 5.4). Reduction of the enone 14 (NaBH4/CeCl3, −78 °C in CH2Cl2/MeOH; 72%) resulted stereoselectively in allylic alcohol 15. A methyl carbonate leaving group was installed on the allylic alcohol by reaction of 15 with methyl chloroformate to form the C4″-carbonate 16 in 75% yield. Unfortunately, exposure of carbonate 16 to the Sinou conditions (TMSN3, [Pd(allyl)Cl]2/1,4-bis(diphenylphosphino)butane) failed to afford the desired regio- and stereoisomeric allylic azide 17. The C-1 kaempferol proved to be the better leaving group, as only products consistent with the hydrolysis at the anomeric position were observed.

163

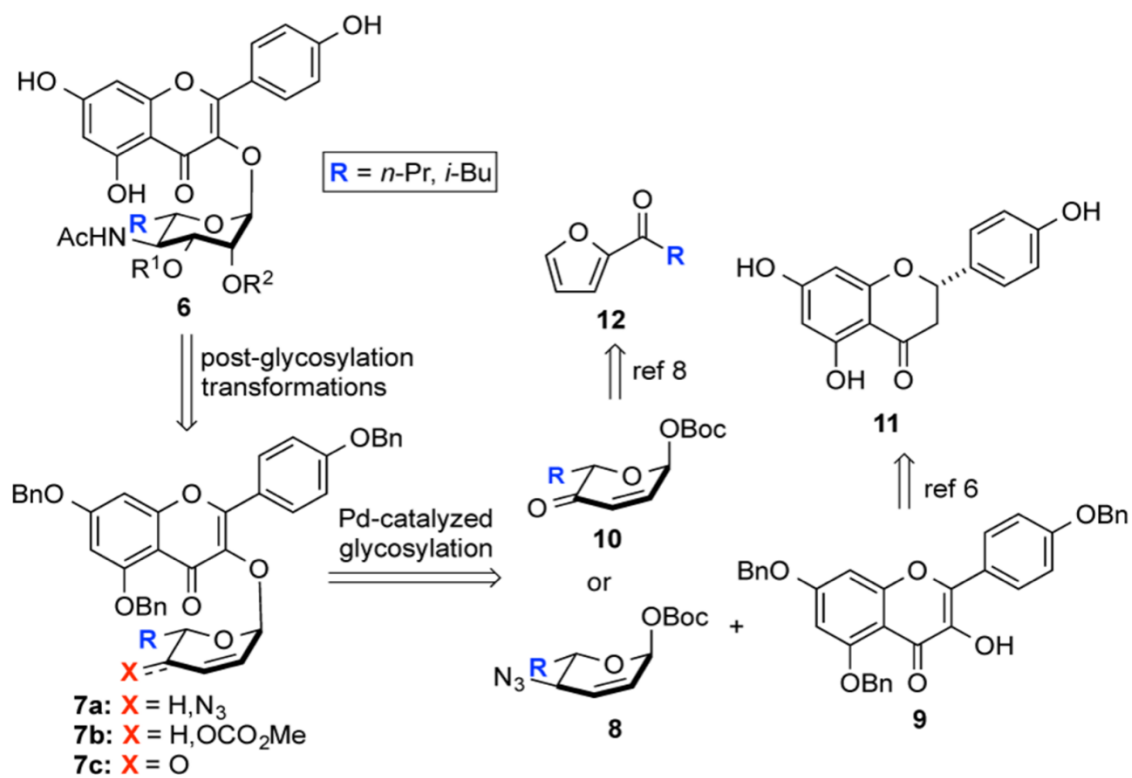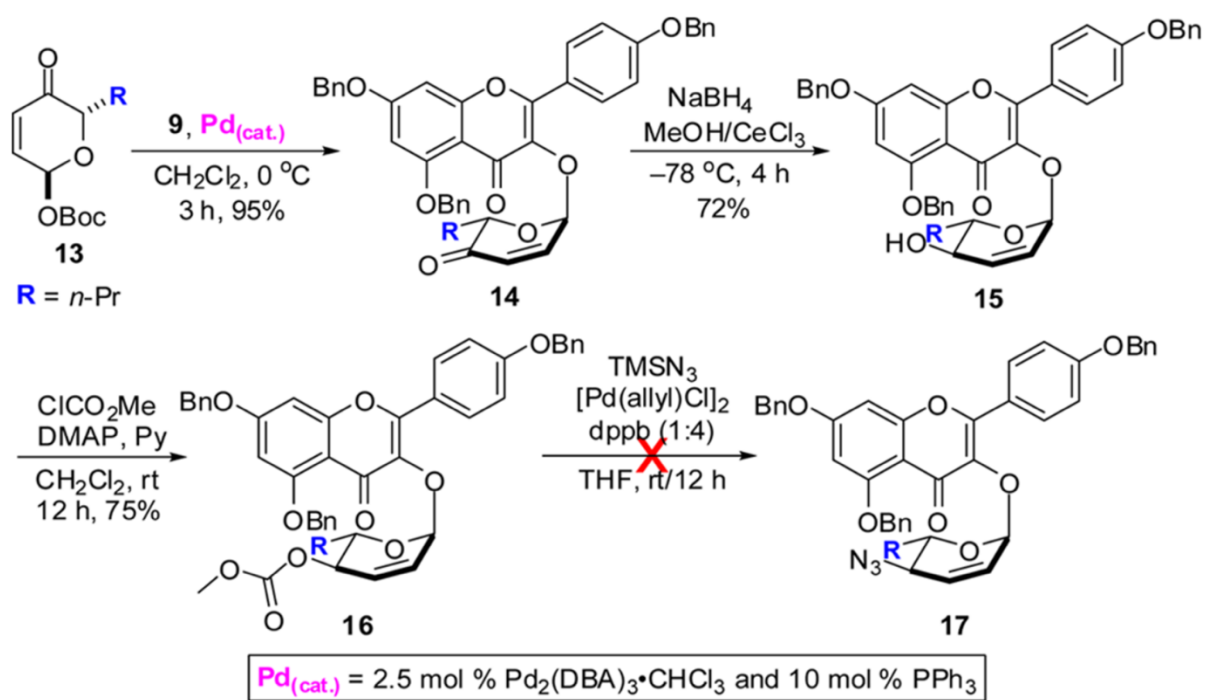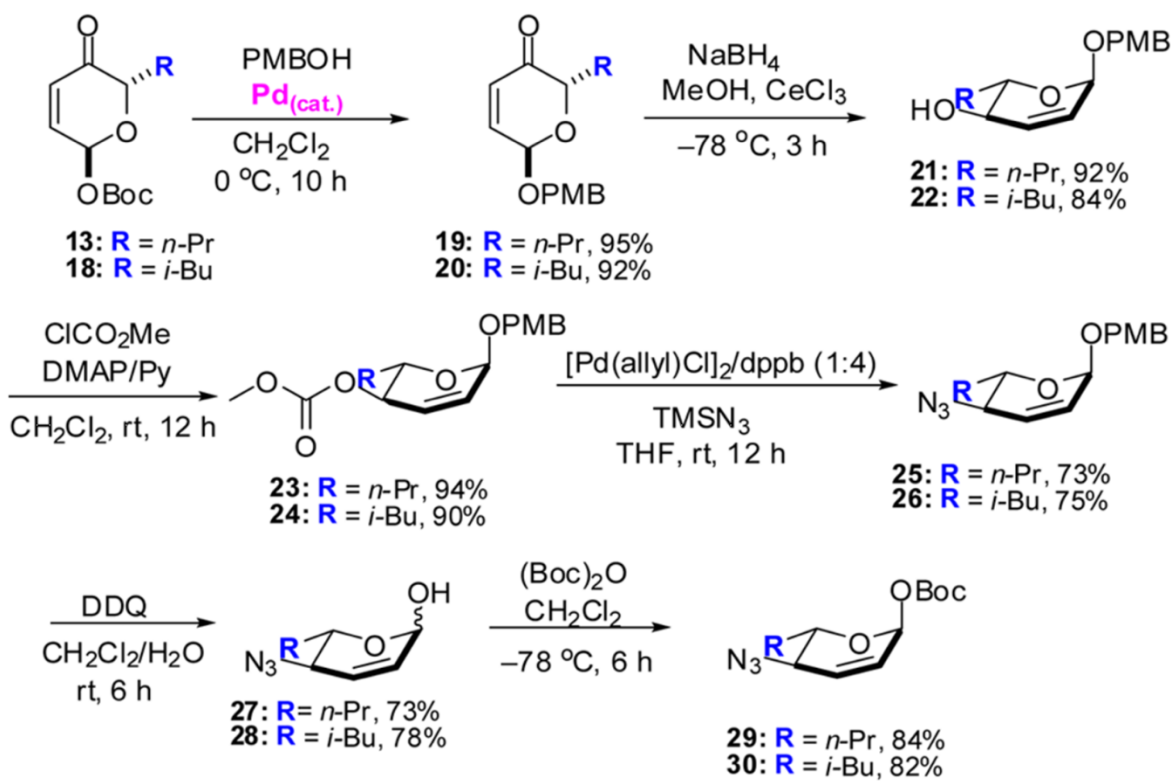# Figure 5. 3 Retrosynthesis of C4"-amide SL0101 analogues.

$R = n\text{-Pr}, i\text{-Bu}$

6

post-glycosylation transformations

7a: X = H,N$_3$
7b: X = H,OCO$_2$Me
7c: X = O

Pd-catalyzed glycosylation

12

ref 8

10

or

8

11

ref 6

9

164

Figure 5. 4 Unsuccessful approach to C4"-azide sugar 17.

To solve this problem, we decided to try reversing the sequence of the two Pd-π-allyl substitution reactions, which required the synthesis of allylic azides 29 and 30 (Fig. 5.5). This began with a palladium-catalyzed glycosylation (Pd(0)/PPh3, 1:2) of p-methoxybenzyl alcohol with Boc-pyranones 13 and 18 which stereoselectively afforded PMB-pyranones 19 and 20 (95% and 92% respectively). Diastereoselective reduction of the two enones (NaBH4/CeCl3, −78 °C in CH2Cl2/MeOH; 92% and 84%) gave allylic alcohols 21 and 22. Treatment of the two allylic alcohols with methyl chloroformate in the presence of a catalytic amount of DMAP gave the allylic carbonates 23 and 24 (94% and 90%). Exposure of the carbonates to the Sinou conditions (TMSN3, [Pd(allyl)Cl]2/1,4-bis(diphenylphosphino)butane) regio- and stereospecifically afforded the desired allylic azides 25 and 26 (73% and 75%). An oxidative PMB deprotection (DDQ/H2O) of 25 and 26 provided anomeric alcohols 27 and 28 as a 13:1 mixture of anomers in 73% and 78% yields. The following Boc-protection of the two alcohols produced the key azido containing intermediates 29 and 30 in 84% and 82% yields with excellent diastereoselectivity.

To our delight, exposure of sugar donor Boc-allylic azides 29 and 30 and acceptor 9 to our typical Pd-catalyzed glycosylation conditions provided our desired glycosylated allylic azides 17 and 31 in excellent yield (98% and 90%) with complete α-selectivity and no sign of hydrolysis at the anomeric position. Exposure of the two allylic azides to Upjohn conditions (OsO4/NMO; 91% and 87%) stereoselectively converted them into the two rhamno-diols 32 and 33, which are poised for further manipulation into the desired SL0101 analogues (Fig. 5.6).

Figure 5. 5 Synthesis of C4'-azide sugar glycosyl donors 29/30.

Reaction scheme:

13: R = n-Pr
18: R = i-Bu

PMBOH, Pd(cat.), CH₂Cl₂, 0 °C, 10 h →

19: R = n-Pr, 95%
20: R = i-Bu, 92%

NaBH₄, MeOH, CeCl₃, −78 °C, 3 h →

21: R = n-Pr, 92%
22: R = i-Bu, 84%

ClCO₂Me, DMAP/Py, CH₂Cl₂, rt, 12 h →

23: R = n-Pr, 94%
24: R = i-Bu, 90%

[Pd(allyl)Cl]₂/dppb (1:4), TMSN₃, THF, rt, 12 h →

25: R = n-Pr, 73%
26: R = i-Bu, 75%

DDQ, CH₂Cl₂/H₂O, rt, 6 h →

27: R= n-Pr, 73%
28: R = i-Bu, 78%

(Boc)₂O, CH₂Cl₂, −78 °C, 6 h →

29: R = n-Pr, 84%
30: R = i-Bu, 82%

Pd(cat.) = 2.5 mol % Pd₂(DBA)₃•CHCl₃ and 10 mol % PPh₃

Figure 5. 6 Synthesis of C4"-azide Rhamno-sugars 32/33.
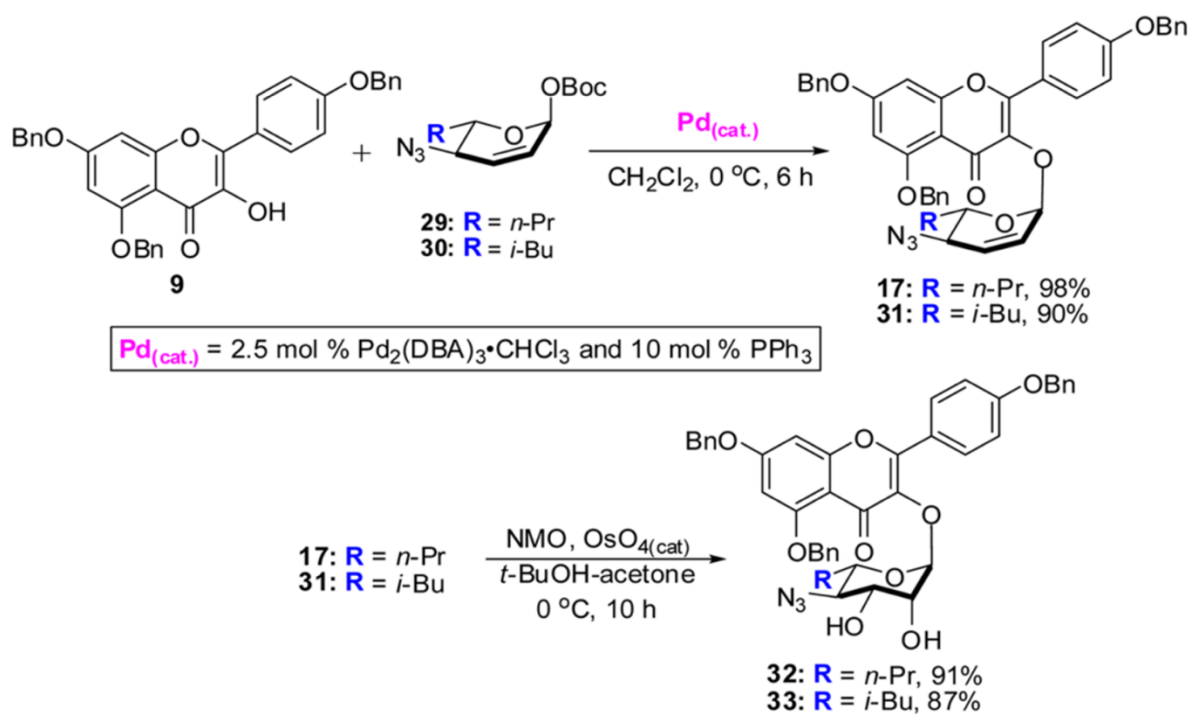
We next investigated the reduction and acylation of azidodiols 32 and 33 (Fig. 5.7) (*225*).

Fortuitously, both the C4 acylated amides 36 and 37 and C3/C4 bis-acylated products 34 and

35 were generated in an ~1:1 mixture in one pot from the reduction of 32 and 33 with zinc dust

in the presence of acetic anhydride and acetic acid. Thus, the reduction acylation of 32 gave the

desired C4″-acetamides 36 (29%) and 34 (27%), whereas the reduction acylation of 33 gave the

desired C4″-acetamides 37 (36%) and 35 (32%).

The intermediates 34–37 were globally deprotected by an exhaustive hydrogenolysis,

which produced four of the desired analogues. Thus, exposure of 34 and 35 to typical

hydrogenolysis conditions (1 atm of hydrogen with Pd/C) furnished 4b and 5b in good yields

(86% and 88%, respectively). Exposure of 36 and 37 to similar hydrogenolysis conditions

furnished 4a and 5a in good yields (90% and 86%, respectively). Finally the last two analogues

4c and 4d were prepared by an acylation deprotection sequence. The peracylated product 4d

was prepared from 34 in 91% overall yield by bis-acylation (Ac2O, DMAP/Py; 97%) and

exhaustive hydrogenolysis. Similarly, the C2 acylated product 4c was prepared from 36 via an

ortho-ester mediated C2-acylation (CH3C(OMe)3, 10% p-TsOH in CH2Cl2; then excess 90%

AcOH/H2O; 85%) and per-hydrogenolysis (94% overall yield).

Figure 5. 7 Synthesis of C4"-Amide analogues of SL0101 4/5.

170
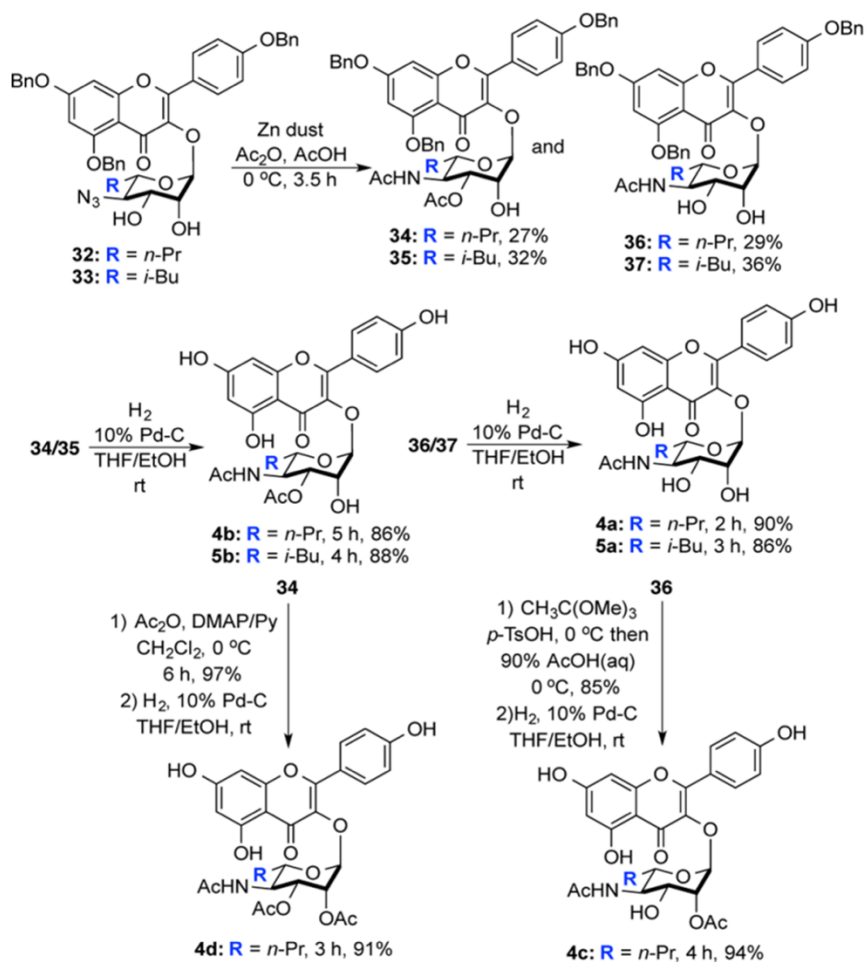
The efficacy of the analogues 4a–d and 5a–b to inhibit RSK2 activity was determined in an in vitro kinase assay using purified recombinant RSK2 (Table 5.1). The data were fit using nonlinear regression analysis. In the n-Pr series, 4b and 4c with a single acetate at the C3″- or C2″-position had significantly lower (~5-fold) IC50's compared to SL0101. However, when compared with our best analogue 2a (C3″/C4″-diacetate, Fig. 5.2) the related C4″-acetamide 4b had a 10-fold increase in IC50 (*224*). The IC50's for 4a with no C2″- or C3″-acetate and 4d with two acetates were not statistically different from that of SL0101. These results are similar to those obtained in the series in which the acetyl group was at the C4″-position. In the isobutyl series the C3″-acetate 5b had a 3-fold improved IC50 compared to that of SL0101, whereas 5a with no C2″- or C3″-acetate had a much poorer IC50 than SL0101. This suggests that, in the n-Pr-series, the C4″-acetamide can replace the C4″-acetate without dramatically compromising the affinity of the analogues for RSK2.

The six analogues were evaluated for their ability to decrease proliferation of the breast cancer cell line, MCF-7 (Table 5.1). Initially, each analogue was tested at a dose of 100 microM and compared to SL0101 (1). Analogue 4d was the only analogue that inhibited proliferation to a greater extent than SL0101 (1). A dose response curve with 4d showed that cytostasis occurred at ~35 microM and substantial cell death occurred at ~50 microM (see online Suppporting Information (SI)). For comparison SL0101 (1) at 100 microM (maximum concentration) induces a reduction in proliferation (~60%). To evaluate whether 4d was specific for RSK, we compared its antiproliferative effects in MCF-7 cells versus MCF-10A, an immortalized nontransformed human breast cell line. We previously found that a preferential ability to inhibit MCF-7 compared to MCF-10A proliferation correlates with specificity for RSK inhibition (142, (*224*). At 25 microM 4d inhibited proliferation of MCF-7 cells by 50% and marginally inhibited MCF-10A proliferation (see online version, Supporting Information). However, at 50 microM of 4d, a cytotoxic dose in MCF-7 cells, proliferation of MCF-10A cells was inhibited by 70%. Thus, 4d shows a very limited

ability to preferentially inhibit MCF-7 proliferation and survival compared to MCF-10A cells.

These results suggest that 4d is not a specific RSK inhibitor in intact cells.

Table 5.1 In vitro potency of SL0101 and analogues. RSK2 IC50: concentration needed for 50% RSK2 inhibition (n ≥ 2; quadruplicate; mean ± S.D.; p(SL0101) Student's t test compared to SL0101). MCF-7 proliferation: (n ≥ 2; triplicate; mean ± S.D.; p(DMSO) Student's t test compared to control; p(SL0101) Student's t test compared to SL0101. P < 0.01 considered significant.

Table 5. 1 In vitro potency of SL0101 and analogues.

Name	RSK2 IC50 (microM)	RSK2 IC50 p(SL0101)	MCF-7 proliferation (% control)	MCF-7 proliferation p(DMSO)	MCF-7 proliferation p(SL0101)
SL0101	1.04 ± 0.60		38.6 ± 14.6	<0.01	
4a	0.76 ± 0.43	0.17	94.5 ± 21.6	0.41	
4b	0.23± 0.07	<0.01	39.2 ± 7.2	<0.01	0.91
4c	0.11 ±0.09	<0.01	47.8 ± 10.6	<0.01	0.16
4d	0.44 ± 0.39	0.02	-80.0 ± 6.6	<0.01	<0.01
5a	2.33 ± 0.88	<0.01	47.5 ± 19.1	<0.01	0.21
5b	0.32 ± 0.18	<0.01	24.6 ± 10.4	<0.01	0.03

To further evaluate the specificity of 4d at inhibiting RSK, we compared the efficacy of

SL0101 (1) and 4d to alter the phosphorylation of known RSK substrates. We chose to test 4d

at both cytostatic (25 microM) and cytotoxic (50 microM) concentrations. To increase the

phosphorylation of substrates MCF-7 cells were stimulated with the mitogen, phorbol myristate

acetate (*10*), after a pretreatment with inhibitor or vehicle. RSK phosphorylates and inhibits the

activity of eukaryotic elongation factor 2 (eEF2) kinase (*112*). Thus, inhibition of RSK relieves

the inhibition of eEF2 kinase, which results in an increase in p-eEF2. As expected activation of

RSK by PMA led to a decrease in p-eEF2 and inhibition of RSK with SL0101 increased p-eEF2

compared to the PMA control (Fig. 5.8).

Ribosomal protein S6, a component of the 40S ribosomal subunit, is phosphorylated by

RSK, and in agreement with these data SL0101 (1) inhibits PMA-induced phosphorylation of S6.

We have also found that RSK regulates the levels of the oncogene, cyclin D1, in MCF-7 cells.

Consistent with these observations SL0101 (1) inhibited cyclin D1 levels. In contrast with our

observations with SL0101 the analogue 4d did not alter the phosphorylation status of eEF2, S6

or the levels of cyclin D1. To further investigate the ability of 4d to inhibit RSK in intact cells, we

immunoblotted the lysates with an antibody against the phosphorylation motif that is recognized

by numerous kinases, including RSK. Treatment with SL0101 increased the phosphorylation of

a band at ~60 kDa and decreased the intensity of a band at ~27 kDa. Analogue 4d did not alter

the phosphorylation pattern as compared to PMA. Consistent with these results we observed

that analogue 4b (100 microM) did not alter the phosphorylation of RSK biomarkers or cyclin D1

levels in intact cells (data not shown). These results suggest that the amide analogues of

SL0101 (1) are not specific for RSK.

Figure 5.8 RSK2 biomarker comparisons with 4d and SL0101 (1). Comparison of analogues 4d and SL0101 (1) was made against known RSK biomarkers in intact cells. MCF-7 cells were pretreated with 4d at the indicated concentrations and then treated with vehicle of PMA. Lysates were analyzed by immunoblotting. The motif, (K/R)x(K/R)xx(pS/pT), is recognized by a number of kinases, including RSK. The arrows indicate bands whose intensity is altered upon treatment of cells with SL0101 (1).

Figure 5. 8 RSK2 biomarker comparisons with 4d and SL0101 (1).
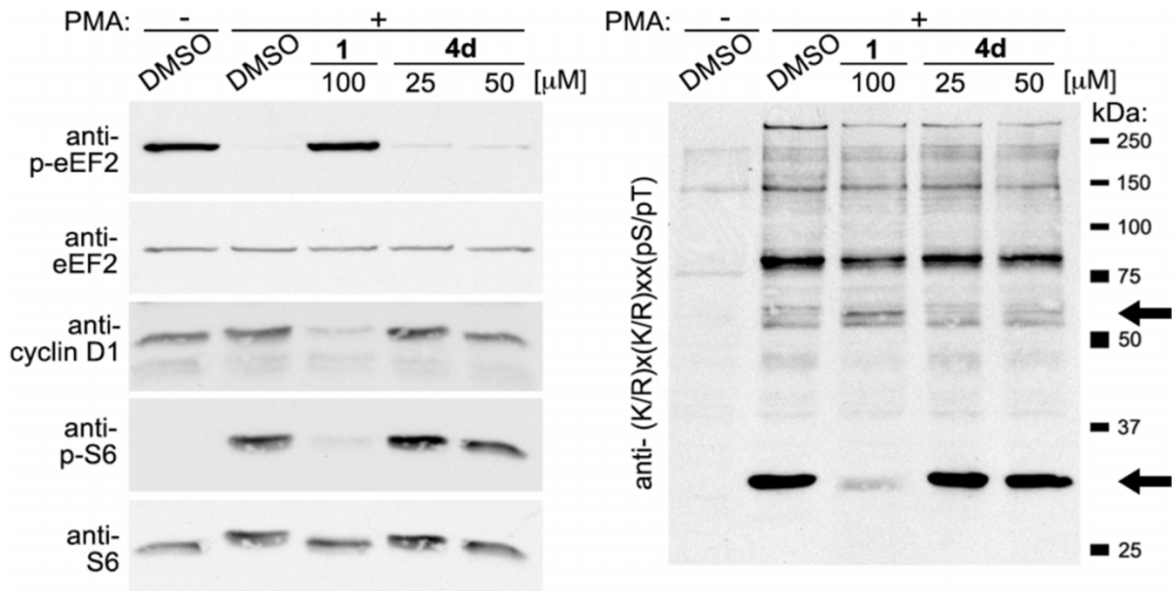
Conclusion

In conclusion, using de novo synthesis C4″-acetamide analogues of SL0101 with a C6″ substitution were prepared and evaluated as RSK inhibitors. Analogues with improved in vitro kinase inhibitory activities were identified; however, this increase in activity came at a loss of selectivity for RSK. Further studies aimed at defining the requirements for a specific-RSK inhibition are ongoing and will be reported in due course.
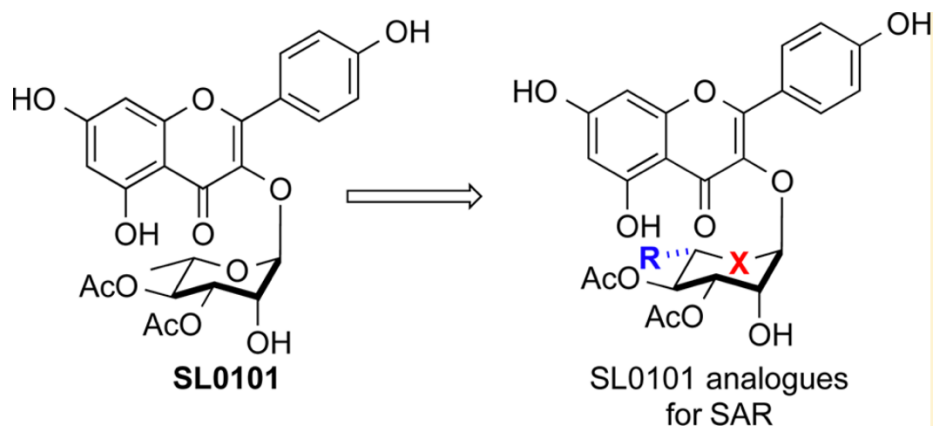
Chapter 6

Synthesis and structure−activity relationship study of 5a-carbasugar analogues of SL0101

Adapted from: (211)

Summary

The Ser/Thr protein kinase, RSK, is associated with oncogenesis, and therefore, there are ongoing efforts to develop RSK inhibitors that are suitable for use in vivo. SL0101 is a natural product that demonstrates selectivity for RSK inhibition. However, SL0101 has a short biological half-life in vivo. To address this issue we designed a set of eight cyclitol analogues, which should be resistant to acid catalyzed anomeric bond hydrolysis. The analogues were synthesized and evaluated for their ability to selectively inhibit RSK in vitro and in cell-based assays. All the analogues were prepared using a stereodivergent palladium-catalyzed glycosylation/cyclitolization for installing the aglycon. The L-cyclitol analogues were found to inhibit RSK2 in in vitro kinase activity with a similar efficacy to that of SL0101, however, the analogues were not specific for RSK in cell-based assays. In contrast, the D-isomers showed no RSK inhibitory activity in in vitro kinase assay.

Figure 6. 1 Graphical abstract.

SL0101

SL0101 analogues for SAR

Materials and methods

General chemistry methods and materials 1 H and 13C spectra were recorded on 400 MHz and 500 MHz spectrometers. Chemical shifts were reported relative to CDCl3 (δ 7.26 ppm), CD3OD (δ 3.31 ppm), acetone-d6 (δ 2.05 ppm) for 1 H, and CDCl3 (δ 77.0 ppm), CD3OD (δ 49.15 ppm), acetone-d6 (δ 29.92 ppm) for 13C. Optical rotations were measured with a digital polarimeter at sodium D line (589 nm) and were reported in concentration of g/100 mL at 25 ºC in the solvent specified. Infrared (IR) spectra were obtained on a FT-IR spectrometer. Flash chromatography was performed using the indicated solvent system on silica gel standard grade 60 (230-400 mesh). Rf values are reported for analytical TLC using the specified solvents and 0.25 mm silica gel 60 F254 plates that were visualized by UV irradiation (254 nm and 365 nm) or by staining with KMnO4 stain or p-anisaldehyde stain. Ethyl ether, tetrahydrofuran, methylene chloride, toluene, and triethylamine were dried by passing through activated alumina (8 x 14 mesh) column with argon gas pressure. Commercial reagents were used without purification unless otherwise noted. Air and/or moisture-sensitive reactions were carried out under an atmosphere of argon/nitrogen using oven/flamed-dried glassware and standard syringe/septum techniques. Melting points are uncorrected. Matrix-assisted laser desorption ionization time-of-flight (MALDI-TOF) mass spectra were obtained using α-cyano-4-hydroxycinnamic acid (CCA) as the matrix on a MALDI-TOF mass spectrometer. Biologic Methods Purified recombinant RSK2 Baculovirus encoding His-tagged RSK2 cDNA was generated using the Bac-to-Bac Baculovirus Expression System (Invitrogen, Carlsbad, CA). Recombinant RSK2 was expressed in Sf9 cells and activated by a 20 min treatment with phorbol 12-myristate 13-acetate (*10*). Protein was purified using the Ni-NTA Spin Kit (Qiagen, Valencia, CA).

In vitro kinase assays were performed as previously described (*210*). Briefly, a fusion protein consisting of glutathione S-transferase and the amino acid sequence RRRLASTNDKG (1 microg/well) was adsorbed to MaxiSorp-treated LumiNunc 96-well white polystyrene plates

(Thermo Scientific, Roskilde, Denmark). The wells were blocked with 3% tryptone in phosphate-buffered saline. Kinase (5 nM) in kinase buffer (25 mM HEPES pH 7.4, 150 mM NaCl, 5 mM β-glycerophosphate, 1.5 mM DTT, 30 mM MgCl2, 1% BSA) was added. Reactions were incubated with or without inhibitor. Reactions were initiated by the addition of ATP (10 microM) for 20 min, which is in the linear range of the assay. The reactions were terminated by addition of EDTA (500 mM, pH 8.0). The plates were washed and phosphorylation was measured using rabbit polyclonal anti- LApSTND1 and horseradish peroxidase (HRP)-conjugated donkey anti-rabbit (Jackson ImmunoResearch Laboratories, West Grove, PA) antibodies. Western Lightning Enhanced Chemiluminescent Reagent Plus (PerkinElmer Life Sciences, Waltham, MA) was used to measure HRP activity. To determine IC50 values, non-linear regression analysis was performed using GraphPad Prism version 6.0a (La Jolla, CA). Proliferation assays were performed as previously described (*210*). Briefly, 200,000 MCF-7 or MCF-10A cells were seeded in 24-well tissue culture treated plates in media recommended by ATCC. Inhibitor or vehicle was added and proliferation was measured after 48 h using CellTiterGlo reagent (Promega, Madison, WI) according to the manufacturer's protocol. To determine IC50 values, non-linear regression analysis was performed using GraphPad Prism version 6.0a (La Jolla, CA). Immunoblot analysis were performed as previously described (*210*) . Briefly, 250,000 MCF-7 cells were seeded onto a 35-mm tissue culture dish. The next day the medium was replaced with serum-free medium. After 16 hours, the medium was changed for serum-free medium with DMSO, serum-containing medium with DMSO, or serum-containing medium with inhibitor. Cells were treated for 2 hours before stimulation with PMA (500 nM) for 20 minutes. Cell lysis was performed as previously described (*210*). Lysates were normalized for total protein, electrophoresed, and immunoblotted. Antibodies used for immunoblotting include: anti-(K/R)x(K/R)xx(pS/pT) motif (9611), anti-(K/R)(K/R)x(pS/pT) motif (9621), anti-(K/R)x(pS/pT)Φ(K/R) motif (2261), monoclonal anti-phospho-Y (9411), anti-eEF2 (2332), anti-phospho-eEF2 (2331), and anti-cyclin D1 (2926), from Cell Signaling Technology (Danvers,

MA). Secondary antibodies used were HRP-conjugated donkey anti-rabbit and goat anti-mouse (Jackson ImmunoResearch Laboratories, West Grove, PA)

Results

The Ser/Thr kinases, RSK, have emerged as a potential drug target for numerous cancers (*137*). A number of RSK inhibitors have been identified (*99, 199, 200, 205, 207, 208, 226-229*) and of these the kaempferol L-rhamnoside SL0101 (1a) is the only allosteric inhibitor of RSK (Fig. 6.2) (*200*), which most likely accounts for its specificity (*199*).

**Figure 6. 2 Structures of SL0101 (1a) and top analogue (2).**
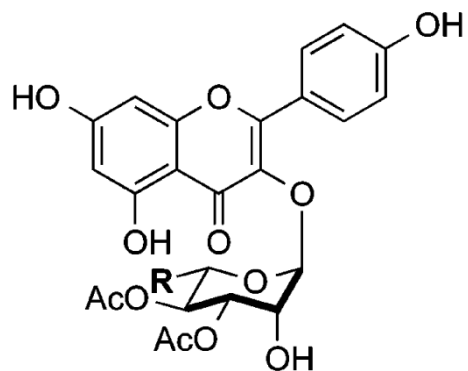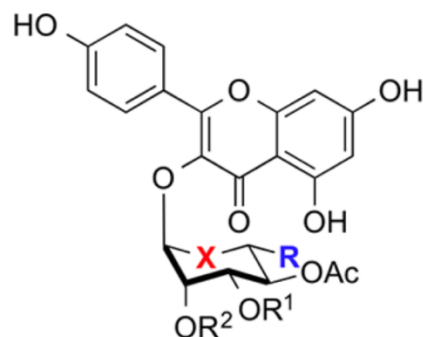

1a: R = Me; **SL0101**: 0.99 μM (IC$_{50}$)
2: R = *n*-Pr; **Best Analogue**: 0.02 μM (IC$_{50}$)

RSK is unusual in that it contains two nonidentical kinase domains (*230*). On the basis of the crystal structure of SL0101 in complex with the RSK2 N-terminal kinase domain (NTKD) we generated the derivative, C3″/C4″-diacetate with a C6″-npropyl substituent 2, which has a 50-fold higher affinity for RSK than SL0101 (*210, 231, 232*). In an effort to further explore the structure− activity relationship of SL0101 as it relates to RSK inhibition, we targeted for synthesis cyclitol (aka, 5a-carbasugar) analogues of SL0101 (e.g., 3 and 4, Figure 6.3) (*233, 234*). We hypothesized that the cyclitol analogues (3a−c) (i.e., sans-anomeric stabilization) would serve as exact conformational mimics of the natural sugar; whereas the enantiomeric analogues (ent)-3a−c serve as control molecules. Finally, to further test the importance of the C6″ alkyl group, we envisioned preparing and evaluating the desmethyl cyclitol analogue 4.

Figure 6. 3 Structure of D-/L-SL0101 analogues 1-4.
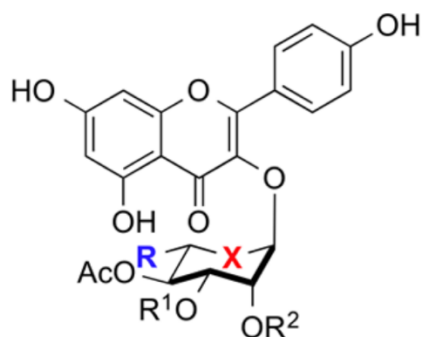
1a: R = Me, **X** = O, R^1 = Ac, R^2 = H	**(ent)-1a: R** = Me, **X** = O, R^1 = Ac, R^2 = H
1b: R = Me, **X** = O, R^1 = H, R^2 = H	**(ent)-1b: R** = Me, **X** = O, R^1 = H, R^2 = H
1c: R = Me, **X** = O, R^1 = H, R^2 = Ac	**(ent)-1c: R** = Me, **X** = O, R^1 = H, R^2 = Ac
3a: R = Me, **X** = CH$_2$, R^1 = Ac, R^2 = H	**(ent)-3a: R** = Me, **X** = CH$_2$, R^1 = Ac, R^2 = H
3b: R = Me, **X** = CH$_2$, R^1 = H, R^2 = H	**(ent)-3b: R** = Me, **X** = CH$_2$, R^1 = H, R^2 = H
3c: R = Me, **X** = CH$_2$, R^1 = H, R^2 = Ac	**(ent)-3c: R** = Me, **X** = CH$_2$, R^1 = H, R^2 = Ac
4: R = H, **X** = CH$_2$, R^1 = Ac, R^2 = H	**(ent)-4: R** = H, **X** = CH$_2$, R^1 = Ac, R^2 = H

We have been developing practical and generalizable approaches to both pyranose (*235-239*) and 5a-carbasugar (*233, 234, 240*) and have reported synthetic approaches to SL0101 and its derivatives. The general approach to these analogues is outlined in Fig. 6.2. The technology that enables this approach was the use of a Pd-catalyzed glycosylation (*233, 234, 241-243*) or cyclitolization (*234, 240*) and subsequent post-glycosylation transformations. Using the Pd-catalyzed glycosylation, the desired pyranose analogues 1a−c and (ent)-1a−c were produced in five to seven steps from pyranones α-L-5 and α-D-5, respectively. Using the related Pd-catalyzed cyclitolization and in the same number of steps, the desired cyclitol analogues 3a−c and (ent)-3a−c were produced from the corresponding enones α-L-6 and α-D-6.

The key to the success of this approach is the reliance of an enantio-divergent (i.e., D/L) and highly stereocontrolled synthesis of both glycosyl- and cyclitol-donors from readily available intermediates (8 and 9, Fig. 6.2). For instance, the pyranose glycosyl donors were readily prepared in three steps from achiral acylfuran intermediate 8. In contrast, the carbasugar cyclitol donor 6 was significantly more difficult to prepare. Like the pyranones 5, the cyclitol 6 can also be prepared from a single intermediate, D-quinic acid 9. Thus, in 11 steps, D-quinic acid was converted into α-D-enone α-D-6, whereas in a related 12-step sequence quinic acid can be also converted into its enantiomeric enone, α-L-6.

Figure 6. 4 Enantiodivergent synthesis of SL0101 analogues 1 and 3.
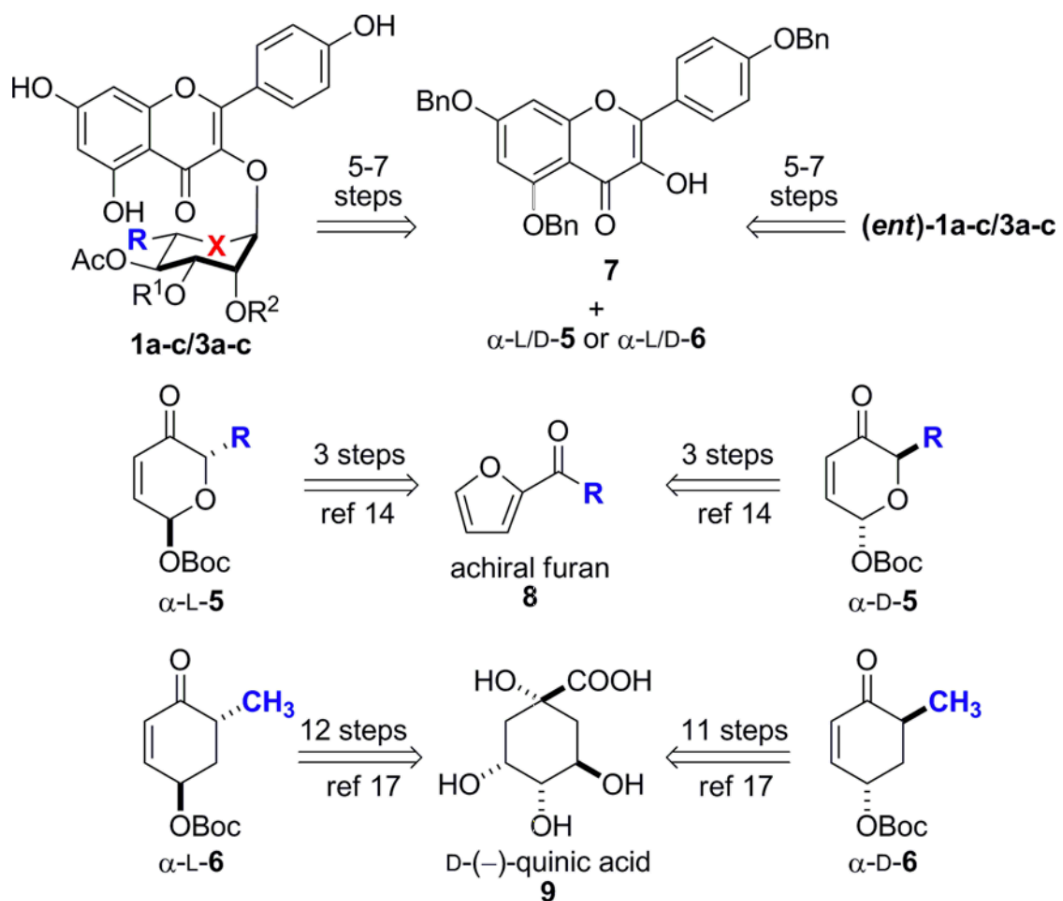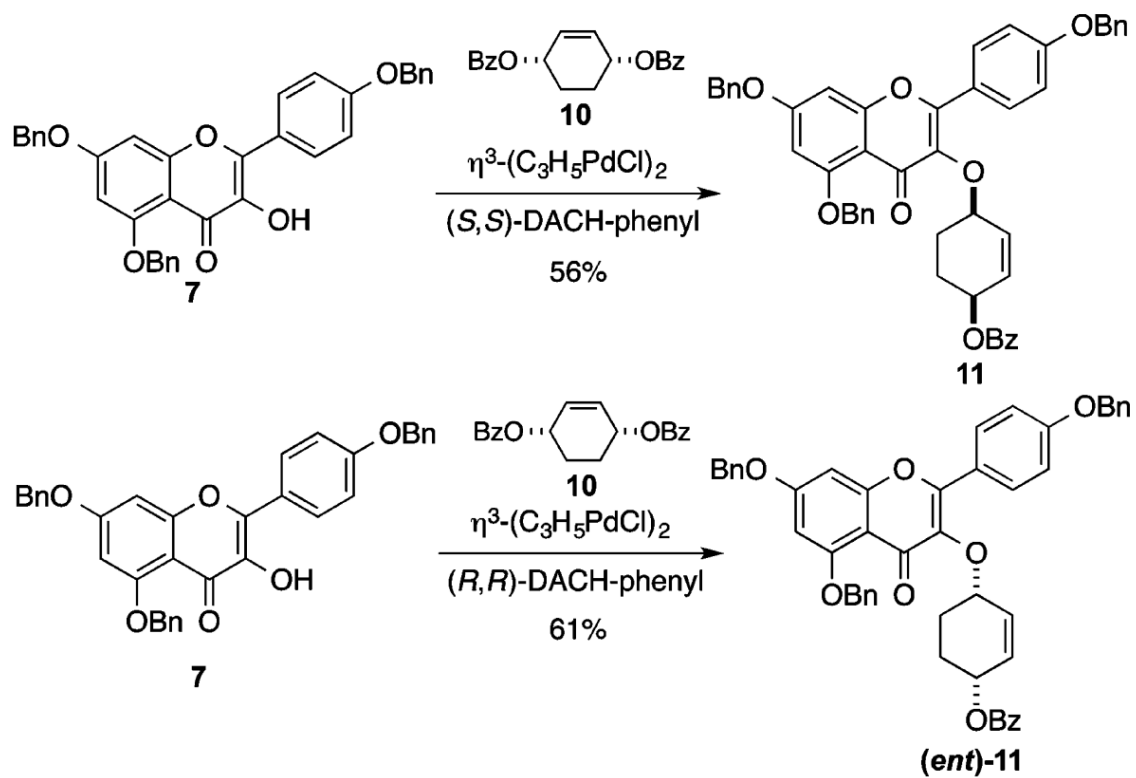
Figure 6. 5 Enantiodivergent cyclitolization of aglycon 7.

With access to the cyclitol analogues 3, we next pursued the de novo asymmetric synthesis of the desmethyl cyclitol analogues 4 and (ent)-4 (Fig. 6.4 and 6.5). Interestingly, the removal of the C6″-methyl group greatly simplifies the analogue synthesis. The simplicity of this approach is enabled by the use of the Trost asymmetric allylation of 7 with meso1,4-bis-benzoate 10 to form either enantiomer of cyclitol 11 (*244-246*). Thus, by appropriate choice of the chiral ligand, cyclitol 11 (via (S,S)-DACH) or its enantiomer (ent)-11 (via (R,R)-DACH) was prepared in only one stereodivergent step. The enantiomeric excess of 12 and (ent)-12 were determined to be >96% ee by Mosher ester analysis. This was accomplished by converting 12 and (ent)-12 into their corresponding Mosher ester and integrating resolved diasteromeric vinyl protons in the 1 H NMR (see online Supporting Information).

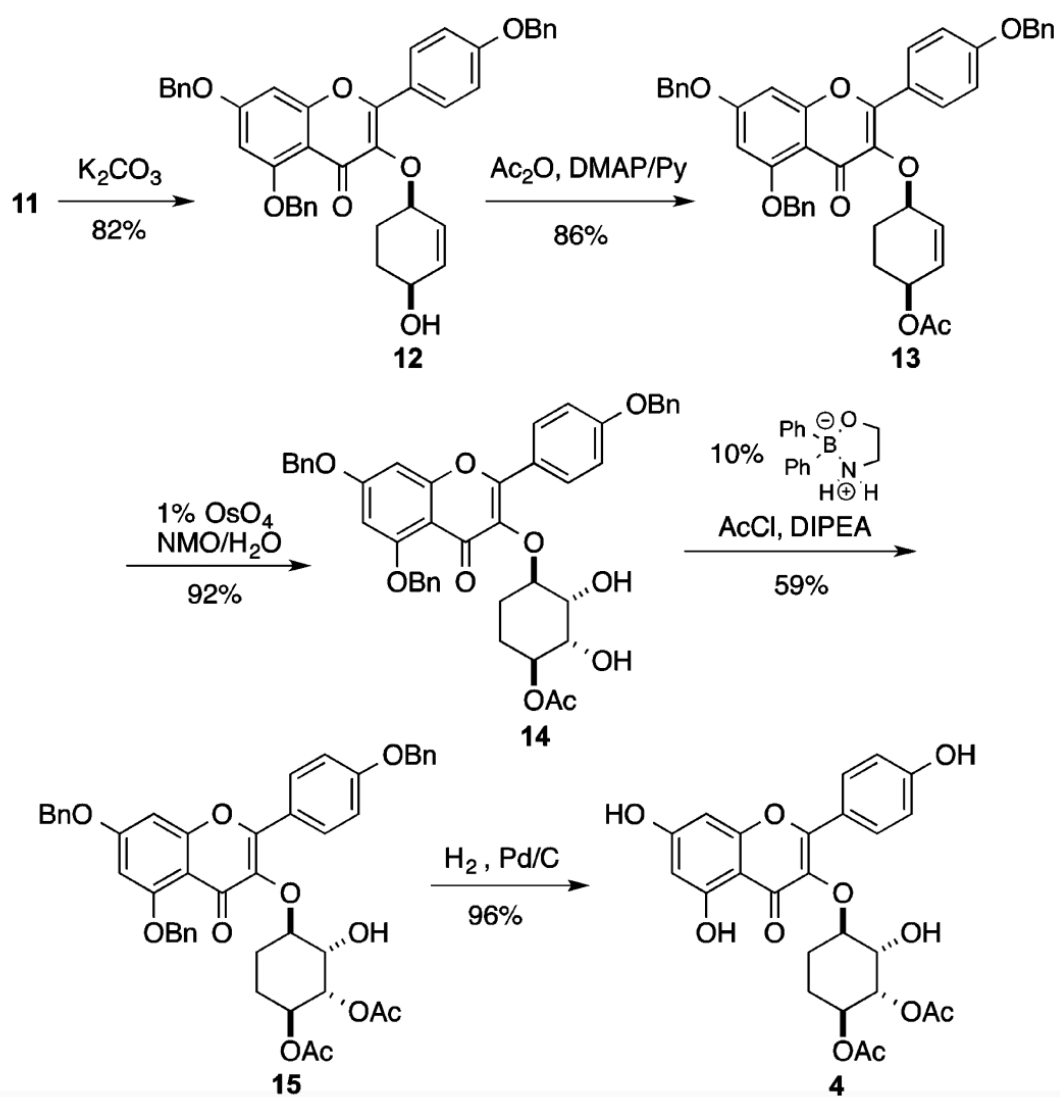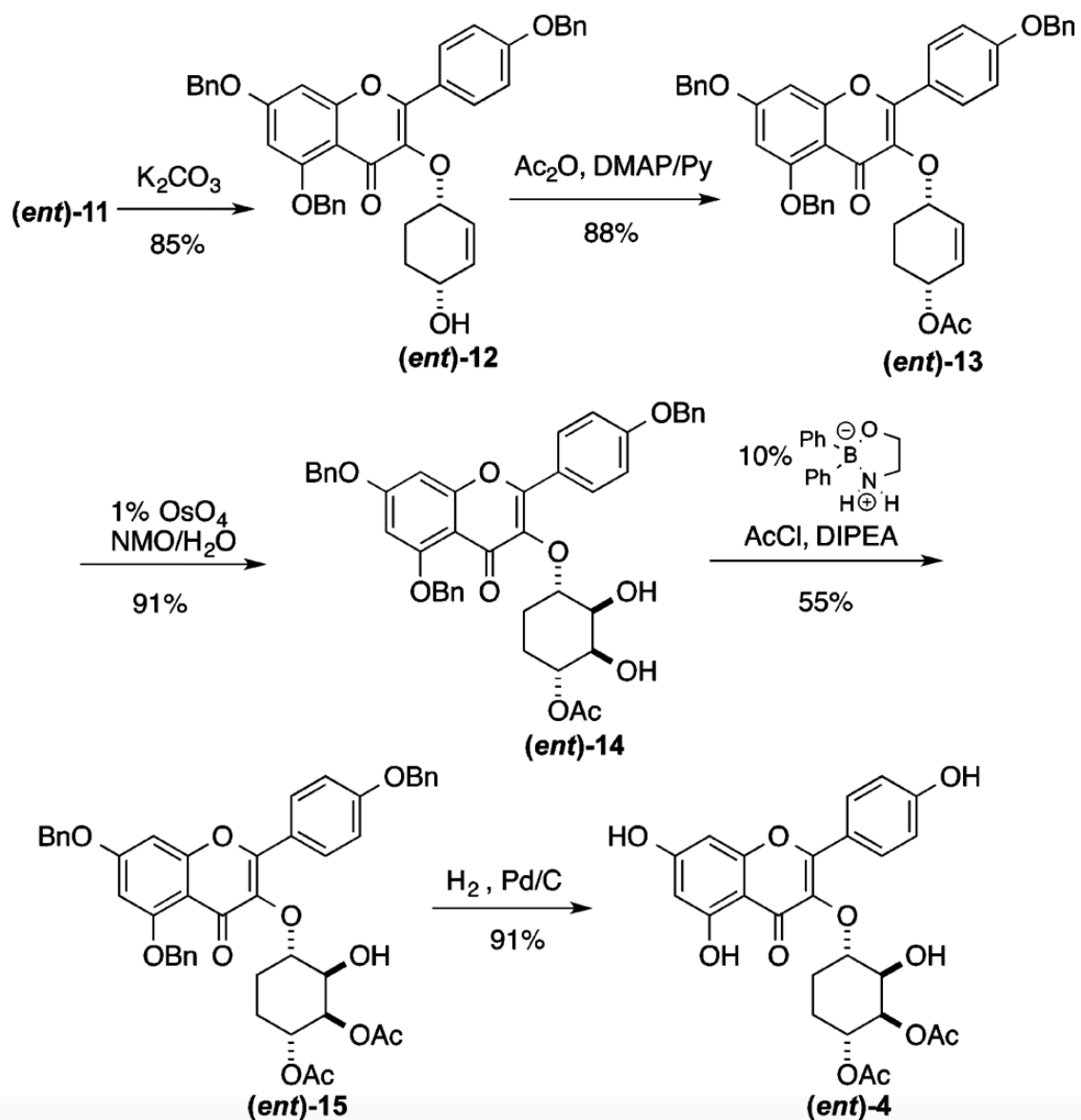**Figure 6. 6 Synthesis of SL0101 cyclitol analogue 4.**

Figure 6. 7 Synthesis of SL0101 cyclitol analogue (ent)-4.

With the C1″/C4″ stereochemistry installed in 11, the C4″ benzoate was transformed into an acetate (Fig. 6.4), via a hydrolysis and acylation sequence (11 to 13). Using an Upjohn dihydroxylation (1% OsO4/NMO),35 the C2″/C3″-hydroxyl groups were stereoselectively installed in 14. The required C3″ acetate was regioselectively installed by means of the Taylor catalysis (14 to 15).36−39 Finally hydrogenolysis was used for a global debenzylation of 15 to give the desired cyclitol analogue 4. Using an identical sequence, the enantiomer 11 was converted into the enantiomeric analogue (ent)-4 (Fig. 6.5).

Using purified recombinant RSK2 enzyme in an in vitro kinase assay, the analogues (ent)-1a, 3a−c, (ent)-3a−c, 4 and (ent)-4 were evaluated for their ability to inhibit RSK2 kinase activity (*113*). Nonlinear regression analysis was used to fit the data (Table 6.1). Regardless of substitution, we found an absolute requirement for the L-isoform, as none of the D-isoforms displayed any RSK2 kinase inhibitory activity at concentrations ≤30 microM.

Interestingly, we found that replacing the ring oxygen in the rhamnose ring with a methylene did not interfere with in vitro RSK2 inhibitory activity (Table 6.1). In fact, the cyclitol analogue 3a was a slightly better inhibitor of RSK than SL0101, albeit the difference is unlikely to be biologically meaningful. In contrast, the cyclitols with varied acetate substitution (3b and 3c) had higher IC50s. This trend was consistent to what was observed for the related rhamnose sugar analogues (1b and 1c) (*247*). The C6″ methyl group proved to be important for activity, as the desmethyl analogue 4 was a poor inhibitor. Even in the less active desmethyl series, the importance of the sugar absolute stereochemistry could be seen, as 4 was significantly more active than its enantiomer (ent)-4. This result is consistent with our crystal structure of the RSK2 NTKD/SL0101 complex. Specifically, we observed SL0101 in a specific 3D orientation with the C6″ methyl group residing in a key hydrophobic pocket (*200*) and that alkyl substitution of the C6″ alkyl group (Me to n-Pr) increased the affinity for RSK2 (*210*).

Table 6.1 In vitro potency of SL0101 (1a) and analogues. RSK2 IC50: concentration needed

for 50% RSK2 inhibition (n > 2; quadruplicate; mean ± S.D.; p(SL0101) Student's t test

compared to SL0101). N.D. no inhibition detected.

Table 6. 1 In vitro potency of SL0101 and analogues.

name	RSK2 IC50 (microM)	RSK2 IC50 p(SL0101)
Sl0101 (1a)	0.37 ≥ 0.13	
(ent)-1a	N.D.	
3a	0.27 ≥ 0.15	0.0404
(ent)-3a	N.D.	
3b	1.23 ≥ 0.62	<0.0001
(ent)-3b	N.D.	
3c	1.60 ≥ 0.66	<0.0001
(ent)-3c	N.D.	
4	8.93 ≥ 1.02	<0.0001
(ent)-4a	N.D.	

The ability of the analogues to inhibit the proliferation of the breast cancer cell line, MCF-7, was compared to that obtained with the immortalized nontransformed human breast cell line, MCF-10A. We have found that a preferential ability to inhibit MCF-7 compared to MCF-10A proliferation correlates with RSK inhibition (*113, 210, 247-249*). The cyclitol analogue 3b inhibited both cell lines to the same extent, which suggests that it does not specifically inhibit RSK (Fig. 6.8). In contrast, the enantiomer (ent)-3b showed no inhibition of either cell line. At 25 μM the analogue 3a inhibited MCF-7 proliferation by ~60% but also significantly inhibited MCF-10A proliferation (Fig. 6.9 A). For comparison, at 100 μM SL0101 (1a) inhibited MCF-7 proliferation by ~60% but had no effect on MCF-10A proliferation. Both analogues 3a and 3c were able to completely inhibit proliferation of MCF-7 cells at ~50 microM, but they also significantly inhibited MCF-10A proliferation at that concentration (Fig. 6.9). For both 3a and 3c the dose response differed by ~3-fold between MCF-7 and MCF-10A cells. This modest differential effect suggests that the inhibitors are not specific for RSK, as we have found that MCF-10A proliferation is not dependent on RSK.

Figure 6.8 C3", C4" acetates are essential for preferential inhibition of MCF-7 proliferation. ATP content was measured after 48 h of treatment. Values are the fold proliferation as a % of the control within each cell line (n ≥ 2; triplicate; mean ≥ S.D.; * p < 0.01 Student's t test compared to control.
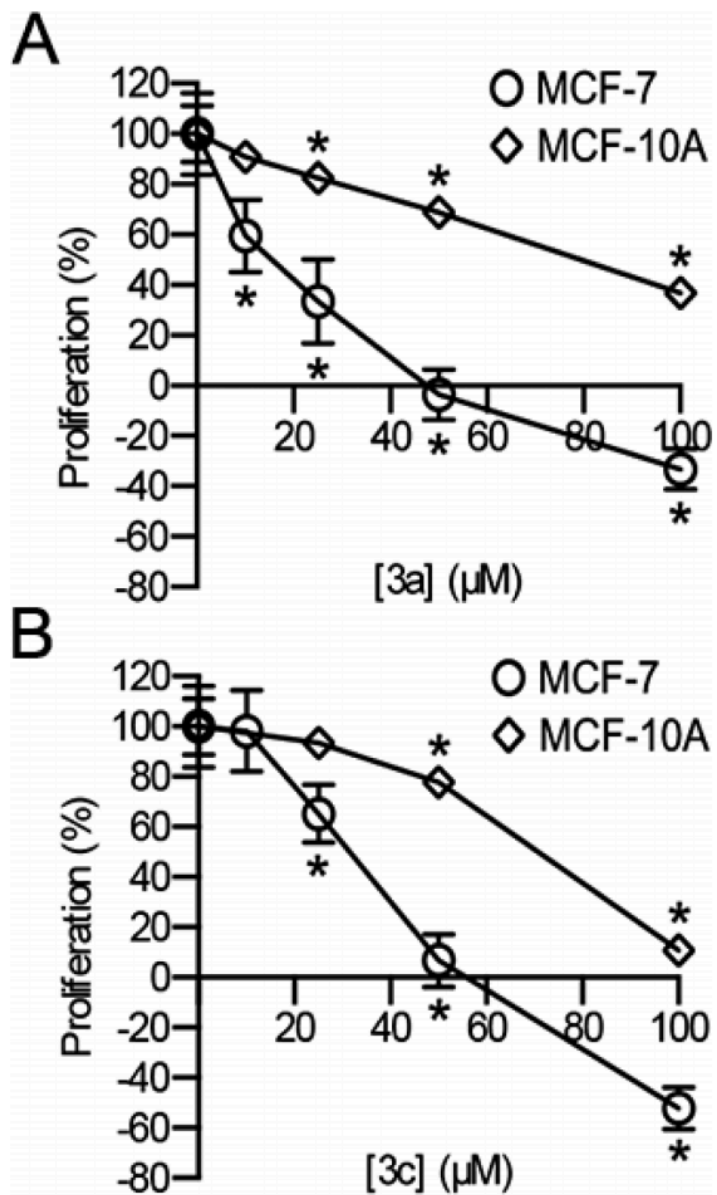
Figure 6. 8 C3", C4" acetates are essential for preferential inhibition of MCF-7 proliferation.
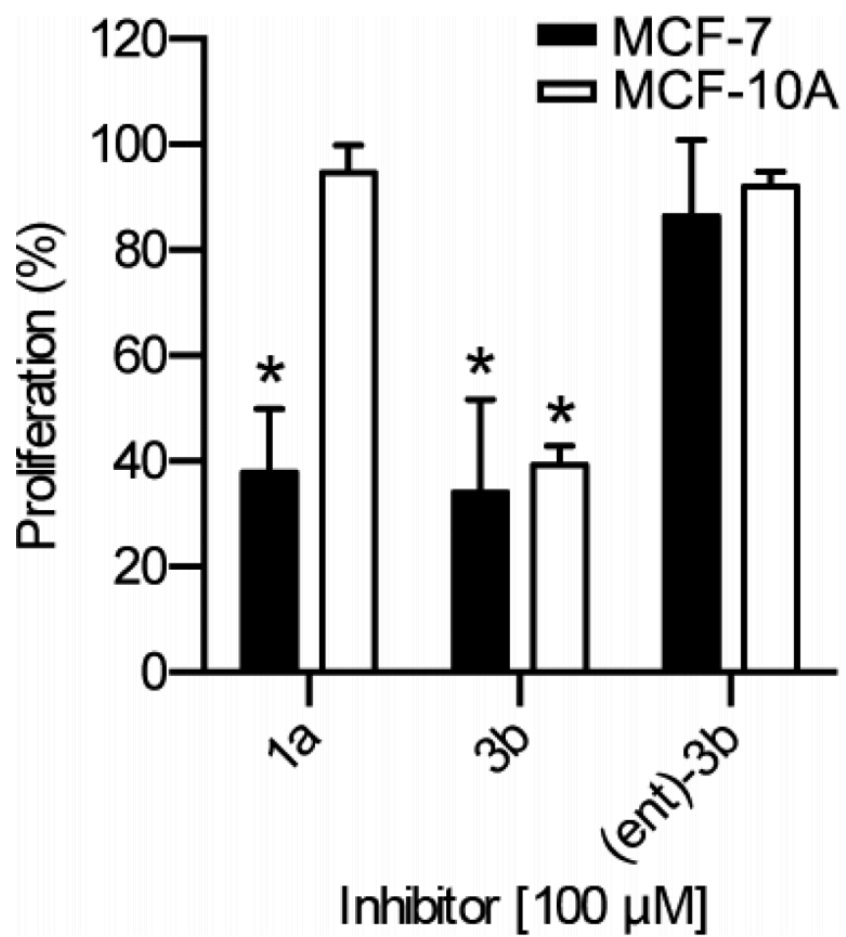
Figure 6.9 Efficacy and specificity of analogues 3a and 3c for inhibition of RSK. As

described in Figure 3 (n ≥ 2; triplicate; mean ± S.D.; * p ≥ 0.01 Student's t test compared to

control).

Figure 6. 9 Efficacy and specificity of analogues 3a and 3c for inhibition of RSK.

To further investigate the specificity of 3a and 3c for inhibition of RSK we determined their ability to inhibit known RSK substrates in comparison to SL0101. We tested the compounds 3a and 3c at 50 microM, which is the cytostatic concentration. Lysates were generated from MCF-7 cells that had been treated with the mitogen, phorbol myristate acetate (10) after a pretreatment with inhibitor or vehicle. Inhibition of RSK is known to result in an increase in the phosphorylation of eukaryotic elongation factor 2 (p-eEF2) via release of the RSK-induced repression of eEF2 kinase (143). As expected SL0101 dramatically enhanced p-eEF2 levels, but 3a and 3c induced only a minor increase (Fig. 6.10 A). To further evaluate whether the analogues could alter RSK biomarkers we used an antibody against a phosphorylation motif, which is recognized by a subset of the AGC family of kinases, which includes RSK. SL0101 decreased the intensity of a band at ~65 and ~27 kDa, but 3a and 3c did not alter the phosphorylation pattern compared to the PMA control (Fig. 6.10 B). We have also determined that RSK regulates the levels of the oncogene, cyclin D1. In agreement with our previous observations SL0101 decreased cyclin D1 levels, whereas 3a and 3c had no effect (Fig. 6.10 A). We conclude that 3a and 3c are not specific for RSK inhibition in cell-based assays.

Figure 6.10 Evaluation of SL0101 (1a), 3a, and 3c as RSK-specific inhibitors in MCF-7 cells. MCF-7 cells were treated with PMA after pretreatment with the indicated inhibitors. Lysates of the cells were immunoblotted. The arrows indicate bands whose intensity decreases upon treatment with SL0101 (1a).

Figure 6. 10 Evaluation of SL0101 (1a), 3a, and 3c as RSK-specific inhibitors in MCF-7 cells.
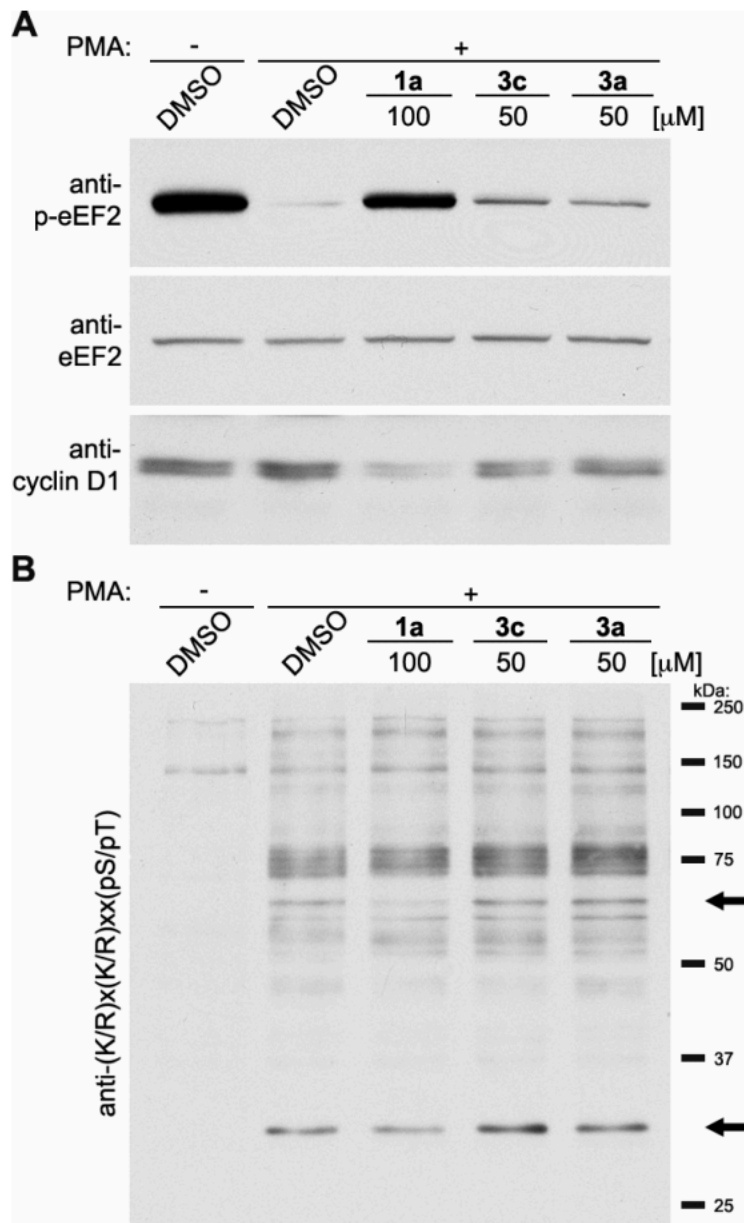
To obtain insight into kinases that 3a and 3c could target we used antibodies that detect the phosphorylation motif of protein kinase A (PKA), protein kinase C (PKC), and tyrosine kinases. Cyclitols 3a and 3c did not alter the phosphorylation pattern obtained with antibodies to the PKC and tyrosine kinase phosphorylation motifs (Fig. 6.11). However, 3a and 3c resulted in the partial increase in the intensity of a band at ~90 kDa. In contrast, SL0101 dramatically increased the intensity of this band compared to PMA. The PKA motif antibody is able to detect phosphorylations generated by RSK, and therefore, observing changes with SL0101 is expected. On the basis of our immunoblot analysis, 3a and 3c do not inhibit kinases that prefer an Arg at the -5 position but do inhibit kinases that prefer an Arg at the -3 and -2 positions from the Ser or Thr phosphorylation site. This information narrows down the possible candidate kinases from within the AGC kinase family that 3a and 3c target.

Figure 6.11 Characterization of selectivity of 3a and 3c compared to SL0101 (1a) in MCF-7 cells. MCF-7 cells were treated with PMA after pre-treatment with the indicated inhibitors. Lysates were electrophoresed and immunoblotted. The arrows indicate bands whose intensity changes upon treatment with SL0101 (1a). Immunblotting with antibodies to detect the PKA phosphorylation motif (A), the PKC phosphorylation motif (B), or the tyrosine kinase motif (C).

Figure 6. 11 Characterization of selectivity of 3a and 3c compared to SL0101.

Conclusion

In conclusion, using a Pd-catalyzed glycosylation or cyclitolization in combination with post-glycosylation transformation, an enantiomerically diverse set of SL0101 analogues were prepared and evaluated as RSK inhibitors. Replacement of the L-rhamno-sugar with a L-rhamno-5a-carbasugar did not substantially alter the ability of the analogues to inhibit RSK kinase activity in vitro; however, the compounds demonstrated off-target effects in cell-based assays. Further efforts aimed at identifying cyclitol analogues that specifically target RSK inhibition are ongoing and will be reported in due course.
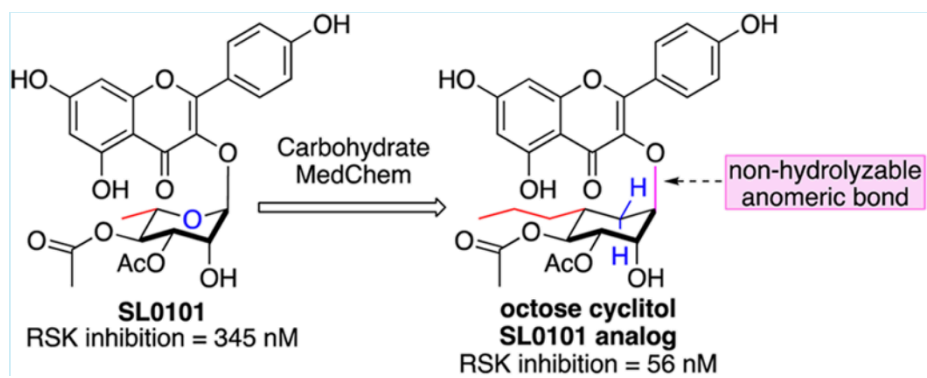
Chapter 7

Stereoselective synthesis and evaluation of C6″-substituted 5a carbasugar analogues of SL0101 as inhibitors of RSK1/2

Adapted from: (142)

Summary

A convergent synthesis of 5a-carbasugar analogues of the nPr-variant of SL0101 is described. The analogues were synthesized in an effort to find compounds with potent in vivo efficacy in the inhibition of p90 ribosomal S6 kinase (RSK1/2). The synthesis derived the desired C-4 L-rhamnose stereochemistry from quinic acid and used a highly selective cuprate addition, $NaBH_4$ reduction, Mitsunobu inversion, and alkene dihydroxylation to install the remaining stereochemistry. A Pd-catalyzed cyclitolization stereoselectively installed the aglycon at the anomeric position. The analogues were evaluated as RSK1/2 inhibitors and found to have 3- to 6-fold improved activity.

Figure 7. 1 Graphical abstract.

SL0101
RSK inhibition = 345 nM

Carbohydrate MedChem

octose cyclitol
SL0101 analog
RSK inhibition = 56 nM

non-hydrolyzable anomeric bond

Materials and methods

General chemistry methods and materials

1 H and 13C spectra were recorded on 400 MHz and 500 MHz spectrometers. Chemical shifts were reported relative to CDCl3 (d 7.26 ppm), CD3OD (d 3.31 ppm), acetone-d6 (d 2.05 ppm) for 1 H, and CDCl3 (d 77.0 ppm), CD3OD (d 49.15 ppm), acetone-d6 (d 29.92 ppm) for 13C. Optical rotations were measured with a digital polarimeter at sodium D line (589 nm) and were reported in concentration of g/100 mL at 25 ºC in the solvent specified. Infrared (IR) spectra were obtained on a FT-IR spectrometer. Flash chromatography was performed using the indicated solvent system on silica gel standard grade 60 (230-400 mesh). Rf values are reported for analytical TLC using the specified solvents and 0.25 mm silica gel 60 F254 plates that were visualized by UV irradiation (254 nm and 365 nm) or by staining with KMnO4 stain or p-anisaldehyde stain. Ethyl ether, tetrahydrofuran, methylene chloride, toluene, and triethylamine were dried by passing through activated alumina (8 x 14 mesh) column with argon gas pressure. Commercial reagents were used without purification unless otherwise noted. Air and/or moisture-sensitive reactions were carried out under an atmosphere of argon/nitrogen using oven/flamed-dried glassware and standard syringe/septum techniques. Melting points are uncorrected. Matrix-assisted laser desorption ionization time-of-flight (MALDI-TOF) mass spectra were obtained using α-cyano-4-hydroxycinnamic acid (CCA) as the matrix on a MALDI-TOF mass spectrometer.

Purified recombinant RSK2

His-tagged RSK2 cDNA was generated using the Bac-to-Bac Baculovirus Expression System (Invitrogen, Carlsbad, CA). Recombinant RSK2 was expressed in Sf9 cells and activated by a 20 min treatment with phorbol 12-myristate 13-acetate (10). Protein was purified using the Ni-NTA Spin Kit (Qiagen, Valencia, CA).

In vitro kinase assays

The assays were performed as previously described (137). Briefly, a fusion protein consisting of glutathione Stransferase and the amino acid sequence RRRLASTNDKG (1 microg/well) was adsorbed to MaxiSorp-treated LumiNunc 96-well white polystyrene plates (Thermo Scientific, Roskilde, Denmark). The wells were blocked with 3% tryptone in phosphate-buffered saline. Kinase (5 nM) in kinase buffer (25 mM HEPES pH 7.4), 150 mM NaCl, 5 mM "-glycerophosphate, 1.5 mM DTT, 30 mM MgCl2, 1% BSA) was added.

Reactions were incubated with or without inhibitor. Reactions were initiated by the addition of ATP (10 microM) for 20 min, which is in the linear range of the assay. The reactions were terminated by addition of EDTA (500 mM, pH 8.0). The plates were washed and phosphorylation was measured using rabbit polyclonal anti- LApSTND1 and horseradish peroxidase (HRP)-conjugated donkey anti-rabbit (Jackson ImmunoResearch Laboratories, West Grove, PA) antibodies. Western Lightning Enhanced Chemiluminescent Reagent Plus (PerkinElmer Life Sciences, Waltham, MA) was used to measure HRP activity. To determine IC50 values, non-linear regression analysis was performed using GraphPad Prism version 6.0a (La Jolla, CA).
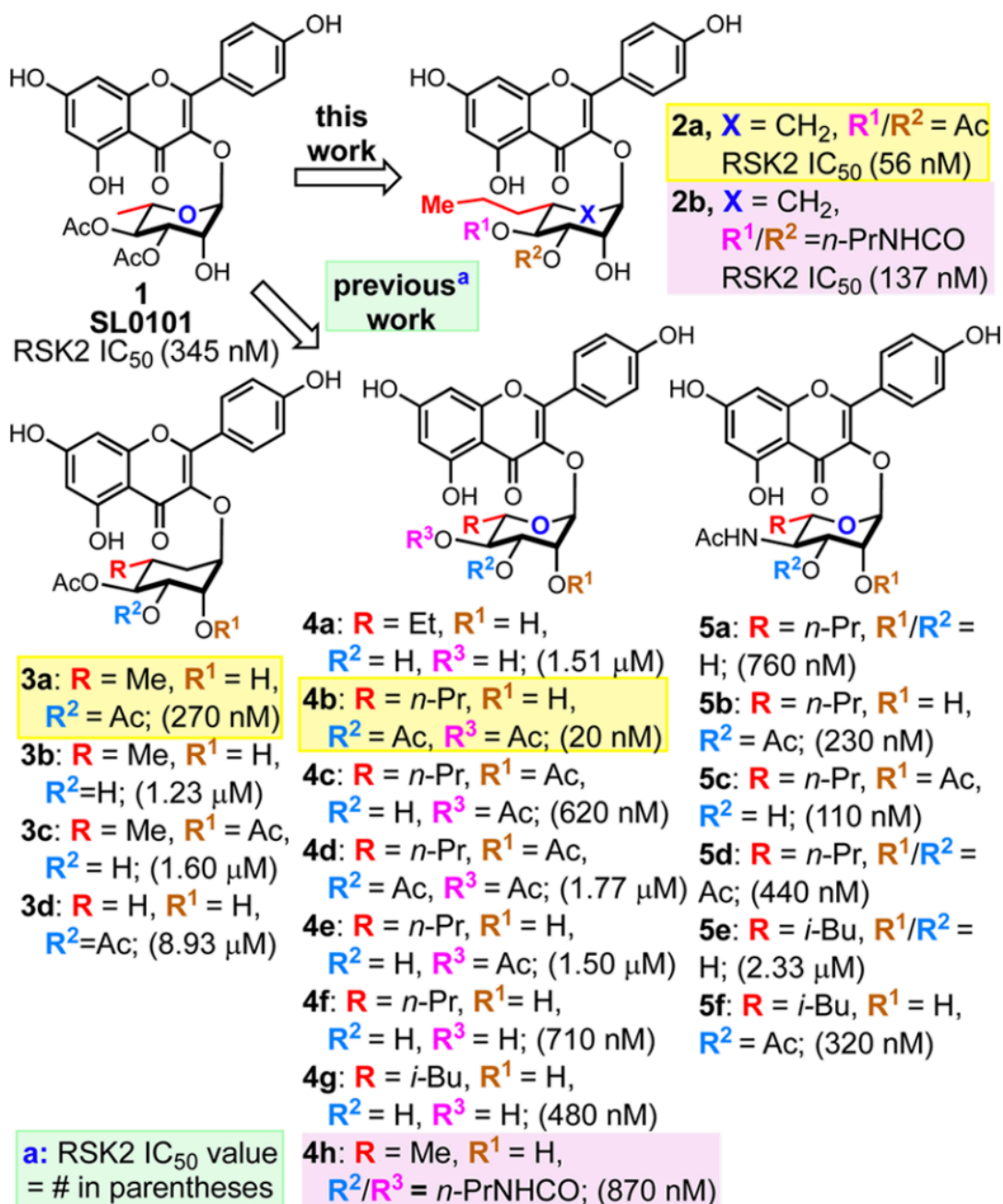
Results

The p90 ribosomal S6 kinases (RSK) are a family of Ser/Thr protein kinases (*137*). Two isoforms (RSK1/2) from this family are involved in the etiology of a number of different cancers (*99, 221*). In an effort aimed at identifying RSK1/2 inhibitors, the flavonoid glycoside natural product SL0101 (1) was discovered as a relatively selective inhibitor of the N-terminal kinase domain (NTKD) of RSK (*113*). RSK has two kinase domains where the Nterminal domain (NTKD) is responsible for phosphorylation of target substrates (*230*). Based on the crystal structure of the RSK2 NTKD complexed with SL0101, a major conformational rearrangement of the N-lobe of the kinase domain generates the inhibitor-binding pocket (*200*).

Inspired by its unique activity and selectivity, we have been exploring structure−activity relationship (SAR) requirements associated with SL0101 (1) (*113, 247, 249*). As part of these studies, we have developed a de novo asymmetric synthesis (*250*) (*251, 252*) of SL0101, its enantiomer, and several congeners (*232, 234*). Our studies have identified several analogues with improved activity and have emphasized the importance of the rhamnose sugar and its C-3 and C-4 acetates. In addition, we have found that substitution at the C-6 position (*231, 232, 234*) and the ring oxygen (2 and 3) of the sugar gives improved efficacy in the in vitro kinase assays and cell-based studies (*231, 232, 234*).

SL0101 (1) has a short biological half-life in vivo (*200*), which is presumably due to the hydrolyzable C-3/C-4-acetates on the sugar, as well as an O-glycosidic bond. To identify less labile groups that could replace the ester without loss of affinity, we have investigated replacing the rhamnose C-4-acetate (e.g., 5a−f with a C-4 acetamide), the C-3/C-4-acetates (e.g., 4h with a C-3/ C-4-n-Pr-carbamates), and the ring oxygen with a methylene group (i.e., 3a−d carbasugars) (*232, 234*). As part of our ongoing effort to identify RSK1/2-inhibitors as potential therapeutics, we decided to test the effects of combining these three substitutions and targeted two analogues 2a−b (Fig. 7.2). Herein we disclose the synthesis of cyclitol analogues 2a and 2b as well as the relative RSK2 inhibitory activity.

Figure 7. 2 SAR for SL0101 and RSK inhibition.

2a, X = CH_2, **R^1/R^2** = Ac
RSK2 IC_{50} (56 nM)

2b, X = CH_2,
R^1/R^2 =n-PrNHCO
RSK2 IC_{50} (137 nM)

1
SL0101
RSK2 IC_{50} (345 nM)

this work

previous^a work

3a: R = Me, **R^1** = H,
R^2 = Ac; (270 nM)
3b: R = Me, **R^1** = H,
R^2=H; (1.23 μM)
3c: R = Me, **R^1** = Ac,
R^2 = H; (1.60 μM)
3d: R = H, **R^1** = H,
R^2=Ac; (8.93 μM)

4a: **R** = Et, **R^1** = H,
R^2 = H, **R^3** = H; (1.51 μM)
4b: R = n-Pr, **R^1** = H,
R^2 = Ac, **R^3** = Ac; (20 nM)
4c: R = n-Pr, **R^1** = Ac,
R^2 = H, **R^3** = Ac; (620 nM)
4d: R = n-Pr, **R^1** = Ac,
R^2 = Ac, **R^3** = Ac; (1.77 μM)
4e: R = n-Pr, **R^1** = H,
R^2 = H, **R^3** = Ac; (1.50 μM)
4f: R = n-Pr, **R^1**= H,
R^2 = H, **R^3** = H; (710 nM)
4g: **R** = i-Bu, **R^1** = H,
R^2 = H, **R^3** = H; (480 nM)
4h: **R** = Me, **R^1** = H,
R^2/R^3 = n-PrNHCO; (870 nM)

5a: R = n-Pr, **R^1/R^2** =
H; (760 nM)
5b: R = n-Pr, **R^1** = H,
R^2 = Ac; (230 nM)
5c: R = n-Pr, **R^1** = Ac,
R^2 = H; (110 nM)
5d: R = n-Pr, **R^1/R^2** =
Ac; (440 nM)
5e: R = i-Bu, **R^1/R^2** =
H; (2.33 μM)
5f: R = i-Bu, **R^1** = H,
R^2 = Ac; (320 nM)

a: RSK2 IC_{50} value = # in parentheses

Retrosynthetically, we envisioned preparing 2a and 2b in a route analogous to our previously established routes to SL0101 analogues 1−5 (e.g., 6 + 7, Fig. 7.3). Specifically, we expected that 2a/b would arise from the Pd-catalyzed cyclitolization of 7 with enone 8 (211, *232-234*). Base on our previous success, we viewed the cyclitol donor 8 would arise from quinic acid 10 via enone 9 (*253, 254*), where the quinic acid tertiary alcohol would become the C-4 ketone and the central alcohol of the triol would become the C-1 anomeric position.

At the outset, our efforts to extend our previous cyclitol synthesis (R = H) encountered difficulty, associated primarily with achieving high stereocontrol in the conversion of 9 into 12b. Specifically, we explored the possibility of installing the sugar Lstereochemistry at C-5 by means of a selective hydrogenation of the enone 11 from the exoface to selectively provide 12b over 12a. To our surprise, when we exposed 11 to typical hydrogenation conditions (1 atm of H2 with Pd/C), we found 12a was the major isomer, but with poor diastereoselectivity (3:1) (Fig. 7.4). This problem was exacerbated by the fact that isomerization of the position α to the ketone occurred when we tried to deprotect the acetonide (*233*). These two compounding factors prompted a search for an alternative approach (*243, 255, 256*).

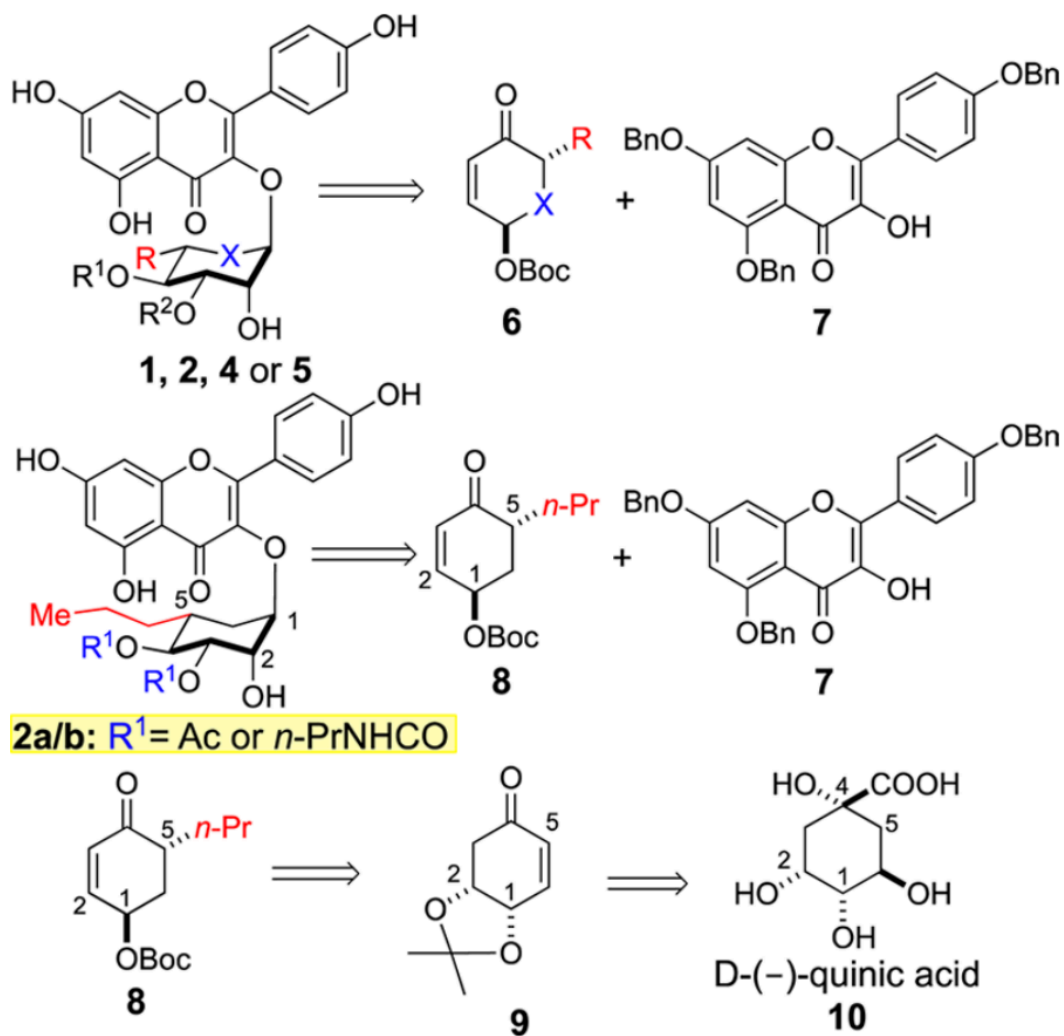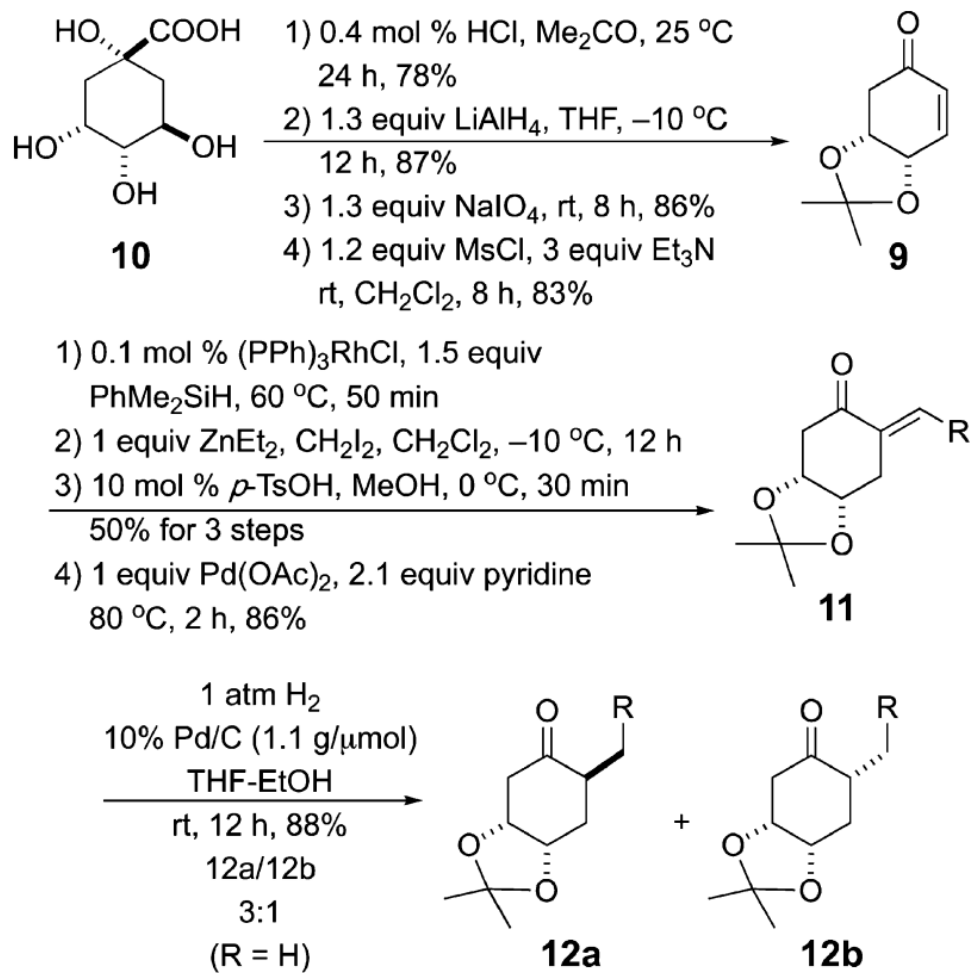**Figure 7. 3 Retrosynthesis of n-Pr carbasugar analogues.**

2a/b: R¹= Ac or n-PrNHCO

Figure 7. 4 Initial attempt to a-L-cyclitol donors.

1) 0.4 mol % HCl, Me$_2$CO, 25 °C
   24 h, 78%
2) 1.3 equiv LiAlH$_4$, THF, −10 °C
   12 h, 87%
3) 1.3 equiv NaIO$_4$, rt, 8 h, 86%
4) 1.2 equiv MsCl, 3 equiv Et$_3$N
   rt, CH$_2$Cl$_2$, 8 h, 83%

10 → **9**

1) 0.1 mol % (PPh)$_3$RhCl, 1.5 equiv
   PhMe$_2$SiH, 60 °C, 50 min
2) 1 equiv ZnEt$_2$, CH$_2$I$_2$, CH$_2$Cl$_2$, −10 °C, 12 h
3) 10 mol % p-TsOH, MeOH, 0 °C, 30 min
   50% for 3 steps
4) 1 equiv Pd(OAc)$_2$, 2.1 equiv pyridine
   80 °C, 2 h, 86%

11

1 atm H$_2$
10% Pd/C (1.1 g/μmol)
THF-EtOH
rt, 12 h, 88%
12a/12b
3:1
(R = H)

12a + **12b**

216

Our redesigned retrosynthesis turned the original design 180° (Fig. 7.5), with the quinic acid tertiary alcohol becoming the carbasugar C-1 anomeric position and the central alcohol of the triol becoming the C-4 enone 8. Because of complications with its conversion to enone 8 this effort turned to the synthesis of allylic acetate 17. Specifically, the allylic benzoate 17 already had a Pd-π-allyl leaving group at the pseudoanomeric position for the cyclitolization reaction. In addition, benzoate 17 also had the desired carbasugar C-4 acetate in the correct rhamno-stereochemistry. The question that remained was could we find conditions to selectively ionize the axial C-1 allylic p-NO2Bz group without touching the allylic C-4 acetate. In addition, we were concerned that the C-4 acetate may not control the regiochemistry of nucleophilic attack to the π-allyl intermediate (i.e., TS-1) as well as the C-4 ketone (i.e., TS-2) (*235*). In general, we found a C-4 ketone both improved the electrophilicity of the Pdπ-allyl intermediate and helped direct nucleophilic addition to the C-1 position. In this regard, we were hopeful that the regiocontrol issues could also be controlled by the C-5 n-propyl substituent (232). Altenatively, chiral ligands on the Pd-π-allyl could be used if the C-4 acetate is not sufficient for controlling the regiochemistry.

Figure 7. 5 Synthesis of Pd-cyclitolization donor.
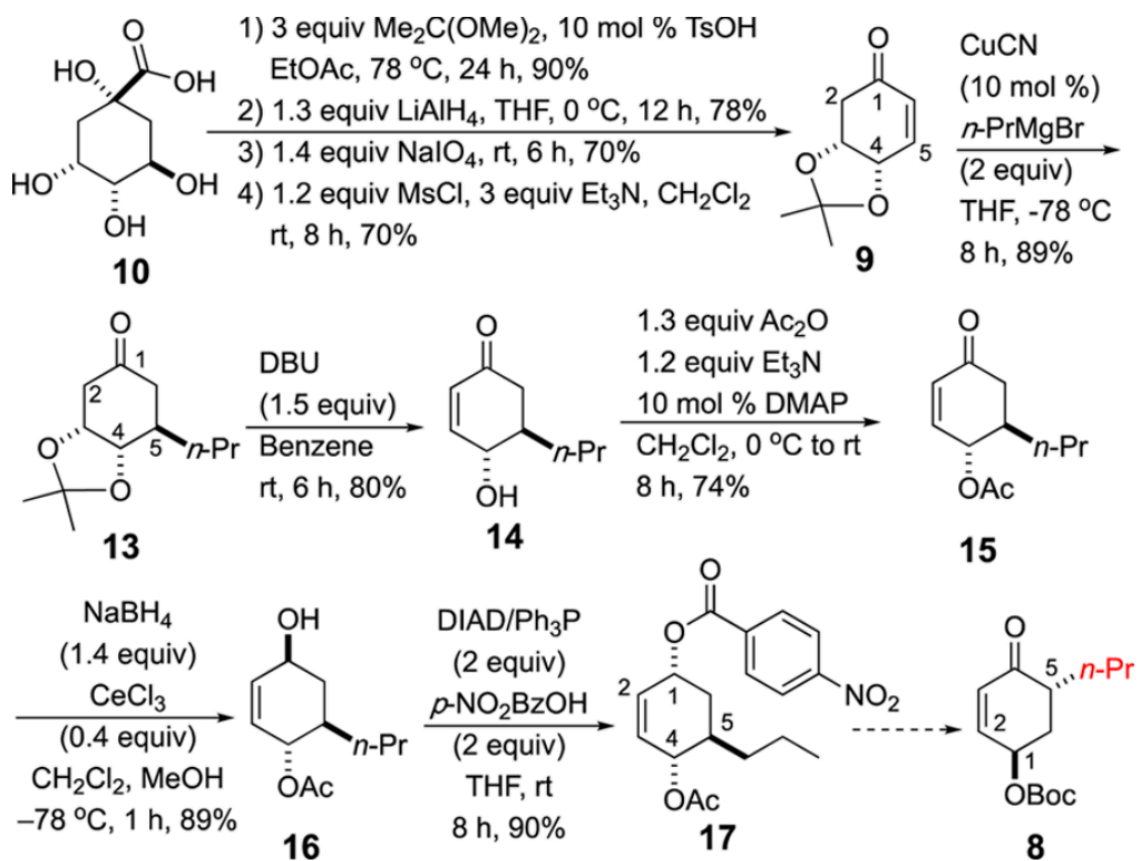
Our redesigned synthesis returned to enone 9, which underwent a highly stereoselective cuprate-promoted addition of n-propyl anion to furnish ketone 13 in an excellent yield and as a single diastereomer (89%). Exposure of 13 to DBU in benzene gave allylic alcohol 14 in good yield (80%). The required C-4 acetate was then installed by an acylation of 14 with acetic anhydride/DMAP with Et3N to deliver allylic acetate 15 (74%). A stereoselective 1,2-reduction of enone 15 under Luche conditions gave the allylic alcohol 16 in good yield (89%) and diastereoselectivity (>10:1). Analysis of the allylic coupling constants in the 1 H NMR for 16 indicated that the Luche reduction occurred via axial attack to install an equatorial alcohol, which corresponds to β-anomeric stereochemistry in the resulting carbasugar. Thus, a Mitsunobu reaction was preformed on 16 with DIAD/PPh3 and p-nitrobenzoic acid to yield the desired cyclitol donor 17 in excellent yield (90%).

Unfortunately, the conversion of the bis-allylic ester 17 to enone 8 proved to be untenable, as conditions for the selective hydrolysis of either of the two esters were not found. In an effort to find a viable alternative, we decided to explore the use of allylic p-NO2-benzoate 17 as a cyclitol donor, in the cyclitolization reactions. The allylic p-nitrobenzoate 17 had some potential advantages to 8 in our planned synthesis of SL0101 analogue 2a. Specifically, the C-1 allylic-benzoate 17 already had a Pd-π-allyl leaving group at the anomeric position for the cyclitolization reaction. In addition, the p-nitrobenzoate 17 also had the desired C-4 acetate with the correct stereochemistry installed, and thus, the aglycon portion would go through two less transformations (Fig. 7.6).

Figure 7. 6 Competing Pd-p-allyl mechanisms.

R = Me, *n*-Pr, *i*-Bu
X = O, CH$_2$
Y = Me, *n*-Pr, *i*-Bu
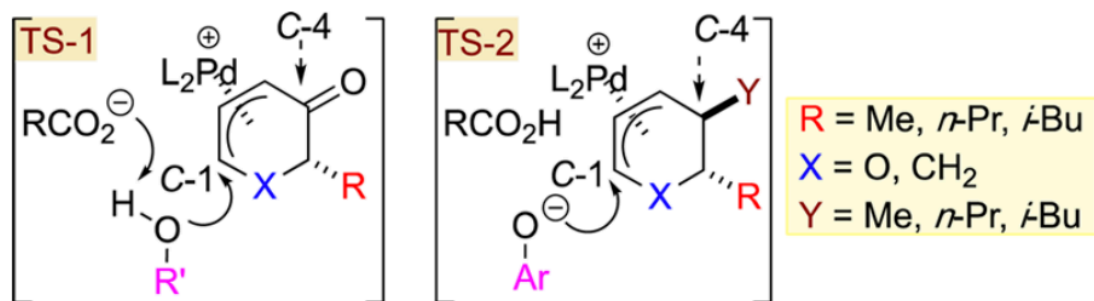
To our delight, when a mixture of p-nitrobenzoate 17 and flavonol 7 was exposed to our typical glycosylation conditions (2.5 mol % Pd2(dba)3·CHCl3 and 10 mol % of PPh3 in CH2Cl2 at 0 °C) the reaction proceeded smoothly to provide the desired product in good yield (80%), in excellent regio- and stereoselectivity (Fig. 7.7). Exposure of the allylic acetate 18 to the Upjohn conditions (OsO4/NMO; 70%) stereoselectively converted it into the rhamno-diol 19 which, when acylated with acetyl chloride and Hunig's base, gave a mixture of the C-3 and C-2 acetates 20 and 21 (1:1.6) in 38% yield. Fortunately, the undesired C-2 acetate 21 could be isomerized to a mixture of acetates which favored the desired C-3 acetate 20 (3:1). Finally, the desired regioisomer 20 was globally deprotected by an exhaustive hydrogenolysis (1 atm of hydrogen with Pd/C), which produced the target C-3/C-4 diacetate 2a in good yield (70%).

With access to the desired diacetate 2a having been established, we turned our attention to the second target compound biscarbamate 2b (Fig. 7.8). Our approach to biscarbamate 2b returned us to allylic acetate 18, which could be hydrolyzed into allylic alcohol 22 with K2CO3 in methanol (84%). The allylic alcohol 22 was converted into n-Pr-carbamate 23 by exposure of it to n-Pr-isocyanate and base (10% DBU/ Et3N in MeCN). Exposure of the allylic carbamate 23 to the Upjohn conditions (OsO4/NMO; 73%) stereoselectively converted it into the rhamno-diol 24. Re-exposure of the C-2/ C-3 diol 24 to the carbamate forming conditions (n-Prisocyanate, 10% DBU/Et3N in MeCN) gave a mixture of C-3 and C-2 carbamates 20 and 21 (1:1). The desired C-3/C-4 biscarbamate 25 could be isolated from that mixture in a 40% overall yield. Unfortunately, the undesired C-2/C-4 biscarbamate 26 could not be isomerized under basic conditions as was the case with the diacetate. Finally, the desired C-3/C-4 regioisomer 25 was globally deprotected by an exhaustive hydrogenolysis (1 atm of hydrogen with Pd/C), to afford the target C-3/C-4 biscarbamate 2b in good overall yield (72%).

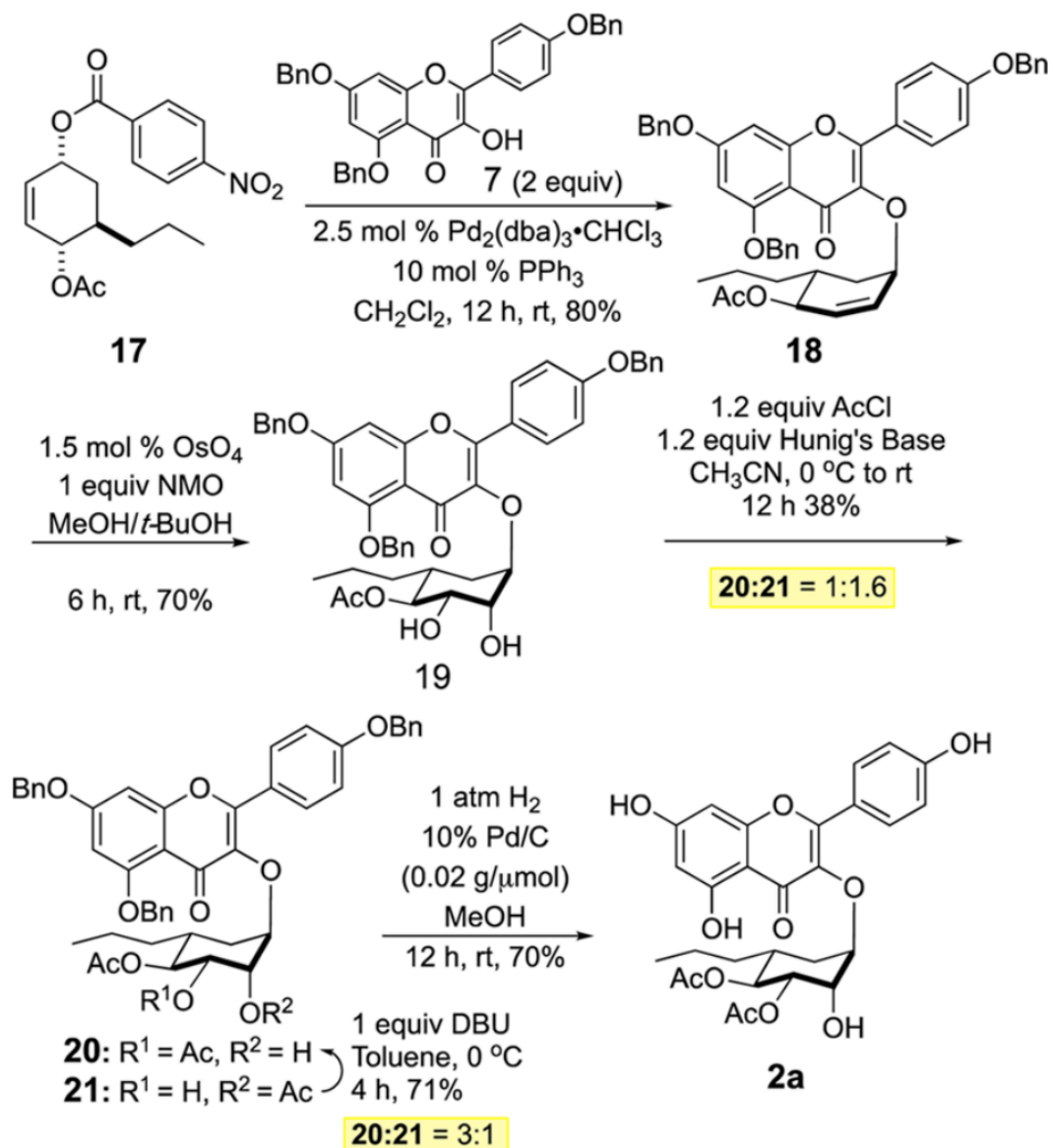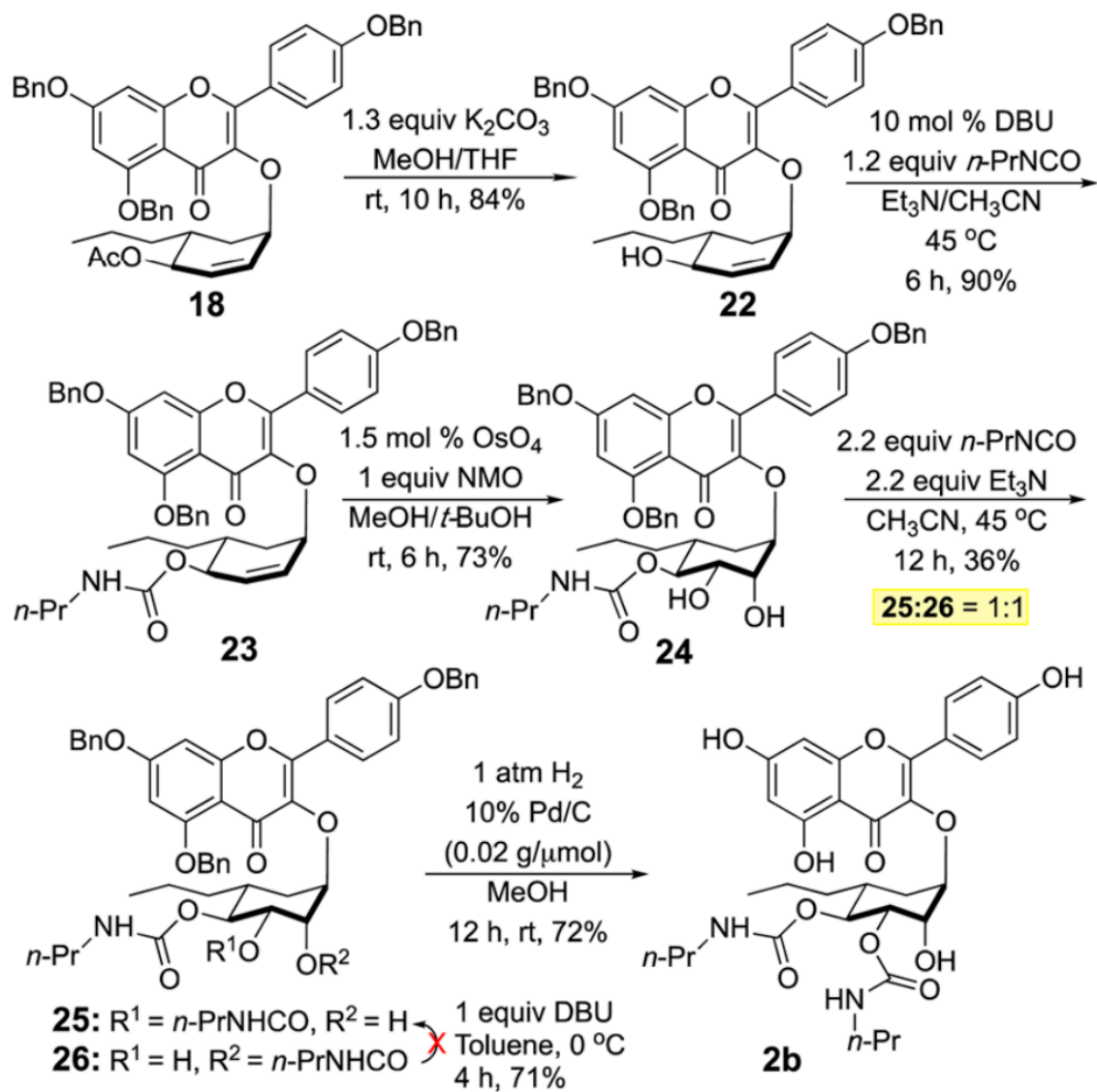**Figure 7. 7 Synthesis of n-Pr carbasugar SL0101 analogue.**
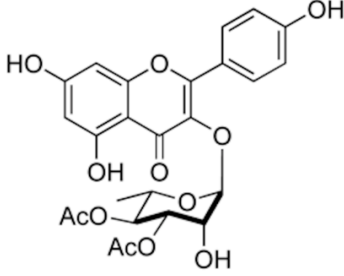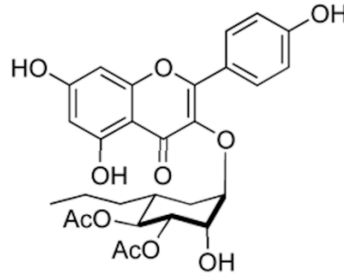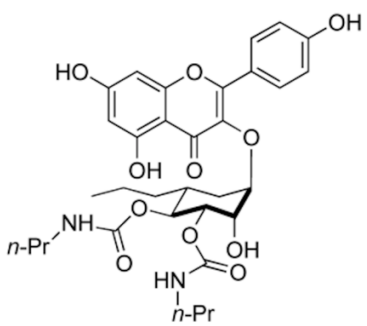
Figure 7. 8 Synthesis of Bis-carbamate analogues.

The efficacy of the two cyclitol analogues 2a and 2b to inhibit RSK2 activity was determined in in vitro kinase assays using purified recombinant RSK2 (Table 7.1). The data were fit using nonlinear regression analysis. Both SL0101 analogues showed improved RSK inhibition over the lead structure SL0101, the nPr cyclitol diacetate 2a having a >6-fold decrease in IC50 (54 nM), whereas the bis-carbamate 2b had an ~3-fold decrease in IC50 (137 nM). In the parent series, cyclitol substitution (i.e., 1 to 3a) led to a modest improvement in the inhibitory activity (345 to 270 nM). In the n-Pr-series, however, the effect of cyclitol substitution (i.e., 4b to 2a) trended toward reduced efficacy (20 to 56 nM). This loss in activity should be easily compensated for by the expected improved bioavailability that results from the hydrolysis-resistant cyclitol substitution. There was also a loss in inhibitory activity (345 to 870 nM) by the n-Pr-carbamate substitution in the parent series (1 to 4h). This negative effect was also observed with the cyclitol series (i.e., 2a to 2b: 56 to 137 nM).

Table 7. 1 In vitro potency of SL0101 and analogues.

Name	Structure	RSK2 IC50 (nM)
SL0101		345 ± 100
2a		56± 27
2b		137 ± 59

Conclusion

In conclusion, using a highly stereoselective Pd-cyclitolization reaction, two new cyclitol analogues of the natural product SL0101 were synthesized and evaluated. These analogues 2a and 2b showed significant improvement in RSK inhibitory activity. Improved bioavailability has already been shown for 2a (115). The synthesis of these new SL0101 cyclitol analogues required the discovery of a novel synthesis of a new cyclitol donor, which demonstrated that the previously believed requirement of a C-4 ketone in the cyclitol donor is not necessary for the reaction with phenol-like nucleophiles. Further studies aimed at defining the requirements for a specific-RSK1/2 inhibition are ongoing and will be reported in due course.
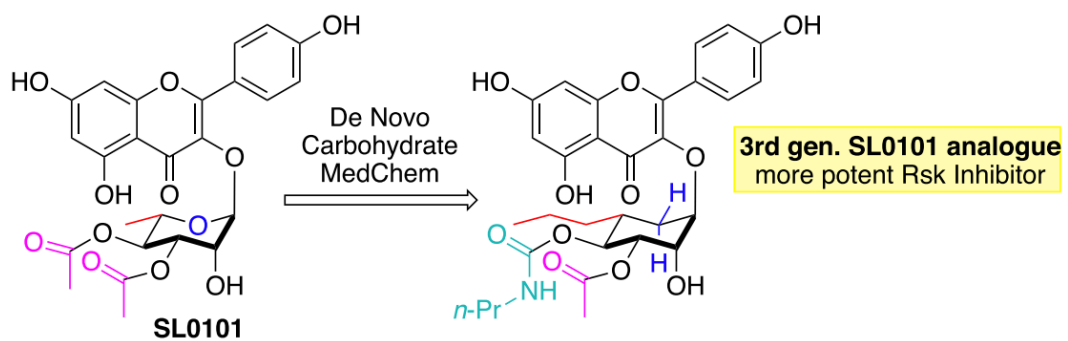
Chapter 8

Regioselective synthesis of a C-4" carbamate, C-6" n-Pr substituted cyclitol analogue of SL0101

Adapted from: (Li et al., 2020, Org Lett)

Summary

An asymmetric synthesis of two analogues of SL0101 (1) has been achieved. The effort is aimed at the discovery of inhibitors of the p90 ribosomal S6 kinase (RSK) with improved bioavailability. The route relies upon the use of the Taylor catalyst to regioselectively install C-3" acetyl or carbamate functionality. This study led to the identification of a third-generation analogue of SL0101 with a C-4" n-Pr-carbamate and a C-3" acetate with improved RSK inhibitory activity.

Figure 8. 1: Graphical abstract.

Materials and methods

General chemistry methods and materials 1 H and 13C spectra were recorded on 400 MHz and 500 MHz spectrometers. Chemical shifts were reported relative to CDCl3 (δ 7.26 ppm), CD3OD (δ 3.31 ppm), acetone-d6 (δ 2.05 ppm) for 1 H, and CDCl3 (δ 77.0 ppm), CD3OD (δ 49.15 ppm), acetone-d6 (δ 29.92 ppm) for 13C. Optical rotations were measured with a digital polarimeter at sodium D line (589 nm) and were reported in concentration of g/100 mL at 25 ºC in the solvent specified. Infrared (IR) spectra were obtained on a FT-IR spectrometer. Flash chromatography was performed using the indicated solvent system on silica gel standard grade 60 (230-400 mesh). Rf values are reported for analytical TLC using the specified solvents and 0.25 mm silica gel 60 F254 plates that were visualized by UV irradiation (254 nm and 365 nm) or by staining with KMnO4 stain or p-anisaldehyde stain. Ethyl ether, tetrahydrofuran, methylene chloride, toluene, and triethylamine were dried by passing through activated alumina (8 x 14 mesh) column with argon gas pressure. Commercial reagents were used without purification unless otherwise noted. Air and/or moisture-sensitive reactions were carried out under an atmosphere of argon/nitrogen using oven/flameddried glassware and standard syringe/septum techniques. Melting points are uncorrected. Matrix-assisted laser desorption ionization time-of-flight (MALDI-TOF) mass spectra were obtained using α-cyano-4-hydroxycinnamic acid (CCA) as the matrix on a MALDI-TOF mass spectrometer. In vitro kinase assay Purified recombinant RSK2. The constitutively active His-tagged RSK2(Y707A) cDNA was generated using the Bac-to-Bac Baculovirus Expression System (Invitrogen, Carlsbad, CA). Recombinant RSK2 was expressed in Sf9 cells and activated by a 20 min treatment with phorbol 12-myristate 13-acetate (*10*). Protein was purified using the Ni-NTA agarose (Qiagen, Valencia, CA).

In vitro kinase assays were performed as previously described (*137*) . Briefly, a fusion protein consisting of glutathione Stransferase and the amino acid sequence RRRLASTNDKG (1 microg/well) was adsorbed to MaxiSorp-treated LumiNunc 96-well white polystyrene plates

(Thermo Scientific, Roskilde, Denmark). The wells were blocked with 3% tryptone in phosphate-buffered saline. Kinase (5 nM) in kinase buffer (25 mM HEPES pH 7.4), 150 mM NaCl, 5 mM β-glycerophosphate, 1.5 mM DTT, 30 mM MgCl2, 1% BSA) was added. Reactions were incubated with or without inhibitor. Reactions were initiated by the addition of ATP (10 microM) for 20 min, which is in the linear range of the assay. The reactions were terminated by addition of EDTA (500 mM, pH 8.0). The plates were washed and phosphorylation was measured using rabbit polyclonal anti- LApSTND1 and horseradish peroxidase (HRP)-conjugated donkey anti-rabbit (Jackson ImmunoResearch Laboratories, West Grove, PA) antibodies. Western Lightning Enhanced Chemiluminescent Reagent Plus (PerkinElmer Life Sciences, Waltham, MA) was used to measure HRP activity. To determine IC50 values, non-linear regression analysis was performed using GraphPad Prism version 6.0a (La Jolla, CA).

Results

Treatments for metastatic breast cancer are limited to reducing disease progression (*186*). In the five-year period after diagnosis, patients with triple negative breast cancer (TNBC) have a reduced survival rate compared to other subtypes (*187*). The MEK-ERK1/2 cascade has been identified as a viable target for TNBC (*188-191*), but drugs that inhibit global regulators like MEK cause side effects that reduce the drug's efficacy (*194*). To circumvent this issue, we focused our efforts on the MEK downstream effector, RSK, which is active in the majority of TNBC tumors (*98, 196, 197*) RSK, is a Ser/Thr protein kinase, which contains an N-terminal kinase domain (NTKD) responsible for substrate phosphorylation (*115*). The flavonoid glycoside natural product SL0101 (1) has been identified as a selective inhibitor of the NTKD of RSK (Ki ≈ 1 microM) (*113*).

As part of a larger structure activity medicinal chemistry effort (Fig. 8.2) (*200, 225*), we have identified SL0101 rhamnopyranose (2) and carbasugar (3) analogues with C-6″-

substitutions that showed improved efficacy in the in vitro kinase assays (*210, 231*). The

carbasugar substitution (2, Y = O to 3, Y = CH2) (*233, 234*) was designed to address the short

in vivo half-life of the pyranose forms. In a similar vein, we have explored the substitution of the

C-3″/C-4″-acetates with nonhydrolyzable isosteres (115). This includes the substitution of the C-

4″-acetate with a C-4″-acetamide (e.g., 2a to 2b).

Unfortunately, these efforts to identify amide isosteres only found analogues (e.g., 2b

with reduced affinity for RSK compared to 2a). In contrast, the bis-carbamate 4 showed some

improvement in activity compared to 3a. With this in mind, we decided to target the regio-

isomeric monoacetate/ monocarbamates 5 and 6 for synthesis and evaluation as an inhibitor of

RSK (*249*).

Figure 8. 2 SL0101 structure-activity relationship.
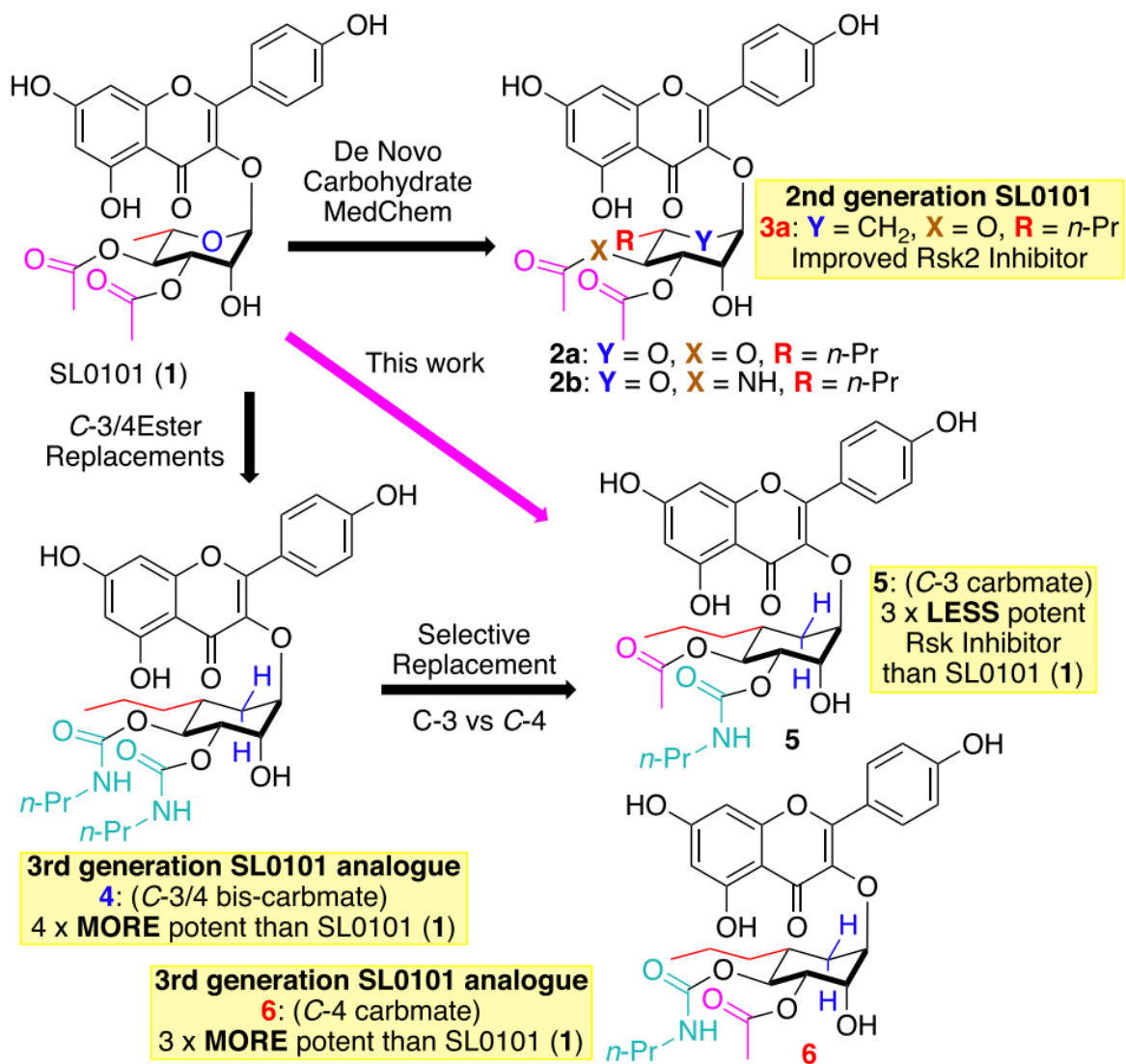
Our de novo synthesis of SL0101 (1) and its analogues 2−6 is outlined in Fig. 8.3. The approach to both the pyranose and carbasugar motifs relies on the construction of the anomeric bond as C-1 via a Pd-catalyzed glycosylation/ cyclitolization reaction (i.e., 8 from 9 + 10 or 11). The glycosyl-donor 10 can be made from achiral furan 12 in only three steps whereas the corresponding cyclitol donor 11 requires 9 steps from quinic acid 13. The Pd-catalyzed coupling reaction sequence that prepares both the pyran and cyclohexene in 8 allows for the selective introduction of the C4 substituent. In contrast, the C-3″ substituent is introduced by means of an Upjohn dihydroxylation to form diol 7 and then a differentiation of the C-3″ equatorial from the C-2″ axial alcohol, which can require more steps than is ideally desired (Fig. 8.4). Herein we describe our efforts to explore the use of the Taylor catalyst (*235, 257-259*) to regioselectively install ester and carbamate functionality on the SL0101 rhamno-pyranose and carbasugar framework and its use in the synthesis of monoacetate/monocarbamates 5 and 6.
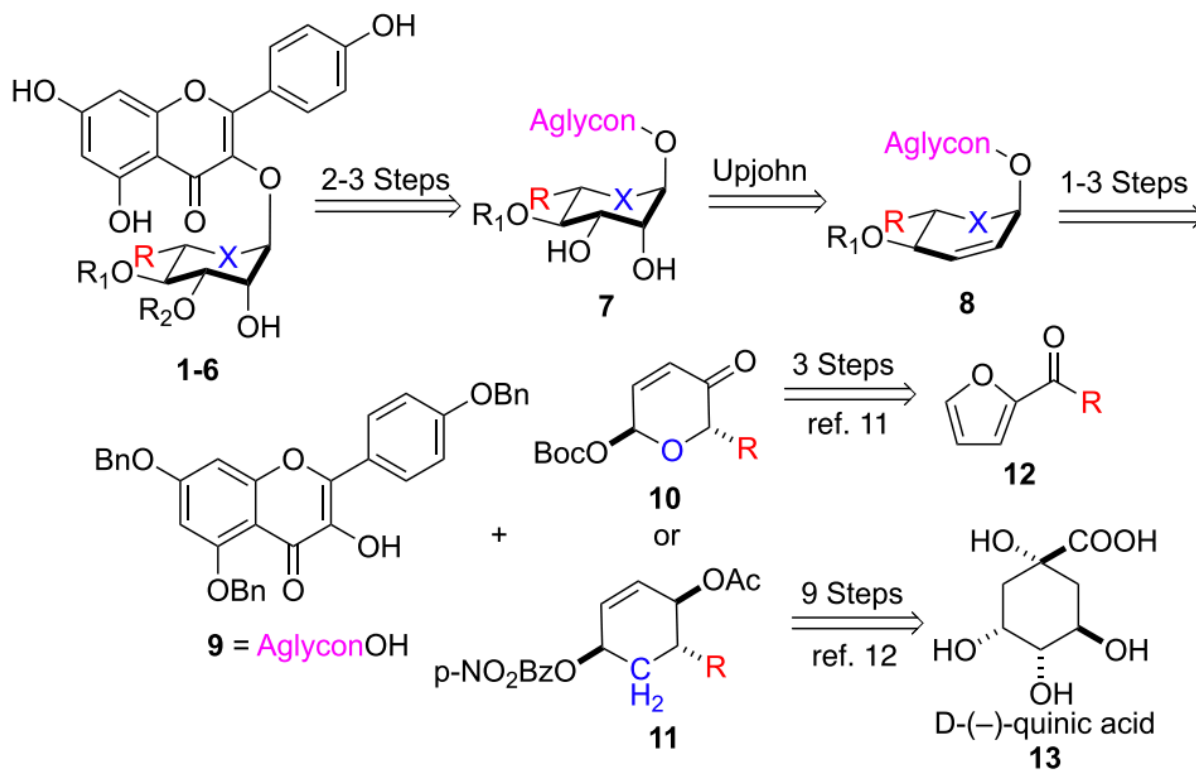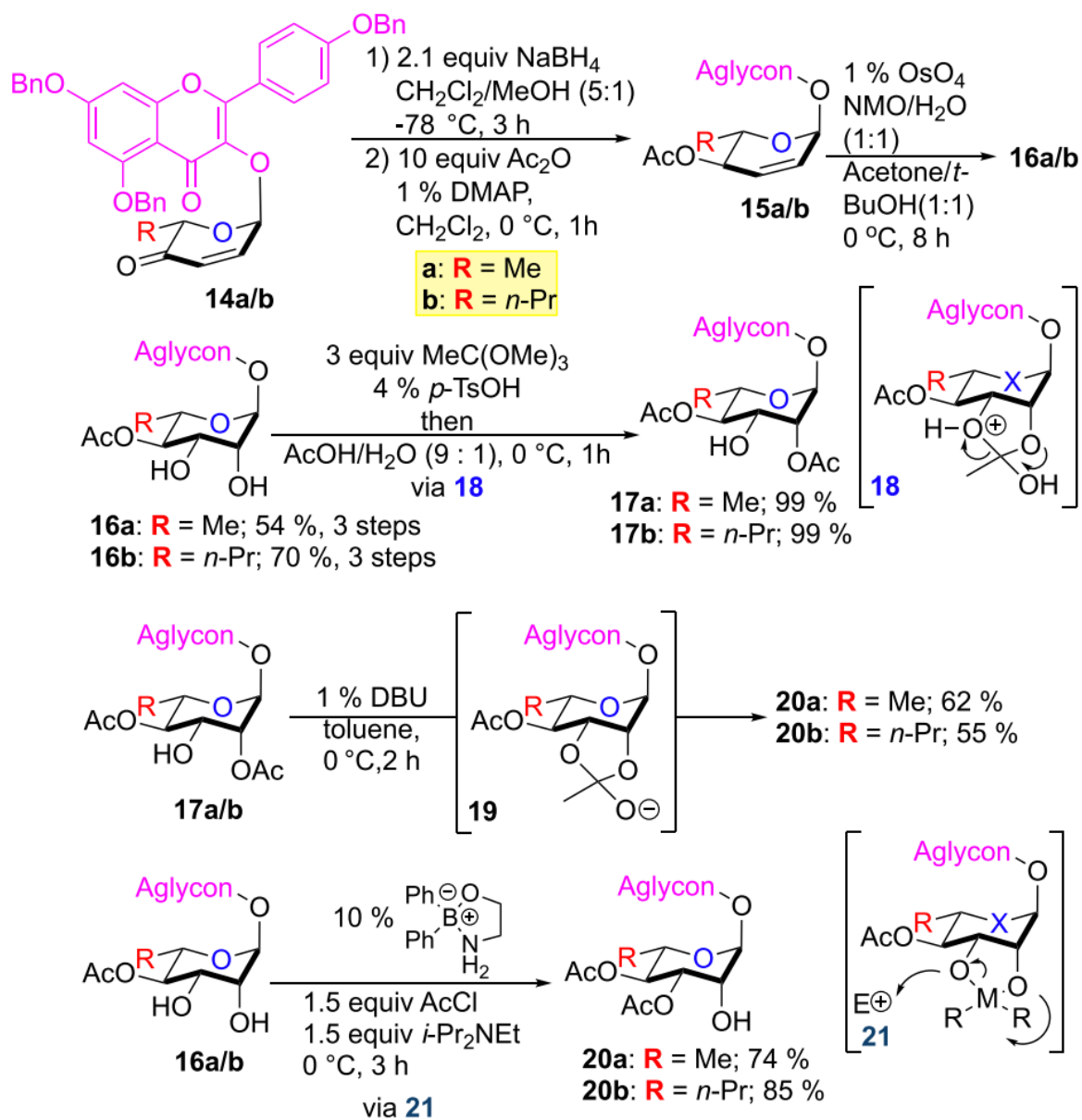
Figure 8. 3 De novo approach to SL0101 and analogues.
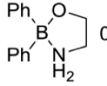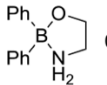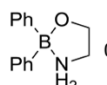
Figure 8. 4 C-3 acylation of pyranose analogues.
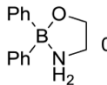
This de novo approach to the SL0101 and its analogues is both highly stereoselective

and generalizable (Fig. 8.4). For example, the Pd-glycosylation products 14a/b could be

stereoselectively reduced, acylated, and dihydroxylated to form 16a/b in excellent overall yield

(54% and 70% for three steps). In contrast to the stereoselectivity, there were issues associated

with the regioselective introduction of the C3″ acetate. Our efforts to directly acylate 16a

(Ac2O/Py/ DMAP) gave a 1:1:1 mixture of diacetates (17a/20a) as well as the triacetate. Using

the ortho-acetate/hydrolysis protocol on 16a/b, the C-2″ acetate could be selectively installed to

form 17a/b, both in near-quantitative yield as a single regioisomer, via intermediate 18.

Regardless of the C-6″ substituent, the C-2″ axial acetate could be isomerized to an ~2:1

mixture of C-3″/C-2″ acetates with the more stable C-3″ acetate favored. Fortunately, the

regioisomers were separable by silica gel chromatography affording diacetates 20a and 20b

(62% and 55%, respectively). While this approach was able to provide enough material for initial
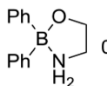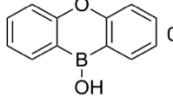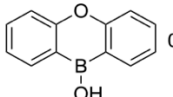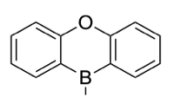
testing, our interest in scaling up the synthesis inspired us to explore protocols for the

regioselective introduction of the C-3″ acetate directly on diols 16a/b. We first turned to the

stochiometric use of Bu2SnO and Bu2Sn(OMe)2, unfortunately these conditions irreproducibly

gave a mixture of regio-isomers 16a/b and 20a/b. To our delight, a highly regioselective and

reproduceable procedure resulted when we switch to the diphenyl borinic ester catalyst

developed by Taylor. Thus, in the presence of 10% Ph2BO(CH2)2NH2 both 16a and 16b

reacted with AcCl to form 20a (74%) and 20b (85%) with excellent regioselectivity (>90%) via

intermediate 21. It is worth noting that the same stereoelectronic effect directs the

regioselectivity in both the ortho-ester and borinic ester acylation reactions (i.e., greater C3″

nucleophilicity in 18 and 21).

Building upon the success of the Taylor catalyst (Ph2BO- (CH2)2NH2) for the

regioselective C-3″ acylation of 16a/b, we decided to explore its use in the regioselective

acylation and carbamate formation of the cyclitol variants (i.e., diols 23 and 28, vide inf ra). This

effort began with diol 23 (Fig. 8.5), which can be easily prepared by the Upjohn dihydroxylation

(1% OsO4/NMO) of cyclohexene 22 (70%) (142). Similar to the pyran cases, the direct acylation of the diol gave a 1:1.6 mixture of diacetates 24 and 25 (entry 1) and the DBU isomerization of the mixture gave a 3:1 mixture of C-3″/C-2″ acetates with the more stable C-3″ acetate 24 being favored. In contrast to the pyranose series, the acylation via the ortho-ester formation/ hydrolysis condition failed to show any significant preference for the axial acylation, affording an excellent yield of a 1:1.6 mixture of 24 and 25. However, the yield for this ortho-ester formation/hydrolysis remained high (95%), so when used in combination with the DBU isomerization this began a viable two-step method for the formation of 24. The stochiometric use of Bu2SnO only slightly improved the selectivity for the C3 acetyl group (entry 4).

Figure 8. 5 Regioselective C-3 acetylation of diol 23.
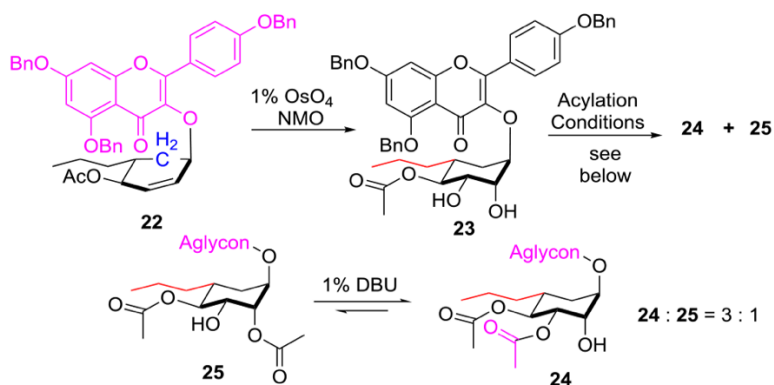
Entry	Reagent	Additive	Temp.	24 : 25	Overall Yield (Yield of 24)
1	AcCl/DIPEA	None	r.t.	1 : 1.6	38%
2	AcCl/DIPEA	[Ph, Ph, B, O, N, H₂] 0.1 eq	r.t.	5 : 1	72% (60%)
3	AcCl/DIPEA	[Ph, Ph, B, O, N, H₂] 0.3 eq	r.t.	4.5 : 1	70%
4	AcCl/DIPEA	Bu₂SnO 1.1eq	Reflux at 82°C	1.4 : 1	46%
5	p-TsOH HOAc triethyl orthoacetate	None	0 °C	1 : 1.3	95%
6	AcCl/DIPEA	[Ph, Ph, B, O, N, H₂] 0.1eq	0 °C	1.2 : 1	35%
7	AcCl/DIPEA	[Ph, Ph, B, O, N, H₂] 0.3 eq	-20 °C	1.6 : 1	46%
8	AcCl/DIPEA	[Ph, Ph, B, O, N, H₂] 0.1 eq	- 78 °C	1.04 : 1	27%
9	AcCl/DIPEA	[phenoxaborine, B, OH] 0.1 eq	r.t.	3.6 : 1	58%
10	AcCl/DIPEA	[phenoxaborine, B, OH] 0.3 eq	r.t.	3.2 : 1	65%
11	AcCl/DIPEA	[phenoxaborine, B, OH] 1 eq	r.t.	3.0 : 1	63%

238
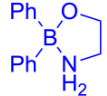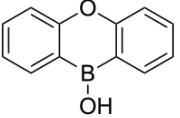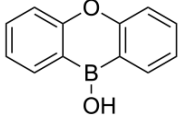
The poor selectivity in both the ortho-ester and tin acetal chemistry suggested that there was a reduction in the rigidity of the carbasugar ring system that led to a diminishment in the stereoelectronic effect in the carbasugar variants of 18 and 21 (X = CH2). Fortunately, this was less the case for the borinic ester catalysis, albeit it did require a great degree of optimization to obtain the desired regioselectivity. Thus, under our optimized conditions (entry 2), using only 10% of the Taylor catalyst, a good yield (72%) of a 5:1 mixture of 24 and 25 could be achieved, reproducibly affording the desired regioisomer in 60% yield. Interestingly, we were not able to find conditions with the more reactive tricyclic borinic acid catalyst that would give as high a regioselectivity (entries 9− 10) as the commercially available catalyst.

We next turned to the regioselective installation of an npropyl carbamate to the C-3″ position of diol 23 (Fig. 8.6). Exposure of diol 23 to n-propyl-isocyanate and DBU gave a slow reaction. Incr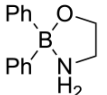easing the reaction temperature to 45 °C gave a 1:1 ratio of carbamates 26 and 27 in 38% yield. Unfortunately, the minor carbamate isomer cannot be isomerized with DBU. When the same reaction was performed in the presence of a catalytic amount of Taylor's catalyst (10%), we observed improved yields and regioselectivity of the desired regioisomer carbamate 26. Interestingly, when the temperature was lowered the regioselectivity switched to prefer the axial carbamate isomer 27. Switching DBU for tertiary amine bases leads to slightly lower yields and regioselectivities. When the conditions that are outlined in entry 2 were scaled up, the desired isomer was isolated in a 41% yield.

Figure 8. 6 Regioselective C-3 carbamate formation.
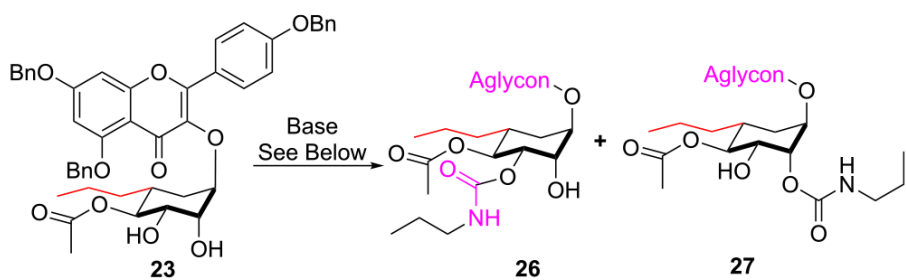
Entry	Additive		Temp.	26 : 27	Overall Yield (Yield of 26)
1	Et$_3$N PrNCO ACN	0.1 eq	45 °C	2.7 : 1	48%
2	Et$_3$N PrNCO ACN	0.3 eq	45 °C	3.7 : 1	51% (41%)
3	Et$_3$N PrNCO ACN	0.3 eq	45 °C	3 : 1	40%
4	Et$_3$N PrNCO ACN	1 eq	45 °C	4 : 1	44%

240

Focus was next turned toward the regioselective acylation of diol 28 with the C-4 carbamate (Fig. 8.7). The carbamate 28 could be easily prepared from the Pd-cyclitolization product 22 by a three-step ester hydrolysis, carbamate formation, and dihydroxylation reaction sequence (55%). Once again, acylation of diol 28 using typical acylation conditions (AcCl/ Base) led to a mixture of regioisomers. Gratifyingly, we saw only minimal effects from the carbamate substitution at C-4. Thus, application of our optimized borinic ester catalyzed acylation conditions on diol 28 gave a nearly identical yield (64%) and ratio (4.4:1) of regioisomeric monoacetates 29 and 30. As with 25 the undesired regioisomer 30 could be recycled by DBU isomerization to a 1:2.5 mixture of 29 to 30, with the more stable isomer being the major product.

We next looked at the regioselective C-3″ carbamate installation to form bis-carbamate 4 from diol 28 (Fig. 8.8). Exposure of diol 28 to n-propyl-isocyanate and DBU at 45 °C gave a 1:1 ratio of carbamates 31 and 32 in 38% yield. Similarly, the minor carbamate isomer could not be isomerized with DBU. The same reaction was performed in the presence of a catalytic amount Taylor catalyst (10%) which improved the yield and regioselectivity (3:1) for the desired regioisomer carbamate 31. Thus, using entry 2, the optimized procedure, we scaled up, affording 31 in a 34% yield. Once again, when the temperature was lowered the regioselectivity switched to prefer the axial carbamate isomer 32. Surprisingly, in this case (entry 4) the undesired C-3 regioisomer was the major isomer, albeit at low conversion (17% yield). Because 32 could not be isomerized back to the desired regioisomer 31, we did not further pursue lower temperature conditions.

Figure 8. 7 Regioselective C-3 acetylation of diol 28.
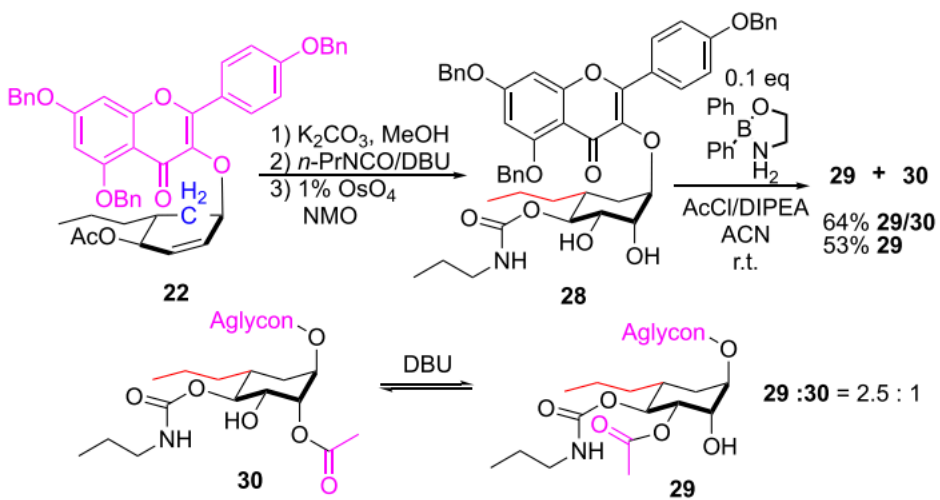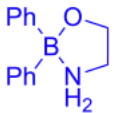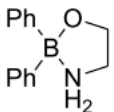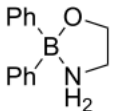
Figure 8. 8 Regioselective C-3 carbamate formation.
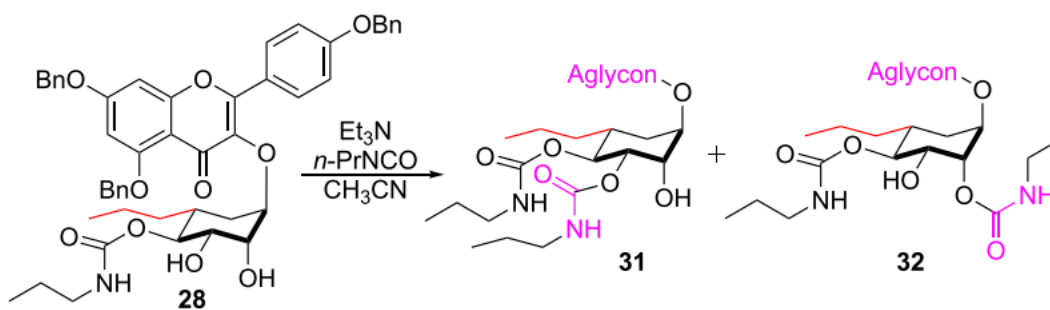
Entry	Additive		Temp.	**31** : **32**	Overall Yield (Yield of **31**)
1	None		45 °C	1 : 1	38%
2	(Ph, Ph, B, O, N, H₂ boron reagent)	0.1 eq	45 °C	3 : 1	45% (34%)
3	(Ph, Ph, B, O, N, H₂ boron reagent)	0.1 eq	20 °C	1.5 : 1	40%
4	(Ph, Ph, B, O, N, H₂ boron reagent)	0.1 eq	0 °C	1 : 3	17%

Finally, with the required carbamate regioisomers 26 and 29 in hand, we explored their conversion into the desired target compounds 5 and 6 (Fig. 8.9). This was accomplished by global deprotection with exhaustive hydrogenolysis. Thus, exposure of the C-3″ carbamate 26 to 1 atm of H2 in the presence of 10% Pd/C gave the C-3″ carbamate 5 in excellent yield (71%). Similarly, exposure of the C-4″ carbamate 29 to 1 atm of H2 in the presence of 10% Pd/C gave the C-4″ carbamate 5 in excellent yield (70%).

The bis-carbamate and two new monocarbamate containing cyclitol SL0101 analogues 5 and 6 were evaluated as RSK2 inhibitors in an in vitro kinase assay (Table 8.1). In this assay, the analogue 5 with a C-3″ n-Pr-carbamate group and a C-4″ acetate had a 3-fold decreased IC50 relative to SL0101. In contrast, the analogues 4 and 6 with a C-4″ n-Pr-carbamate group had a higher affinity than SL0101, with 4 having a 4-fold and 6 having a 3-fold higher affinity. The potency difference between 2a and analogues C-4″ n-Pr-carbamate 6 and the C-3″/C4″ bis-n-Pr-carbamate 4 group is moderate. Importantly, these results are the first demonstration that modifications to the rhamnose at the 4″ position can be introduced without substantially reducing RSK affinity for the compound.

Figure 8. 9 Preparation of SL0101 analogues 5 and 6.
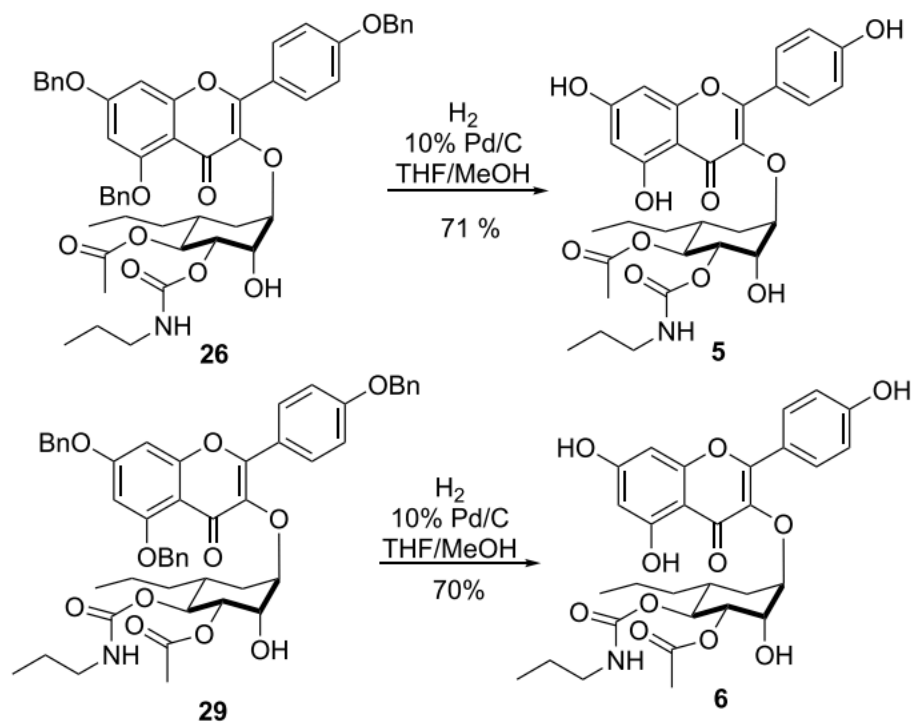
Table 8.1 RSK inhibitory activity of carbamates 4-6. RSK2IC50 Assay: concentration need for 50% RSK2 inhibition (n > 2; sextuplicate; mean ± 95% confidence interval). The in vitro kinase assay provides a relative IC50 as the absolute value depends on batch-to-batch variation of the reagents. SL0101 is used as a positive control for every assay and therefore, the potencies are relative to SL0101.

Table 8. 1 In vitro potency of SL0101 carbamate analogues.

Name	RSK2 IC50 (microM)	95% confidence interval
4	0.14	± 0.06
5	1.16	± 0.24
6	0.17	± 0.05

Conclusion

In conclusion the use of Taylor's borinic ester catalyst for the regioselective introduction of acetyl and carbamate functional groups on rhamno-5a-carbasugar motifs was investigated. The Taylor borinic ester catalyst was found to be superior at controlling regioselectivity in the rhamnocarbasugar environment compared to traditional tin and orthoester methods. Conditions were found that allowed for the efficient synthesis of C-3/C-4 regioisomeric acetate/n-Prcarbamate analogues of the RSK1/2 inhibitor, SL0101. This synthetic effort led to the discovery of a new cyclitol analogue of SL0101 with improved RSK inhibitory activity.

Chapter 9

Discussion

For the discussion, I am attempting to place my work in the field in the context of two topics, estrogen signaling and RSK signaling. In estrogen signaling, I have focused on the major results from my thesis, presented in chapter 2. For RSK signaling, there was a general theme in committee questions about RSK in development, immunity, cardiology and insight into RSK drug development. Therefore, I am attempting to address these questions about RSK using the literature on RSK knockout mice.

ERalpha transcription activity controls homeostasis of many tissues in men and women. Ligand activation of ERalpha promotes post-translational modification through crosstalk with other signaling pathways (*260*). These ERalpha modifications include phosphorylation and ubiquitination (*31*). Phosphorylation of ERalpha is required for full transcription activity (*261*). Many ERalpha transcriptional coactivators have a dual role as ubiquitin ligases (*30*). In this work, we have discovered regulation of estrogen signaling homeostasis in the mammary gland by the ERK1/2-RSK2 pathway. This regulatory mechanism involves ERalpha phosphorylation and transcription-coupled proteolysis. Ultimately, RSK2 is required for in vivo maintenance of mammary ER+ cells. (Figure 9.1). Identification of the specific factors driving ERalpha proteolysis may have important therapeutic implications for ER+ breast cancer and other endocrine-related diseases.

ERalpha transcriptional activity is dependent on proteolysis. Ligand induced degradation is observed in vivo in multiple estrogen responsive tissues, demonstrating the physiological relevance (*62, 262*). Although inhibition of the proteasome increases ERalpha protein levels, the transcriptional activity of ERalpha is decreased, supporting a link between ERalpha proteolysis and transcription. Related nuclear hormone receptors have also been found to use a

transcription-coupled proteolysis mechanism including androgen receptor (*263*), progesterone receptor (*57*) and thyroid receptor (*264*). A unifying model has not been developed for transcription-coupled proteolysis, which is complicated by the ability of the proteasome to activate and repress different ERalpha responsive genes (*265*). It is possible that regulation of ERalpha transcription-coupled proteolysis is very complex, occurring in a dynamic manner with a tissue- and gene-specific context.

Our studies implicate the 26S proteasome pathway in control of ERalpha transcription-coupled proteolysis. The addition of poly-ubiquitin chains to target proteins signals them for degradation through the 26S proteasome. Ubiquitination involves three classes of enzymes, ubiquitin activating (UBA), ubiquitin conjugating (UBC), and ubiquitin ligases (UBL). The ubiquitination of ERalpha is observed rapidly after ligand activation (*55, 266, 267*). ERalpha is ubiquitinated at Lys302 and Lys303 in the linker domain, although ubiquitination of ERalpha is observed when these sites are mutated, suggesting other ubiquitination sites exist (*67*). Ubiquitination of Lys302/303 has been implicated in prognosis of ER+ breast cancer (*268*). In addition to ubiquitination, proteins are targeted to the 26S proteasome by the NEDDylation and SUMOylation pathways. These pathways involve addition of NEDD8 or SUMO, which are structurally similar to the ubiquitin peptide and are added by a similar three step enzyme pathway. NEDDylation of ERalpha has been reported to decrease ERalpha activity (*269*) and major crosstalk exists between the NEDDylation and the ubiquitin-proteasome pathway (*270*). The SUMOylation of ERa is also reported to decrease ERalpha transcription (*271*). Degradation of ERalpha through the lysosome pathway is not connected to ERalpha transcription (*267, 272*). Taken together, many routes for ERalpha degradation have been described with potential for targeting in ERalpha related diseases.

The importance of phospho-Ser118 ERalpha in normal homeostasis remains to be established. In breast cancer, phospho-Ser118 ERalpha is a predictive marker for response to tamoxifen, suggesting this site indicates intact estrogen signaling (*39*). In agreement with

phospho-Ser118 ERalpha indicating active receptor, genomic analysis of phospho-Ser118 ERalpha in cell lines found that the phosphorylated receptor is enriched at enhancer elements (*41*). Additionally, exogenous expression of the phospho-mimetic Ser118Glu ERalpha has revealed a role for phospho-Ser118 in ERalpha degradation (*58*). However, no mouse models for mutant Ser-118 ERalpha have been developed. The most relatable model, the AF-1 domain null mice (Esr1 AF1^0), demonstrate phenotypes similar to AF-2 null mice (Esr1 AF2^0) and ERalpha knockout mice (ERalpha-KO) (*79*). Furthermore, we found no suitable antibodies for detection of mouse phospho-Ser118. It is intriguing to speculate that phospho-Ser118 ER alpha generates a phospho-degron for recruitment of co-activators, transcriptional activation, and receptor degradation (*58*). In the future, studying these factors in non-transformed tissues may aid identification of core factors that are hijacked in disease.

In the mammary gland, ERalpha is a major regulator of development. Knockout of ERalpha blocks development of the mammary epithelium and overexpression of ERalpha results in mammary tumors (*32, 128*). ERalpha in the mammary epithelium has therefore been linked to proliferation of mammary epithelial cells. Traditionally, ER+ mammary epithelial cells were thought to be terminally differentiated and post-mitotic, but more recent studies have challenged this theory. Lineage tracing of ER+ cells in the mammary epithelium found that the ER+ population is heterogenous and contains a long-lived progenitor cell, which may have significance for ER+ breast cancer (*80, 81*). In line with these studies, the mammary ER+ cell subpopulation has been shown to proliferate with each estrous cycle in the adult mouse (*82*). Therefore, the ER+ cell population is more heterogenous and active than previously thought. In future studies, it will be interesting to understand how susceptible the ER+ progenitor cells are to transformation. Additionally, it will be important to understand differences in estrogen signaling in ER+ progenitors versus differentiated cells.

A myriad of UBL proteins have been found to regulate ERalpha in breast cancer cell lines (*30*). Notably, E6AP (gene name UBE3A), is a UBL that is associated with ERalpha protein

regulation in vivo. In the mouse mammary gland, overexpression of E6AP delays mammary development and decreases protein levels of ERalpha and progesterone receptor (*69*). In addition to UBL activity, E6AP was the first UBL identified as an ERalpha coactivator (*61*) and can ubiquitinate phospho-Ser118 ERalpha (*58*). Two other UBLs, MDM2 and BRCA1, are noteworthy because they are ERalpha coactivators with established tumor suppressor roles in breast cancer (*68, 273-276*). However, their in vivo significance for ERalpha control remains to be established.

Previous studies have implicated RSK2 in ER+ breast cancer. In transgenic mice, expression of nuclear RSK2 in the mammary gland promotes ER+ tumor initiation and progression (*115*). This suggests that a RSK2 inhibitor may be beneficial in ER+ breast cancer. Additionally, it is possible that regulation of ERalpha protein levels, which we found is influenced by RSK2, is disrupted in breast cancer. In a phase II study of advanced ER+ breast cancer patients, targeting the proteasome with bortezomib provides only a modest benefit (*277*). It remains to be explored if more directly targeting the proteasome components in ERalpha transcription-coupled proteolysis, such as UBLs, will provide a greater benefit. The only FDA approved therapy that is considered UBL targeted is thalidomide for multiple myeloma (*278*). However, many other molecules are under preclinical or early phase clinical development (*279*).

A role for RSK2 in development of the mammary gland is not surprising, as the importance of RSKs in other tissues has been established using RSK knockout mice. Two RSK2 knockout mouse models were independently developed using similar strategies of inserting stop codons into the RSK2 gene (*105, 280*). Together, these mice have been used to study RSK2 in ~17 peer-reviewed studies. The Yang mouse has phenotypes consistent with Coffin-Lowry Syndrome, including osteopenia with deformed face and skull bones as well as learning and hippocampal neuron defects (*106, 281, 282*). The Dufresne mouse has defects in skeletal muscle and insulin resistance, inflammatory signaling in adaptive immune cells, and vasoconstriction in smooth muscle cells (*283-286*). Importantly, in our studies we eliminate the

possibility for systemic effects of RSK2 knockout on ERalpha by performing tissue transplant experiments.

Other than RSK2, there are no reports on RSK1 or RSK4 individual knockout mice. A RSK3 knockout mouse was developed by the Kapiloff group which has established a role for RSK3 activity in cardiac pathology (*287-289*). Furthermore, RSK1/2/3 triple-knockout mice are reported viable (*106*). The viability and fertility of these mice is promising for development of RSK inhibitors for targeted treatment of diseases with increased RSK activity.

Figure 9.1 The ERK1/2-RSK pathway controls mammary estrogen degradation in vivo. A) The hormone responsive nature of the mammary gland makes it an ideal model for this study. B) Edu-labeling of proliferating mammary epithelial cells in response to the endogenous estrous cycle demonstrates that RSK2 controls proliferation of normal ER+ cells. C) In-situ immunofluorescence of the mammary gland identifies a role for RSK2 in 26S proteasome mediated ERalpha degradation.

Figure 9. 1 The ERK1/2-RSK pathway controls mammary estrogen receptor alpha degradation in vivo.
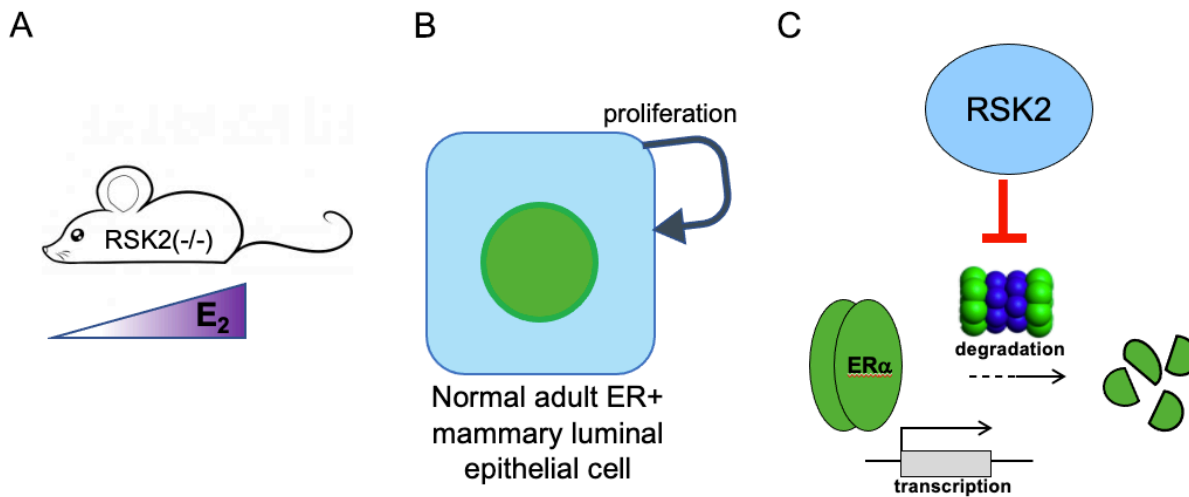
References

1. R. J. Epstein, P. J. Smith, Estrogen-induced potentiation of DNA damage and cytotoxicity in human breast cancer cells treated with topoisomerase II-interactive antitumor drugs. *Cancer Res* **48**, 297-303 (1988).
2. D. Roy, J. G. Liehr, Estrogen, DNA damage and mutations. *Mutat Res* **424**, 107-115 (1999).
3. C. G. o. H. F. i. B. Cancer, Menarche, menopause, and breast cancer risk: individual participant meta-analysis, including 118 964 women with breast cancer from 117 epidemiological studies. *Lancet Oncol* **13**, 1141-1151 (2012).
4. M. Lambe *et al.*, Transient increase in the risk of breast cancer after giving birth. *N Engl J Med* **331**, 5-9 (1994).
5. J. F. Couse, K. S. Korach, Estrogen receptor null mice: what have we learned and where will they lead us? *Endocr Rev* **20**, 358-417 (1999).
6. J. E. Rossouw *et al.*, Risks and benefits of estrogen plus progestin in healthy postmenopausal women: principal results From the Women's Health Initiative randomized controlled trial. *Jama* **288**, 321-333 (2002).
7. J. H. Morrison, R. D. Brinton, P. J. Schmidt, A. C. Gore, Estrogen, menopause, and the aging brain: how basic neuroscience can inform hormone therapy in women. *J Neurosci* **26**, 10332-10348 (2006).
8. G. M. Anstead, K. E. Carlson, J. A. Katzenellenbogen, The estradiol pharmacophore: ligand structure-estrogen receptor binding affinity relationships and a model for the receptor binding site. *Steroids* **62**, 268-303 (1997).
9. R. M. Blair *et al.*, The estrogen receptor relative binding affinities of 188 natural and xenochemicals: structural diversity of ligands. *Toxicol Sci* **54**, 138-153 (2000).
10. R. Qureshi *et al.*, The Major Pre- and Postmenopausal Estrogens Play Opposing Roles in Obesity-Driven Mammary Inflammation and Breast Cancer Development. *Cell Metab* **31**, 1154-1172 e1159 (2020).
11. I. E. Smith, M. Dowsett, Aromatase inhibitors in breast cancer. *N Engl J Med* **348**, 2431-2442 (2003).
12. A. H. Eliassen *et al.*, Endogenous steroid hormone concentrations and risk of breast cancer among premenopausal women. *J Natl Cancer Inst* **98**, 1406-1415 (2006).
13. R. Kaaks *et al.*, Postmenopausal serum androgens, oestrogens and breast cancer risk: the European prospective investigation into cancer and nutrition. *Endocr Relat Cancer* **12**, 1071-1082 (2005).
14. A. F. Minsart, A. Van Onderbergen, F. Jacques, C. Kurt, Y. Gillerot, Indication of prenatal diagnosis in pregnancies complicated by undetectable second-trimester maternal serum estriol levels. *J Prenat Med* **2**, 27-30 (2008).
15. R. C. Bonney, M. J. Reed, K. Davidson, P. A. Beranek, V. H. James, The relationship between 17 beta-hydroxysteroid dehydrogenase activity and oestrogen concentrations in human breast tumours and in normal breast tissue. *Clin Endocrinol (Oxf)* **19**, 727-739 (1983).

16. A. A. van Landeghem, J. Poortman, M. Nabuurs, J. H. Thijssen, Endogenous concentration and subcellular distribution of estrogens in normal and malignant human breast tissue. *Cancer Res* **45**, 2900-2906 (1985).
17. A. E. Herbison, Control of puberty onset and fertility by gonadotropin-releasing hormone neurons. *Nat Rev Endocrinol* **12**, 452-466 (2016).
18. S. P. Wu, R. Li, F. J. DeMayo, Progesterone Receptor Regulation of Uterine Adaptation for Pregnancy. *Trends Endocrinol Metab* **29**, 481-491 (2018).
19. C. Brisken *et al.*, A paracrine role for the epithelial progesterone receptor in mammary gland development. *Proc Natl Acad Sci U S A* **95**, 5076-5081 (1998).
20. S. L. Byers, M. V. Wiles, S. L. Dunn, R. A. Taft, Mouse estrous cycle identification tool and images. *PLoS One* **7**, e35538 (2012).
21. K. De Bosscher, W. Vanden Berghe, G. Haegeman, Cross-talk between nuclear receptors and nuclear factor kappaB. *Oncogene* **25**, 6868-6886 (2006).
22. D. T. Baird, A. F. Glasier, Hormonal contraception. *N Engl J Med* **328**, 1543-1549 (1993).
23. L. S. Morch *et al.*, Contemporary Hormonal Contraception and the Risk of Breast Cancer. *N Engl J Med* **377**, 2228-2239 (2017).
24. D. B. Petitti, Clinical practice. Combination estrogen-progestin oral contraceptives. *N Engl J Med* **349**, 1443-1450 (2003).
25. C. G. o. H. F. i. B. Cancer, Breast cancer and hormone replacement therapy: collaborative reanalysis of data from 51 epidemiological studies of 52,705 women with breast cancer and 108,411 women without breast cancer. . *Lancet* **350**, 1047-1059 (1997).
26. C. B. Hanna *et al.*, Development of WEE2 kinase inhibitors as novel non-hormonal female contraceptives that target meiosis†. *Biol Reprod* **103**, 368-377 (2020).
27. M. S. Post *et al.*, Effect of oral and transdermal estrogen replacement therapy on hemostatic variables associated with venous thrombosis: a randomized, placebo-controlled study in postmenopausal women. *Arterioscler Thromb Vasc Biol* **23**, 1116-1121 (2003).
28. J. Cuzick *et al.*, Long-term results of tamoxifen prophylaxis for breast cancer--96-month follow-up of the randomized IBIS-I trial. *J Natl Cancer Inst* **99**, 272-282 (2007).
29. D. B. Lubahn *et al.*, Alteration of reproductive function but not prenatal sexual development after insertional disruption of the mouse estrogen receptor gene. *Proc Natl Acad Sci U S A* **90**, 11162-11166 (1993).
30. W. Zhou, J. M. Slingerland, Links between oestrogen receptor activation and proteolysis: relevance to hormone-regulated cancer therapy. *Nat Rev Cancer* **14**, 26-38 (2014).
31. M. Le Romancer *et al.*, Cracking the estrogen receptor's posttranslational code in breast tumors. *Endocr Rev* **32**, 597-622 (2011).
32. Y. Feng, D. Manka, K. U. Wagner, S. A. Khan, Estrogen receptor-alpha expression in the mammary epithelium is required for ductal and alveolar morphogenesis in mice. *Proc Natl Acad Sci U S A* **104**, 14718-14723 (2007).

33. S. Mallepell, A. Krust, P. Chambon, C. Brisken, Paracrine signaling through the epithelial estrogen receptor alpha is required for proliferation and morphogenesis in the mammary gland. *Proc Natl Acad Sci U S A* **103**, 2196-2201 (2006).

34. J. H. Krege *et al.*, Generation and reproductive phenotypes of mice lacking estrogen receptor beta. *Proc Natl Acad Sci U S A* **95**, 15677-15682 (1998).

35. N. A. Marjon, C. Hu, H. J. Hathaway, E. R. Prossnitz, G protein-coupled estrogen receptor regulates mammary tumorigenesis and metastasis. *Mol Cancer Res* **12**, 1644-1654 (2014).

36. J. Chinsomboon *et al.*, The transcriptional coactivator PGC-1alpha mediates exercise-induced angiogenesis in skeletal muscle. *Proc Natl Acad Sci U S A* **106**, 21401-21406 (2009).

37. C. Brisken, B. O'Malley, Hormone action in the mammary gland. *Cold Spring Harb Perspect Biol* **2**, a003178 (2010).

38. S. Kato *et al.*, Activation of the estrogen receptor through phosphorylation by mitogen-activated protein kinase. *Science* **270**, 1491-1494 (1995).

39. J. Bergqvist *et al.*, Activated ERK1/2 and phosphorylated oestrogen receptor alpha are associated with improved breast cancer survival in women treated with tamoxifen. *Eur J Cancer* **42**, 1104-1112 (2006).

40. H. Yamashita *et al.*, Low phosphorylation of estrogen receptor alpha (ERalpha) serine 118 and high phosphorylation of ERalpha serine 167 improve survival in ER-positive breast cancer. *Endocr Relat Cancer* **15**, 755-763 (2008).

41. K. T. Helzer *et al.*, The Phosphorylated Estrogen Receptor α (ER) Cistrome Identifies a Subset of Active Enhancers Enriched for Direct ER-DNA Binding and the Transcription Factor GRHL2. *Mol Cell Biol* **39**, (2019).

42. H. Yamashita *et al.*, Phosphorylation of estrogen receptor alpha serine 167 is predictive of response to endocrine therapy and increases postrelapse survival in metastatic breast cancer. *Breast Cancer Res* **7**, R753-764 (2005).

43. J. Jiang *et al.*, Phosphorylation of estrogen receptor-alpha at Ser167 is indicative of longer disease-free and overall survival in breast cancer patients. *Clin Cancer Res* **13**, 5769-5776 (2007).

44. L. C. Murphy, Y. Niu, L. Snell, P. Watson, Phospho-serine-118 estrogen receptor-alpha expression is associated with better disease outcome in women treated with tamoxifen. *Clin Cancer Res* **10**, 5902-5906 (2004).

45. N. Sarwar *et al.*, Phosphorylation of ERalpha at serine 118 in primary breast cancer and in tamoxifen-resistant tumours is indicative of a complex role for ERalpha phosphorylation in breast cancer progression. *Endocr Relat Cancer* **13**, 851-861 (2006).

46. L. C. Murphy *et al.*, The relevance of phosphorylated forms of estrogen receptor in human breast cancer in vivo. *J Steroid Biochem Mol Biol* **114**, 90-95 (2009).

47. R. Michalides *et al.*, Tamoxifen resistance by a conformational arrest of the estrogen receptor alpha after PKA activation in breast cancer. *Cancer Cell* **5**, 597-605 (2004).

48. M. Kok *et al.*, PKA-induced phosphorylation of ERα at serine 305 and high PAK1 levels is associated with sensitivity to tamoxifen in ER-positive breast cancer. *Breast Cancer Res Treat* **125**, 1-12 (2011).

49. J. Bostner, L. Skoog, T. Fornander, B. Nordenskjöld, O. Stål, Estrogen receptor-alpha phosphorylation at serine 305, nuclear p21-activated kinase 1 expression, and response to tamoxifen in postmenopausal breast cancer. *Clin Cancer Res* **16**, 1624-1633 (2010).

50. C. Holm *et al.*, Phosphorylation of the oestrogen receptor alpha at serine 305 and prediction of tamoxifen resistance in breast cancer. *J Pathol* **217**, 372-379 (2009).

51. Y. Cui *et al.*, Phosphorylation of estrogen receptor alpha blocks its acetylation and regulates estrogen sensitivity. *Cancer Res* **64**, 9199-9208 (2004).

52. R. Jeselsohn, G. Buchwalter, C. De Angelis, M. Brown, R. Schiff, ESR1 mutations—a mechanism for acquired endocrine resistance in breast cancer. *Nat Rev Clin Oncol* **12**, 573-583 (**2015**).

53. J. Adams, The proteasome: a suitable antineoplastic target. *Nat Rev Cancer* **4**, 349-360 (2004).

54. W. P. Tansey, Transcriptional activation: risky business. *Genes Dev* **15**, 1045-1050 (2001).

55. Z. Nawaz, D. M. Lonard, A. P. Dennis, C. L. Smith, B. W. O'Malley, Proteasome-dependent degradation of the human estrogen receptor. *Proc Natl Acad Sci U S A* **96**, 1858-1862 (1999).

56. A. Dace *et al.*, Hormone binding induces rapid proteasome-mediated degradation of thyroid hormone receptors. *Proc Natl Acad Sci U S A* **97**, 8985-8990 (2000).

57. T. Shen, K. B. Horwitz, C. A. Lange, Transcriptional hyperactivity of human progesterone receptors is coupled to their ligand-dependent down-regulation by mitogen-activated protein kinase-dependent phosphorylation of serine 294. *Mol Cell Biol* **21**, 6122-6131 (2001).

58. P. Rajbhandari *et al.*, Pin1 modulates ERα levels in breast cancer through inhibition of phosphorylation-dependent ubiquitination and degradation. *Oncogene* **33**, 1438-1447 (2014).

59. S. Bhatt, Z. Xiao, Z. Meng, B. S. Katzenellenbogen, Phosphorylation by p38 mitogen-activated protein kinase promotes estrogen receptor α turnover and functional activity via the SCF(Skp2) proteasomal complex. *Mol Cell Biol* **32**, 1928-1943 (2012).

60. W. Zhou, S. Srinivasan, Z. Nawaz, J. M. Slingerland, ERα, SKP2 and E2F-1 form a feed forward loop driving late ERα targets and G1 cell cycle progression. *Oncogene* **33**, 2341-2353 (2014).

61. Z. Nawaz *et al.*, The Angelman syndrome-associated protein, E6-AP, is a coactivator for the nuclear hormone receptor superfamily. *Mol Cell Biol* **19**, 1182-1189 (1999).

62. G. B. Silberstein, K. Van Horn, E. Hrabeta-Robinson, J. Compton, Estrogen-triggered delays in mammary gland gene expression during the estrous cycle: evidence for a novel timing system. *J Endocrinol* **190**, 225-239 (2006).

63. Y. Shang, X. Hu, J. DiRenzo, M. A. Lazar, M. Brown, Cofactor dynamics and sufficiency in estrogen receptor-regulated transcription. *Cell* **103**, 843-852 (2000).

64. G. Reid *et al.*, Cyclic, proteasome-mediated turnover of unliganded and liganded ERalpha on responsive promoters is an integral feature of estrogen signaling. *Mol Cell* **11**, 695-707 (2003).

65. R. Métivier *et al.*, Estrogen receptor-alpha directs ordered, cyclical, and combinatorial recruitment of cofactors on a natural target promoter. *Cell* **115**, 751-763 (2003).

66. Y. Ma *et al.*, BRCA1 regulates acetylation and ubiquitination of estrogen receptor-alpha. *Mol Endocrinol* **24**, 76-90 (2010).

67. N. B. Berry, M. Fan, K. P. Nephew, Estrogen receptor-alpha hinge-region lysines 302 and 303 regulate receptor degradation by the proteasome. *Mol Endocrinol* **22**, 1535-1551 (2008).

68. C. M. Eakin, M. J. Maccoss, G. L. Finney, R. E. Klevit, Estrogen receptor alpha is a putative substrate for the BRCA1 ubiquitin ligase. *Proc Natl Acad Sci U S A* **104**, 5794-5799 (2007).

69. S. Ramamoorthy, S. C. Dhananjayan, F. J. Demayo, Z. Nawaz, Isoform-specific degradation of PR-B by E6-AP is critical for normal mammary gland development. *Mol Endocrinol* **24**, 2099-2113 (2010).

70. E. Lim *et al.*, Aberrant luminal progenitors as the candidate target population for basal tumor development in BRCA1 mutation carriers. *Nat Med* **15**, 907-913 (2009).

71. L. Ciarloni, S. Mallepell, C. Brisken, Amphiregulin is an essential mediator of estrogen receptor alpha function in mammary gland development. *Proc Natl Acad Sci U S A* **104**, 5455-5460 (2007).

72. T. C. G. Atlas, Comprehensive molecular portraits of human breast tumours. *Nature* **490**, 61-70 (2012).

73. M. P. van Bragt, X. Hu, Y. Xie, Z. Li, RUNX1, a transcription factor mutated in breast cancer, controls the fate of ER-positive mammary luminal cells. *Elife* **3**, e03881 (2014).

74. G. M. Bernardo *et al.*, FOXA1 is an essential determinant of ERalpha expression and mammary ductal morphogenesis. *Development* **137**, 2045-2054 (2010).

75. Y. Liu *et al.*, Foxa1 is essential for mammary duct formation. *Genesis* **54**, 277-285 (2016).

76. H. Kouros-Mehr, E. M. Slorach, M. D. Sternlicht, Z. Werb, GATA-3 maintains the differentiation of the luminal cell fate in the mammary gland. *Cell* **127**, 1041-1055 (2006).

77. I. Del Barco Barrantes *et al.*, Regulation of Mammary Luminal Cell Fate and Tumorigenesis by p38α. *Stem Cell Reports* **10**, 257-271 (2018).

78. K. A. Ludwik *et al.*, RSK2 Maintains Adult Estrogen Homeostasis by Inhibiting ERK1/2-Mediated Degradation of Estrogen Receptor Alpha. *Cell Rep* **32**, 107931 (2020).

79. S. Cagnet *et al.*, Oestrogen receptor α AF-1 and AF-2 domains have cell population-specific functions in the mammary epithelium. *Nat Commun* **9**, 4723 (2018).

80. C. Wang, J. R. Christin, M. H. Oktay, W. Guo, Lineage-Biased Stem Cells Maintain Estrogen-Receptor-Positive and -Negative Mouse Mammary Luminal Lineages. *Cell Rep* **18**, 2825-2835 (2017).

81. A. Van Keymeulen *et al.*, Lineage-Restricted Mammary Stem Cells Sustain the Development, Homeostasis, and Regeneration of the Estrogen Receptor Positive Lineage. *Cell Rep* **20**, 1525-1532 (2017).

82.	R. R. Giraddi *et al.*, Stem and progenitor cell division kinetics during postnatal mouse mammary gland development. *Nat Commun* **6**, 8487 (2015).

83.	H. W. Jackson *et al.*, The single-cell pathology landscape of breast cancer. *Nature* **578**, 615-620 (2020).

84.	C. J. Park *et al.*, Generation and characterization of an estrogen receptor alpha-iCre knock-in mouse. *Genesis* **55**, (2017).

85.	K. S. Korach *et al.*, Estrogen receptor gene disruption: molecular characterization and experimental and clinical phenotypes. *Recent Prog Horm Res* **51**, 159-186; discussion 186-158 (1996).

86.	L. Gagniac *et al.*, Membrane expression of the estrogen receptor ERα is required for intercellular communications in the mammary epithelium. *Development* **147**, (2020).

87.	S. A. Best *et al.*, Dual roles for Id4 in the regulation of estrogen signaling in the mammary gland and ovary. *Development* **141**, 3159-3164 (2014).

88.	J. R. Carr *et al.*, FoxM1 regulates mammary luminal cell fate. *Cell Rep* **1**, 715-729 (2012).

89.	C. Forster *et al.*, Involvement of estrogen receptor beta in terminal differentiation of mammary gland epithelium. *Proc Natl Acad Sci U S A* **99**, 15578-15583 (2002).

90.	E. Erikson, J. L. Maller, A protein kinase from Xenopus eggs specific for ribosomal protein S6. *Proc Natl Acad Sci U S A* **82**, 742-746 (1985).

91.	P. P. Roux *et al.*, RAS/ERK signaling promotes site-specific ribosomal protein S6 phosphorylation via RSK and stimulates cap-dependent translation. *J Biol Chem* **282**, 14056-14064 (2007).

92.	D. C. Fingar, J. Blenis, Target of rapamycin (TOR): an integrator of nutrient and growth factor signals and coordinator of cell growth and cell cycle progression. *Oncogene* **23**, 3151-3171 (2004).

93.	T. W. Sturgill, L. B. Ray, E. Erikson, J. L. Maller, Insulin-stimulated MAP-2 kinase phosphorylates and activates ribosomal protein S6 kinase II. *Nature* **334**, 715-718 (1988).

94.	M. Zeniou, T. Ding, E. Trivier, A. Hanauer, Expression analysis of RSK gene family members: the RSK2 gene, mutated in Coffin-Lowry syndrome, is prominently expressed in brain structures essential for cognitive function and learning. *Hum Mol Genet* **11**, 2929-2940 (2002).

95.	J. Kim *et al.*, Rsk-mediated phosphorylation and 14-3-3ε binding of Apaf-1 suppresses cytochrome c-induced apoptosis. *Embo j* **31**, 1279-1292 (2012).

96.	S. Kang *et al.*, p90 ribosomal S6 kinase 2 promotes invasion and metastasis of human head and neck squamous cell carcinoma cells. *J Clin Invest* **120**, 1165-1177 (2010).

97.	N. Fujita, S. Sato, T. Tsuruo, Phosphorylation of p27Kip1 at threonine 198 by p90 ribosomal protein S6 kinases promotes its binding to 14-3-3 and cytoplasmic localization. *J Biol Chem* **278**, 49254-49260 (2003).

98.	G. A. Smolen *et al.*, A genome-wide RNAi screen identifies multiple RSK-dependent regulators of cell migration. *Genes Dev* **24**, 2654-2665 (2010).

99.   U. Doehn *et al.*, RSK is a principal effector of the RAS-ERK pathway for eliciting a coordinate promotile/invasive gene program and phenotype in epithelial cells. *Mol Cell* **35**, 511-522 (2009).

100.   S. W. Jones, E. Erikson, J. Blenis, J. L. Maller, R. L. Erikson, A Xenopus ribosomal protein S6 kinase has two apparent kinase domains that are each similar to distinct protein kinases. *Proc Natl Acad Sci U S A* **85**, 3377-3381 (1988).

101.   T. L. Fisher, J. Blenis, Evidence for two catalytically active kinase domains in pp90rsk. *Mol Cell Biol* **16**, 1212-1219 (1996).

102.   Y. Romeo, X. Zhang, P. P. Roux, Regulation and function of the RSK family of protein kinases. *Biochem J* **441**, 553-569 (2012).

103.   P. M. Pereira, A. Schneider, S. Pannetier, D. Heron, A. Hanauer, Coffin-Lowry syndrome. *Eur J Hum Genet* **18**, 627-633 (2010).

104.   R. Poirier *et al.*, Deletion of the Coffin-Lowry syndrome gene Rsk2 in mice is associated with impaired spatial learning and reduced control of exploratory behavior. *Behav Genet* **37**, 31-50 (2007).

105.   X. Yang *et al.*, ATF4 is a substrate of RSK2 and an essential regulator of osteoblast biology; implication for Coffin-Lowry Syndrome. *Cell* **117**, 387-398 (2004).

106.   V. Laugel-Haushalter *et al.*, RSK2 is a modulator of craniofacial development. *PLoS One* **9**, e84343 (2014).

107.   J. J. Facher *et al.*, Cardiomyopathy in Coffin-Lowry syndrome. *Am J Med Genet A* **128a**, 176-178 (2004).

108.   J. Dumont, M. Umbhauer, P. Rassinier, A. Hanauer, M. H. Verlhac, p90Rsk is not involved in cytostatic factor arrest in mouse oocytes. *J Cell Biol* **169**, 227-231 (2005).

109.   P. A. Bignone *et al.*, RPS6KA2, a putative tumour suppressor gene at 6q27 in sporadic epithelial ovarian cancer. *Oncogene* **26**, 683-700 (2007).

110.   J. Cai *et al.*, Low expression of RSK4 predicts poor prognosis in patients with colorectal cancer. *Int J Clin Exp Pathol* **7**, 4959-4970 (2014).

111.   S. B. Dewdney *et al.*, Aberrant methylation of the X-linked ribosomal S6 kinase RPS6KA6 (RSK4) in endometrial cancers. *Clin Cancer Res* **17**, 2120-2129 (2011).

112.   K. A. Ludwik, D. A. Lannigan, Ribosomal S6 kinase (RSK) modulators: a patent review. *Expert Opin Ther Pat* **26**, 1061-1078 (2016).

113.   J. A. Smith *et al.*, Identification of the first specific inhibitor of p90 ribosomal S6 kinase (RSK) reveals an unexpected role for RSK in cancer cell proliferation. *Cancer Res* **65**, 1027-1034 (2005).

114.   M. Li *et al.*, Stereoselective Synthesis and Evaluation of C6″ -Substituted 5a-Carbasugar Analogues of SL0101 as Inhibitors of RSK1/2. *Org Lett* **19**, 2410-2413 (2017).

115.   K. A. Ludwik *et al.*, Development of a RSK Inhibitor as a Novel Therapy for Triple-Negative Breast Cancer. *Mol Cancer Ther* **15**, 2598-2608 (2016).

116.   R. P. Barros, J. A. Gustafsson, Estrogen receptors and the metabolic network. *Cell Metab* **14**, 289-299 (2011).

117. J. L. Lovett *et al.*, Oral contraceptives cause evolutionarily novel increases in hormone exposure: A risk factor for breast cancer. *Evol Med Public Health* **2017**, 97-108 (2017).

118. D. K. Walmer, M. A. Wrona, C. L. Hughes, K. G. Nelson, Lactoferrin expression in the mouse reproductive tract during the natural estrous cycle: correlation with circulating estradiol and progesterone. *Endocrinology* **131**, 1458-1466 (1992).

119. P. M. Vogel, N. G. Georgiade, B. F. Fetter, F. S. Vogel, K. S. McCarty, Jr., The correlation of histologic changes in the human breast with the menstrual cycle. *Am J Pathol* **104**, 23-34 (1981).

120. D. M. Lonard, Z. Nawaz, C. L. Smith, B. W. O'Malley, The 26S proteasome is required for estrogen receptor-alpha and coactivator turnover and for efficient estrogen receptor-alpha transactivation. *Mol Cell* **5**, 939-948 (2000).

121. H. Zhang *et al.*, The catalytic subunit of the proteasome is engaged in the entire process of estrogen receptor-regulated transcription. *EMBO J* **25**, 4223-4233 (2006).

122. C. C. Valley, N. M. Solodin, G. L. Powers, S. J. Ellison, E. T. Alarid, Temporal variation in estrogen receptor-alpha protein turnover in the presence of estrogen. *J Mol Endocrinol* **40**, 23-34 (2008).

123. M. B. Deutsch, V. Bhakri, K. Kubicek, Effects of cross-sex hormone treatment on transgender women and men. *Obstet Gynecol* **125**, 605-610 (2015).

124. W. Xie, A. J. Paterson, E. Chin, L. M. Nabell, J. E. Kudlow, Targeted expression of a dominant negative epidermal growth factor receptor in the mammary gland of transgenic mice inhibits pubertal mammary duct development. *Mol Endocrinol* **11**, 1766-1781 (1997).

125. L. Pasic *et al.*, Sustained activation of the HER1-ERK1/2-RSK signaling pathway controls myoepithelial cell fate in human mammary tissue. *GEnes & Dev* **25**, 1641-1653 (2011).

126. A. E. Maennling *et al.*, Molecular Targeting Therapy against EGFR Family in Breast Cancer: Progress and Future Potentials. *Cancers (Basel)* **11**, (2019).

127. P. B. Joel *et al.*, pp90rsk1 regulates estrogen receptor-mediated transcription through phosphorylation of Ser-167. *Mol Cell Biol* **18**, 1978-1984 (1998).

128. K. A. Ludwik, O. G. McDonald, D. R. Brenin, D. A. Lannigan, ERalpha-mediated nuclear sequestration of RSK2 is required for ER+ breast cancer tumorigenesis. *Cancer Res*, (2018).

129. G. A. Wood, J. E. Fata, K. L. Watson, R. Khokha, Circulating hormones and estrous stage predict cellular and stromal remodeling in murine uterus. *Reproduction* **133**, 1035-1044 (2007).

130. B. Brill, N. Boecher, B. Groner, C. S. Shemanko, A sparing procedure to clear the mouse mammary fat pad of epithelial components for transplantation analysis. *Laboratory animals* **42**, 104-110 (2008).

131. I. Pardo *et al.*, Next-generation transcriptome sequencing of the premenopausal breast epithelium using specimens from a normal human breast tissue bank. *Breast Cancer Res* **16**, R26 (2014).

132. J. E. Fata, V. Chaudhary, R. Khokha, Cellular turnover in the mammary gland is correlated with systemic levels of progesterone and not 17beta-estradiol during the estrous cycle. *Biol Reprod* **65**, 680-688 (2001).

133. M. Shehata *et al.*, Phenotypic and functional characterization of the luminal cell hierachy of the mammary gland. *Breast Cancer Res* **14**, R134 (2012).

134. R. G. Mehta *et al.*, Differential roles of ERalpha and ERbeta in normal and neoplastic development in the mouse mammary gland. *PLoS One* **9**, e113175 (2014).

135. C. Brisken, D. Ataca, Endocrine hormones and local signals during the development of the mouse mammary gland. *Wiley Interdiscip Rev Dev Biol* **4**, 181-195 (2015).

136. N. E. Hynes, C. J. Watson, Mammary gland growth factors: roles in normal development and in cancer. *Cold Spring Harb Perspect Biol* **2**, a003186 (2010).

137. T. S. Eisinger-Mathason, J. Andrade, D. A. Lannigan, RSK in tumorigenesis: connections to steroid signaling. *Steroids* **75**, 191-202 (2010).

138. O. Pinter, Z. Beda, Z. Csaba, I. Gerendai, Differences in the onset of puberty in selected inbred mouse strains. *Endocrine Abstracts* **14**, P617 (2007).

139. K. N. Dalby, N. Morrice, F. B. Caudwell, J. Avruch, P. Cohen, Identification of regulatory phosphorylation sites in mitogen-activated protein kinase (MAPK)-activated protein kinase-1a/p90rsk that are inducible by MAPK. *J Biol Chem* **273**, 1496-1505 (1998).

140. M. Dutertre *et al.*, Estrogen regulation and physiopathologic significance of alternative promoters in breast cancer. *Cancer Res* **70**, 3760-3770 (2010).

141. G. Reid *et al.*, Cyclic, proteasome-mediated turnover of unliganded and liganded ERalpha on responsive promoters is an integral feature of estrogen signaling. *Mol Cell* **11**, 695-707 (2003).

142. M. Li *et al.*, Stereoselective Synthesis and Evaluation of C6"-Substituted 5a-Carbasugar Analogues of SL0101 as Inhibitors of RSK1/2. *Org Lett* **19**, 2410-2413 (2017).

143. X. Wang *et al.*, Regulation of elongation factor 2 kinase by p90(RSK1) and p70 S6 kinase. *EMBO J* **20**, 4370-4379 (2001).

144. P. Filipcik, J. R. Curry, P. D. Mace, When Worlds Collide-Mechanisms at the Interface between Phosphorylation and Ubiquitination. *J Mol Biol* **429**, 1097-1113 (2017).

145. I. Robertshaw, F. Bian, S. K. Das, Mechanisms of uterine estrogen signaling during early pregnancy in mice: an update. *J Mol Endocrinol* **56**, R127-138 (2016).

146. W. Winuthayanon, S. C. Hewitt, K. S. Korach, Uterine epithelial cell estrogen receptor alpha-dependent and -independent genomic profiles that underlie estrogen responses in mice. *Biol Reprod* **91**, 110 (2014).

147. J. Eeckhoute *et al.*, Positive cross-regulatory loop ties GATA-3 to estrogen receptor alpha expression in breast cancer. *Cancer Res* **67**, 6477-6483 (2007).

148. M. Uhlen *et al.*, A pathology atlas of the human cancer transcriptome. *Science* **357**, (2017).

149. D. Tian *et al.*, A kinetic model identifies phosphorylated estrogen receptor-alpha (ERalpha) as a critical regulator of ERalpha dynamics in breast cancer. *FASEB J* **29**, 2022-2031 (2015).

150. P. B. Joel, A. M. Traish, D. A. Lannigan, Estradiol-induced phosphorylation of serine 118 in the estrogen receptor is independent of p42/p44 mitogen-activated protein kinase. *J Biol Chem* **273**, 13317-13323 (1998).

151. B. Perillo *et al.*, DNA oxidation as triggered by H3K9me2 demethylation drives estrogen-induced gene expression. *Science* **319**, 202-206 (2008).

152. C. C. Wentworth, A. Alam, R. M. Jones, A. Nusrat, A. S. Neish, Enteric commensal bacteria induce extracellular signal-regulated kinase pathway signaling via formyl peptide receptor-dependent redox modulation of dual specific phosphatase 3. *J Biol Chem* **286**, 38448-38455 (2011).

153. T. Tanaka, H. D. Halicka, X. Huang, F. Traganos, Z. Darzynkiewicz, Constitutive histone H2AX phosphorylation and ATM activation, the reporters of DNA damage by endogenous oxidants. *Cell Cycle* **5**, 1940-1945 (2006).

154. P. P. Roux, I. Topisirovic, Signaling Pathways Involved in the Regulation of mRNA Translation. *Mol Cell Biol* **38**, (2018).

155. H. E. Scharfman, N. J. MacLusky, Estrogen-growth factor interactions and their contributions to neurological disorders. *Headache* **48 Suppl 2**, S77-89 (2008).

156. A. M. Kelleher, G. W. Burns, S. Behura, G. Wu, T. E. Spencer, Uterine glands impact uterine receptivity, luminal fluid homeostasis and blastocyst implantation. *Sci Rep* **6**, 38078 (2016).

157. P. Zhang *et al.*, Estradiol inhibits fMLP-induced neutrophil migration and superoxide production by upregulating MKP-2 and dephosphorylating ERK. *Int Immunopharmacol* **75**, 105787 (2019).

158. J. M. Denu, K. G. Tanner, Specific and reversible inactivation of protein tyrosine phosphatases by hydrogen peroxide: evidence for a sulfenic acid intermediate and implications for redox regulation. *Biochemistry* **37**, 5633-5642 (1998).

159. T. C. Meng, T. Fukada, N. K. Tonks, Reversible oxidation and inactivation of protein tyrosine phosphatases in vivo. *Mol Cell* **9**, 387-399 (2002).

160. H. G. Moon *et al.*, Phosphorylation of p90RSK is associated with increased response to neoadjuvant chemotherapy in ER-positive breast cancer. *BMC cancer* **12**, 585 (2012).

161. G. E. Weitsman, W. Weebadda, K. Ung, L. C. Murphy, Reactive oxygen species induce phosphorylation of serine 118 and 167 on estrogen receptor alpha. *Breast Cancer Res Treat* **118**, 269-279 (2009).

162. D. Chen *et al.*, Activation of estrogen receptor alpha by S118 phosphorylation involves a ligand-dependent interaction with TFIIH and participation of CDK7. *Mol Cell* **6**, 127-137 (2000).

163. G. Bunone, P. A. Briand, R. J. Miksicek, D. Picard, Activation of the unliganded estrogen receptor by EGF involves the MAP kinase pathway and direct phosphorylation. *EMBO J* **15**, 2174-2183 (1996).

164. J. Park, Y. Lee, Hypoxia induced phosphorylation of estrogen receptor at serine 118 in the absence of ligand. *J Steroid Biochem Mol Biol* **174**, 146-152 (2017).

165. L. Gonzalez *et al.*, Activation of the unliganded estrogen receptor by prolactin in breast cancer cells. *Oncogene* **28**, 1298-1308 (2009).

166. C. C. Valley *et al.*, Differential regulation of estrogen-inducible proteolysis and transcription by the estrogen receptor alpha N terminus. *Mol Cell Biol* **25**, 5417-5428 (2005).

167. X. R. Yang *et al.*, Estrogen receptor and progesterone receptor expression in normal terminal duct lobular units surrounding invasive breast cancer. *Breast Cancer Res Treat* **137**, 837-847 (2013).

168. B. Sigurgeirsson *et al.*, Comprehensive RNA sequencing of healthy human endometrium at two time points of the menstrual cycle. *Biol Reprod* **96**, 24-33 (2017).

169. Breast cancer and hormonal contraceptives: further results. Collaborative Group on Hormonal Factors in Breast Cancer. *Contraception* **54**, 1S-106S (1996).

170. I. Romieu, M. Hernandez-Avila, M. H. Liang, Oral contraceptives and the risk of rheumatoid arthritis: a meta-analysis of a conflicting literature. *Br J Rheumatol* **28 Suppl 1**, 13-17; discussion 18-23 (1989).

171. D. J. Hunter *et al.*, Oral contraceptive use and breast cancer: a prospective study of young women. *Cancer Epidemiol Biomarkers Prev* **19**, 2496-2502 (2010).

172. J. Simin, R. Tamimi, J. Lagergren, H. O. Adami, N. Brusselaers, Menopausal hormone therapy and cancer risk: An overestimated risk? *Eur J Cancer* **84**, 60-68 (2017).

173. J. N. Upshaw, Cardioprotective Strategies to Prevent Cancer Treatment-Related Cardiovascular Toxicity: a Review. *Curr Oncol Rep* **22**, 72 (2020).

174. J. Caron, A. Nohria, Cardiac Toxicity from Breast Cancer Treatment: Can We Avoid This? *Curr Oncol Rep* **20**, 61 (2018).

175. S. Gallo, A. Vitacolonna, A. Bonzano, P. Comoglio, T. Crepaldi, ERK: A Key Player in the Pathophysiology of Cardiac Hypertrophy. *Int J Mol Sci* **20**, (2019).

176. Y. Takeishi *et al.*, Activation of mitogen-activated protein kinases and p90 ribosomal S6 kinase in failing human hearts with dilated cardiomyopathy. *Cardiovascular research* **53**, 131-137 (2002).

177. N. T. Le *et al.*, p90RSK targets the ERK5-CHIP ubiquitin E3 ligase activity in diabetic hearts and promotes cardiac apoptosis and dysfunction. *Circulation research* **110**, 536-550 (2012).

178. S. Gao, D. Ho, D. E. Vatner, S. F. Vatner, Echocardiography in Mice. *Curr Protoc Mouse Biol* **1**, 71-83 (2011).

179. A. G. Cadar, L. Zhong, A. Lin, M. O. Valenzuela, C. C. Lim, Upstream open reading frame in 5'-untranslated region reduces titin mRNA translational efficiency. *Biochem Biophys Res Commun* **453**, 185-191 (2014).

180. C. Y. Huang *et al.*, Mitochondrial ROS-induced ERK1/2 activation and HSF2-mediated AT1 R upregulation are required for doxorubicin-induced cardiotoxicity. *J Cell Physiol* **233**, 463-475 (2018).

181. C. S. Abdullah *et al.*, Doxorubicin-induced cardiomyopathy associated with inhibition of autophagic degradation process and defects in mitochondrial respiration. *Sci Rep* **9**, 2002 (2019).

182. S. Zhang *et al.*, Identification of the molecular basis of doxorubicin-induced cardiotoxicity. *Nat Med* **18**, 1639-1642 (2012).

183. J. S. Lee, S. E. Yost, Y. Yuan, Neoadjuvant Treatment for Triple Negative Breast Cancer: Recent Progresses and Challenges. *Cancers (Basel)* **12**, (2020).

184. C. Li, J. Dai, F. Wu, H. Zhang, Impacts of different anesthetic agents on left ventricular systolic function in mice assessed by echocardiography. *Physiol Res* **68**, 365-374 (2019).

185. K. P. Hoeflich *et al.*, In vivo antitumor activity of MEK and phosphatidylinositol 3-kinase inhibitors in basal-like breast cancer models. *Clin Cancer Res* **15**, 4649-4664 (2009).

186. M. Banys-Paluchowski, N. Krawczyk, F. Meier-Stiegen, T. Fehm, Circulating tumor cells in breast cancer--current status and perspectives. *Crit Rev Oncol Hematol* **97**, 22-29 (2016).

187. R. Dent *et al.*, Triple-negative breast cancer: clinical features and patterns of recurrence. *Clin Cancer Res* **13**, 4429-4434 (2007).

188. D. W. Craig *et al.*, Genome and transcriptome sequencing in prospective metastatic triple-negative breast cancer uncovers therapeutic vulnerabilities. *Mol Cancer Ther* **12**, 104-116 (2013).

189. J. R. Infante *et al.*, A phase 1b study of trametinib, an oral Mitogen-activated protein kinase kinase (MEK) inhibitor, in combination with gemcitabine in advanced solid tumours. *Eur J Cancer* **49**, 2077-2085 (2013).

190. J. S. Duncan *et al.*, Dynamic reprogramming of the kinome in response to targeted MEK inhibition in triple-negative breast cancer. *Cell* **149**, 307-321 (2012).

191. J. M. Giltnane, J. M. Balko, Rationale for targeting the Ras/MAPK pathway in triple-negative breast cancer. *Discov Med* **17**, 275-283 (2014).

192. P. Cossu-Rocca *et al.*, Analysis of PIK3CA Mutations and Activation Pathways in Triple Negative Breast Cancer. *PLoS One* **10**, e0141763 (2015).

193. J. Jing *et al.*, Comprehensive predictive biomarker analysis for MEK inhibitor GSK1120212. *Mol Cancer Ther* **11**, 720-729 (2012).

194. A. A. Samatar, P. I. Poulikakos, Targeting RAS-ERK signalling in cancer: promises and challenges. *Nat Rev Drug Discov* **13**, 928-942 (2014).

195. M. D. Larrea *et al.*, RSK1 drives p27Kip1 phosphorylation at T198 to promote RhoA inhibition and increase cell motility. *Proc Natl Acad Sci U S A* **106**, 9268-9273 (2009).

196. D. Vial, P. J. McKeown-Longo, Epidermal growth factor (EGF) regulates α5β1 integrin activation state in human cancer cell lines through the p90RSK-dependent phosphorylation of filamin A. *J Biol Chem* **287**, 40371-40380 (2012).

197. J. E. Gawecka *et al.*, RSK2 protein suppresses integrin activation and fibronectin matrix assembly and promotes cell migration. *J Biol Chem* **287**, 43424-43437 (2012).

198. A. L. Stratford *et al.*, Targeting p90 ribosomal S6 kinase eliminates tumor-initiating cells by inactivating Y-box binding protein-1 in triple-negative breast cancers. *Stem Cells* **30**, 1338-1348 (2012).

199. J. Bain *et al.*, The selectivity of protein kinase inhibitors: a further update. *Biochem J* **408**, 297-315 (2007).

200. D. Utepbergenov *et al.*, Insights into the inhibition of the p90 ribosomal S6 kinase (RSK) by the flavonol glycoside SL0101 from the 1.5 Å crystal structure of the N-terminal domain of RSK2 with bound inhibitor. *Biochemistry* **51**, 6499-6510 (2012).

201. G. P. Sapkota *et al.*, Phosphorylation of the protein kinase mutated in Peutz-Jeghers cancer syndrome, LKB1/STK11, at Ser431 by p90(RSK) and cAMP-

dependent protein kinase, but not its farnesylation at Cys(433), is essential for LKB1 to suppress cell vrowth. *J Biol Chem* **276**, 19469-19482 (2001).

202. T. M. Kirrane *et al.*, Indole RSK inhibitors. Part 2: optimization of cell potency and kinase selectivity. *Bioorg Med Chem Lett* **22**, 738-742 (2012).

203. A. J. Edgar, M. Trost, C. Watts, R. Zaru, A combination of SILAC and nucleotide acyl phosphate labelling reveals unexpected targets of the Rsk inhibitor BI-D1870. *Biosci Rep* **34**, (2014).

204. R. M. Fryer *et al.*, Mitigation of off-target adrenergic binding and effects on cardiovascular function in the discovery of novel ribosomal S6 kinase 2 inhibitors. *J Pharmacol Exp Ther* **340**, 492-500 (2012).

205. I. Aronchik *et al.*, Novel potent and selective inhibitors of p90 ribosomal S6 kinase reveal the heterogeneity of RSK function in MAPK-driven cancers. *Mol Cancer Res* **12**, 803-812 (2014).

206. R. Jain *et al.*, Discovery of Potent and Selective RSK Inhibitors as Biological Probes. *J Med Chem* **58**, 6766-6783 (2015).

207. M. S. Cohen, H. Hadjivassiliou, J. Taunton, A clickable inhibitor reveals context-dependent autoactivation of p90 RSK. *Nat Chem Biol* **3**, 156-160 (2007).

208. M. S. Cohen, C. Zhang, K. M. Shokat, J. Taunton, Structural bioinformatics-based design of selective, irreversible kinase inhibitors. *Science* **308**, 1318-1321 (2005).

209. I. M. Serafimova *et al.*, Reversible targeting of noncatalytic cysteines with chemically tuned electrophiles. *Nat Chem Biol* **8**, 471-476 (2012).

210. R. M. Mrozowski *et al.*, Improving the affinity of SL0101 for RSK using structure-based design. *ACS Med Chem Lett* **4**, 175-179 (2012).

211. M. Li *et al.*, Synthesis and Structure-Activity Relationship Study of 5a-Carbasugar Analogues of SL0101. *ACS Med Chem Lett* **6**, 95-99 (2015).

212. D. E. Clark, C. E. Poteet-Smith, J. A. Smith, D. A. Lannigan, Rsk2 allosterically activates estrogen receptor alpha by docking to the hormone-binding domain. *Embo j* **20**, 3484-3494 (2001).

213. T. S. Eisinger-Mathason *et al.*, Codependent functions of RSK2 and the apoptosis-promoting factor TIA-1 in stress granule assembly and cell survival. *Mol Cell* **31**, 722-736 (2008).

214. M. Ammirati *et al.*, Discovery of an in Vivo Tool to Establish Proof-of-Concept for MAP4K4-Based Antidiabetic Treatment. *ACS Med Chem Lett* **6**, 1128-1133 (2015).

215. B. D. Lehmann *et al.*, Identification of human triple-negative breast cancer subtypes and preclinical models for selection of targeted therapies. *J Clin Invest* **121**, 2750-2767 (2011).

216. B. D. Lehmann, J. A. Pietenpol, Identification and use of biomarkers in treatment strategies for triple-negative breast cancer subtypes. *J Pathol* **232**, 142-150 (2014).

217. C. Neuzillet *et al.*, MEK in cancer and cancer therapy. *Pharmacol Ther* **141**, 160-171 (2014).

218. A. B. Turke *et al.*, MEK inhibition leads to PI3K/AKT activation by relieving a negative feedback on ERBB receptors. *Cancer Res* **72**, 3228-3237 (2012).

219. E. Jokinen, J. P. Koivunen, MEK and PI3K inhibition in solid tumors: rationale and evidence to date. *Ther Adv Med Oncol* **7**, 170-180 (2015).

220. D. Li *et al.*, The prometastatic ribosomal S6 kinase 2-cAMP response element-binding protein (RSK2-CREB) signaling pathway up-regulates the actin-binding protein fascin-1 to promote tumor metastasis. *J Biol Chem* **288**, 32528-32538 (2013).

221. R. Lara *et al.*, An siRNA screen identifies RSK1 as a key modulator of lung cancer metastasis. *Oncogene* **30**, 3513-3521 (2011).

222. Y. Zhou *et al.*, Crucial roles of RSK in cell motility by catalysing serine phosphorylation of EphA2. *Nat Commun* **6**, 7679 (2015).

223. K. Zaman *et al.*, Fulvestrant with or without selumetinib, a MEK 1/2 inhibitor, in breast cancer progressing after aromatase inhibitor therapy: a multicentre randomised placebo-controlled double-blind phase II trial, SAKK 21/08. *Eur J Cancer* **51**, 1212-1220 (2015).

224. Y. Li *et al.*, Regioselective Synthesis of a C-4″ Carbamate,C-6″ n-Pr Substituted Cyclitol Analogue of SL0101. *Org Lett* **22**, 1448-1452 (2020).

225. D. J. Maloney, S. M. Hecht, Synthesis of a potent and selective inhibitor of p90 Rsk. *Org Lett* **7**, 1097-1099 (2005).

226. T. L. Nguyen *et al.*, Homology model of RSK2 N-terminal kinase domain, structure-based identification of novel RSK2 inhibitors, and preliminary common pharmacophore. *Bioorg Med Chem* **14**, 6097-6105 (2006).

227. H. I. Lowe, C. O. Facey, N. J. Toyang, J. L. Bryant, Specific RSK kinase inhibition by dibenzyl trisulfide and implication for therapeutic treatment of cancer. *Anticancer Res* **34**, 1637-1641 (2014).

228. A. Costales *et al.*, 2-Amino-7-substituted benzoxazole analogs as potent RSK2 inhibitors. *Bioorg Med Chem Lett* **24**, 1592-1596 (2014).

229. Y. Zhong *et al.*, Substituted indolin-2-ones as p90 ribosomal S6 protein kinase 2 (RSK2) inhibitors: Molecular docking simulation and structure-activity relationship analysis. *Bioorg Med Chem* **21**, 1724-1734 (2013).

230. R. Anjum, J. Blenis, The RSK family of kinases: emerging roles in cellular signalling. *Nat Rev Mol Cell Biol* **9**, 747-758 (2008).

231. H. Y. Wang *et al.*, C5'-Alkyl Substitution Effects on Digitoxigenin α-l-Glycoside Cancer Cytotoxicity. *ACS Med Chem Lett* **2**, 259-263 (2011).

232. R. M. Mrozowski *et al.*, De novo synthesis and biological evaluation of C6″-substituted C4″-amide analogues of SL0101. *Org Lett* **16**, 5996-5999 (2014).

233. M. Shan, G. A. O'Doherty, Synthesis of carbasugar C-1 phosphates via Pd-catalyzed cyclopropanol ring opening. *Org Lett* **10**, 3381-3384 (2008).

234. M. Shan, G. A. O'Doherty, Synthesis of SL0101 carbasugar analogues: carbasugars via Pd-catalyzed cyclitolization and post-cyclitolization transformations. *Org Lett* **12**, 2986-2989 (2010).

235. S. O. Bajaj, E. U. Sharif, N. G. Akhmedov, G. A. O'Doherty, De novo asymmetric synthesis of the mezzettiaside family of natural products via the iterative use of a dual B-/Pd-catalyzed glycosylation. *Chem Sci* **5**, 2230-2234 (2014).

236. A. Z. Aljahdali, P. Shi, Y. Zhong, G. A. O'Doherty, De novo asymmetric synthesis of the pyranoses: from monosaccharides to oligosaccharides. *Adv Carbohydr Chem Biochem* **69**, 55-123 (2013).

237. J. M. Harris, M. D. Keranen, G. A. O'Doherty, Syntheses of D- and L-Mannose, Gulose, and Talose via Diastereoselective and Enantioselective Dihydroxylation Reactions. *J Org Chem* **64**, 2982-2983 (1999).

238. J. M. Harris, M. D. Keränen, H. Nguyen, V. G. Young, G. A. O'Doherty, Syntheses of four D- and L-hexoses via diastereoselective and enantioselective dihydroxylation reactions. *Carbohydr Res* **328**, 17-36 (2000).

239. R. S. Babu, M. Zhou, G. A. O'Doherty, De novo synthesis of oligosaccharides using a palladium-catalyzed glycosylation reaction. *J Am Chem Soc* **126**, 3428-3429 (2004).

240. M. Shan, G. A. O'Doherty, De novo asymmetric syntheses of SL0101 and its analogues via a palladium-catalyzed glycosylation. *Org Lett* **8**, 5149-5152 (2006).

241. R. S. Babu, G. A. O'Doherty, A palladium-catalyzed glycosylation reaction: the de novo synthesis of natural and unnatural glycosides. *J Am Chem Soc* **125**, 12406-12407 (2003).

242. R. S. Babu, S. R. Guppi, G. A. O'Doherty, Synthetic studies toward mannopeptimycin-E: synthesis of the O-linked tyrosine 1,4-alpha,alpha-manno,manno-pyranosyl pyranoside. *Org Lett* **8**, 1605-1608 (2006).

243. H. Guo, G. A. O'Doherty, De Novo Asymmetric Syntheses of d-, l- and 8-epi-Swainsonine. *Tetrahedron* **64**, 304-313 (2008).

244. B. M. Trost, D. L. Van Vranken, Asymmetric Transition Metal-Catalyzed Allylic Alkylations. *Chem Rev* **96**, 395-422 (1996).

245. B. M. Trost, M. L. Crawley, Asymmetric transition-metal-catalyzed allylic alkylations: applications in total synthesis. *Chem Rev* **103**, 2921-2944 (2003).

246. B. M. Trost, M. R. Machacek, A. Aponick, Predicting the stereochemistry of diphenylphosphino benzoic acid (DPPBA)-based palladium-catalyzed asymmetric allylic alkylation reactions: a working model. *Acc Chem Res* **39**, 747-760 (2006).

247. J. A. Smith *et al.*, Influence of rhamnose substituents on the potency of SL0101, an inhibitor of the Ser/Thr kinase, RSK. *Bioorg Med Chem* **14**, 6034-6042 (2006).

248. M. K. Hilinski, R. M. Mrozowski, D. E. Clark, D. A. Lannigan, Analogs of the RSK inhibitor SL0101: optimization of in vitro biological stability. *Bioorg Med Chem Lett* **22**, 3244-3247 (2012).

249. J. A. Smith, D. J. Maloney, S. M. Hecht, D. A. Lannigan, Structural basis for the activity of the RSK-specific inhibitor, SL0101. *Bioorg Med Chem* **15**, 5018-5034 (2007).

250. A. K. Iyer *et al.*, A Direct Comparison of the Anticancer Activities of Digitoxin MeON-Neoglycosides and O-Glycosides: Oligosaccharide Chain Length-Dependent Induction of Caspase-9-Mediated Apoptosis. *ACS Med Chem Lett* **1**, 326-330 (2010).

251. P. Shi *et al.*, Structure Activity Relationship Study of the Cleistriosides and Cleistetrosides for Antibacterial/Anticancer Activity. *ACS Med Chem Lett* **3**, 1086-1090 (2012).

252. B. Wu, M. Li, G. A. O'Doherty, Synthesis of several cleistrioside and cleistetroside natural products via a divergent de novo asymmetric approach. *Org Lett* **12**, 5466-5469 (2010).

253. B. M. Trost, A. G. Romero, Synthesis of optically active isoquinuclidines utilizing a diastereoselectivity control element. *The Journal of Organic Chemistry* **51**, 2332-2342 (1986).

254. J. E. Audia, L. Boisvert, A. D. Patten, A. Villalobos, S. J. Danishefsky, Synthesis of two useful, enantiomerically pure derivatives of (S)-4-hydroxy-2-cyclohexenone. *The Journal of Organic Chemistry* **54**, 3738-3740 (1989).

255. J. N. Abrams *et al.*, De novo asymmetric synthesis of 8a-epi-swainsonine. *J Org Chem* **73**, 1935-1940 (2008).

256. S. A. Borisova *et al.*, A de novo approach to the synthesis of glycosylated methymycin analogues with structural and stereochemical diversity. *Org Lett* **12**, 5150-5153 (2010).

257. L. Chan, M. S. Taylor, Regioselective alkylation of carbohydrate derivatives catalyzed by a diarylborinic acid derivative. *Org Lett* **13**, 3090-3093 (2011).

258. D. Lee, C. L. Williamson, L. Chan, M. S. Taylor, Regioselective, borinic acid-catalyzed monoacylation, sulfonylation and alkylation of diols and carbohydrates: expansion of substrate scope and mechanistic studies. *J Am Chem Soc* **134**, 8260-8267 (2012).

259. M. S. Taylor, Catalysis based on reversible covalent interactions of organoboron compounds. *Acc Chem Res* **48**, 295-305 (2015).

260. D. A. Lannigan, Estrogen receptor phosphorylation. *Steroids* **68**, 1-9 (2003).

261. T. T. Duplessis, C. C. Williams, S. M. Hill, B. G. Rowan, Phosphorylation of Estrogen Receptor alpha at serine 118 directs recruitment of promoter complexes and gene-specific transcription. *Endocrinology* **152**, 2517-2526 (2011).

262. S. J. Han *et al.*, The Dual Estrogen Receptor alpha Inhibitory Effects of the Tissue-Selective Estrogen Complex for Endometrial and Breast Safety. *Mol Pharmacol* **89**, 14-26 (2016).

263. P. Chymkowitch, N. Le May, P. Charneau, E. Compe, J. M. Egly, The phosphorylation of the androgen receptor by TFIIH directs the ubiquitin/proteasome process. *EMBO J* **30**, 468-479 (2011).

264. J. W. Lee, F. Ryan, J. C. Swaffield, S. A. Johnston, D. D. Moore, Interaction of thyroid-hormone receptor with a conserved transcriptional mediator. *Nature* **374**, 91-94 (1995).

265. G. L. Powers, S. J. Ellison-Zelski, A. J. Casa, A. V. Lee, E. T. Alarid, Proteasome inhibition represses ERalpha gene expression in ER+ cells: a new link between proteasome activity and estrogen signaling in breast cancer. *Oncogene* **29**, 1509-1518 (2010).

266. P. B. Nirmala, R. V. Thampan, Ubiquitination of the rat uterine estrogen receptor: dependence on estradiol. *Biochem Biophys Res Commun* **213**, 24-31 (1995).

267. E. T. Alarid, N. Bakopoulos, N. Solodin, Proteasome-mediated proteolysis of estrogen receptor: a novel component in autologous down-regulation. *Mol Endocrinol* **13**, 1522-1534 (1999).

268. S. A. Fuqua *et al.*, A hypersensitive estrogen receptor-alpha mutation in premalignant breast lesions. *Cancer Res* **60**, 4026-4029 (2000).

269. M. Fan, R. M. Bigsby, K. P. Nephew, The NEDD8 pathway is required for proteasome-mediated degradation of human estrogen receptor (ER)-alpha and

essential for the antiproliferative activity of ICI 182,780 in ERalpha-positive breast cancer cells. *Mol Endocrinol* **17**, 356-365 (2003).

270. R. I. Enchev, B. A. Schulman, M. Peter, Protein neddylation: beyond cullin-RING ligases. *Nat Rev Mol Cell Biol* **16**, 30-44 (2015).

271. T. Traboulsi, M. El Ezzy, V. Dumeaux, E. Audemard, S. Mader, Role of SUMOylation in differential ERalpha transcriptional repression by tamoxifen and fulvestrant in breast cancer cells. *Oncogene* **38**, 1019-1037 (2019).

272. M. Fan, A. Park, K. P. Nephew, CHIP (carboxyl terminus of Hsc70-interacting protein) promotes basal and geldanamycin-induced degradation of estrogen receptor-alpha. *Mol Endocrinol* **19**, 2901-2914 (2005).

273. V. Duong *et al.*, Differential regulation of estrogen receptor alpha turnover and transactivation by Mdm2 and stress-inducing agents. *Cancer Res* **67**, 5513-5521 (2007).

274. S. Saji *et al.*, MDM2 enhances the function of estrogen receptor alpha in human breast cancer cells. *Biochem Biophys Res Commun* **281**, 259-265 (2001).

275. K. Kim *et al.*, MDM2 regulates estrogen receptor alpha and estrogen responsiveness in breast cancer cells. *J Mol Endocrinol* **46**, 67-79 (2011).

276. E. Dizin, I. Irminger-Finger, Negative feedback loop of BRCA1-BARD1 ubiquitin ligase on estrogen receptor alpha stability and activity antagonized by cancer-associated isoform of BARD1. *Int J Biochem Cell Biol* **42**, 693-700 (2010).

277. K. Adelson *et al.*, Randomized phase II trial of fulvestrant alone or in combination with bortezomib in hormone receptor-positive metastatic breast cancer resistant to aromatase inhibitors: a New York Cancer Consortium trial. *NPJ Breast Cancer* **2**, 16037 (2016).

278. T. Ito *et al.*, Identification of a primary target of thalidomide teratogenicity. *Science* **327**, 1345-1350 (2010).

279. X. Huang, V. M. Dixit, Drugging the undruggables: exploring the ubiquitin system for drug development. *Cell Res* **26**, 484-498 (2016).

280. S. D. Dufresne *et al.*, Altered extracellular signal-regulated kinase signaling and glycogen metabolism in skeletal muscle from p90 ribosomal S6 kinase 2 knockout mice. *Mol Cell Biol* **21**, 81-87 (2001).

281. J. P. David *et al.*, Essential role of RSK2 in c-Fos-dependent osteosarcoma development. *J Clin Invest* **115**, 664-672 (2005).

282. C. Castillon *et al.*, Selective alteration of adult hippocampal neurogenesis and impaired spatial pattern separation performance in the RSK2-deficient mouse model of Coffin-Lowry syndrome. *Neurobiol Dis* **115**, 69-81 (2018).

283. K. El-Haschimi *et al.*, Insulin resistance and lipodystrophy in mice lacking ribosomal S6 kinase 2. *Diabetes* **52**, 1340-1346 (2003).

284. K. Yao *et al.*, RSK2 phosphorylates T-bet to attenuate colon cancer metastasis and growth. *Proc Natl Acad Sci U S A* **114**, 12791-12796 (2017).

285. K. Yao *et al.*, RSK2 is required for TRAF6 phosphorylation-mediated colon inflammation. *Oncogene* **37**, 3501-3513 (2018).

286. M. V. Artamonov *et al.*, RSK2 contributes to myogenic vasoconstriction of resistance arteries by activating smooth muscle myosin and the Na(+)/H(+) exchanger. *Sci Signal* **11**, (2018).

287. J. Li *et al.*, Anchored p90 ribosomal S6 kinase 3 is required for cardiac myocyte hypertrophy. *Circulation research* **112**, 128-139 (2013).
288. C. L. Passariello *et al.*, p90 ribosomal S6 kinase 3 contributes to cardiac insufficiency in alpha-tropomyosin Glu180Gly transgenic mice. *Am J Physiol Heart Circ Physiol* **305**, H1010-1019 (2013).
289. C. L. Passariello *et al.*, RSK3 is required for concentric myocyte hypertrophy in an activated Raf1 model for Noonan syndrome. *J Mol Cell Cardiol* **93**, 98-105 (2016).